The role of Titania in the formation of MgO - A1(_2)O(_3)-SiO(_2) glass ceramics

Hutton, William

THE ROLE OF TITANIA IN THE FORMATION OF $MgO - Al_2O_3 - SiO_2$ GLASS CERAMICS

by

William Hutton B.Sc.

(Graduate Society)

A Thesis submitted to the University of Durham in Candidature for the degree of

Doctor of Philosophy

December 1979

To

Pamela, Gayle and Abigail

ABSTRACT

Glasses and ceramics of the $MgO-Al_2O_3-SiO_2$ system have been founded and characterised by X-Ray Diffraction and optical and electron microscopy (Chapter 3).

The hole and electron trapping centres generated by γ-irradiation of the specimens have been studied by electron spin resonance, (x-band), and optical absorption spectroscopy, (Chapters 4 and 5). Computer simulations of the e.s.r. spectra have been used to deduce the Hamiltonian parameters and distributions of each 'defect' site. We conclude that the traps responsible for the hole resonances are non-bonding oxygen ions singly bonded to an SiO_4 tetrahedra in the glass specimens, and oxygen ions bridging between SiO_4 and AlO_4 tetrahedra in the ceramics.

I.R. absorption and Raman scattering studies are reported in Chapter 6. A phase separated glass structure is indicated consisting of a high silica phase with a framework silicate structure, and a high modifier (Mg) phase which degrades from a cyclosilicate structure to a chain silicate structure as TiO_2 is added to the base glass.

Corresponding changes in the hole resonance lineshape are also interpreted in terms of structural changes within the high modifier glass phase and found to be consistent with 'sheet' and 'chain' silicate structures.

TiO_2 appears to promote the phase separation by the formation of Al-Ti complexes. Analysis of the e.s.r. and optical absorption spectra from the radiochemically reducted Ti^{3+} ions suggests titanium sites with the essential symmetry of a tetragonally compressed octahedron (D_{4h}). We are unable to suggest a specific Al-Ti complex.

The e.s.r. and vibrational spectra are invariant with heat treatments of the glasses at temperatures below that at which the first crystalline phase appears, and we find no evidence therefore of structural changes associated with such heat treatments.

In Chapter 7 we consider a model for the promotion of phase separation in the $MgO-Al_2O_3-SiO_2$ system by TiO_2, and also present evidence which suggests that the first metastable crystalline phase to form originates from the TiO_2 rich glass phase. Thereby the secondary role of the TiO_2 in the production of fine grain glass ceramics is indicated.

ACKNOWLEDGEMENTS

I should like to express my thanks to the following:-

The Science Research Council for their financial support of this work.

Professors D A Wright and G G Roberts for making available the research facilities of their department.

The technical staff of the Department of Applied Physics and Electronics, led by Mr. F Spence. In particular Mr. R Waite and Mr. C Savage for their continual assistance during the course of the work. Also Mr. T Harcourt for his careful specimen preparation.

Principally I acknowledge the contributions made by my supervisor, Dr. J S Thorp, and by Dr. G Brown. Without their considerable guidance and assistance this work would not have been concluded. I thank them.

My colleagues and friends in the Department, especially Mr. R Vasquez, Mr. G T Quayle and Dr. E A E Ammar, who gave unhesitatingly of their time and knowledge.

Finally I thank Mrs. J Henderson for typing and greatly assisting in the preparation of the manuscript, and Mrs. E Johnson for the tracing of the drawings.

CONTENTS

CHAPTER 1

INTRODUCTION

1.1 Glass Ceramics

Glass is a supercooled liquid with a viscosity of greater than 10^{14} poise, and the glass technologist's problem has always been to select a system in which the inevitable tendency to nucleate and crystallize whilst passing through the metastable zone of supercooling, is not so great that the limiting viscosity of 10^{14} poise, at which such processes are almost entirely arrested, cannot be reached before there are any detectable signs of crystallization.

Glass ceramics were initially developed at Corning Glass in the U.S.A. in the late 1950's, and the criteria for these systems are rather different. The parent glass must be such that the nucleation and crystallization stages can be controlled to produce a fine grain, (0.1 μ - 1.0 μ crystals), polycrystalline product, which, in conventional glass ceramics is 90-95% crystalline, and in some special transparent ceramics is 50-60% crystalline (1.1). When compared with the parent glasses, the glass ceramics almost always show an improvement in most of their 'useful' properties, i.e. they are mechanically stronger, more chemically durable, more refractory, and they have reduced dielectric losses (1.2). The commercial attractiveness of glass ceramics when compared with conventional sintered ceramics is largely in the fact that the parent glasses can be cast into the final product form and then, by appropriate heat treatments, the glass - glass ceramic conversion effected. In this process the dimensional changes are small and thus final machining costs are small compared with conventional ceramics which typically contract by 20-40% during the firing and drying stages (1.2). In addition, glass ceramics have many technical advantages

over conventional ceramics. This is principally due to the fact that the glass ceramic process is applicable to a wide range of compositions, and this, together with the variations which are possible within a system by different heat treatment schedules, means that a wide range of ceramics with a great variety of properties may be produced for specific applications.

1.2 Controlled Crystallization

The classical theories of nucleation and crystallization are reviewed in (1.2) and (1.3). The controlled crystallization of a glass requires a controlled nucleation stage and Porai-Koshits (1.1) has reviewed the possible processes of 'nucleation' in glasses. The formation of stable nuclei in a glass requires that a free energy barrier be overcome. We quote a result due to Stookey and Maurer (1.4):

$$\Delta F = \frac{16\pi \left[\Delta f_s\right]^3}{3\left[\Delta f_v\right]^2} \qquad (1.1)$$

where ΔF is the free energy barrier to stable nucleus formation, Δf_s is the energy per unit surface area between the two phases, and Δf_v is the difference in free energy between the liquid and solid phases.

Nucleation centres may be homogeneous or heterogeneous. In the first case, compositional fluctuations in a supersaturated solution result in the spontaneous formation of crystal nuclei, which, in order to grow and crystallization to proceed, must be greater than a minimum 'critical' dimension. This is equivalent to overcoming the energy barrier of equation (1.1), and therefore the 'ease' with which nuclei form is a balance between the Gibbs free energy difference of the liquid and solid phases Δf_v, which is a function of the supercooling, and the interfacial tension Δf_s between the nucleus and the melt. Heterogeneous nucleation involves the seeding of the melt with nuclei, upon which crystals of the primary phase

can grow. Essentially, these nucleation centres reduce the free energy barrier to nucleation by reducing the interfacial tension term of equation (1.1).

In most glasses, crystallization proceeds from the surface of the specimen where the interfacial free energy is reduced. The resulting ceramics are mechanically weak and of little use. The volume crystallization of the melt is achieved by ensuring many evenly dispersed nuclei through the body of the specimen. Historically, this was first accomplished by doping the glass melt with photosensitive agents such as Ag and Cu, which precipitated into colloidal particles after irradiation of the quenched glass with u.v. radiation, and provided heterogeneous nuclei upon which the glass could crystallize (1.5). Much more common now is the use of 'complex nucleants' such as TiO_2, P_2O_5 and ZrO_2, and the mechanisms by which one of these materials, TiO_2, effects the conversion of a Magnesium-Aluminium-Silicate glass from a coarsely crystalline material into a strong, fine grained glass ceramic is the subject of this study.

1.3 Mechanisms of Nucleation by TiO_2

It was originally proposed (1.6) that the solubility of TiO_2 in the glass melt was high, and upon cooling, the reduced solubility, caused a precipitation by homogeneous nucleation of the TiO_2 into small rutile crystals which then acted as heterogeneous growth centres for the subsequent crystallization of the principal phase. However this proposal did not satisfactorily account for the general observation that in many glasses containing TiO_2, phases other than rutile or a titanate were first to appear in X-ray diffraction measurements, and often a titania phase appeared only in the final stages of crystallization, or even did not appear at all (1.7).

The next suggestion, favoured particularly by many Russian workers, was that the TiO_2 was instrumental in creating a phase separated structure within the glasses. It was proposed that a coordination change from 4-fold

in the melt to 6-fold upon cooling would cause the Ti ions to become incompatible with the silicate network, and that these ions, probably in association with other ions in the melt, would separate into a distinct Ti-rich phase (1.8). However, many silicate and borosilicate glasses phase separate, (e.g. 'Pyrex'), without subsequently producing homogeneous fine grained ceramics on crystallization. Indeed there is evidence to suggest that the glass system studied here, the $MgO-Al_2O_3-SiO_2$ system, itself phase separates without producing useful glass ceramics until significant amounts of TiO_2, (5-20% by weight), are added to the melt, i.e. phase separation is not of itself sufficient to produce fine grain ceramics (1.9).

Some workers have proposed that the titanium converts the relatively coarse phase separation of the systems referred to above, (macrophase separation), into a system with a widely dispersed and uniform emulsion of very fine droplets, (microphase separation), the surfaces of which act as heterogeneous nuclei for the crystallization of the glass matrix. Barry et al (1.10,1.11) are rather more specific in terms of how the TiO_2 produces this microphase separation. These authors suggest that the Ti ion can best achieve its required 6-fold coordination with oxygen by associating with the non-bridged oxygens in the glass, which are most likely to be found at the boundary between the droplets and the matrix. The suggestion is therefore that the titanium ions congregate at the boundary between regions of high order and facilitate the uniform distribution of finely dispersed droplets and the subsequent growth of the crystals upon the 'nuclei', by reducing the interfacial tension term Δf_s (equation (1.1)). In this role the titanium is acting as a surfactant.

While still accepting the importance of a phase separation within the glass, other authors (1.12,1.13) have argued for a rather different nucleation mechanism. They have suggested that the titanium enters one of the

glass phases, and that in the initial stages of crystallization a titanium rich phase, possibly a pseudobrookite solid solution on the composition line $MgO.2TiO_2$ - $Al_2O_3.TiO_2$, is precipitated and acts as heterogeneous nuclei for the crystallization of the major phase.

It seems unlikely at this time that a single universal mechanism by which TiO_2 effects the conversion of a glass system into a fine grained ceramic, will be appropriate to all systems.

1.4 Pre-crystallization, (Nucleation), heat treatments

It is even yet a question of debate as to the necessity or significance of the pre-crystallization heat treatment in the production of a glass ceramic. Most work would suggest that the grain size and crystal type of the final ceramic may be influence by such a treatment (1.1,1.2,1.14,1.15). The optimum 'nucleation' temperature, i.e. that which produces ceramics with the smallest grain size, is in the region of the peak of the endotherm on the thermogram of the glass, (1.14), corresponding to a viscosity of 10^{11} to 10^{12} poise, and being some 20° to 50° above the annealing temperature of the glass, ($\eta \sim 10^{13}$). Studies of the physical properties of glasses, e.g. density and coefficient of expansion, have certainly shown that structural changes have occurred as a result of pre-crystallization heat treatments (1.15).

Other workers however have not observed any significant differences between ceramics produced with and without a 'nucleation' stage (1.9,1.16,1.17). They argue that the structural changes take place during the cooling of the melt and the re-heating of the glass when it is crystallized. Clearly it is the rate at which the structural changes take place which determines whether or not the 'nucleation' treatment is necessary, and this of course is dependent upon the particular glass system and its concentration of added 'nucleant'.

A general feature of all work in which a 'nucleation' stage was observed to influence the final ceramic, is that those ceramics crystallized at lower temperatures had a rather greater dependence upon the 'nucleation' treatments than the same specimens crystallized at higher temperature (1.14).

1.5 $MgO - Al_2O_3 - SiO_2$ Glass Ceramics

Glass ceramics based on Cordierite, ($2MgO.2Al_2O_3.5SiO_2$), are highly refractory and have an excellent resistance to thermal shock (1.2,1.18,1.19). It is however the excellent dielectric characteristics of this system at both high temperatures and frequencies which has led to most of the commercial applications of this ceramic. For example, Corning code 9606, a Cordierite based ceramic, is used in both vacuum tubes and Radomes, where for the latter application, the ability of this system to produce a high tolerance, refractory, shock resistant, homogeneous and microwave transparent material, has no counterpart in conventional ceramic technology (1.2).

Without added TiO_2, Cordierite glasses do not produce mechanically strong and fine grained ceramics, i.e. the observed phase separation within many glasses of the Cordierite composition (1.9) is not of itself sufficient to produce useful glass-ceramics. Consequently, such materials as Corning 9606 incorporate approximate 10 wt.% of TiO_2.

1.6 Aims of the work

The broad aim of this work was to understand the role of TiO_2 in the production of ceramics from a $MgO-Al_2O_3-SiO_2$ glass system. Specifically, we have attempted to answer the following questions:-

1. What is the nature of the titanium complexes in the glass, and do they vary with TiO_2 content?

2. Are the titanium complexes changed by pre-crystallization heat treatments?

3. What is the nature of the general glass structure, particularly the silicate network, and what effect does the addition of TiO_2 have upon this network?

4. What changes of the glass structure take place during the pre-crystallization heat treatments?

In this work we have studied questions 1 and 2 by observing, using electron spin resonance (e.s.r.) techniques, the point symmetry of the Ti ion in glasses of varying composition, (i.e. with TiO_2 contents ranging from 0% to 10%), and after a variety of 'nucleation' heat treatments. Most of the titanium in the glasses 'as melted' is in the non-paramagnetic 4+ oxidation state, and consequently it was necessary to radiochemically reduce a small proportion of these ions to the paramagnetic 3+ state in order to sensitise the ions for e.s.r. measurements. In the process of γ-irradiation, other 'defect centres' were generated, and, although initially considered unhelpful, these paramagnetic centres proved to be valuable in the study of questions 3 and 4. The e.s.r. measurements and their analysis are described in Chapter 4.

Principally as an adjunct to the e.s.r. measurements, the optical absorption spectra of the irradiation produced 'defects' were recorded and the results are presented in Chapter 5.

It was realised that 'point defect' measurements of the type just described, had a limited application to questions 3 and 4, i.e. upon the understanding of changes in the glass structure as a whole. Consequently,

Infra Red Absorption and Raman Scattering measurements were recorded for all of the glass specimens, and these results are described in Chapter 6.

In order to relate the structural information gained by the e.s.r., optical, and vibrational measurements, to the nature of the resultant ceramics, i.e. their crystal size, type and morphology, the ceramics from all of the melt compositions, with and without pre-crystallization heat treatments, were characterised by microscopic and X-ray diffraction measurements. These results are presented first in this thesis, in Chapter 3, immediately following the detailed exposition of the experimental techniques in Chapter 2.

Finally, Chapter 7 summarised the principal results from the preceding sections, considers their interrelationships, and draws the conclusions from this work.

REFERENCES

CHAPTER 1

1.1 E A Porai - Koshits in 'Structure of Glass' V5 Ed. E A Porai - Koshits Consultants Bureau 1965

1.2 P W McMillan, 'Glass Ceramics' Academic Press 1964

1.3 H Rawson, 'Inorganic Glass-Forming Systems' Academic Press 1967

1.4 S D Stookey and R D Maurer in 'Prog. in Ceram. Sci.' V2 pp.77-101 Pergamon 1962

1.5 S D Stookey, U S Patent No.2, 515, 941 1950

1.6 S D Stookey and R D Maurer, 'Catallysed Crystallization of Glass - Theory and Practise' in Prog. in Ceram. Sci. V2 Pergamon 1961

1.7 S M Ohlberg et al, 'Crystal Nucleation by Glass in Glass Separation' Nucleation and Cryst. Symp. Ohio 1962 p.55

1.8 W Weyl in 'Coloured Glasses' Pub. by Soc. Glass Technol. Sheffield 1951

1.9 N M Pavlushkin et al, Sci. Tech. Comm. 2 (1971) 1051-67 9th Int. Cong. Glass

1.10 J I Barry et al J Mat. Sci. 4 (1969) 596

1.11 T I Barry et al J Mat. Sci. 5 (1970) 117

1.12 N M Pavlushkin et al, Inorg. Mater. Consult. Bur. Transl. 4(4), (1968) 554-6

1.13 R C De Vekey et al, Proc. Brit. Ceram. Soc. 25 (1975) 1-11

1.14 I Kitaigorodskii et al, Izv. Acad. Nauk. S.S.S.R. Neorgan Mater. 1(5) (1965) 729-33

1.15 I Kita et al in 'Structure of Glass' V5 Ed. E A Porai-Koshits Pub. Consultants Bureau pp.27-33

1.16 M I Kalinin et al in 'Structure of Glass' V5 pp.175-176 Ed. E A Porai-Koshits Pub. Consultants Bureau

1.17 R C de Vekey et al, Phys. Chem. of Glass 16(2) (1975) 31-43

1.18 R C de Vekey, Glass Technol. 14(5) (1973) 125-34

1.19 A G Gregory and T J Veasey, J. Mat. Sci. 6 (1971) 1312-1321

CHAPTER 2

EXPERIMENTAL METHODS AND TECHNIQUES

The experimental programme is here sub-divided into three broad areas of work:

(a) Glass and glass-ceramic production

(b) The characterization of the ceramics resulting from the various melt compositions and heat treatments

(c) The investigation of the glass structure at the atomic/molecular level

We deal with each area in turn.

2.1 Glass and ceramic production

2.1.1 Melt compositions

Glass batches were prepared from fine powders of SiO_2, Al_2O_3, MgO and TiO_2, which, after weighing, were homogenized by prolonged mechanical agitation of the containing capsule. The base glass components, i.e. SiO_2, Al_2O_3 and MgO were all of 4N purity, the 100 p.p.m. of impurities being largely refractory oxides similar to the melt components. Total iron group impurities were less than 10 p.p.m. and the single most abundant paramagnetic species, iron, was present in quantities of less than 5 p.p.m. The TiO_2 which was added to the base glass was of 'specpure' quality with less than 1 p.p.m. of any individual paramagnetic impurity.

In all, five glass compositions were founded, four containing TiO_2, and a base glass without added titania. The melt compositions are given in Table 2.1.

Attempts to found the Stoichiometric Cordierite composition - $5SiO_2.2Al_2O_3.2MgO$ - were only partly successful. The high viscosity of

Table 2.1: Composition of Glasses

Melt Number	Melt Classification	Wt.% of constituents			
		SiO_2	Al_2O_3	MgO	TiO_2
Melt 1	Base Glass (B.G.)	60	20	20	0
Melt 2	B.G. + 0.2% TiO_2	59.88	19.96	19.96	0.20
Melt 3	B.G. + 1% TiO_2	59.41	19.80	19.80	0.99
Melt 4	B.G. + 5% TiO_2	57.14	19.05	19.05	4.76
Melt 5	B.G. + 10% TiO_2	54.55	18.18	18.18	9.09

Melt Number	Mol.% of constituents			
	SiO_2	Al_2O_3	MgO	TiO_2
Melt 1	59.05	11.60	29.35	0
Melt 2	58.96	11.59	29.30	0.15
Melt 3	58.62	11.51	29.13	0.74
Melt 4	56.94	11.19	28.30	3.57
Melt 5	54.99	10.80	27.32	6.89

the melt at the founding temperature, precluded the moulding of specimens with the form required for measurements to be described later. Cutting or grinding of large 'blocks' of the melt was not possible due to the internal stresses 'quenched in' on cooling, and annealing of the specimens was not possible in this work. Thus the choice of base glass composition at 60 : 20 : 20 weight % of SiO_2 : Al_2O_3 : MgO was largely pragmatic, this composition lying close to the ternary eutectic of the system at 61.4 : 18.3 : 20.3 wt.% of the above components. An abbreviated ternary phase diagram of the SiO_2 - Al_2O_3 - MgO system is shown in Figure 2.1.[2.1] The chosen base glass, (melt 1), is seen to lie in the primary phase field of Cordierite.

2.1.2 Melting procedure

Melt batches of approximately 100 gms were founded in a Pt - 10% Rh crucible within a furnace capable of extended operation at 1600°C. The furnace was heated by 'Crystolon' (Morganite Electroheat Ltd.) silicon carbide hot rods, and temperature controlled by Pt - Pt 10% Rh thermocouples operating a Eurotherm type 070 controller. Batches were entered at a furnace temperature of 1000°C, which over a period of ∿ 10 hrs. was raised to the melting temperature of 1600°C. After 40 hrs. at 1600°C the melts were poured into pre-heated moulds (at 450°C to prevent the glasses from shattering), all of which were coated with an aqueous carbon suspension to prevent the glasses 'wetting' the surfaces. The moulds and glasses were then allowed to cool slowly in air. This melting schedule is shown diagrammatically in Figure 2.2.

The glasses from the above procedure were markedly inhomogeneous, i.e. striae and colour variations were clearly visible to the naked eye. Analysis by atomic absorption spectroscopy showed that the titania content of the melt 4 glasses varied from 3 to 7 wt.%, and at these extremes, the

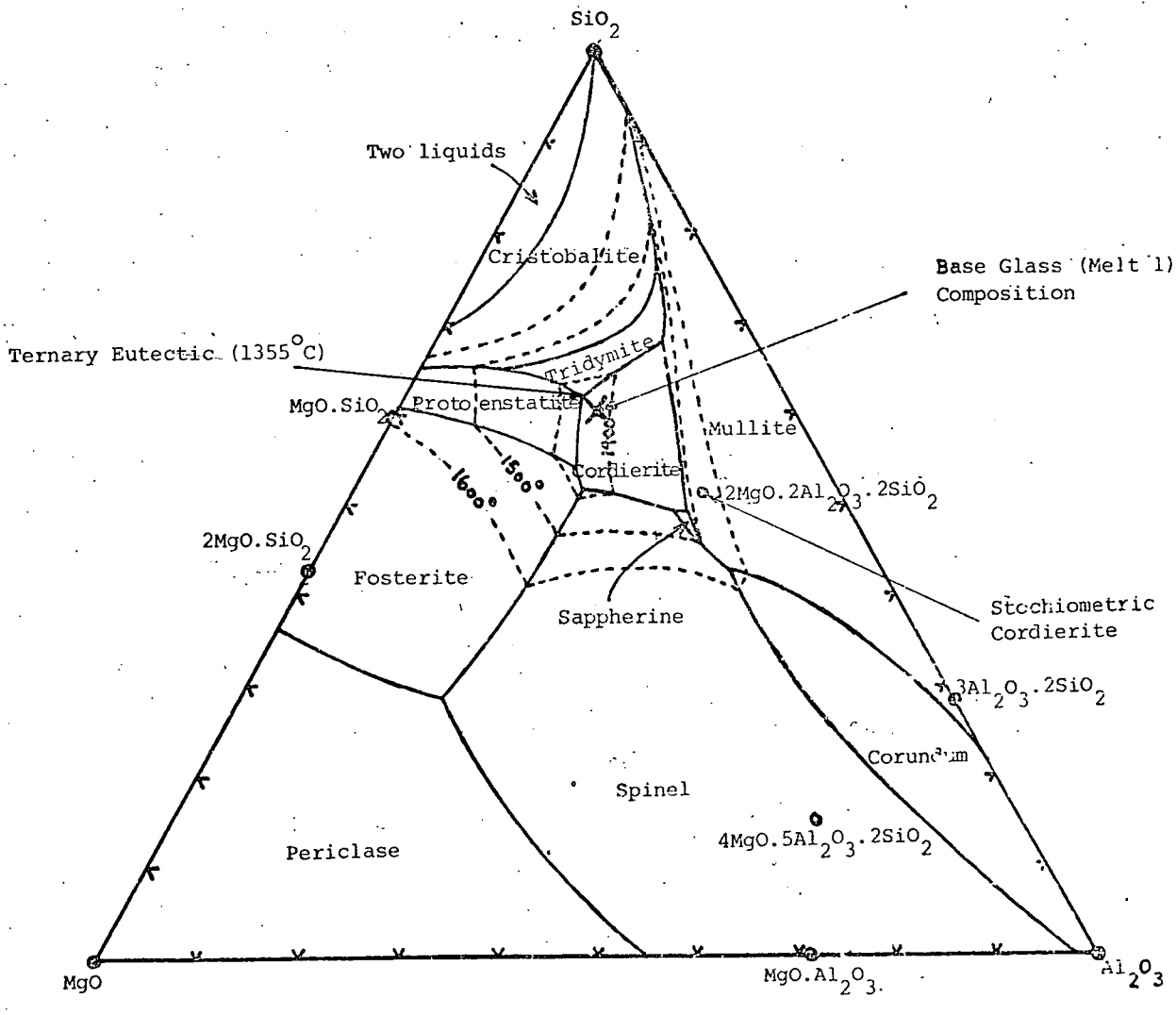

Figure 2.1: THE MgO - Al_2O_3 - SiO_2 SYSTEM

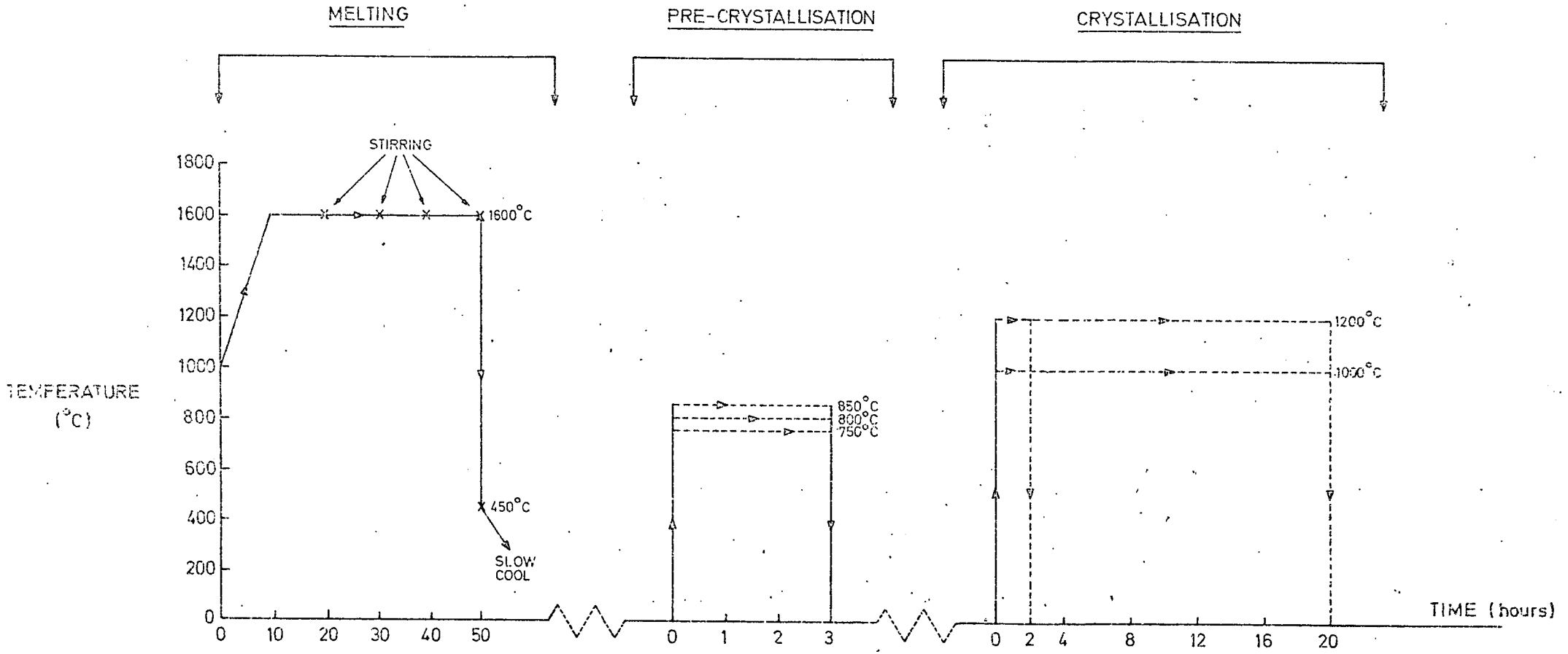

FIG. 2.2. THE MELTING, PRE-CRYSTALLISATION, AND CRYSTALLISATION, HEATING SCHEDULES

properties of the resulting ceramic were found to vary considerably. This effect was thought to be due to the fractionating of the melt in the crucible into layers of varying composition, and homogenizing methods were considered. Multiple crushing and re-melting, oscillation of the crucible, and pouring from crucible to crucible,[2.2] were all either impractical or ineffective, and ultimately a Pt - 10% Rh stirrer was built into the furnace. The stirrer was connected by an alumina rod and a flexible coupling to a low speed electric motor outside of the furnace. At ∿ 10 hour intervals the stirrer was lowered into the melt and the melt stirred for approximately one hour, the final stir being immediately prior to pouring. This was important as striae again occurred if the melt was allowed to stand for more than one hour after the final stir. This procedure produced seed-free and homogeneous glasses. Homogeneity was confirmed by test specimens, which after careful annealing, showed only slight birefringence due to residual stresses when viewed in a 'strain' viewer, there being no indication of composition induced birefringence.

2.1.3 Pre-crystallization, (Nucleation), Heat Treatments

Discussion in the previous chapter has indicated that in most systems the optimum nucleation temperature for glass-ceramic production is in the region between the annealing temperature and 50°C above this temperature. At the onset of annealing, i.e. when the residual stresses are being released, there is an endothermic reaction and differential thermal analysis (D.T.A.) measurements were carried out at the Ceramic Department of Leeds University on a specimen of melt 3, indicated an annealing temperature of 790°C - 800°C. Thus all glass specimens were individually 'nucleated' at either 750°C, 800°C, or 850°C for periods of three hours, see Figure 2.2, within a muffle furnace with a low temperature gradients zone, (< 1°C/cm). Combined with temperature control by a series 010

digital Eurotherm controller, pre-crystallization temperatures were thus accurate and reproducible to within $\pm 2^{\circ}C$. Glass specimens were entered directly into the furnace, achieving the required temperature in under two minutes, and, after three hours, removed to air cool.

2.1.4 Crystallization heat treatments

The conversion of the glass specimens to glass-ceramics was performed in the muffle furnace discussed previously by heat treatments at $1000^{\circ}C$ or $1200^{\circ}C$ for either two or twenty hours, see Figure 2.2.

Thus a series of specimens of varying composition, varying pre-crystallization heat treatments and varying crystallization temperatures and times, were prepared for the investigations to follow.

2.2 Characterization Studies of the Ceramics

In order to characterize the nature of the ceramics which resulted from the various compositions and heat treatments, four main investigative methods were employed. We consider each in turn.

2.2.1 X-Ray Diffraction

The crystalline phases present in each ceramic were established by X-Ray Diffraction. Specimens of the ceramic were ground to 10 μm and smear mounted on to glass slides. Diffractometer traces were obtained from the flat bed recorder of a Phillips PW 1130 diffractometer operating with a C_o target and Fe filter. A small quantity (5%) of BPO_4 (A.S.T.M. index 14-696), was mixed with each of the ceramic powders as a 2θ calibration.

Some specimens were quantitatively phase analysed, and the necessary degree of mixing of the standards and the ceramics was achieved by prolonged mechanical oscillation of the specimen containers.

2.2.2 Optical Microscopy

The size and morphology of the crystals within the polycrystalline ceramics were investigated with the Polarizing Microscope, (Carl Zeiss ULTRAPHOT). 'Thin sections', ($\sim$ 30 μm thick), of the ceramics were prepared by grinding and polishing, following standard mineralogical techniques.

Crystals with non-cubic symmetry are optically anisotropic, and when a 'thin section' is viewed between crossed polars in transmitted light, the birefringence of the randomly orientated crystallites causes interference effects which results in the different crystallites appearing with different degrees of brightness (or 'relief'), ranging from complete extinction to a maximum brightness which in white light may be a greyish white or a colour, depending upon the size and birefringence of the crystals. Rotating the microscope stage from a position of extinction for an individual crystallite causes that crystallite to increase in brightness, reaching a maximum at 45° of rotation, and returning to extinction after 90° of rotation. The glassy regions of the specimens, being optically isotropic, remained dark for all positions of the microscope stage. Photographs of the thin sections in transmitted light were taken (photomicrographs), and the crystal sizes were determined by calibrating each of the microscope objectives using ruled gratings.

2.2.3 Scanning Electron Microscopy

The fracture surfaces, and in some instances the etched surfaces, of the ceramic (or partly ceramic) specimens, were studied using a Scanning Electron Microscope (S.E.M.). The surfaces to be examined were prepared either by fracturing the ceramic and observing the fractured surfaces directly, or by observing the surfaces after polishing to $\frac{1}{4}\mu$ Al_2O_3 and etching in 1% HF for 30 seconds. The S.E.M. was operated in the Secondary Emission Mode and to prevent electrostatic charging of the specimen surfaces

and the resultant loss of resolution, the specimens were mounted by electrically conducting cement to the microscope stages, and thin films of gold evaporated on to the surfaces to be examined. To ensure uniform coating, the specimens were continuously rotated during the deposition of the gold film.

2.2.4 Laue Back-reflection

X-ray back reflection photographs were taken of 2 mm diameter regions of the ceramic fracture surfaces using a Phillips PW 1009/80 X-ray set operating with a Cu target and a Ni filter.

2.3 Investigations of the Structural Natures of the Glasses

In this Section of the work, three spectroscopic techniques were employed. We consider each in turn.

2.3.1 Electron Spin Resonance (E.S.R.) Spectroscopy

In the early stages, the radiochemical reduction of the Ti^{4+} ion with its d^{o} electronic configuration to the paramagnetic 3+ state, (d^{1}), was done by x-irradiation from a commercial x-ray set, and the spin resonance measurements were made on an x-band e.s.r. spectrometer developed by R.A. Vasquez and described fully in a thesis by this author.[2.3] Although the glass specimens visible darkened, no room temperature e.s.r. spectra could be detected. The spectrometer was fitted with cryogenic facilities, (L.He), by the present author, using an Oxford Instruments type MD4A cryostat and remote cavity tuning using an iris coupling unit whose aperture was adjustable from outside of the cryostat. The rationale of this development was:-

(a) the increased sensitivity due to the more favourable Boltzmann distribution factor.

(b) the possibility of discriminating between linewidth effects due to spin-lattice relaxation, a temperature dependent mechanism, and those due to a distribution of the paramagnetic sites, which would be temperature independent.

The calculation of Appendix 1 shows that effect (a) could be expected to increase the absorption signal one hundred times at 4.2 K compared with its value at room temperature. Unfortunately, even at 4.2 K the x-irradiated glasses whilst just indicating a hole resonance, ($g > 2.0023$), gave no evidence of the electron resonance expected from Ti^{3+}. A room temperature sensitivity calibration of the spectrometer using a dilute sample of D.P.P.H. (Diphenylpicrylhydrazyl), a free radical with one free spin per molecule, ($\sim 1.5 \times 10^{21}$ spins/gm), showed that a 2:1 signal to noise ratio required 5×10^{16} spins of D.P.P.H. Assuming a first derivative pk-pk width of 80 gauss for the Ti^{3+} ion, then from formulae presented in reference (2.4), a requirement of 4×10^{19} spins of Ti^{3+} was calculated to be necessary for detection in this spectrometer. Later measurements showed that the quantity of radiochemically produced Ti^{3+} was 5×10^{17} spins/gm in all glass compositions. Sample masses of ~ 2 gms combined with the fact that in practise the increased sensitivity on cooling to 4.2 K was seldom better than 10 X, meant that in fact, the concentration of Ti^{3+} was always an order of magnitude too low for the broad glassy resonance lines to be detected by this instrument.

At this stage in the work, Dr. G Brown of the Royal Military College of Science at Shrivenham, kindly offered to make available the College's commcerial X-band spectrometer - a JEOL series J.E.S.-PE-1X. A block diagram of the spectrometer is shown in Figure 2.3. As a standard

FIG. 2.3.

BLOCK DIAGRAM OF THE JEOL PE-IX E.S.R. SPECTROMETER

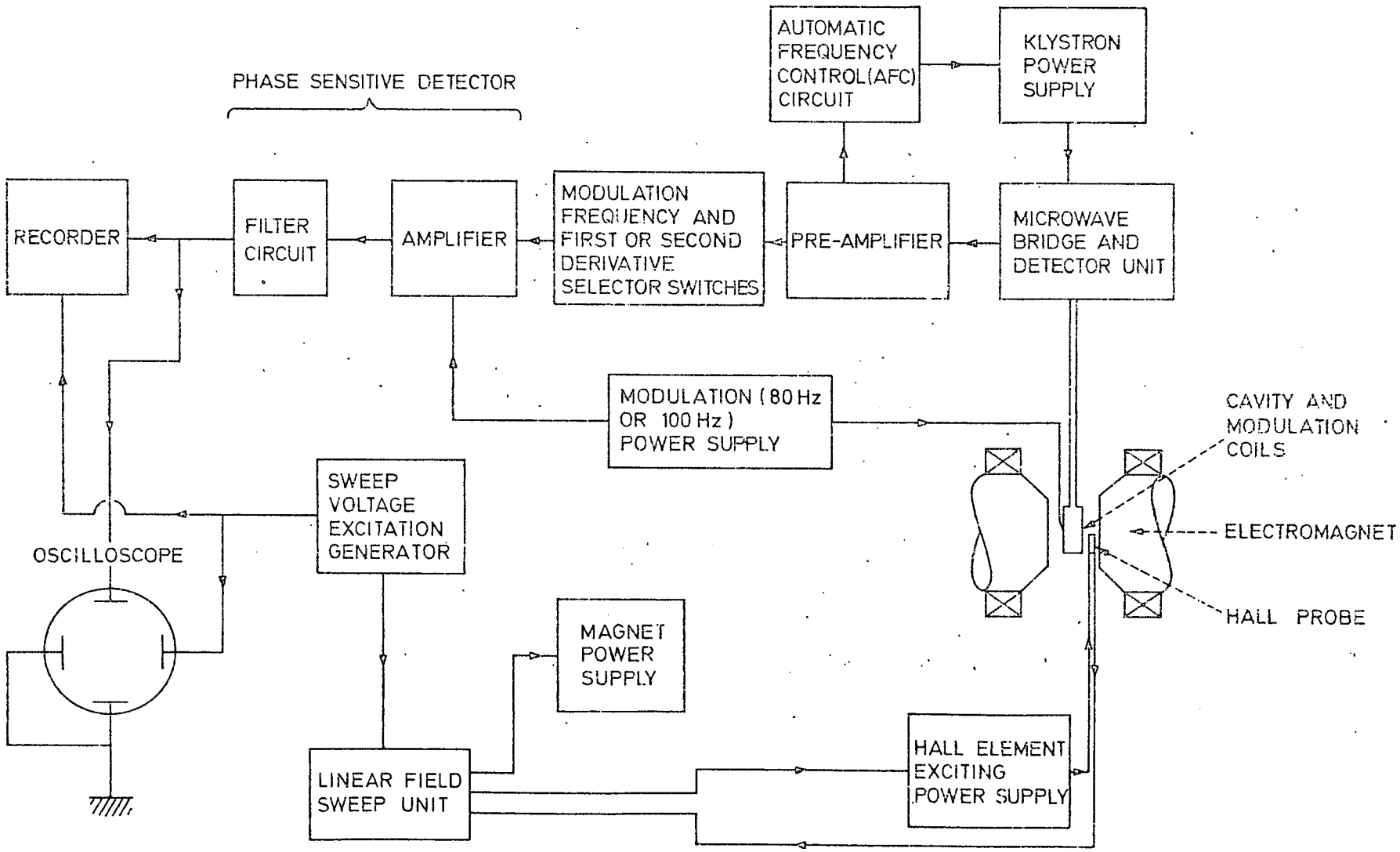

X-band reflection spectrometer operating at 9.4 GHz with a cylindrical cavity in the T.E.$_{011}$ mode, the principle of operation is fully accounted in standard texts, e.g. Ingram,[2.5] Poole[2.6] and Assenheim[2.7] and is not recounted here.

The most significant additional feature of this instrument compared with the one developed at Durham was the Automatic Frequency Control (A.F.C.) system, a feedback circuit which 'locks' the klystron frequency to the resonant frequency of the cavity, thus allowing a much higher Q cavity to be used. Combined with a hot carrier diode μ-wave detector and a tuned modulation/phase sensitive detection system, the sensitivity of the instrument was 5 x 10^{10} spins/gauss. Extrapolating to a line of 80 gauss the spin sensistivity was therefore 3 x 10^{14} spins and the 5 x 10^{17} spins/gm of Ti^{3+} gave strong, low noise e.s.r. signals at room temperature.

MgO crystals with a weak dilution of ^{55}Mn were supplied by the instrument manufacturer as 'g marker' standards. The S-state Mn^{2+} ion has electronic and nuclear spins of $^{5}/_{2}$. In the region of g = 2 therefore the 6-line hyperfine spectrum of the $|-\frac{1}{2}\rangle \rightarrow |+\frac{1}{2}\rangle$ spin transition, if calibrated, may be used to calculate the g values of the specimen lines by extrapolation or interpolation along the $^{1}/_{g}$ (linear field), axis. The standard is inserted into a special cavity location such that the H.F. lines appear antiphase to the specimen lines, and in the spectra following, the specimen and 'g marker' lines may be discriminated by their opposite phase. In this work the g values of the experimental spectra are accurate to ± 0.0005.

The intensities of the e.s.r. lines was calculated using a $CuSO_4 5H_2O$ single crystal standard. The S = ½ Cu^{2+} ion of the standard has a symmetrical hole resonance in the region of g ∿ 2.4. Each molecule of $CuSO_4 5H_2O$ contains one Cu^{2+} ion, i.e. one spin. Thus 1 gm of this standard contains 2.4 x 10^{21} spins. A comparison of the respective areas beneath

the absorption lines from the standard and the specimen, allows the number of spins contributing to the specimen absorption to be calculated from:

$$\text{No. of spins/gm of specimen} = \frac{\text{Area beneath specimen line}}{\text{Area beneath standard line}} \times \frac{\text{mass of standard}}{\text{mass of specimen}} \times \text{No. of spins/gm of standard}$$

The area beneath the absorption lines was found by double integration of the first derivative spectra using Simpson's Rule.

Finally concerning the spectrometer operation, we mention that by double modulation of the magnetic field, (at 80 Hz and 100 kHz), the instrument was capable of generating the second derivative of the absorption line, and with some specimens this facilities was used to resolve their spectra.

A $^{60}C_o$ source and a dose rate of 1.5 Mrad/hr were used to γ - irradiate the specimens to effect the radiochemical reduction of the titanium ion to the 3+ state. Doses of from 0.5 Mrad to 300 Mrad were tried and in all cases two e.s.r. centres emerged, an electron centre and a hole centre. The weaker electron centre, (later identified with the Ti^{3+} ion), saturated at between 1 Mrad and 5 Mrad, and thereafter, for all specimens, doses were standardized to 1 Mrad.

The analysis of the spectra from the glasses and glass-ceramics was performed principally by computer simulation of the first derivative spectra. The theory and practise of this technique is described in the next chapter.

2.3.2 Optical absorption spectroscopy

The absorption spectra of the glass specimens in the region 200 nm → 1000 nm were measured with an 'Optika' type CF4 double beam

spectrophotometer. In a selection of samples the wavelength range was extended to 2000 nm using a Grubb Parsons 'Spectromaster.' Each glass composition was examined as produced, after pre-crystallization heat treatment, and after γ-irradiation.

This section of the work necessitated the production of thin, (< 3 mm), glass prisms, because of the high linear absorption coefficient of the irradiated glasses. The high viscosity of the melts even at 1600^{o}C required a vacuum injection technique. The melts were poured directly into a mould containing many 12 mm x 3 mm rectangular channels. Each channel was continuously evacuated by a rotary pump, and on pouring, the vacuum created caused the glass to be forced some 1 cm to 2 cms down the channels before it solidified. The mould was dismantled and individual specimens polished on each broad face to ¼ μAl_2O_3, leaving the final optical path length as approximately 2.5 mm.

To take account of the multiple reflections at the interfaces, in the calculation of the absorption coefficient, (α), the Refractive Indices of the different melts were measured, (to within 1% at Sodium D - 589.3 nm), using an Abbe refractometer.

The γ-ray induced optical absorption, i.e. the difference between the absorption coefficients before and after irradiation, was calculated and plotted. The resulting curves were analysed into their Gaussian component bands using a Hewlett-Packard curve resolver.

2.3.3 Vibrational Spectroscopy

Infra-red absorption and Raman scattering measurements were made upon all of the glass specimens and a limited number of ceramic specimens.

(a) I.R. absorption

The glasses and ceramics were finely ground and prepared as KBr discs

by a standard die pressing technique. Room temperature absorption spectra between 2.5 μm and 40 μm, (4000 cm^{-1} → 250 cm^{-1}), were measured on a Perkin-Elmer model 475 double beam spectrometer.

(b) Raman Scattering

A Varian-Carey model 82 Raman spectrometer, in conjunction with a Spectra Physics model 164 Argon-Iron laser operating at 514.5 nm, were used to record Raman spectra from the as-produced and pre-crystallization heat treated glasses. For these measurements rectangular glass blocks were founded and two 'ends' and one 'face' polished to ¼ μAl_2O_3 leaving final specimen dimensions of 8 mm x 7 mm x 6 mm (see diagram below). The exciting laser beam was directed through the specimen between the polished ends and a multiple pass arrangement used to intensify the scattered signal. The radiation was incident along the x-axis and polarized in the z-direction. The scattered radiation was collected along the y-axis, i.e. at 90° to the incident beam, the scattered intensity being the sum of radiation polarized in the z and x directions. All spectra were recorded at room temperature with a bandwidth of 10 cm^{-1}.

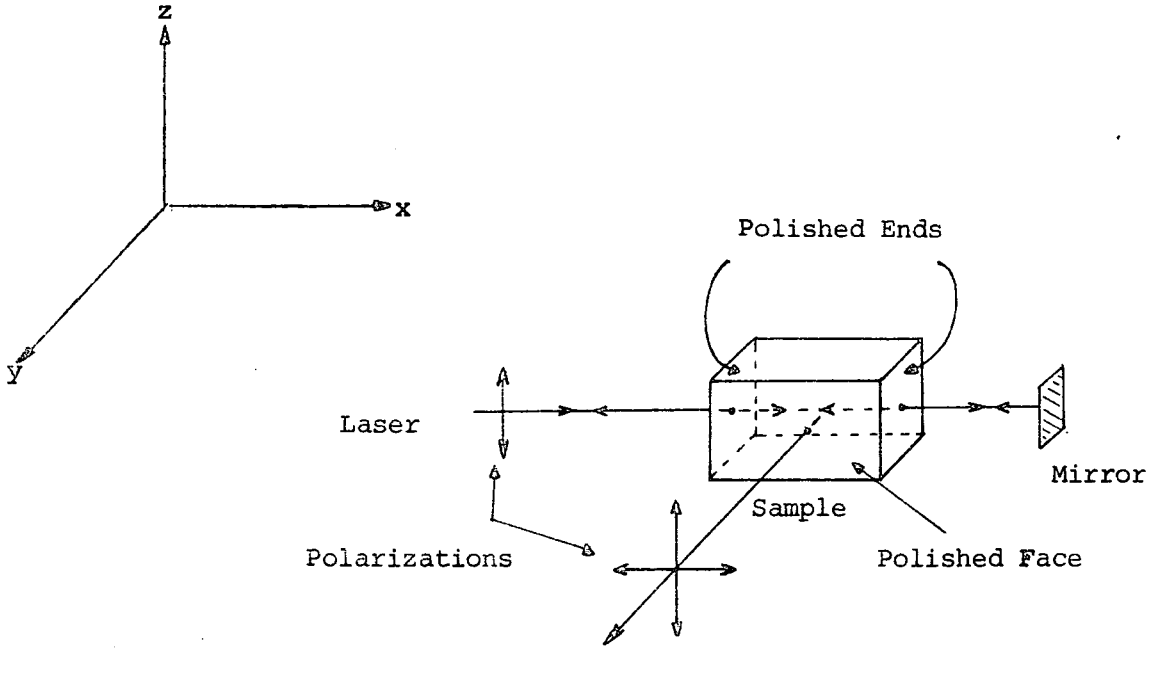

REFERENCES

CHAPTER 2

2.1 E M Levin et al, 'Phase diagrams for ceramicists' American Ceramic Soc. 1969, p.246

2.2 J F Stirling and R G Miselbach, Glass Technol. V.9 No.6 1968, pp.176-178

2.3 R A Vasquez, M.Sc. Thesis, University of Durham (1975)

2.4 P B Ayscough, 'E.S.R. in Chemistry' Methuen 1967, p.165

2.5 D E Ingram, 'Spectroscopy at Radio and Microwave Frequencies' Butterworths 1955

2.6 C P Poole, 'Electron Spin Resonance,' Publisher John Wiley and Sons 1967.

2.7 H M Assenheim, 'Introduction to Electron Spin Resonance,' Pub. Hilger and Watts

CHAPTER 3

CHARACTERISATION STUDIES OF THE GLASS-CERAMICS

The work which this Chapter reports characterises the nature of the ceramics formed from the different melt compositions. The crystalline phases present in each ceramic were established from x-ray diffractometer spectra and the morphology and size of the ceramic crystals was determined by a combination of polarising microscope, scanning electron microscope and x-ray back reflection techniques.

3.1 X-Ray Diffractometer Results

3.1.1 Melts (1), (2) and (3) (the low titania ceramics)

Results described later in the Chapter show that specimens from these melts are, after crystallization for two hours at 1000°C, only partly crystalline, i.e. there is surface crystalization only. Consequently the crystal phases present in the ceramics formed from the above compositions were studied only after twenty hour treatments at 1000°C.

Figure 3.1 shows the x-ray diffraction spectra from glass melt (1) subjected to a variety of pre-crystallization heat treatments followed by crystallization at 1000°C. The spectra are essentially the same, the principal difference being the elimination (on the bottom trace) of the line marked Q. The analysis of these spectra is therefore typified in Figure 3.2 where the fifteen most intense lines (neglecting Q) are labelled, and compared with the A.S.T.M. data for high cordierite (Card No. 13-293). The principal phase is clearly high cordierite (lines 1 to 15), the unaccounted lines being those marked D, E and Q. The line Q is the 100% line of β-quartz, but, at present, the identification of the lines D and E, which are certainly not associated with either the high cordierite nor the

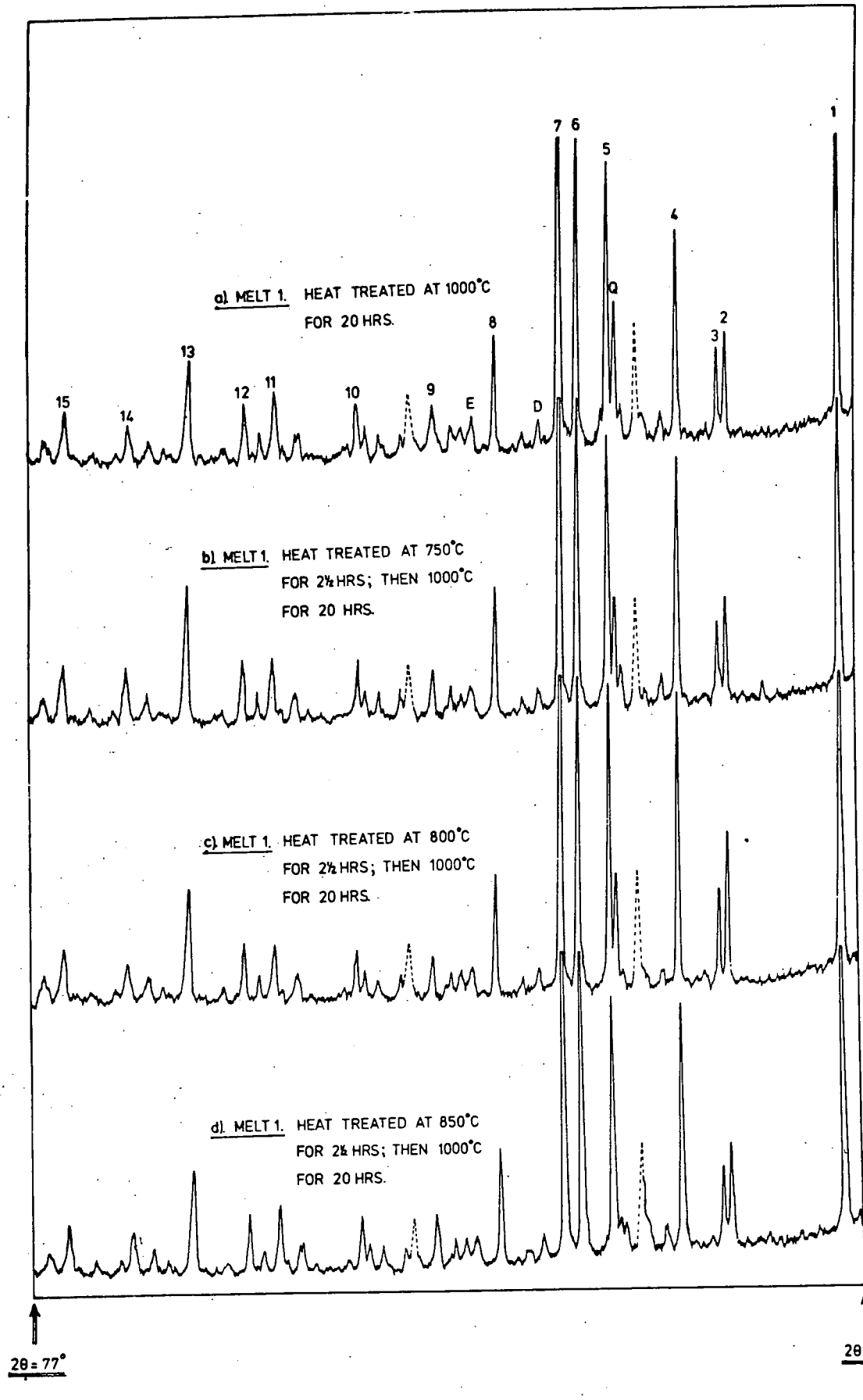

FIG. 3.1. X-RAY DIFFRACTOMETER SPECTRA; 2θ FROM 11° to 77°; CoKα RADIATION.
(DOTTED PEAKS ARE BPO_4 REFERENCE MARKERS)

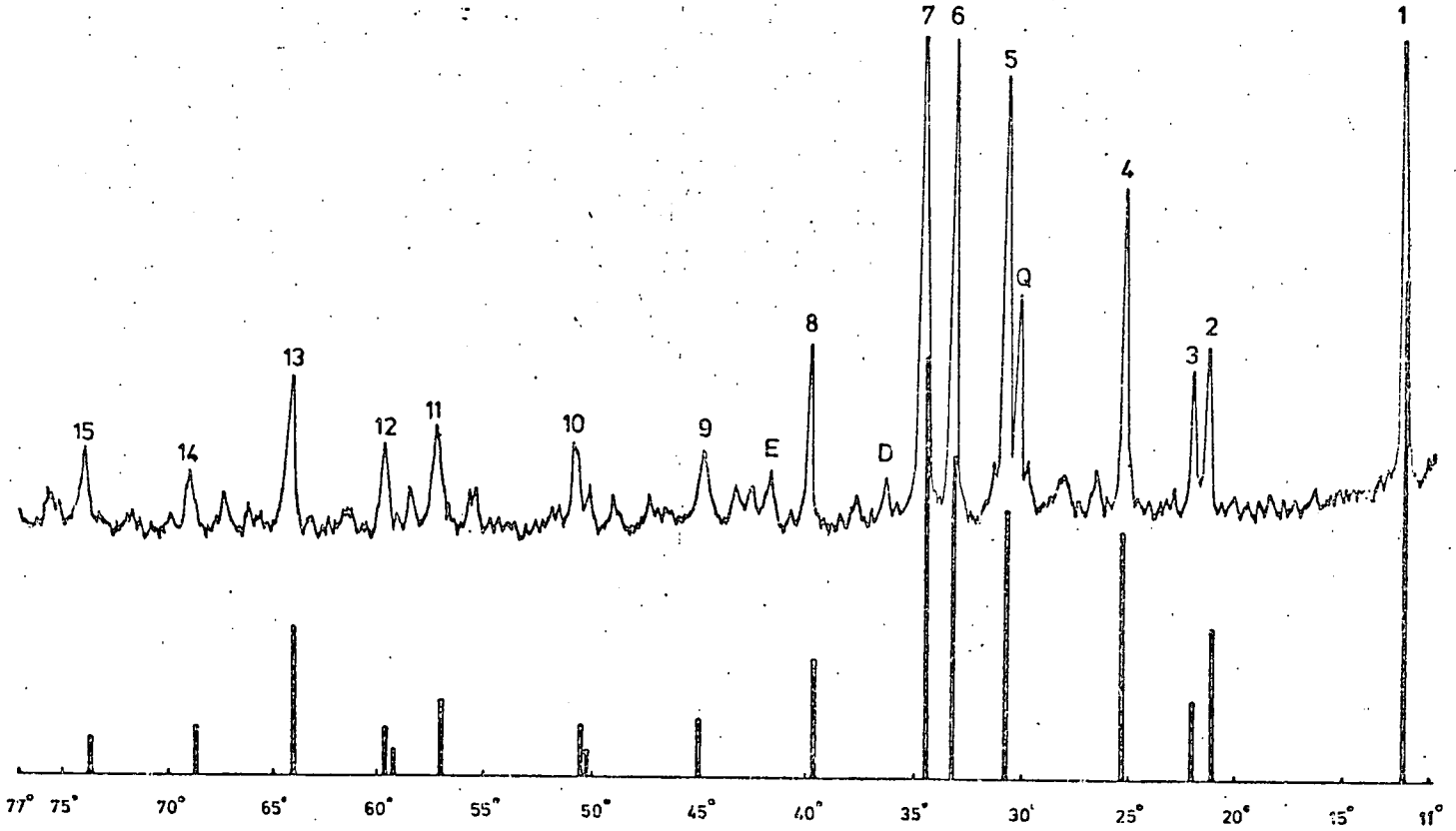

FIG. 3.2. COMPARISON OF DIFFRACTOMETER SPECTRA OF MELT 1 [FIG. 1 trace a)] WITH A.S.T.M. DATA FOR CORDIERITE ($Mg_2Al_4Si_5O_{18}$). [2θ FROM 11° TO 77.° Co.Kα RAD.^{N}]

β-quartz, has not been attempted. Table 3.1a quantifies the results shown in Figure 3.1 and analysed in Figure 3.2.

The spectra from glass (1) crystallized at 1200°C are almost identical to the 1000°C spectra, the differences being the absence of a β-quartz line and the intensification of the lines marked D and E. The experimental spectra are shown in Figure 3.3 and their analysis presented in Figure 3.4, where it is clear that again high cordierite is the principal phase. The lattice parameters of the 1200°C ceramics are identical to those of the 1000°C ceramics and a separate table is not presented. Extending the crystallization period to twenty hours leaves the diffraction spectrum unchanged (see Figure 3.5 traces (a) and (d)).

The crystallized specimens of glasses (2) and (3) have diffraction spectra again dominated by the set of high cordierite lines (1 to 15). This is shown in Figures 3.5 and 3.6. As with glass (1), only the 1000°C spectra show the β-quartz line, which is in turn reduced by increasing the pre-crystallization heat treatment temperature. In addition the lines D and E are again present and perhaps rather more intense on those specimens crystallized at 1200°C. A new line U, not present on the glass (1) spectra is present in the spectra of glasses (2) and (3) crystallized at 1000°C.

The foregoing results may be summarised as follows. Essentially the low titania glasses (glasses (1) (2) and (3)), crystallize out into high cordierite at both 1000°C and 1200°C. The addition of titania in the glass (2) and (3) compositions is not observed to significantly affect the lattice parameters of the cordierite or the intensity ratios of the diffraction lines. Some β-quartz is present in the specimens crystallized at 1000°C, and indeed, the only discernable effect of the pre-crystallization heat treatments is to reduce, and eventually eliminate this phase. The lines as yet not accounted for are those marked D, E and U.

Experimental Data			A.S.T.M. Data	
Peak Identification	Intensity (%) (I)	Parameter ($\times 10^{-10}$ m) (d)	Cordierite* (I)	Lines (d)
1	85	8.36	100	8.48
2	25	4.84	30	4.89
3	20	4.68	16	4.68
4	50	4.09	50	4.09
Q	35	3.42		
5	70	3.36	55	3.38
6	75	3.12	65	3.14
7	100	3.00	85	3.03
D	8	2.87		
8	30	2.62	25	2.64
E	80	2.51		
9	15	2.34	12	2.34
10	15	2.08	12	2.10
11	20	1.867	16	1.875
12	15	1.798	10	1.800
13	25	1.684	30	1.688
14	10	1.580	10	1.589
15	15	1.487	8	1.494

* Card No. 13-293

Table 3.1: The lattice parameters of Melt (1) crystallized at 1000°C. (Intensity figures from Figure 3.2).

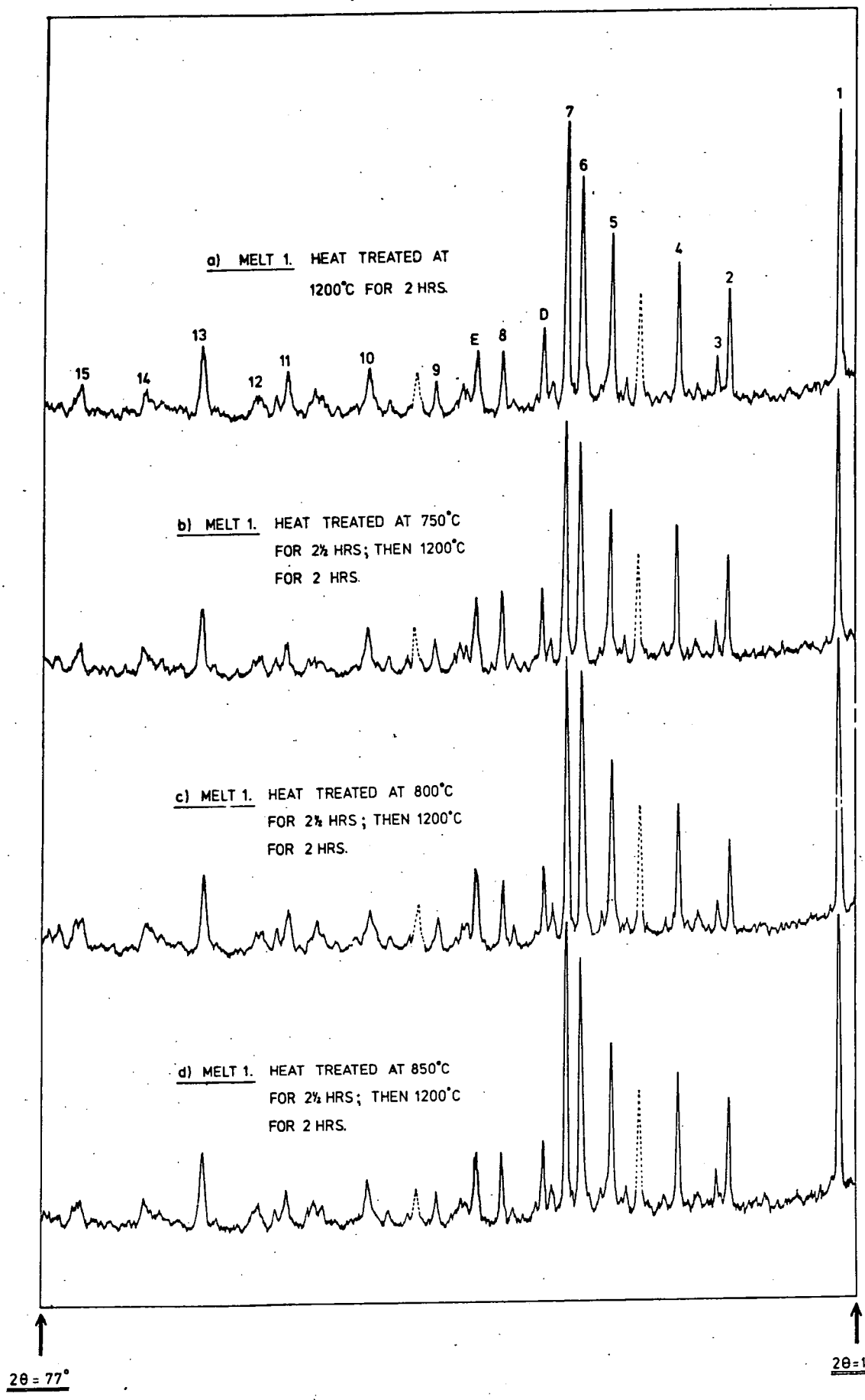

FIG. 3.3. X-RAY DIFFRACTOMETER SPECTRA; 2θ FROM 11° to 77°; CoKα RADIATION.
(DOTTED PEAKS ARE BPO_4 REFERENCE MARKERS)

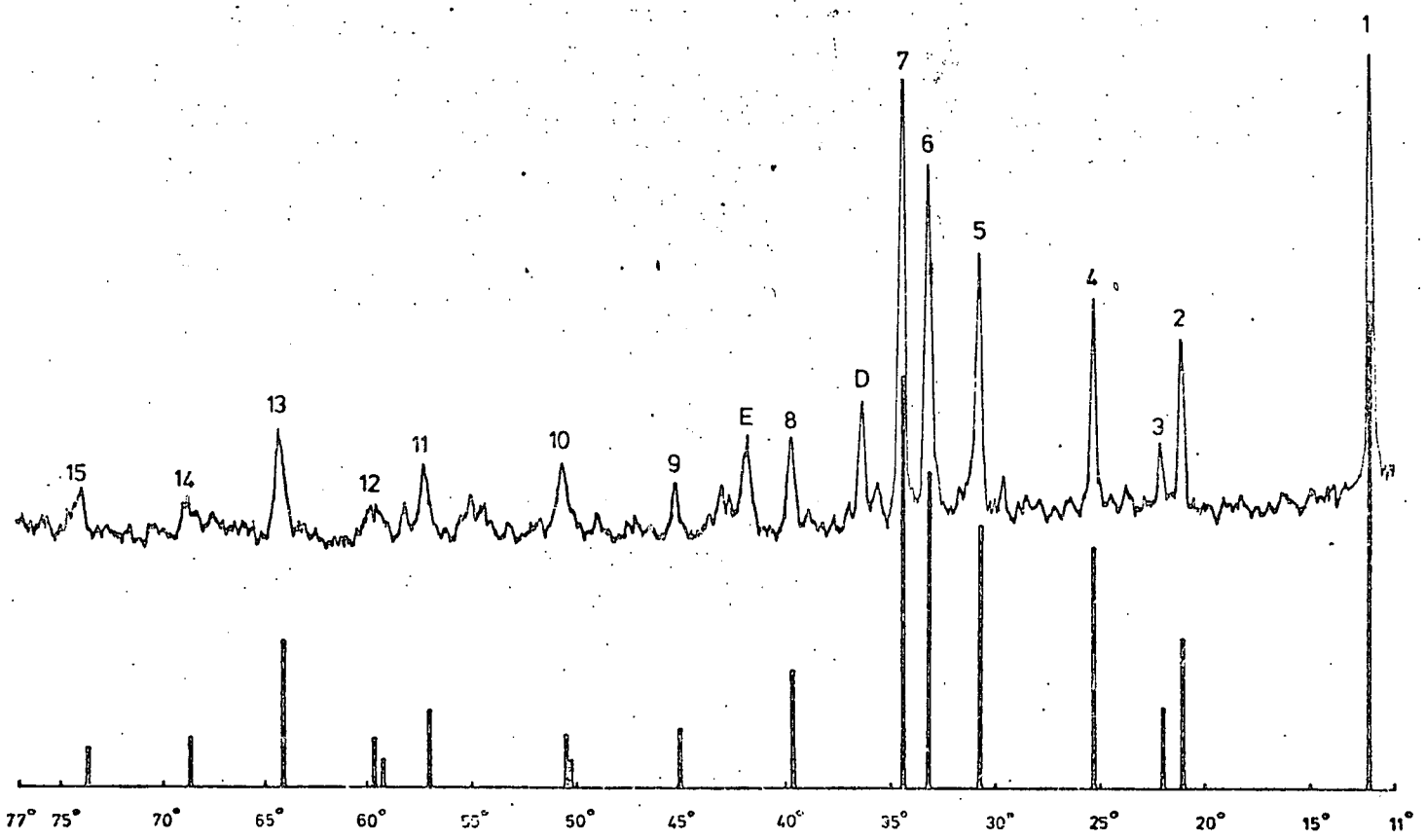

FIG.3.4. COMPARISON OF DIFFRACTOMETER SPECTRA OF MELT 1 [FIG. 3 trace a)] WITH A.S.T.M. DATA FOR CORDIERITE ($Mg_2Al_4Si_5O_{18}$). [2θ FROM 11° TO 77°. Co.Kα RAD^{N}.]

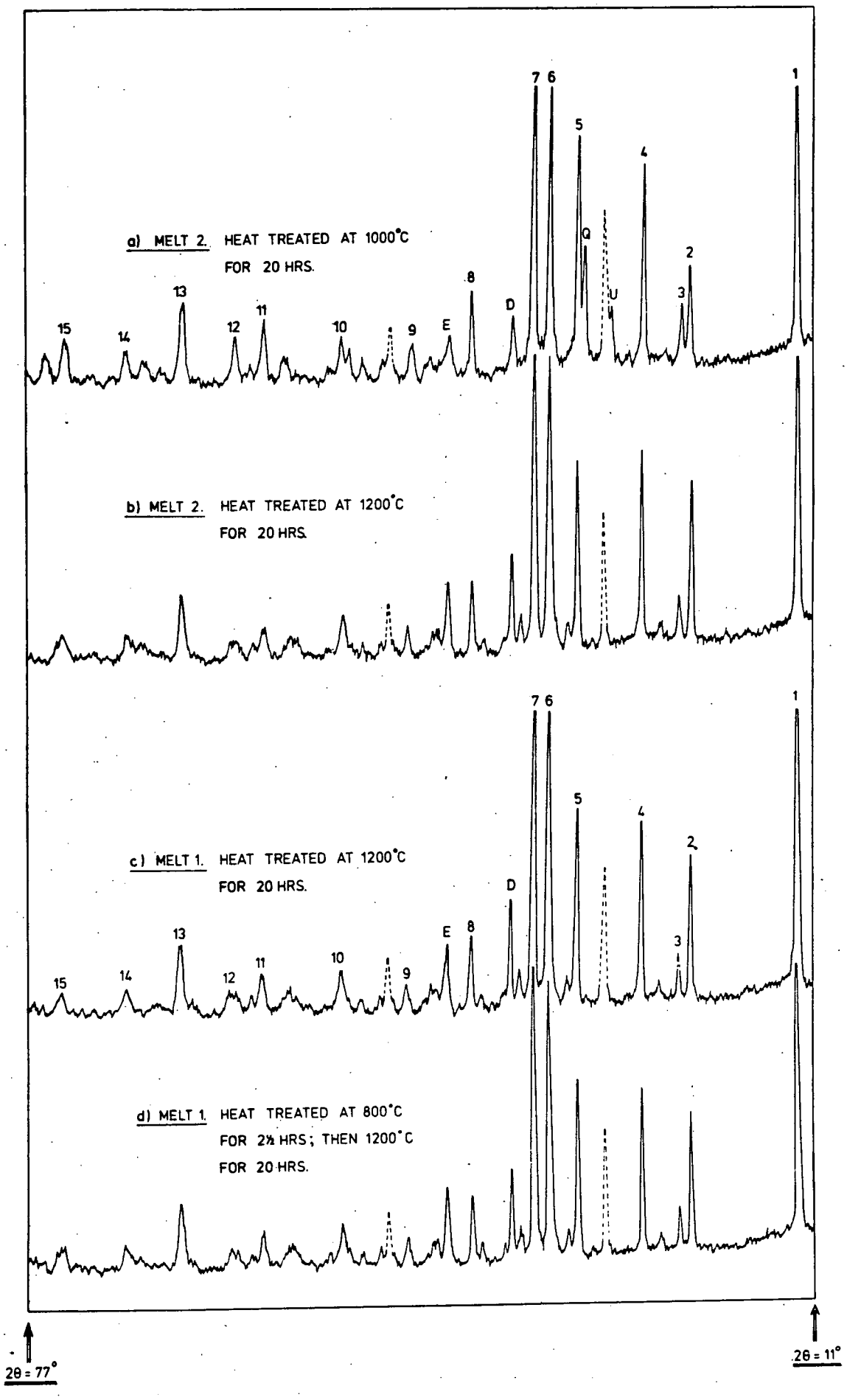

FIG. 3.5. X-RAY DIFFRACTOMETER SPECTRA; 2θ FROM 11° to 77°; CoKα RADIATION.
(DOTTED PEAKS ARE BPO_4 REFERENCE MARKERS)

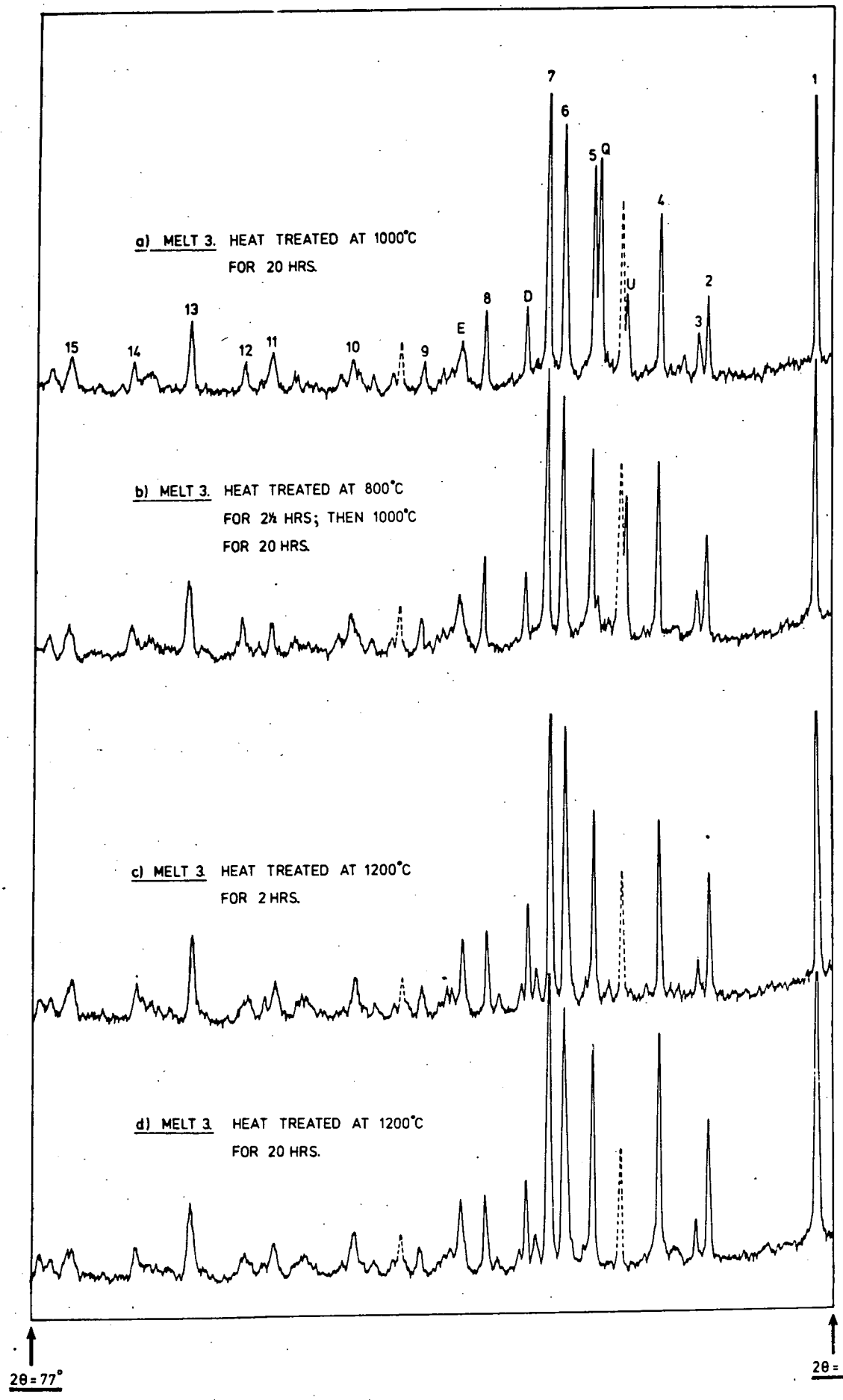

FIG. 3.6. X-RAY DIFFRACTOMETER SPECTRA; 2θ FROM 11° to 77°; CoKα RADIATION.
(DOTTED PEAKS ARE BPO_4 REFERENCE MARKERS)

3.1.2 Melts (4) and (5), (the high titania ceramics), crystallized at 1000°C

The diffraction spectra from melts (4) and (5) crystallized at 1000°C with and without pre-crystallization heat treatments are shown in Figures 3.7 and 3.8. In both compositions the spectrum is dominated by the set of lines marked A to J and the β-quartz line Q. The 2θ positions of the set A → J (and the associated lattice parameters) remain unchanged with both composition, pre-crystallization heat treatments and crystallization period. The pre-crystallization treatments are effective in reducing the β-quartz line.

Figure 3.9 compares a typical trace from Figures 3.7 and 3.8 with A.S.T.M. data for Enstatite (Card No. 7-216). Although not a complete fit, the correlation is good, sufficient to suggest that the set of lines A → J are associated with an enstatite-like phase. It is finally noted that all of the spectra from these samples have a suggestion of a line (X_1) at $2\theta \sim 24^\circ$. This line is not associated with either the enstatite or β-quartz phases and a discussion of its origin is deferred at present. The quantitative details of the spectrum shown in Figure 3.9 are presented in Table 3.2.

This set of results may be summarised as follows. The glass (4) and (5) compositions when crystallized at 1000°C produce ceramics whose major crystalline phase is an enstatite-like phase. This phase is stable, (i.e. its lattice parameters are invarient), with pre-crystallization heat treatments, duration of crystallization and melt composition, although the amount of the minor β-quartz phase is sensitive to these parameters. It is now clear that the D and E lines present in those ceramics who major phase is high cordierite, are the two most intense lines of the enstatite phase; the third most intense line, (B), cannot be resolved from line 6 of the high cordierite phase.

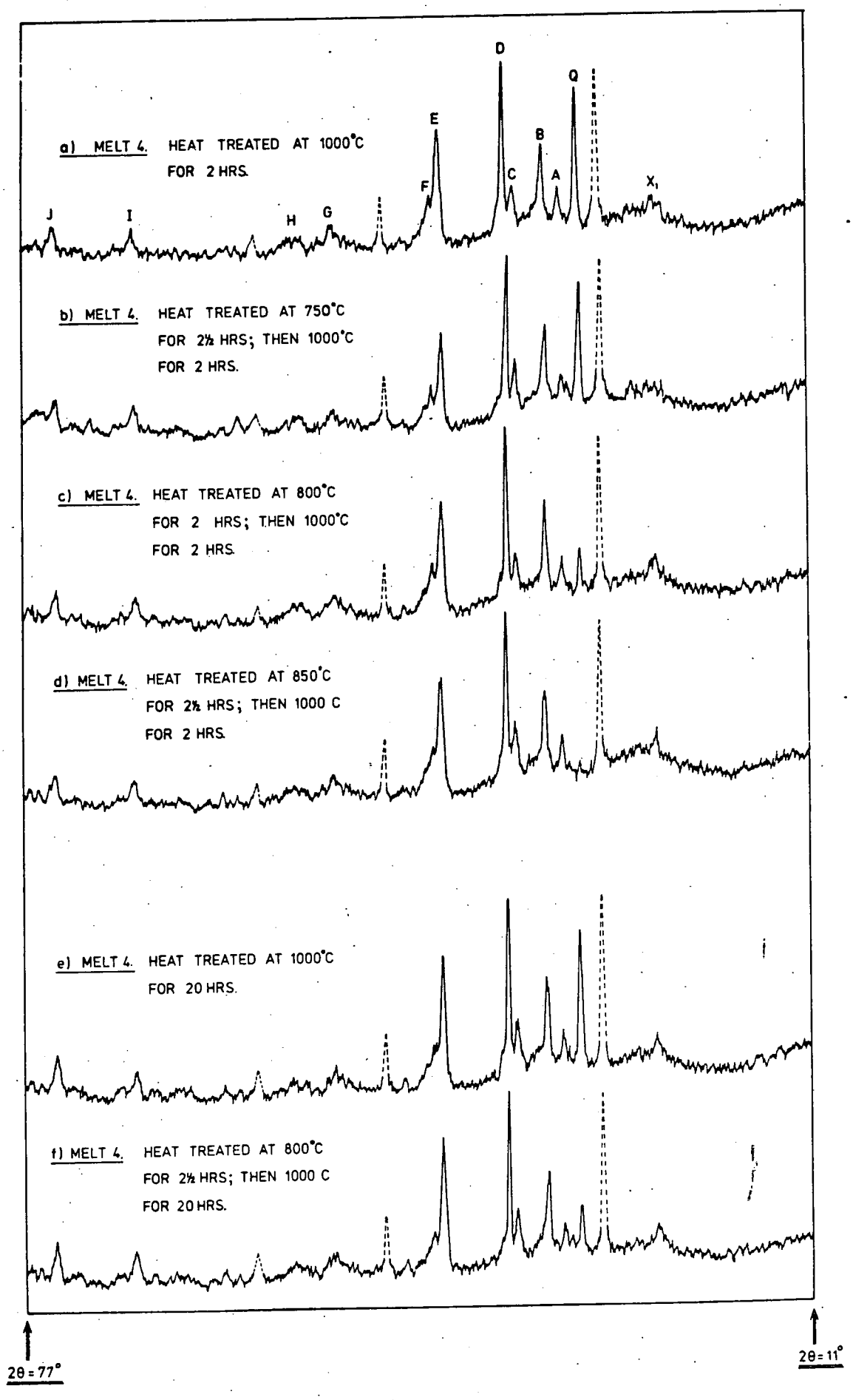

FIG. 3.7. X-RAY DIFFRACTOMETER SPECTRA; 2θ FROM 11° to 77°; CoKα RADIATION.
(DOTTED PEAKS ARE BPO_4 REFERENCE MARKERS)

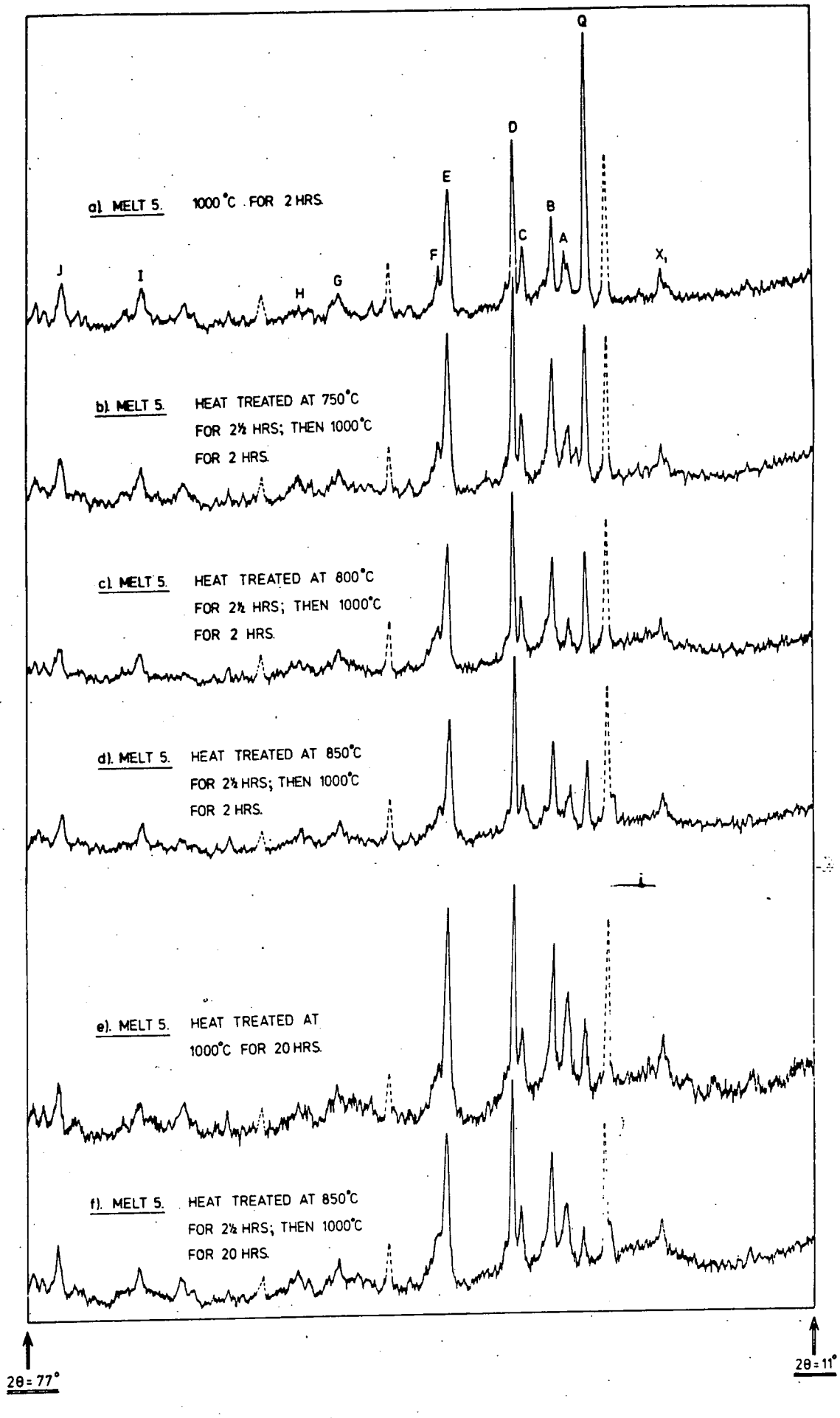

FIG.3.8. X-RAY DIFFRACTOMETER SPECTRA; 2θ FROM 11° to 77°; CoKα RADIATION.
(DOTTED PEAKS ARE BPO_4 REFERENCE MARKERS)

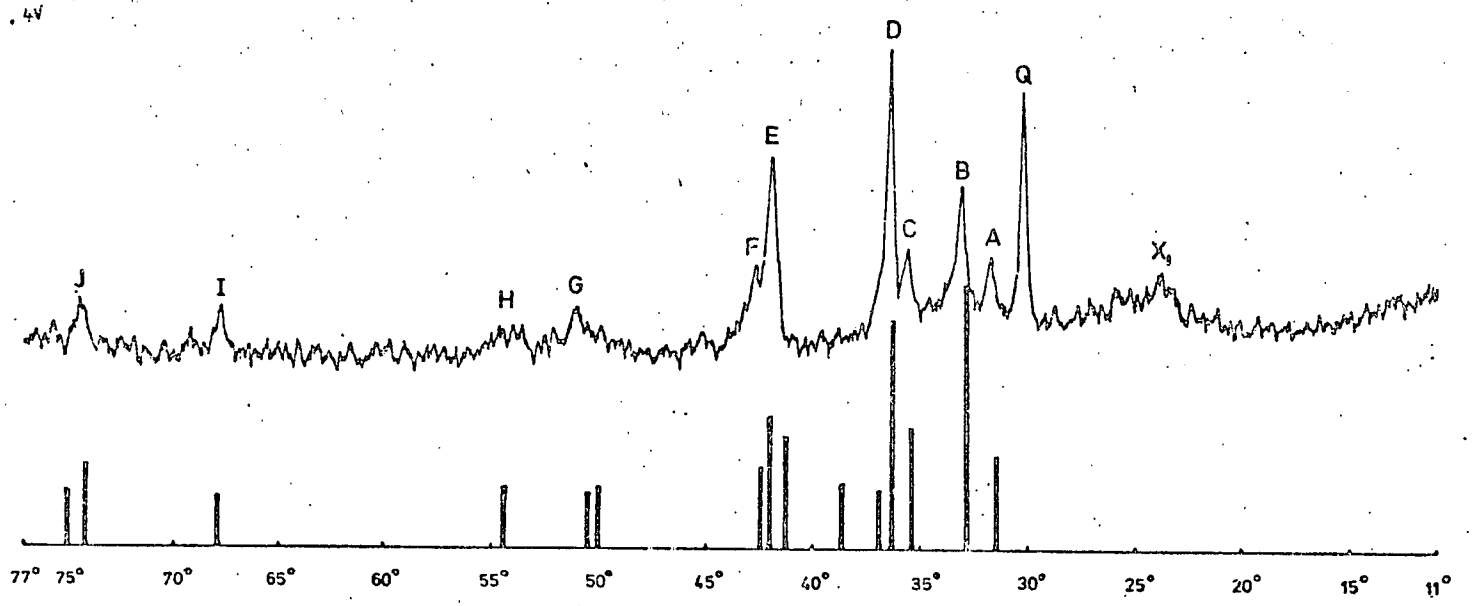

FIG. 3.9. COMPARISON OF DIFFRACTOMETER SPECTRA OF MELT 4 (FIG. 7 trace a)) WITH A.S.T.M. DATA FOR ENSTATITE ($MgSiO_3$). [2θ FROM 11° TO 77° CoKα RAD^N]

Experimental Data			A.S.T.M. Data	
Peak Identification	Intensity (%) (I)	Lattice Parameter ($\times 10^{-10}$ m) (d)	Principal Enstatite* (I)	Lines (d)
X_1	10	4.31		
Q	80	3.42		
A	20	3.27	35	3.30
B	45	3.14	100	3.17
C	20	2.92	44	2.94
D	100	2.87	87	2.87
			23	2.83
			26	2.71
E	70	2.50	43	2.53
			51	2.49
F	10	2.46	31	2.47
G	15	2.08	24	2.11
			21	2.10
H	10	1.960	24	1.960
I	15	1.606	20	1.603
J	20	1.482	34	1.485
			22	1.470

* Card No. 7-216

Table 3.2: The lattice parameters of Melt (4) crystallized at 1000°C. (Intensity figures from Figure 3.9).

3.1.3 Melts (4) and (5) crystallized at 1200°C

The spectra from these ceramics are rather more complex than those previously considered and it is necessary to consider each heat treatment and composition separately.

(i) Melt (4) crystallized at 1200°C for 2 hours:-

The pre-crystallization heat treatments markedly affect the spectra from this range of ceramics. This effect is shown in Figure 3.10. We take for analysis the spectrum of the directly crystallized ceramic, and the spectrum of the specimen crystallized after heat treatment at 850°C, i.e. traces (a) and (d) of Figure 3.10.

The analysis of the spectrum of the directly crystallized specimen is shown in Figure 3.11 where it is apparent that high cordierite is the principal phase, with, in addition, some enstatite, (characterised by the A → J set of lines), as the second most prominent phase. It is interesting to note that the peaks D_1 and D_2, associated with enstatite but not resolved in the 1000°C ceramics, are present in this spectrum. In addition to the two principal phases there are lines due to rutile, (the 100% line is marked 'R'), and the as yet unexplained X_1.

The analysis of the spectrum from a sample identical to that above but for a pre-crystallization heat treatment at 850°C is shown in Figure 3.12. The high cordierite, enstatite and rutile lines are again present, the enstatite : cordierite ratio having significantly increased, but now in addition a set of lines marked X_1 → X_5 is in evidence. The phase giving rise to this group of lines is almost certainly Silica 'O', (A.S.T.M. card No. 12-708), a 'stuffed' silica phase with a distorted quartz structure (see Table 3.3).

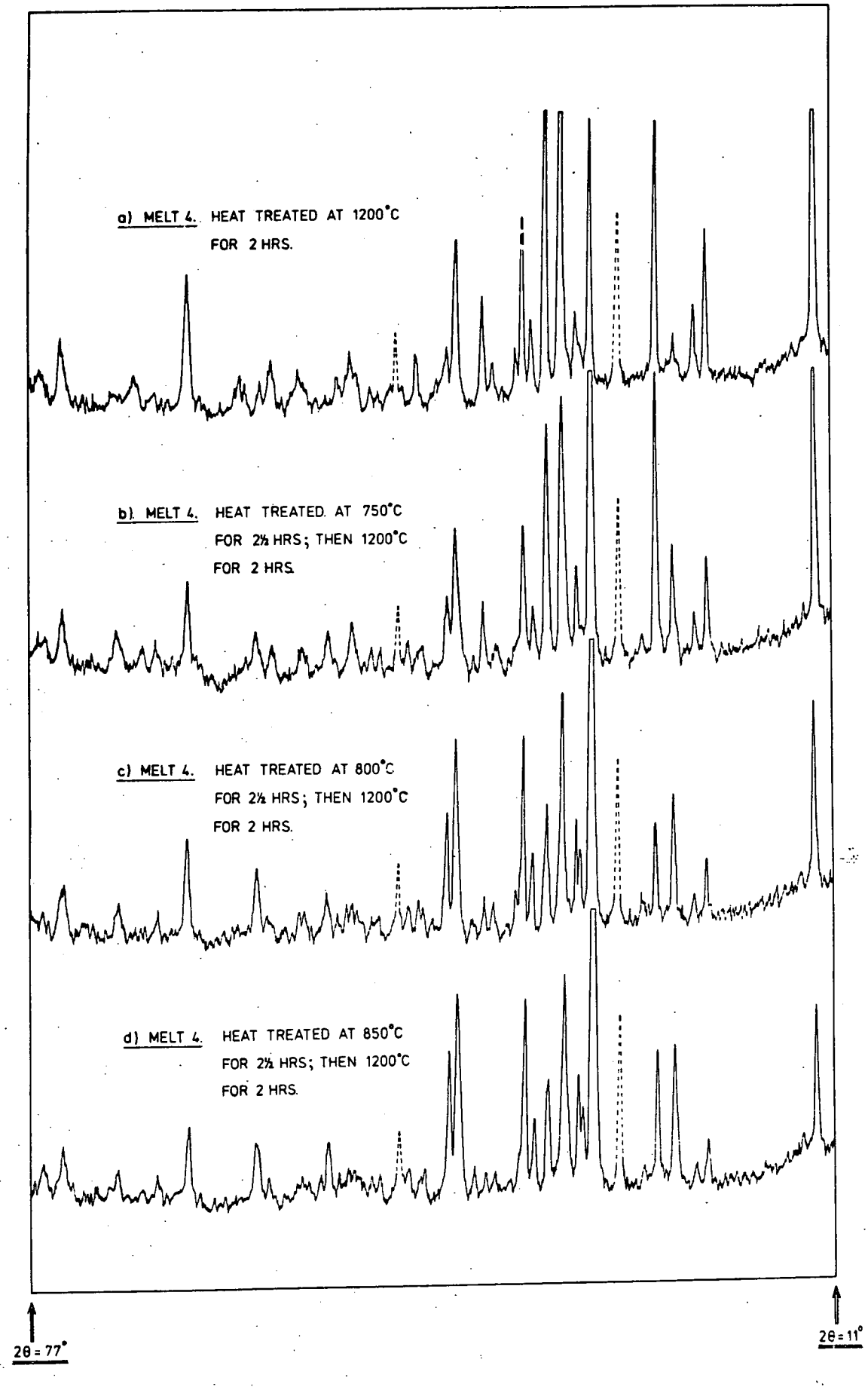

FIG.3.10.X-RAY DIFFRACTOMETER SPECTRA; 2θ FROM 11° to 77°; CoKα RADIATION.
(DOTTED PEAKS ARE BPO_4 REFERENCE MARKERS)

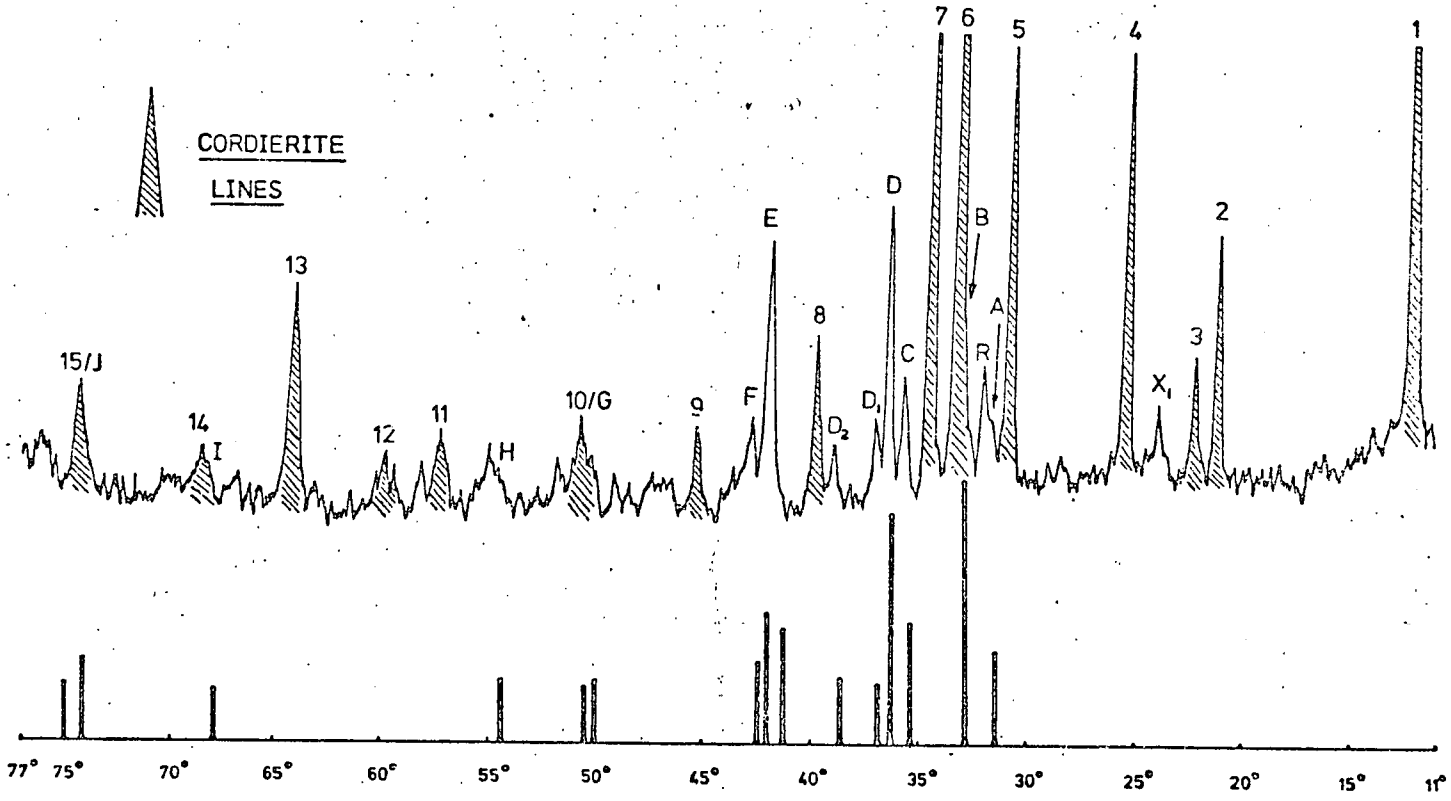

FIG. 3.11. UPPER: ANALYSIS OF DIFFRACTOMETER SPECTRUM OF MELT 4 [FIG. trace a)].

LOWER: ENSTATITE ($MgSiO_3$) SPECTRUM.

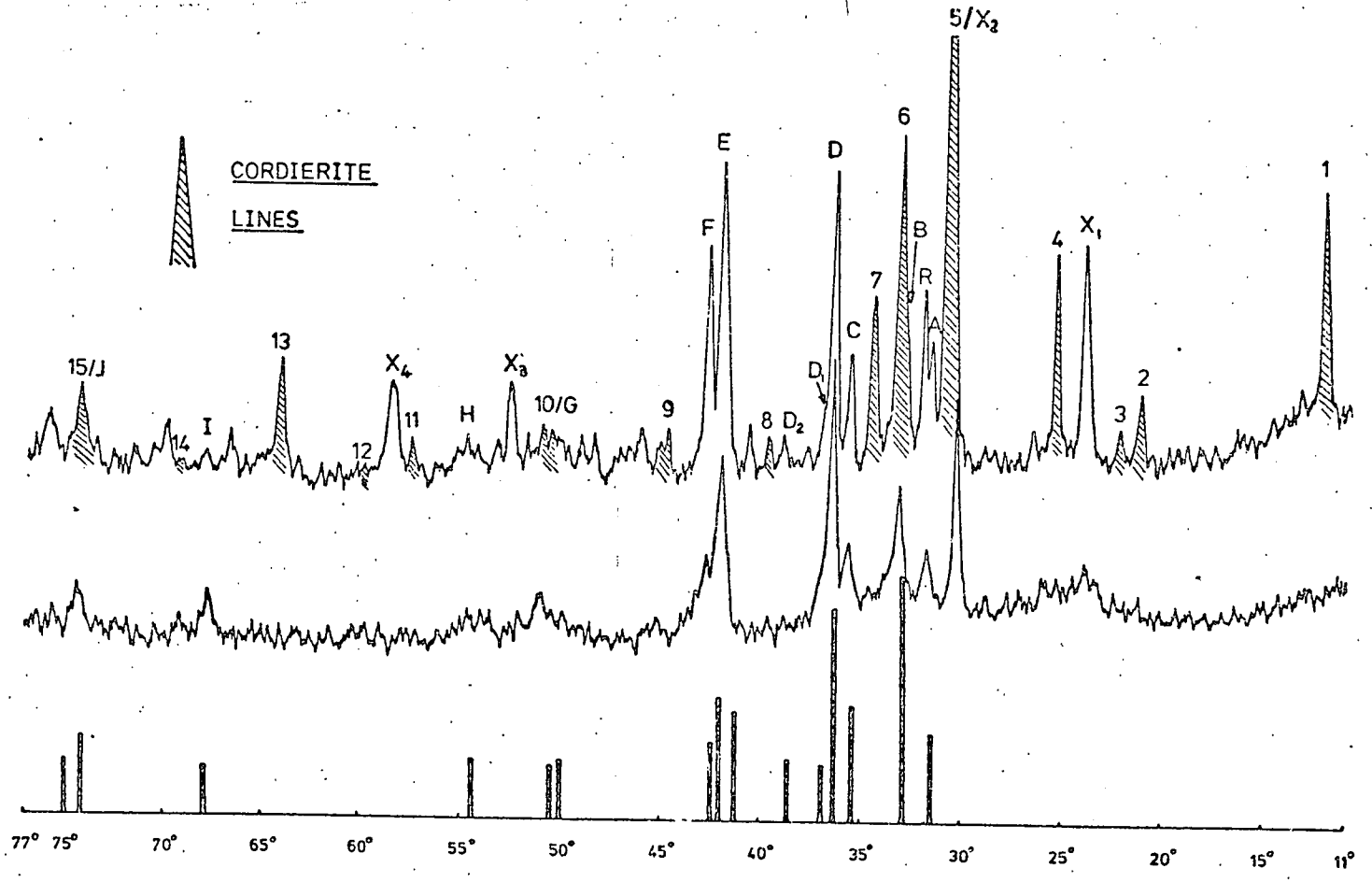

FIG. 3.12. UPPER: ANALYSIS OF DIFFRACTOMETER SPECTRUM OF MELT 4 [FIG. trace d).]

CENTRE: DIFFRACTOMETER SPECTRUM OF MELT 4 [FIG. trace a).]

LOWER: ENSTATITE ($MgSiO_3$) SPECTRUM.

The X series			A.S.T.M. Data for Silca '0' *	
Peak	I	d	I	d
X_1	75	4.33	40	4.32
X_2	100	3.38	100	3.38
X_3	35	2.016	-	-
X_4	40	1.835	60	1.842
X_5	20	1.570	25	1.568

The Y series			A.S.T.M. Data for $MgSiO_3$ **	
Peak	I	d	I	d
Y_1	100	3.175	100	3.17
Y_2	40	2.91	40	2.91
Y_3	20	2.73	20	2.73
Y_4	20	2.55	20	2.55
Y_5	20	2.30	20	2.31
Y_6	30	1.97	20	1.98
			20	1.97

* Card No. 12-708

** Card No. 11-273

Table 3.3: The lattice parameters of the X and Y series of diffraction lines.

(ii) Melt (4) crystallized at 1200°C for 20 hours:-

The diffraction line patterns from these specimens are typified in Figure 3.13. The patterns are very similar to those from the low titania compositions crystallized at this temperature, i.e. a mixture of the dominant cordierite lines and the weaker enstatite lines, with in addition some lines from the rutile present in these ceramics. It is evident also that those ceramics which were pre-heat treated and crystallized at 1200°C for two hours were metastable in terms of their crystalline phases.

(iii) Melt (5) crystallized at 1200°C:-

Typical diffractometer traces from these specimens are shown in Figure 3.14. There are no significant changes in the crystal phases with the varied pre-heat treatments, but the figure shows that the specimens crystallized for two hours have metastable crystal phases, i.e. the two hour and twenty hour specimens have different spectra.

The traces from the specimens crystallized for two hours consist of the dominant set from high cordierite, together with lines from enstatite, rutile and the 'stuffed' silica phase (the X series). The principal change in the pattern on moving to the 20 hours crystallized specimens is the disappearance of the enstatite and silica '0' lines (D, E and the X series), and the emergence of a new set of lines denoted Y_1, Y_2, etc. This set is due to a polymorph of $MgSiO_3$, (A.S.T.M. 11-273), a fact which is established in Table 3.3, and it would seem that the principal change on extending the crystallization period of these samples, is the loss of the metastable $MgSiO_3$ and SiO_2 phases (lines A → J and the X set), and the appearance of a polymorph of the early $MgSiO_3$ phase. During this change the dominant high cordierite phase and the rutile phase remain unaltered.

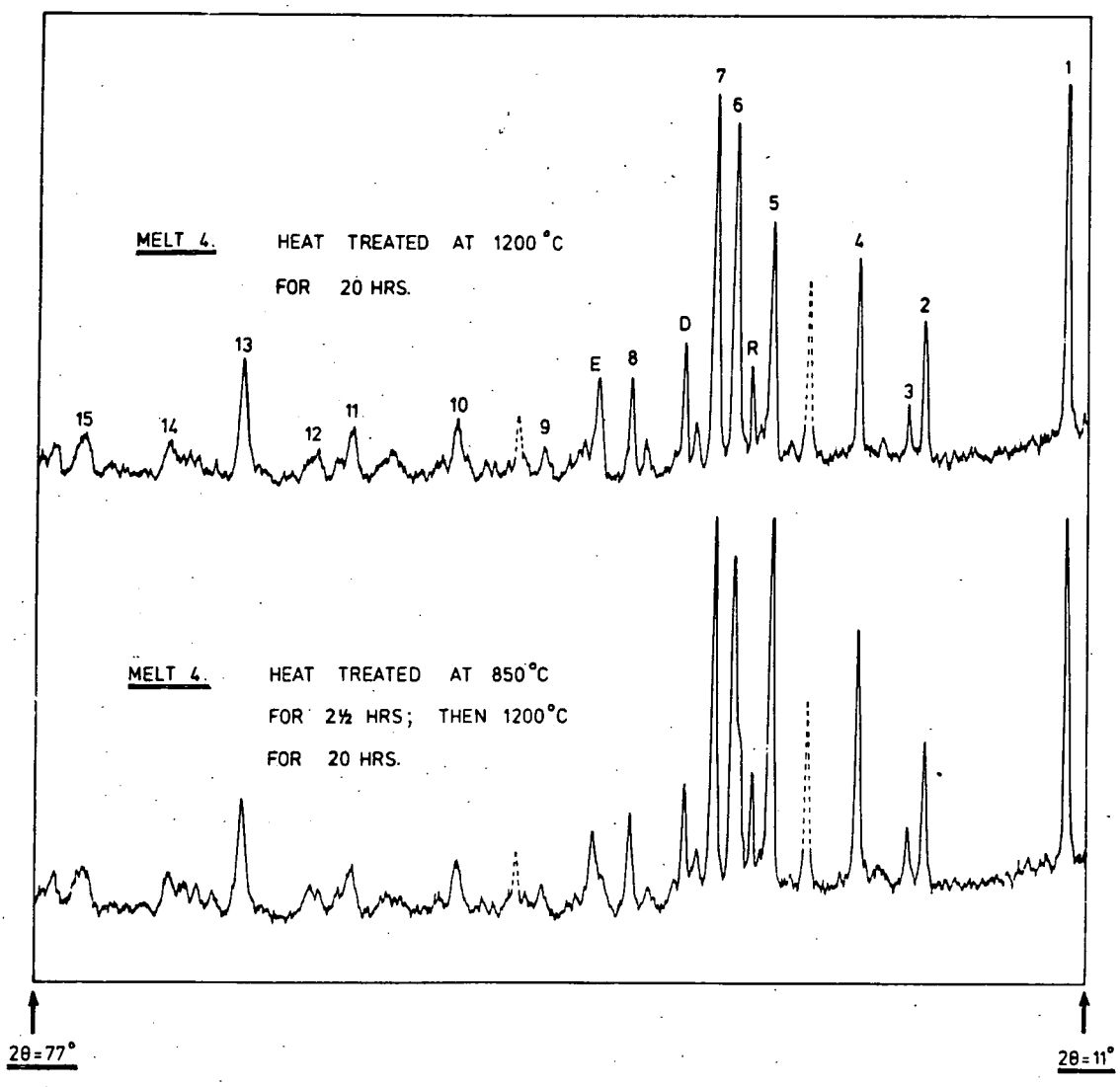

FIG.3.13. X-RAY DIFFRACTOMETER SPECTRA; 2θ FROM 11° to 77°; CoKα RADIATION.
(DOTTED PEAKS ARE BPO_4 REFERENCE MARKERS)

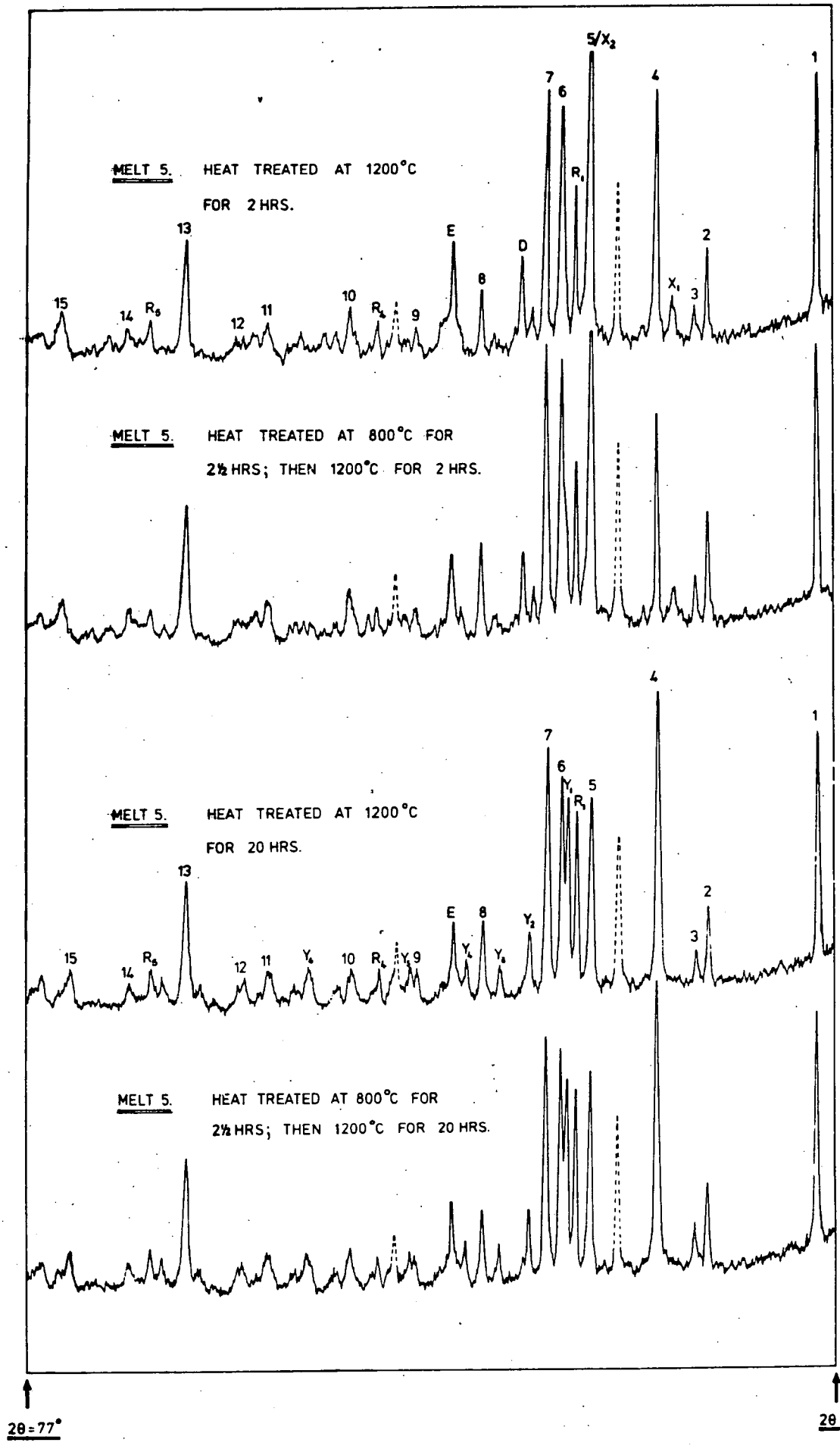

FIG.3.11.4. X-RAY DIFFRACTOMETER SPECTRA; 2θ FROM 11° to 77°; CoKα RADIATION.
(DOTTED PEAKS ARE BPO_4 REFERENCE MARKERS)

A final comment may be made about the one diffraction line as yet unexplained that is the line marked U on the diffraction traces. Figure 3.15 (traces (a) and (b)) shows the diffraction pattern from melts (4) and (5) heat treated at 850°C. The glass (4) pattern is indicative of glassy scatter only, i.e. this sample has not crystallized, but the melt (5) pattern shows a strong line U at $2\theta = 28^{\circ}$ ($d = 3.70$ Å). This is the line observed previously in melts (2) and (3), and a search of the A.S.T.M. index has failed to determine the phase with which it is associated.

Raising the heat treatment temperature of the melt (5) specimens to 900°C produces a diffraction spectrum which is very similar to that from the 1000°C crystallized specimens, and it is clear that the unknown phase has been replaced by the stable enstatite-like phase previously discussed.

3.2 Polarising Microscope, X-Ray back reflection, and SEM results

This work compliments the diffraction results by establishing the size and morphology of the crystallites in the various ceramics.

3.2.1 Melts (1), (2) and (3) (the low titania ceramics)

The ceramic specimens from these melt compositions were studied first with the polarising microscope. Photomicrographs from melt (1) crystallized at 1000°C and 1200°C are shown in Figures 3.16 and 3.17 respectively. It is apparent that the 1000°C specimens have both a 'surface' and a 'bulk' crystallization. The 'surface' crystallites are dendritic in form, and, it can be assumed, originate from nucleation sites at the surface of the sample, whereas the crystallites in the interior of the specimen are spherulitic in form and have apparently originated at nucleation sites in the interior of the specimen. The size of the spherulitic crystals varies by an order of magnitude and is in the region 25 μm → 250 μm.

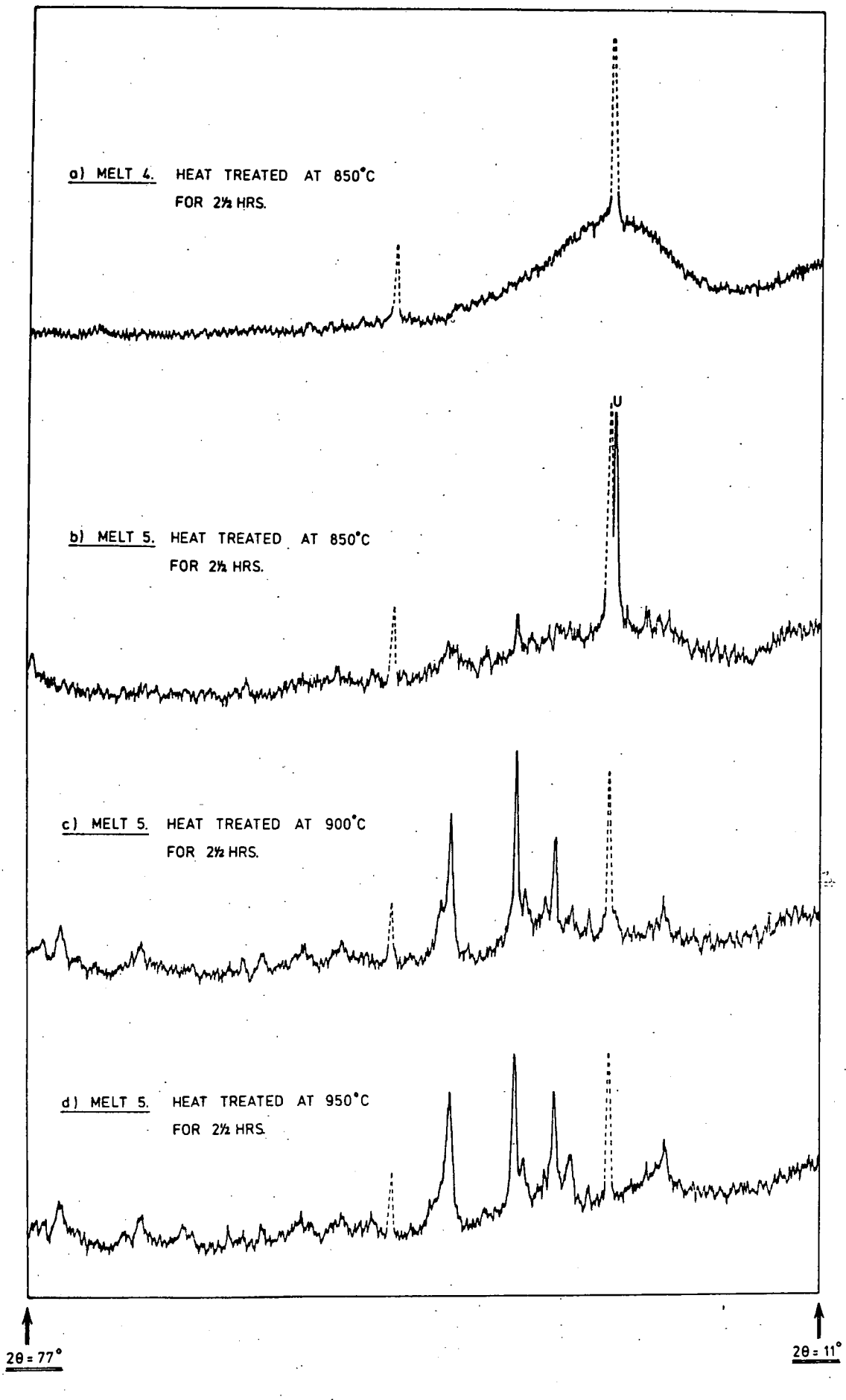

FIG.3.15.X-RAY DIFFRACTOMETER SPECTRA; 2θ FROM 11° to 77°; CoKα RADIATION.
(DOTTED PEAKS ARE BPO_4 REFERENCE MARKERS)

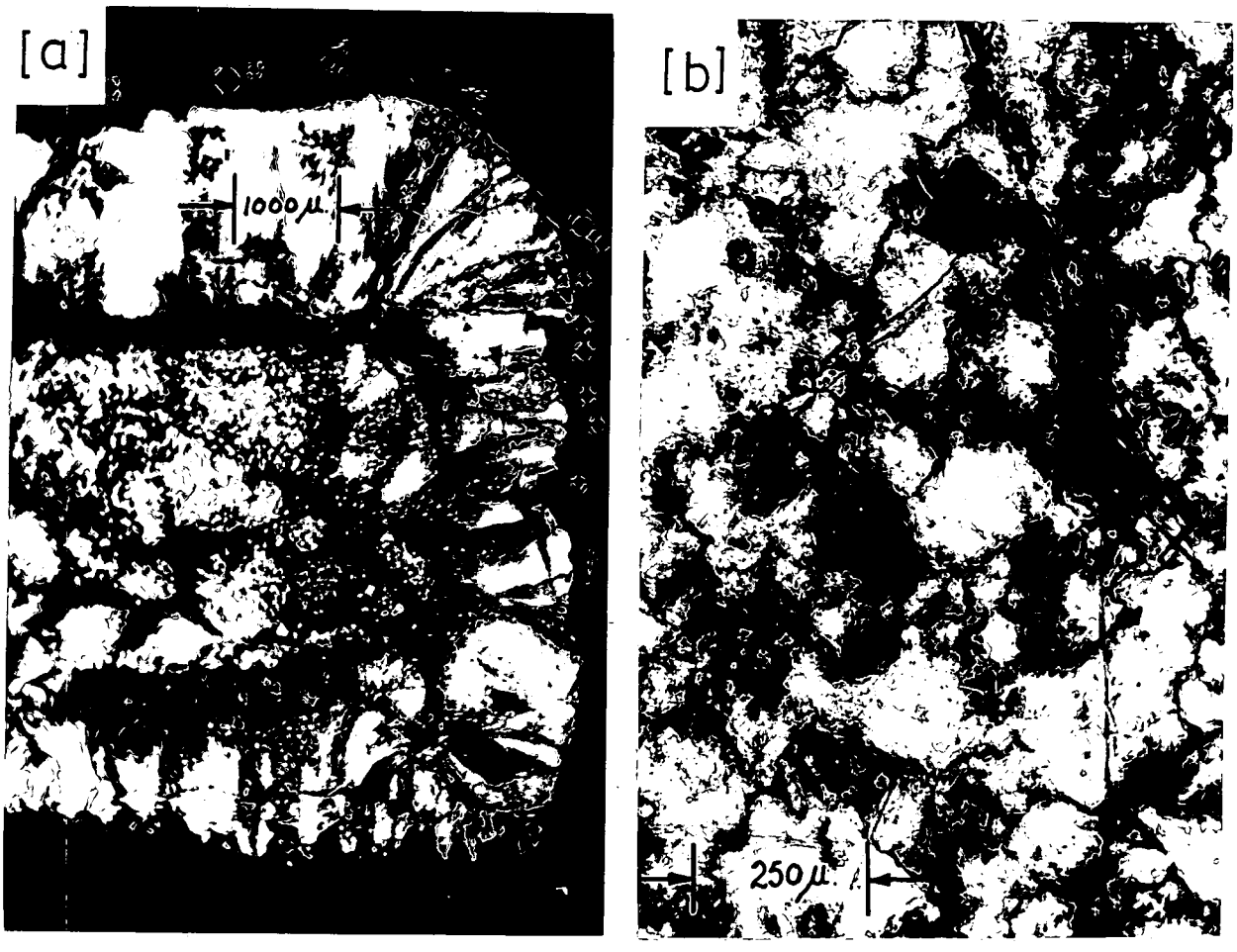

FIG. 3.16. PHOTOMICROGRAPHS OF MELT 1 CRYSTALLIZED AT 1000 °C. (20 hrs.)

[a] Surface and interior of specimen.

[b] Interior of specimen (higher magnification)

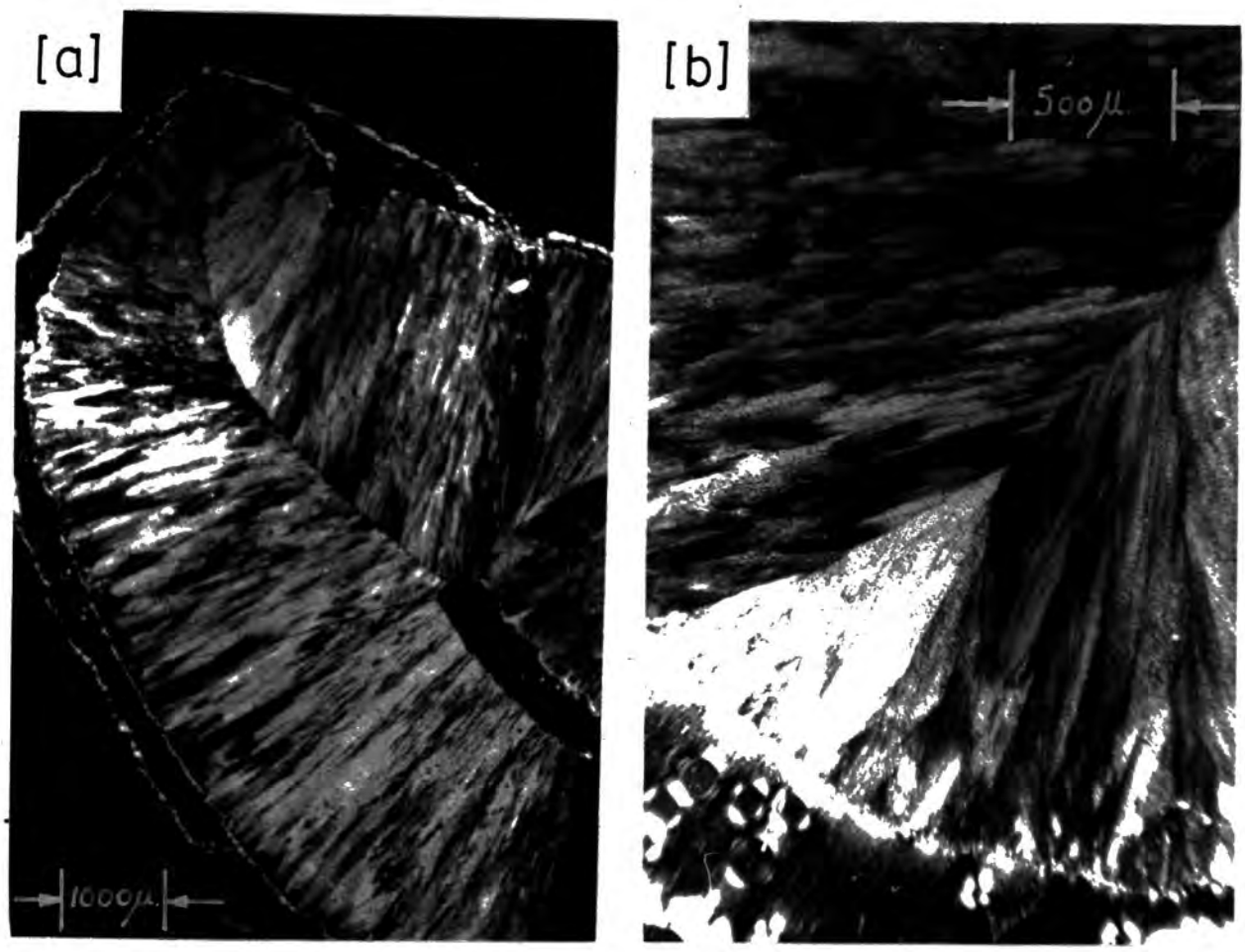

FIG. 3.17. PHOTOMICROGRAPHS OF MELT 1 CRYSTALLIZED AT 1200°C (20 hrs.)

[a] Surface and interior of specimen

[b] As [a], but at a higher magnific.^{n}

The micrographs from the 1200°C specimens show no evidence of a 'bulk' crystallization. The dendritic crystallites, which have presumably originated from the surface of the specimen, extend to the centre of the specimen where their growth is arrested by the dendrites originating from the 'opposite' surface.

Supporting evidence concerning the nature of the crystallites in the melt (1) ceramics was obtained by X-ray back-reflection studies. Figure 3.18(a) shows the photograph from a region in the interior of a melt (1) specimen crystallized at 1000°C. The rings are 'spotty' indicative of a coarse grained material with a significant proportion of its crystallites greater than 100 μm. Back-reflection photographs from the interior of melt (1) specimens crystallized at 1200°C (and from the surface region of the 1000°C specimens), are typified in photograph (c) of Figure 3.18, (the incident beam is $\sim 90^{\circ}$ to the axis of the dendrites). The diffraction rings are continuous in nature but of non-uniform intensity. This is indicative of a fine grained structure with a preferred orientation of the crystal axes, exactly what would be expected from dendritic or columnar crystals nucleated at, and growing from, the surface of the specimen.

Melts (2) and (3) crystallized at 1000°C and 1200°C exhibited a similar type of crystallization behaviour to that of melt (1), i.e. at 1000°C there was evidence of 'surface' and 'bulk' crystallization and at 1200°C the crystallization appeared to have originated at the surface only. Nevertheless a significant quantitative change occurred, most notably between melt (1) and melts (2) and (3). Figure 3.19 presents the micrographs from melts (2) and (3) crystallized at 1000°C and comparison with Figure 3.16 shows that the spherulitic crystals in the interior of melts (2) and (3) are significantly smaller, (20 μm → 100 μm), than those in the melt (1) specimens (25 μm → 250 μm). This observation is supported by the

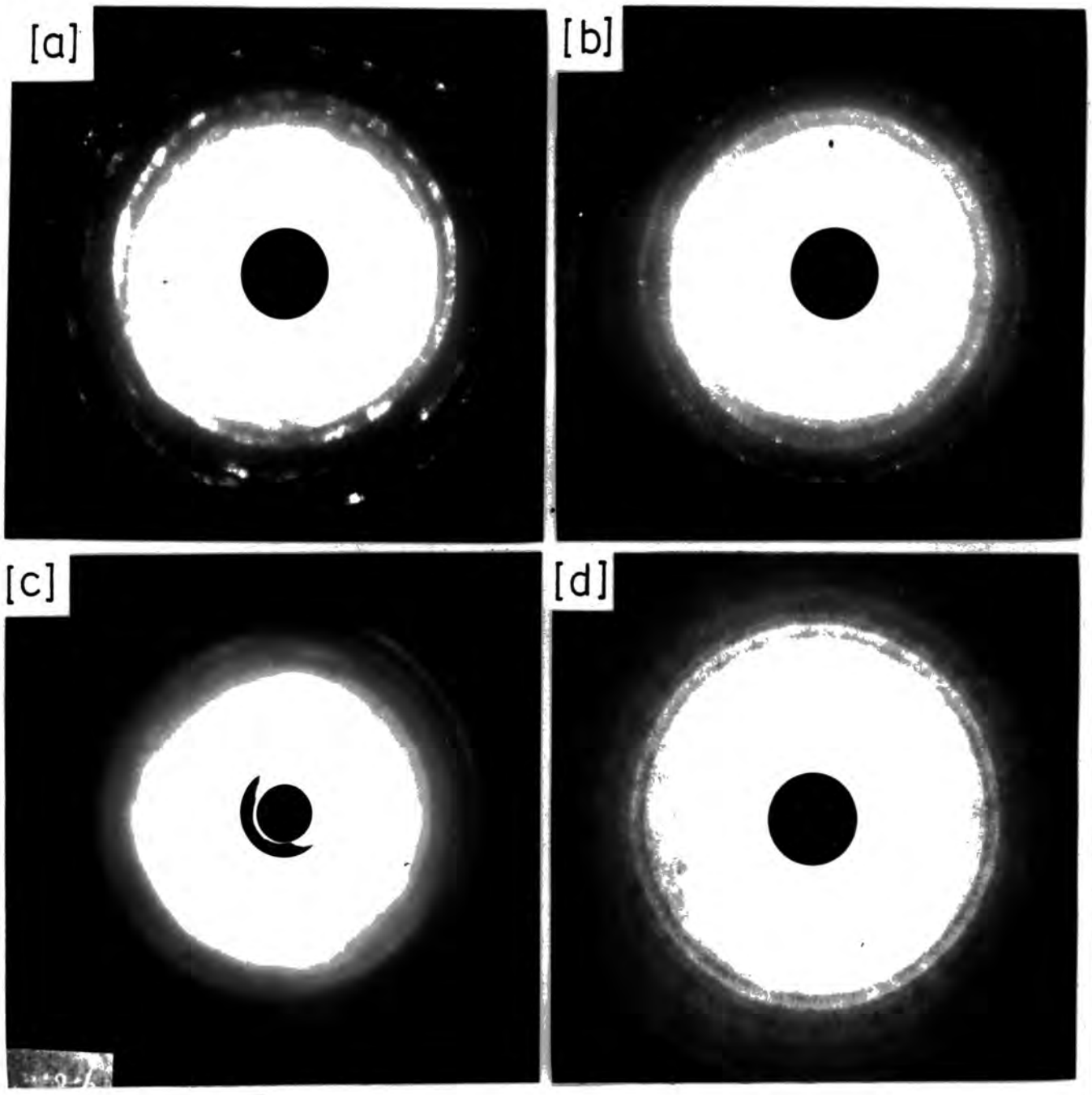

FIG. 3.18. X-RAY BACK REFLECTION PHOTOGRAPHS FROM :—

[a] Interior of melt 1 crystallized at 1000°C (20hrs).
[b] " " " 2 " " " "
[c] " " " 1 " " 1200°C "
[d] " " " 5 " " " "

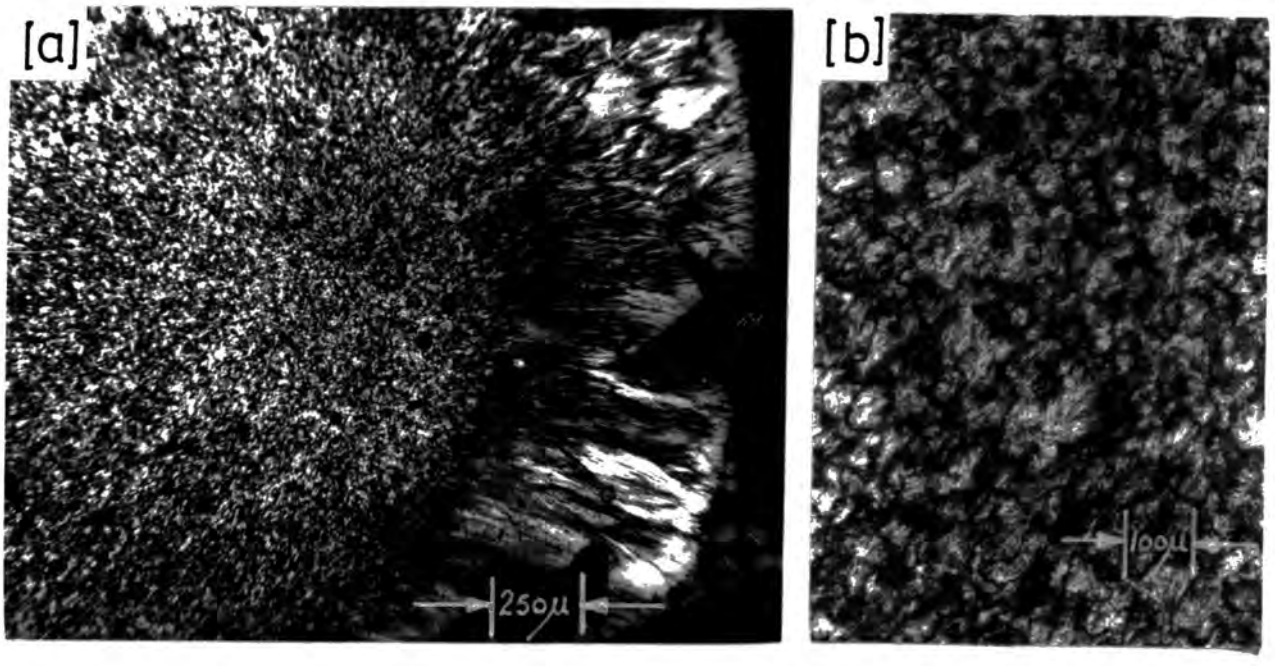

FIG. 3.19. PHOTOMICROGRAPHS OF MELT 3 CRYSTALLIZED AT 1000°C. (20 hrs.)

[a] Surface and interior of specimen.

[b] Interior of specimen at higher magnific.n

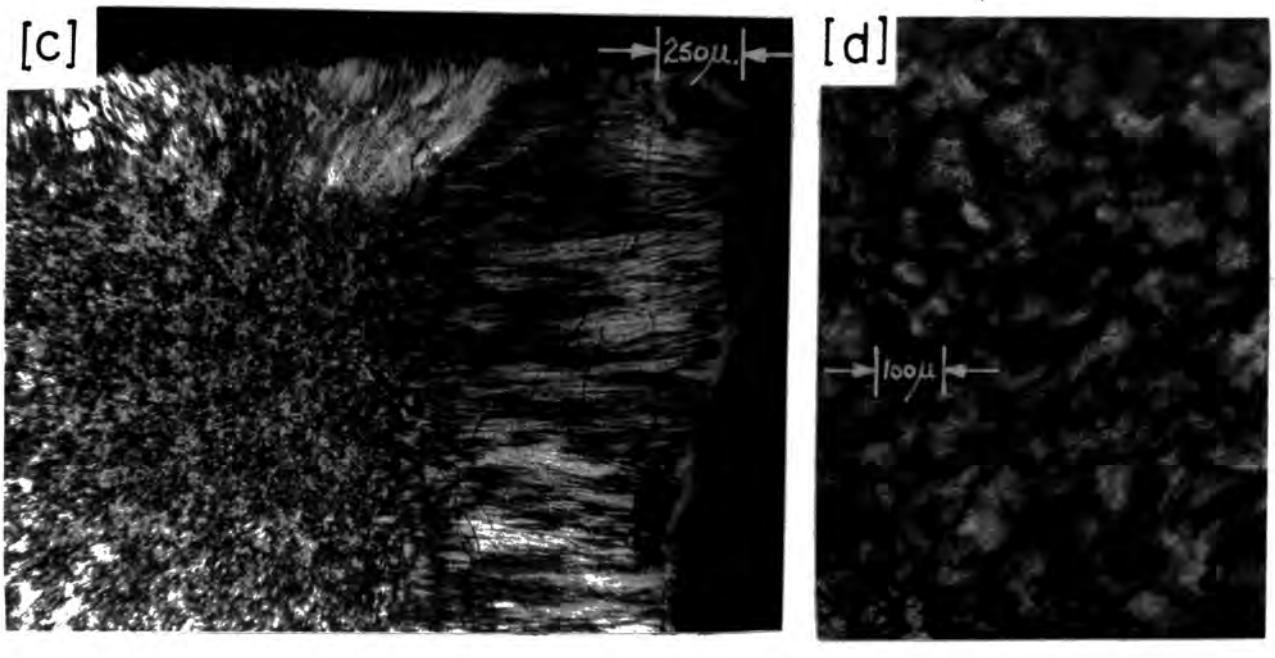

FIG. 3.19. PHOTOMICROGRAPHS OF MELT 2 CRYSTALLIZED AT 1000°C. (20 hrs.)

[a] Surface and interior of specimen

[b] Interior of specimen at higher magnific.n

comparison of back-reflection photographs from melts (1), (2) and (3), i.e. Figure 3.18(a) and (b) shows that the diffraction rings from the melt (1) ceramics, (a), are significantly more 'spotty' than those from melt (2), (b). Figure 3.19 also suggests, and back-reflection results confirm that there is a slight reduction in the average crystallite size when moving from melt (2) to melt (3). A final comparison of Figures 3.16 and 3.19 reveals that in addition to the reduction of the crystallite size, the extent of the surface dendritic growth in the melt (2) and (3) specimens is approximately one half of that in the melt (1) specimens.

Melts (2) and (3) crystallized at 1200°C are characterised by micrographs similar to those of Figure 3.17 and back-reflection photographs similar to Figure 3.18(c), and we conclude that in these specimens, as in melt (1), the crystals are surface nucleated and columnar in nature.

To this point, only 20 hour crystallizations have been considered. This is because samples of melts (1), (2) and (3), although fully crystallized after 2 hours at 1200°C, are only partly crystalline after 2 hours at 1000°C. This is clearly indicated in Figure 3.20 where the fracture surface of melt (2) is shown. The interior of this specimen showed no structure up to the highest magnifications possible with the S.E.M. employed, (10 thousand times), the fracture surface giving all the indications of a glassy fracture. Back-reflection measurements and Polarizing Microscope observations also failed to detect crystals in the interior of the specimens whereas the surface of the specimens was clearly crystalline.

3.2.2 Melts (4) and (5) (the high titania ceramics)

Figures 3.21 and 3.22 are micrographs of melts (4) and (5) respectively, each crystallized at 1000°C. These are three important features. Firstly, the crystal size is greatly reduced in comparison with the low titania specimens; secondly, the dendritic 'surface' crystallization is completely suppressed in favour of the 'bulk' spherulitic crystallites;

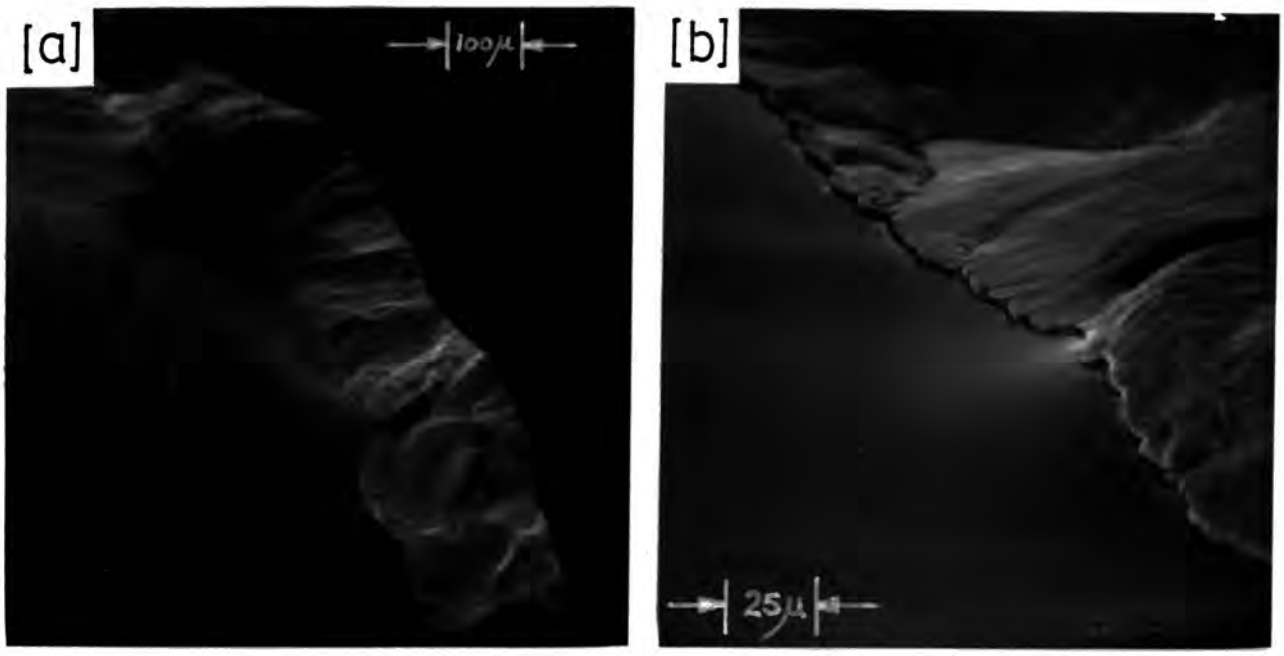

FIG. 3.20. S.E.M. PHOTOGRAPHS OF MELT 2 CRYSTALLIZED AT 1000°C FOR 2hrs.

[a] Surface and interior of specimen.

[b] Interface between crystalline surface and glassy interior of specimen.

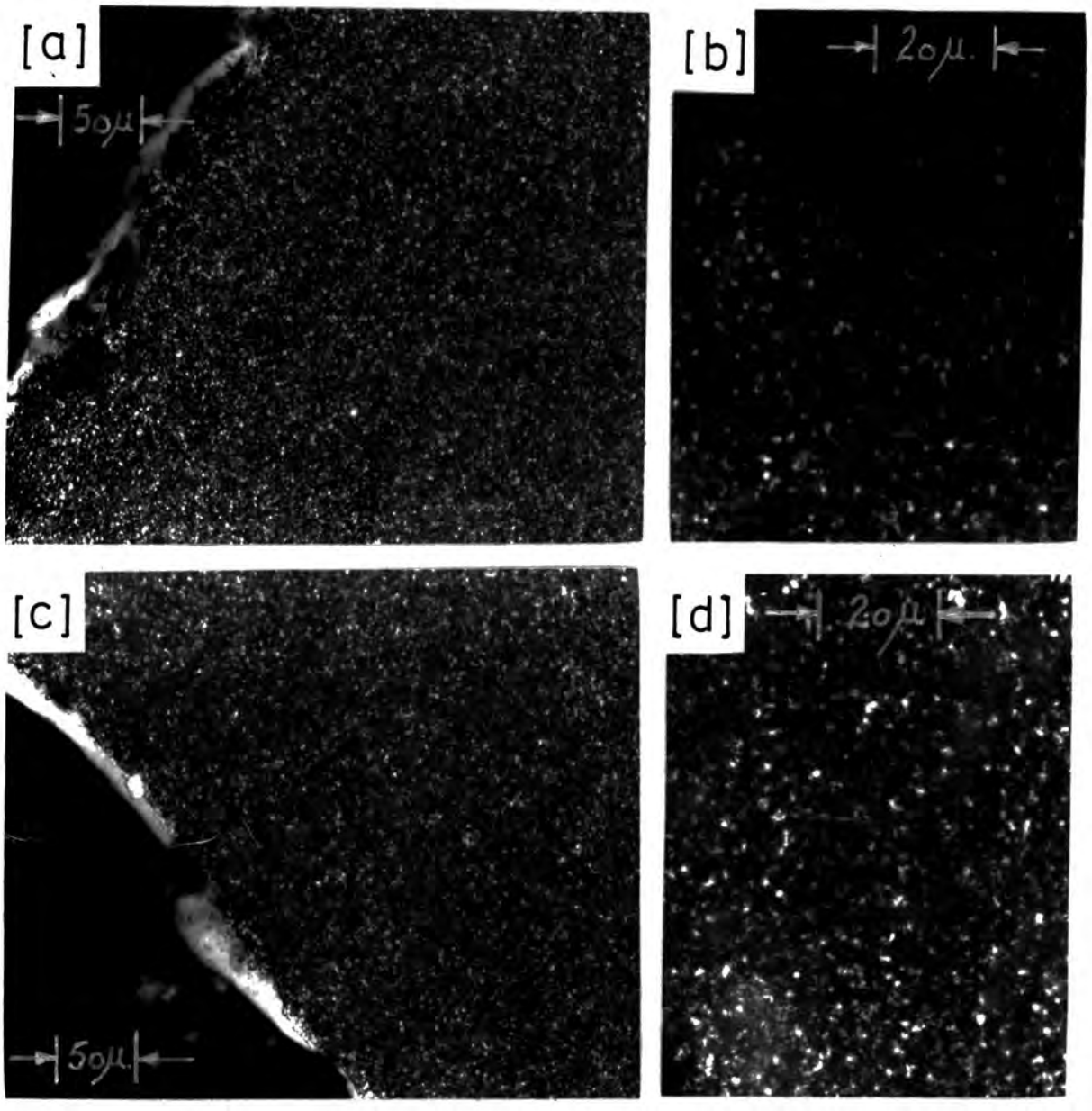

FIG. 3.21. PHOTOMICROGRAPHS OF MELT 4

[a] and [b] :— Crystallized at 1000°C (20 hrs.) without pre-heat treatment.

[a] Surface and interior of specimen.

[b] Surface of [a] at a higher magnific.n

[c] and [d] :— Pre-heated at 800°C for 2½ hrs., then crystallized at 1000°C.

[c] Surface and interior of specimen.

[d] Interior of [c] at a higher magnific.n

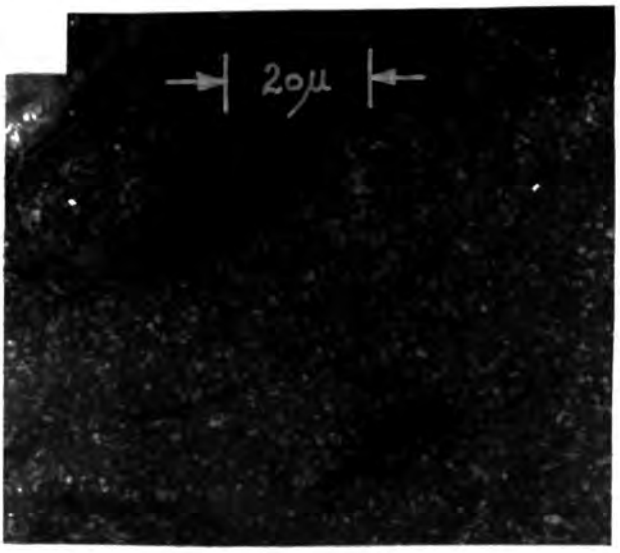

FIG. 3.22.

Photomicrograph of Melt 5
Crystalized at 1000 °C

and thirdly, as Figure 3.21 suggests, the pre-crystallization heat treatments have little, if any, effect upon the nature of the crystallization or upon the size of the crystallites. This final or third feature, shown here for the melt (4) composition, was observed throughout the range of compositions studied, i.e. the size and nature of the crystallites were independent of the pre-crystallization heat treatments.

No details of the crystallization in the melt (4) and (5) compositions crystallized at 1200°C could be discerned under the polarizing microscope and the characterization investigation methods were extended to studies with the Scanning Electron Microscope (S.E.M.). The topography of the fracture surfaces and of the surfaces after polishing and etching in hydrofluoric acid was investigated. As typical of the results from the high titania specimens, the fracture surfaces, ((a) and (c)), and the polished/etched surfaces, ((b) and (d)), of melt (5) specimens crystallized at 1000°C and 1200°C, are shown in Figure 3.23. The interpretation of these photographs cannot be as unequivocal as that of the polarising microscope photographs. Nevertheless, what is apparent is that the melt (5), (and melt (4)), specimens are microcrystalline when crystallized at both 1000°C and 1200°C. Back-reflection results confirm this view; Figure 3.18(d) presents the back-reflection photograph from a sample of melt (5) crystallized at 1200°C and the continuous nature of the rings, even in the absence of polarising microscope information, affirms the microcrystalline nature of these specimens. Studies of the whole region of the fractured and etched surfaces of the 1200°C ceramics showed that the nature of the crystallization was, as with the 1000°C ceramics, identical throughout the specimen, i.e. the 'surface' nucleated crystallization is suppressed by the 'bulk' nucleated crystallization. The precise size of the crystallites in the 1200°C specimens could not be determined with certainty, but a comparison of the etched surface of the 1000°C specimen,

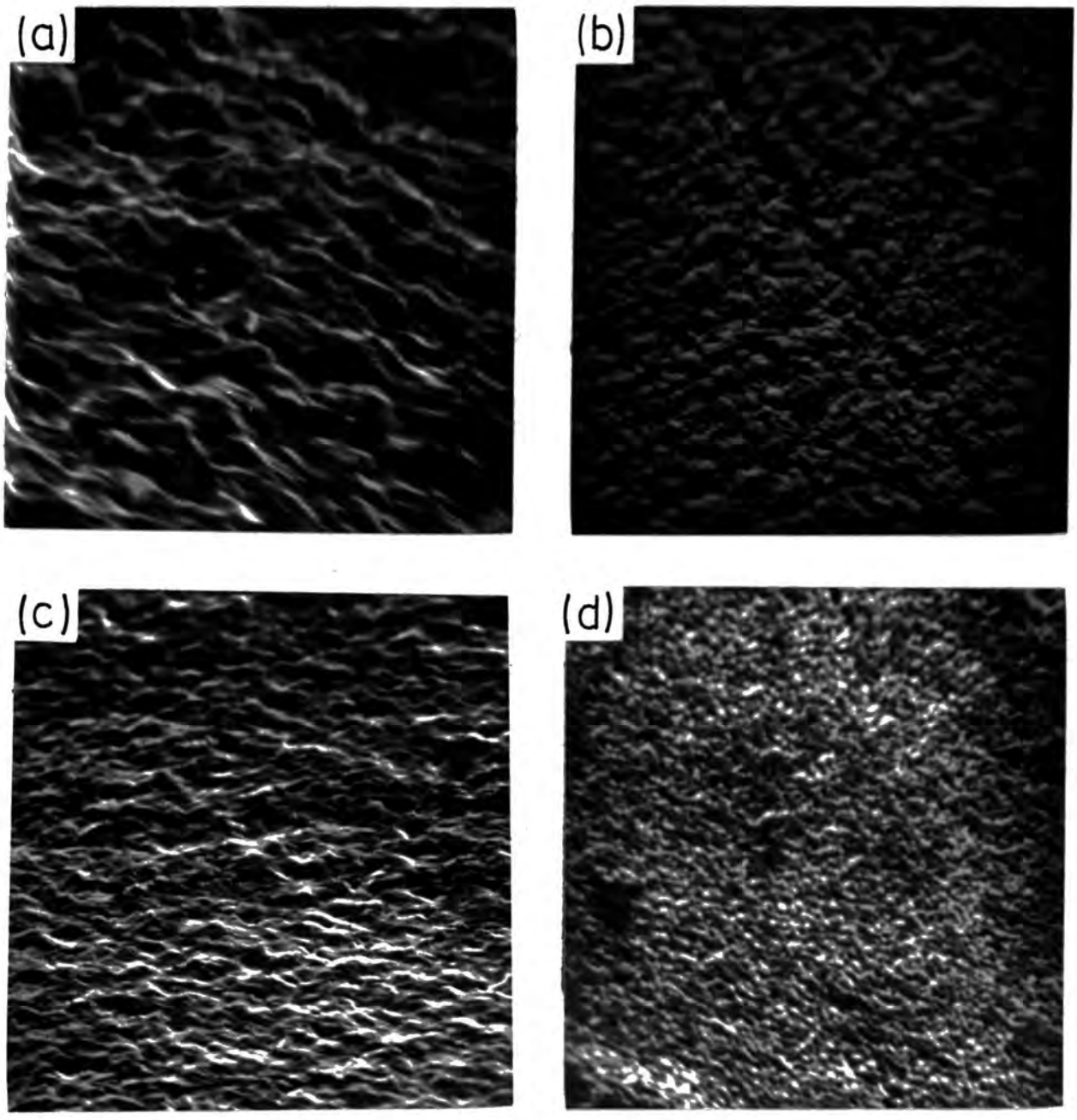

FIG. 3.23. S.E.M. Photographs of Melt 5

(a) Crystalized at 1000°C for 20 hrs. — fracture surface.

(b) Crystalized at 1000°C for 20 hrs. — fracture surface after polishing (¼ μ Al_2O_3) then etching (1% HF) for 30 sec.

(c) Crystalized at 1200°C for 20 hrs. — fracture surface.

(d) Crystalized at 1200°C for 20 hrs. — fracture surface after polishing (¼ μ Al_2O_3) then etching (1% HF) for 30 sec.

(Figure 3.22), shows that the principal areas of relief could reasonably be ascribed to individual crystallites. If therefore, the areas of relief in Figure 3.23(d) are individual crystallites, then there is a significant reduction in the crystallite size within the 1200°C ceramics compared with the 1000°C specimens. This is somewhat speculatory recalling that the crystal type is different in the 1200°C and 1000°C ceramics.

The high Ti 1200°C ceramics, although much stronger than any of the coarse grained low Ti ceramics, were noticeably easier to fracture than the mechanically strong 1000°C specimens. In general, the fracture strength of a glass-ceramic will be enhanced if the fracture takes a tortuous path through the ceramic, and thus fracture strength increases in the direction:- small grain > large grain, and intergranular, (along the grain boundaries), > transgranular fracture (across the grains), (3.1). The nature of the fracture depends upon the stresses in the crystallites and the residual glass. If the expansion coefficient of the crystal is greater than that of the residual glass phase then, in the radial direction, (normal to interface), both crystal and glass are in tensile stress, and in the circumferential direction the stresses are compressive in the glass and tensile in the crystal. This situation favours an intergranular fracture. If the crystal has a smaller expansion coefficient than the surrounding glass then similar stress arguments, (3.1), show that transgranular fracture will be favoured. We do not know the compositions of the residual glasses; however the expansion coefficient of Cordierite is low in comparison with Enstatite (3.2) and it is plausible that transgranular fracture is favoured in the 1200°C Cordierite ceramics, and that intergranular fracture is likely in the 1000°C Enstatite ceramics. This would be consistent with the observation of the relative fracture strengths of these ceramics. Unfortunately, the fracture surfaces themselves, (Figures 3.23 (a) and (c)), partly due to the resolution of the S.E.M. employed, do not clearly indicate the nature of the fracture,

although the appearance of 3.23(a), the surface of the 1000°C ceramic, is very similar to S.E.M. photographs of intergranular fracture surfaces presented in reference (3.2). There is no clear correspondence either between the fractured and etched surfaces of a given specimen, although again, as with Figures 3.23 (b) and (d), a comparison of Figure 3.23(a) amd (c) reinforces the impression that the 1200°C ceramics are rather finer grained than the 1000°C ceramics. Thus the higher mechanical strength of the Enstatite ceramics as compared with the Cordierite ceramics would seem to originate from the relative expansion coefficients of the crystal and glass phases rather than the crystallite size.

The visual appearance of the fracture surfaces suggested that there could be an additional factor to consider. The Enstatite ceramics had shiny specular reflecting surfaces, whereas the Cordierite ceramic surfaces were matt diffuse reflectors. Thus it was plausible that there was a much greater quantity of residual glass in the Enstatite ceramics than in the Cordierite ceramics, and consequently, a quantitative phase analysis study was undertaken.

3.3 Quantitative Phase Analysis

An Internal Standard technique was used to determine the amount of each crystalline phase in the ceramics. This method of analysis has been employed by Kitaigorodskii et al (3.3) upon a similar ceramic system, and a complete theoretical treatment of the technique has been published by Klug and Alexander (3.4). Essentially, a known quantity of an internal standard is mixed into the ceramic powder and the diffraction spectrum recorded. The total intensity of the lines from the standard, (I_s), and the lines from a given crystalline phase in the ceramic, (I_1), are, if the quantity of standard remains constant, related to the weight fraction, (x_1) of the specific crystal phase by

$$x_1 = k \frac{I_1}{I_s}$$

where k is a constant which in practise is determined by preparing mixtures of the standard and crystal phase in varying ratios, and, after analysis of the diffractograms from these mixtures, a calibration curve may be prepared.

Such a method requires pure specimens of the crystal phases to be analysed, and unfortunately in this work, the available mineral specimens of the main crystalline phases, Enstatite and Cordierite, were neither sufficiently pure nor of the correct modification. Thus a quantitative analysis of these phases was not possible and the apparently higher glass content of the Enstatite ceramics could not be verified. We were able however to prepare a calibration curve for Rutile, using BPO_4 as the internal standard, and this calibration is shown in Figure 3.24. Each point is the average of five calibrations at a constant TiO_2:BPO_4 ratio, involving summation of the three most intense rutile lines and the two most intense BPO_4 lines from each diffractogram. The dotted lines represent the extremes of the individual calibrations, and as such are tolerance limits for the calibration curve.

Rutile is clearly indicated in the diffractograms of melts (4) and (5) crystallised at 1200°C (Figures 3.13 and 3.14). The quantity of BPO_4 in these traces is 5 wt.% and by summation of the rutile and BPO_4 lines and the use of Figure 3.24 we make the following assessments:-

(a) Melt (4) - 1200°C for 20 hours:- Rutile content $\sim$ 4.9%
(Tolerance 3.9% → > 5%)

(b) Melt (5) - 1200°C for 2 hours:- Rutile content $\sim$8%
(Tolerance 6.5% → 9%)

(c) Melt (5) - 1200°C for 20 hours:- Rutile content $\sim$9.4%
(Tolerance 7.8% → > 10%)

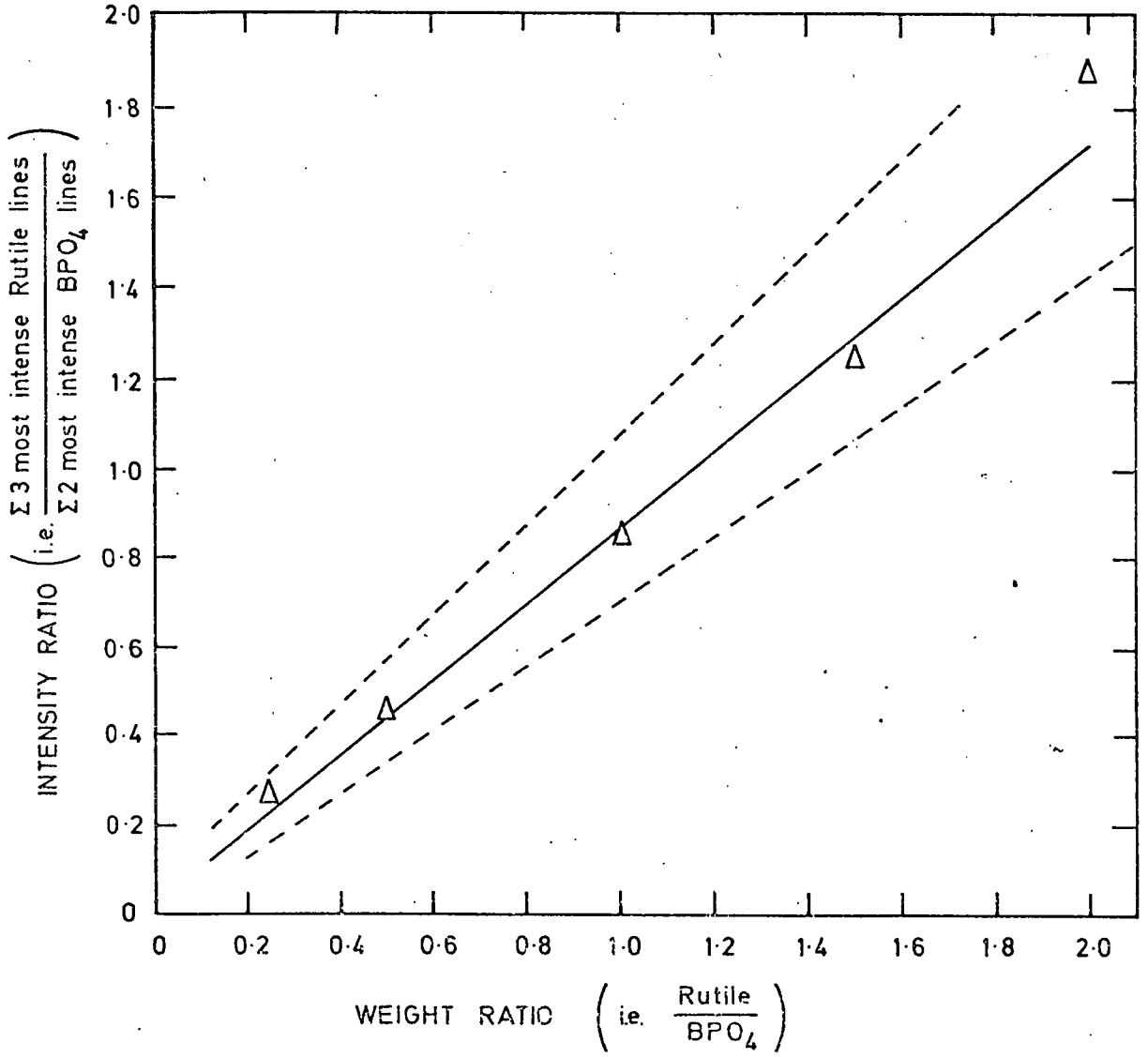

FIG 3.24. INTERNAL STANDARD CALIBRATION CURVE FOR RUTILE, (STANDARD BPO_4).

It would seem therefore that the Rutile phase accounts for most if not all of the added TiO_2 in those high titania ceramics which have Cordierite as the major crystal phase. The analysis above however does not preclude the presence of spectroscopically significant quantities of titanium in phases other than Rutile.

REFERENCES

CHAPTER 3

3.1 P W McMillan, Glass Technology 15(1) (1974) 5-15

3.2 P W McMillan, 'Glass Ceramics' Academic Press 1964

3.3 I I Kitaigorodskii et al, Zh. Neorgan. Mater. 2 (1966) 623-632

3.4 H P Klug, L E Alexander, 'X-Ray Diffraction Procedures' John Wiley and Sons. Inc. 1954

CHAPTER 4

ELECTRON SPIN RESONANCE

4.1 Theory

4.1.1 Free Ion and Solid State Resonance

In a free atom or ion of the 3d transition series, Russell-Saunders (L-S) and spin-orbit coupling combine to form spectroscopic states characterised by their spin, orbital and total angular momenta (i.e. S, L and J). The (2J + 1) spatial degeneracy of each state is lifted by an external magnetic field, (H), and a small oscillating magnetic field perpendicular to H can induce transitions between the levels when the resonance condition

$$h\nu = g_J \beta H$$

(β is the Bohr magneton, ν = frequency of oscillation).

is satisfied. The Lande splitting factor g_J, is specified exactly for a given S, L, J term, having the value 2, (2.0023 with corrections), for spin-only magnetism (L = 0) and 1 for orbital-only magnetism (S = 0). Within a given term the (2J + 1) levels are equally spaced, and resonance occurs at a single field whatever may be its orientation.

In the solid, the 3d electrons of the iron group are fully exposed to the electrostatic field (crystal field) of its neighbours with the effect that the orbitals are 'locked' into the field, and the orbital contribution to the magnetic moment of the ion is largely 'quenched'. The spin moment, however, having no direction interaction with the crystal field is free to orientate in an external magnetic field.

The complete Hamiltonian, with the orders of magnitude of the energy terms appropriate to a paramagnetic ion of the first transition series, takes the form

$$H_{total} = H_c \text{ (Coulomb term } \sim 10^5 \text{ cm}^{-1}) + H_F \text{ (crystal field term } 10^4 \text{ cm}^{-1})$$

$$+ H_{L.S.} \text{ (spin-orbit coupling term } \sim 10^2 \text{ cm}^{-1} \text{ in the free ion)}$$

$$+ H_Z \text{ (Zeeman term } \sim 1 \text{ cm}^{-1}) + \text{smaller terms.}$$

As in the free ion, the dominant Coulomb term determines the electronic configuration and L-S term (i.e. $3d^3$, ^4F) but, H_F being greater than $H_{L.S.}$, the spin and orbital magnetic moments are almost completely de-coupled.

4.1.2 The Spin Hamiltonian

E.S.R. measurements are concerned with transitions between levels split at most by a few cm^{-1}, and, in the formalism due to Abraham and Pryce (4.1), only terms of this magnitude in the full Hamiltonian are considered. This truncated expression is the Spin Hamiltonian.

$$H_S = \beta H.(L + 2S) + \lambda L.S + AI.S \quad (+ \text{smaller terms}) \qquad (4.1)$$

The first term is due to the Zeeman interaction with a given LS term, the second expresses the spin-orbit coupling within the term, and the third arises from the interaction of the electronic and nuclear magnetic moments when $I \neq 0$. λ and A are the spin-orbit and hyperfine coupling constants respectively.

In most circumstances the crystal field completely removes the orbital degeneracy and the ground state is an orbital singlet, ($\langle 0|L_p|0\rangle = 0$, $p = x,y,z$). In addition the de-coupling of the spin and orbital momenta allow $\lambda L.S$ to be treated as a perturbation on the Zeeman term, and to second order, i.e. taking account of the mixing of higher orbital states into the ground state due to the remaining spin-orbit coupling, equation (4.1) becomes (4.2):

$$H_S = \beta H.g.S + S.A.I + S.D.S. + \text{(smaller terms)} \qquad (4.2)$$

where g, A and D are tensor quantities which may be satisfactorily defined in terms of their values along 3 principal axes (x, y and z), the z axis being taken by convention to be the principal axis of symmetry of the crystal field.

If the external field H has direction cosines ℓ, m, and n with respect to the x, y and z axes then the Zeeman term in equation (4.2) becomes, (4.2)

$$H_S \text{ (Zeeman)} = g\beta H.S \tag{4.3}$$

where

$$g^2 = \ell^2 g_x^2 + m^2 g_y^2 + n^2 g_z^2 \tag{4.4}$$

Including the hyperfine term the Spin Hamiltonian becomes (4.2):

$$H_S \text{ (Zeeman)} = g\beta H.S + AI.S \tag{4.5}$$

where

$$g^2A^2 = \ell^2 g_x^2 A_x^2 + m^2 g_y^2 A_y^2 + n^2 g_z^2 A_z^2 \tag{4.6}$$

Equations (4.3) to (4.6) express the divergence of the energy levels of the ground LS term in a field H, in terms of the parameters g and A which may be determined directly from the experimental resonance spectrum. Conversely, estimation of the g and A parameters appropriate to a particular term and crystal field allows the prediction, i.e. simulation of, the experimental spectrum.

The third term in the Hamiltonian of equation (2), the spin-spin term, has the effect of splitting the states with differing magnetic quantum numbers, (when the ground term has $S > \frac{1}{2}$ and the crystal field symmetry is less than cubic), even in zero magnetic field. It gives rise to a 'fine structure' in the spectrum with the (2S + 1) individual transitions occurring at different fields.

4.1.3 The Resonance Conditions

Associated with the Spin Hamiltonian of equation (4.3) are the energy levels

$$E = g\beta HM \tag{4.7}$$

where M is the magnetic quantum number appropriate to each of the $(2S + 1)$ states degenerate in zero magnetic field. The selection rule $\Delta M = \pm 1$ for the allowed transitions gives the resonance condition

$$h\nu = g\beta H \tag{4.8}$$

The Hamiltonian of equation (4.5) has energy levels

$$E = g\beta HM + AMm \tag{4.9}$$

where m is the magnetic quantum number of the $(2I + 1)$ nuclear spin states. The selection rule $\Delta M = \pm 1$, $\Delta m = 0$ gives for the main transitions

$$h\nu = g\beta H + Am \tag{4.10}$$

Thus the hyperfine interaction splits a given electronic transition into $(2I + 1)$ components with a field spacing of $(Am/g\beta)$.

4.1.4 The Single Crystal Resonance Spectrum

Figure 4.1 shows the hypothetical spectrum of an ion with $S = \frac{1}{2}$, $I = 0$, when there is complete anisotropy in the g factor, i.e.

$$g_1 \ (\equiv g_x) \neq g_2 (\equiv g_y) \neq g_3 (\equiv g_z)$$

Experimentally, only one absorbtion line would be observed if all of the paramagnetic ions were in identical sites in the single crystal matrix. The magnetic field (H) at which resonance occurs, is determined by the orientation of H with respect to the crystal axes, and would lie

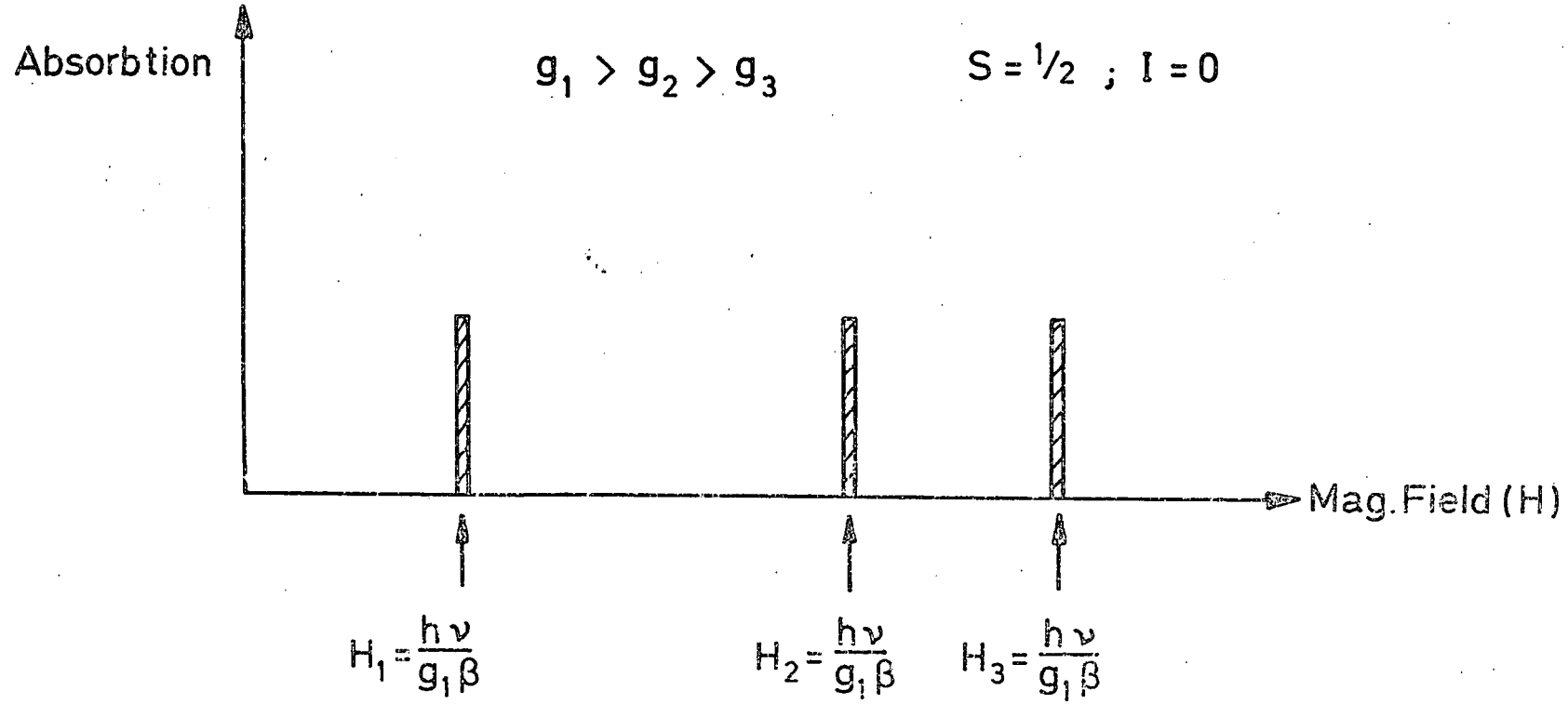

FIG. 4.1. Field positions of the resonance line, (δ function), when H is directed along the three principal axes.

between the extremes H_1 and H_3 and satisfy the condition

$$H_R = \frac{h\nu}{g\beta} \qquad (4.11)$$

where g is given by equation (4.4).

4.1.5 Resonance Spectra of Polycrystalline Materials

Rotating the principal axes of the crystal whilst the direction of the magnetic field is kept constant results in an absorbtion of power at fields between H_1 and H_3 (Figure 4.1) satisfying the resonance condition, (equation (4.11)). A polycrystalline sample approximates to an ensemble of sites randomly orientated to the magnetic field, and thus the absorbtion spectrum is the sum over the resonance conditions satisfied by all of the sites. Such a sum is termed a POWDER PATTERN. For an $S = \frac{1}{2}$, $I = 0$ ion, characteristic powder spectra and their first derivatives are shown in Figure 4.2.

When there is a hyperfine splitting of the electronic transition, the powder pattern will take the form of Figure 4.3, which is drawn for an $S = \frac{1}{2}$, $I = \frac{1}{2}$ ion. Each transition is split into two components and the resultant absorbtion spectrum is in effect the sum of two individual patterns.

When the Hamiltonian contains the Zeeman term only, analytic expressions for the powder pattern are possible and have been evaluated for the case of axial symmetry (4.3) and orthorhombic symmetry (4.4) of the paramagnetic site. However, when additional terms are necessary in the Hamiltonian or when the effects of broadening of the single crystal linewidth are included, numerical methods or computer based techniques become essential.

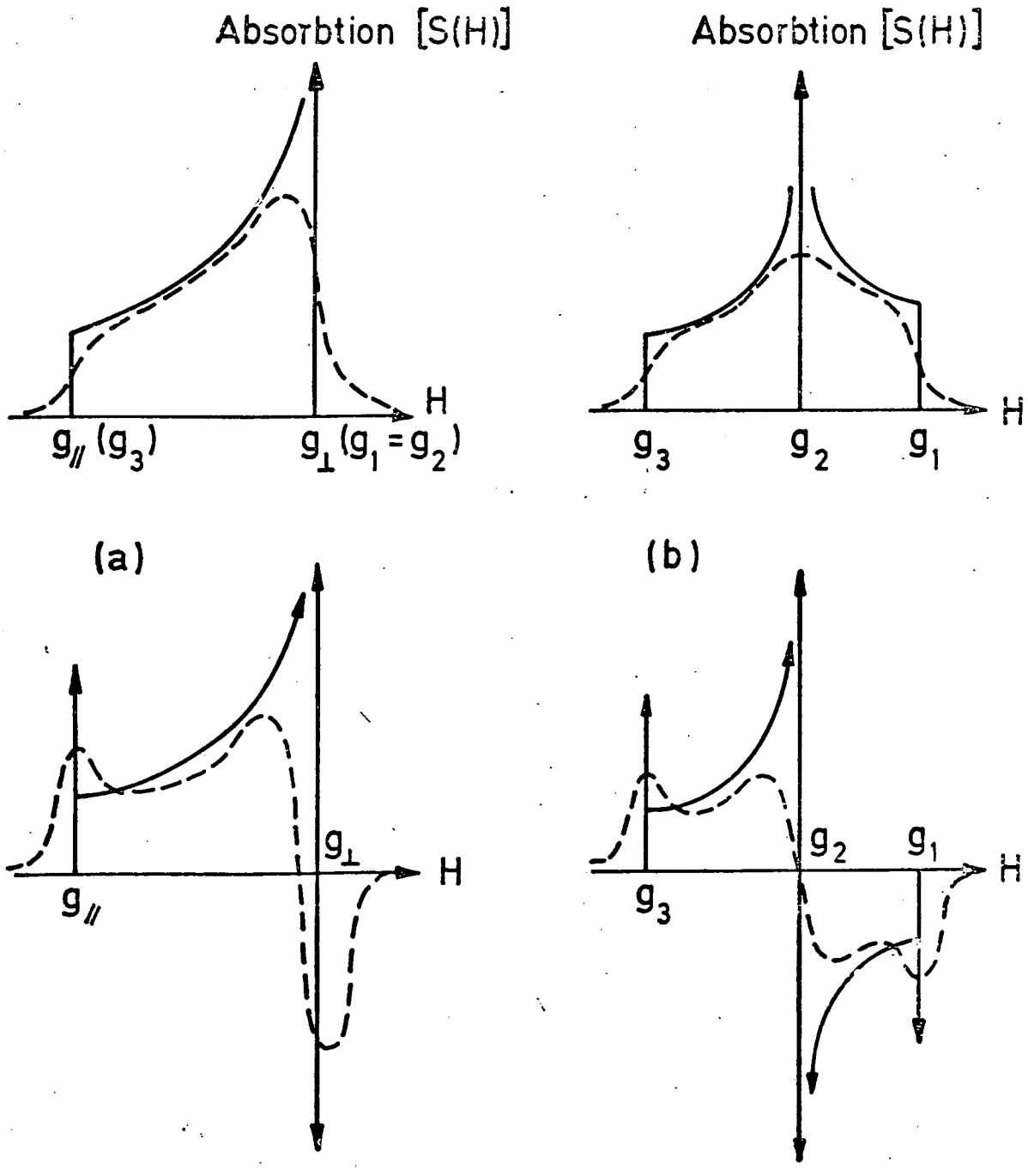

FIG. 4.2. Powder spectra from sites with (a) Axial Symmetry (b) Orthorhombic Symmetry.

Upper Traces:- Absorbtion Spectrum.
Lower Traces:- First Derivative of Spectrum.
Full Lines:- Idealized Spectra with δ Function Absorbtion by Individual Crystallites.
Dotted Lines:- 'Real' Spectra, i.e. the Effect of Crystallite Line Broadening.

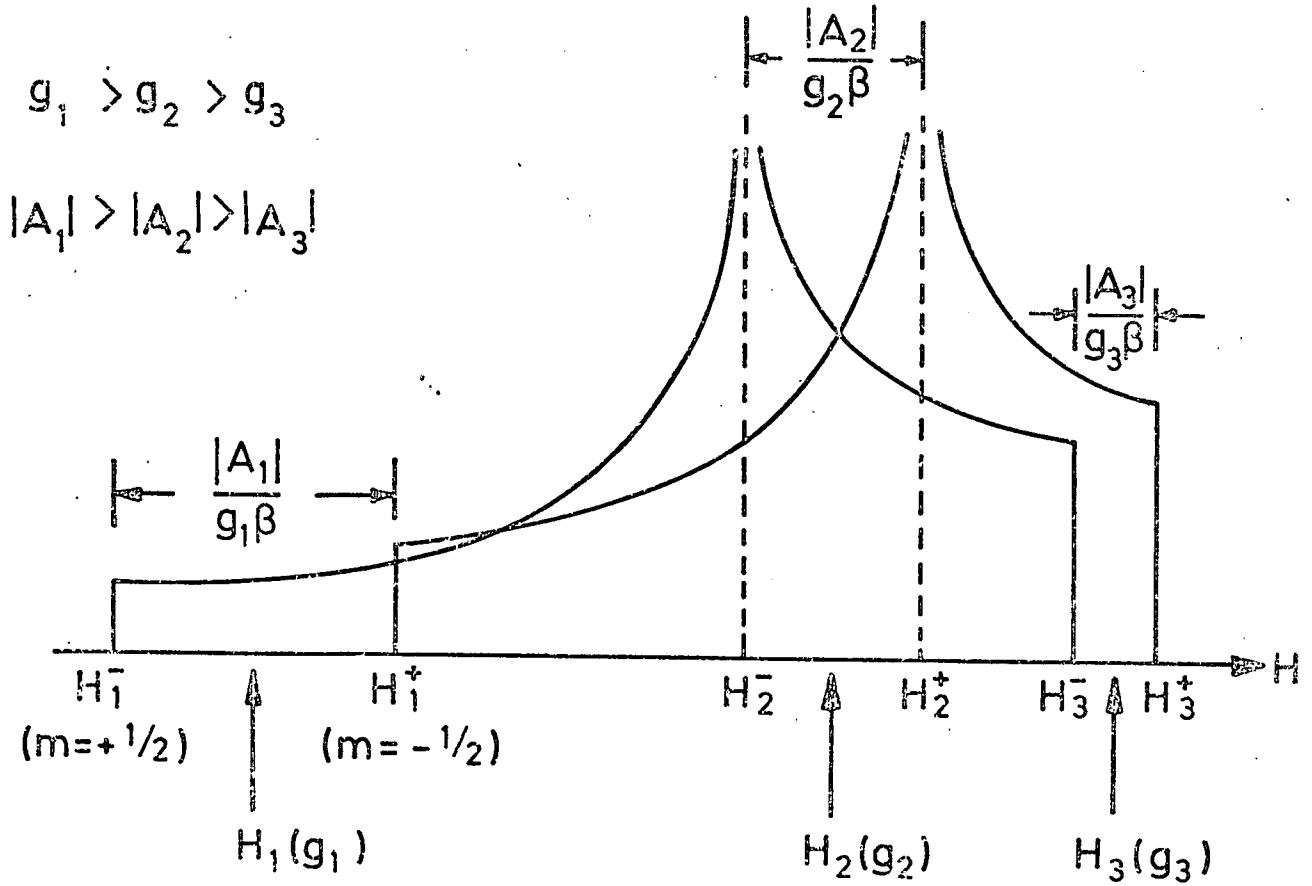

FIG. 4.3. Powder pattern (components) for a paramagnetic centre with $S = 1/2$, $I = 1/2$, in the case of complete anisotropy in the g and A tensors.

4.1.6 Computer Simulation of Powder Spectra

Assuming that each individual or crystallite has an equal probability of being orientated in any element of solid angle $d\Omega$ with respect to the applied field H, the shape function S(H) (or powder pattern) is given by (4.4,4.5,4.6)

$$S(H)\ dH = \frac{1}{4\pi} \sum_m \int_H^{(H + dH)} l_m(\Omega)\ d\Omega(H_m) \qquad (4.12)$$

where S(H) represents the normalized amplitude of the resonance absorbtion signal at the field H. The integration is over the elements of solid angle such that $H < H_m < (H + dH)$ where H_m is the resonance field derived from an appropriate resonance condition, e.g. (equation (4.11)). The quantity $l_m(\Omega)$ is the transition probability for the m^{th} component of the spectrum which, for the $M \leftrightarrow (M - 1)$ electronic transition is proportional to, (4.2):

$$S(S + 1) - M(M - 1)$$

Except for strong anisotropy in g, $l_m(\Omega)$ is independent of the angle which the oscillating field inducing transitions makes with the principal axes of the system and may be taken outside the integral. Thus for a system with only one electronic transition (i.e. $S = \frac{1}{2}$) the $l_m(\Omega)$ term may be neglected, and equation (4.12) reduces to

$$S(H)\ dH = \frac{1}{4\pi} \int_H^{(H + dH)} d\Omega \qquad (4.13)$$

The simulation procedure is effectively a numerical evaluation of equation (4.13).

4.1.7 Details of the Computation

It is convenient to define the orientation of the principal axes of the crystallite with respect to H in terms of the Eulerian angles

θ and ϕ , (see Figure 4.4). Then, equal elements of solid angle $d\Omega$ correspond to equal units of $\sin\theta \cdot d\theta \cdot d\phi$, or equal areas in $d(\cos\theta) \cdot d\phi$ space. In terms of θ and ϕ the g and A parameters defined in equations (4.4) and (4.6) become,

$$g = \left[g_1^2 \sin^2\theta \sin^2\phi + g_2^2 \sin^2\theta \cos^2\phi + g_3^2 \cos^2\theta \right]^{\frac{1}{2}} \qquad (4.14)$$

$$A = \left\{ \frac{\left[A_1^2 g_1^2 \sin^2\theta \sin^2\phi + A_2^2 g_2^2 \sin^2\theta \cos^2\phi + A_3^2 g_3^2 \cos^2\theta \right]}{g} \right\}^{\frac{1}{2}} \qquad (4.15)$$

Thus as $\cos\theta$ and ϕ are incremented over the whole solid angle, the corresponding resonance fields are calculated from

$$\left.\begin{aligned} H_R &= \frac{h\nu}{g\beta} \quad , \\ \text{or} \qquad H_R &= \frac{\hbar\nu}{g\beta} + \frac{Am}{g\beta} \end{aligned}\right\} \qquad (4.16)$$

in which g and A are evaluated for a particular θ and ϕ from (4.14) and (4.15). The number of times that this procedure generates a resonance field between H_x and $H_{(x+1)}$ is then histogrammed on a magnetic field array H_1, $H_2 \rightarrow H_n$. The complete histogram is the shape function S(H) (or powder pattern).

The powder pattern is now convoluted with an appropriate single crystal lineshape function. Essentially, each value $S(H)_1$, $S(H)_2$, $\rightarrow$ corresponding to H_1, H_2, $\rightarrow$ is multiplied by the appropriate normalized function to generate the smoothed absorption lines shown in the upper traces of Figure 4.2 (dashed lines).

The final step is to evaluate the first derivative of the absorption line, (Figure 4.2), for comparison with the expermental data.

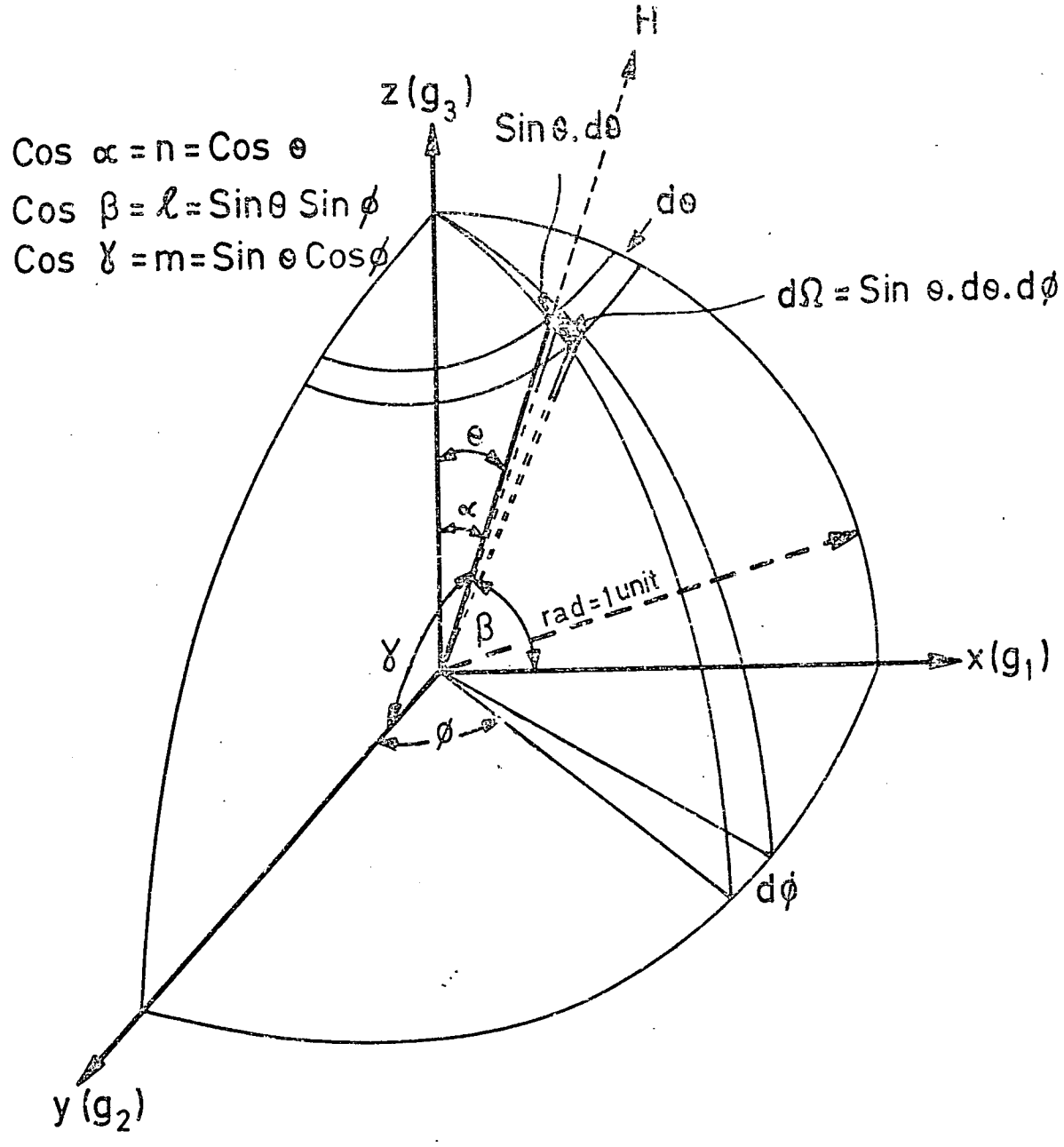

FIG. 4.4. Spherical geometry parameters employed in power pattern simulations.

4.1.8 Resonance Spectra of Amorphous Materials

A glassy material approximates to a polycrystalline or powdered material in that the principal axes of the paramagnetic site are randomly orientated with respect to the applied field. In addition, the basic randomness of the structure itself suggests a smooth distribution of the Hamiltonian parameters describing the site. We make the assumption in this work that there exists an identical ensemble of randomly oriented sites for each local environment. Then, the complete powder pattern is the sum of many individual patterns due to each individual site, i.e. each set of g and A parameters. Following this, the composite pattern is broadened with an isotropic single crystal line function and the first derivative taken. Figure 4.5 illustrates this process for an axially symmetric site with a distribution in the $g_{\parallel}$ parameter.

4.1.9 The Lineshape Functions

Other than instrumental sources of broadening the resonance line is broadened by two main mechanisms, spin-lattice interaction and spin-spin interaction.

Spin-lattice interactions are the means whereby the spin system reduces its spin temperature to equilibrium following the absorption of microwave power. The characteristic relaxation time for the process T_1 is related through the Uncertainty Principle to the linewidth $2\Delta H$ at half peak absorption by ,

$$\Delta H = \frac{h}{g\beta} \cdot \frac{1}{2\pi T_1}$$

and the lineshape associated with this process is the Lorentzian function ,

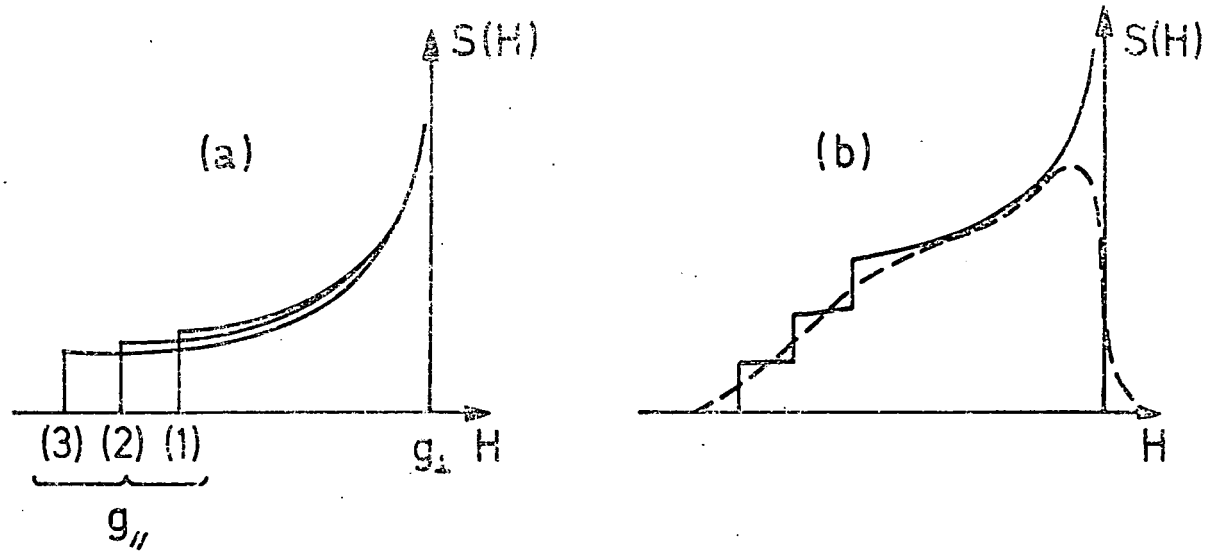

FIG. 4.5. Powder pattern shape functions for 3 sites with identical $g_{\perp}$ parameters but differing $g_{//}$ parameters. (a) Components of pattern.
(b) Total pattern (not to scale), with the effect of line broadening shown dotted.

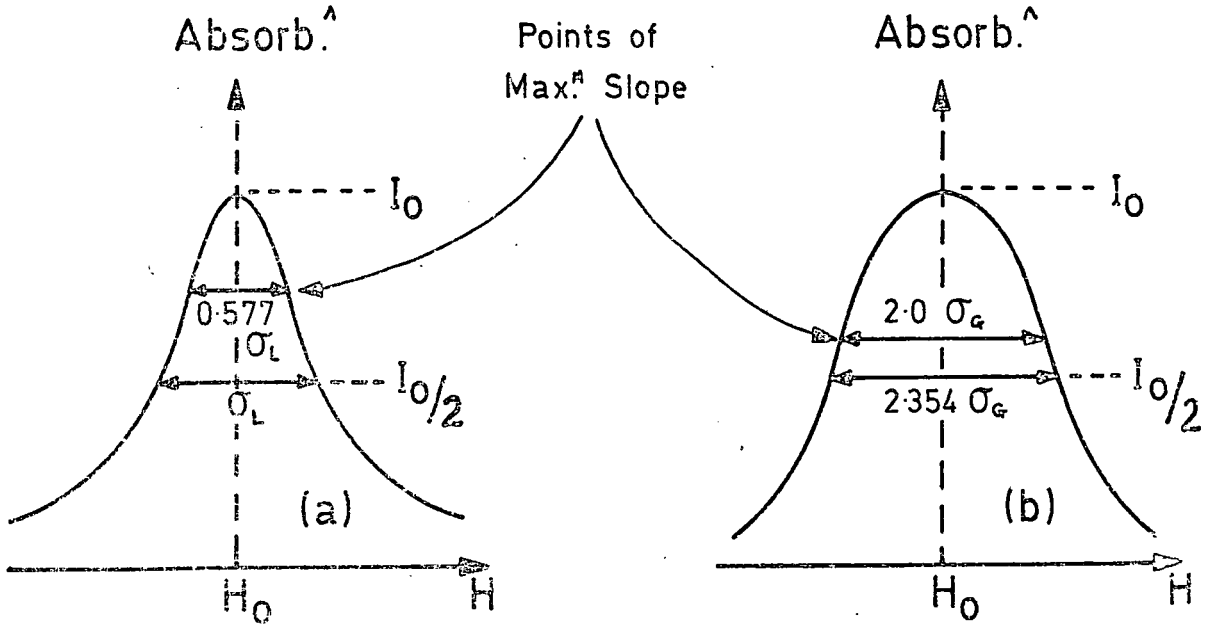

FIG. 4.5. Characteristic (a) Lorentzian
(b) Gaussian line shapes.

$$F(H_o - H) = \frac{1}{\pi} \frac{2/\sigma_L}{\left(2/\sigma_L\right)^2 \left(H_o - H\right) + 1} \qquad (4.17)$$

(the function is normalized i.e.

$$\int_o^\infty F(H_o - H)\, dH = 1$$

where the parameter σ_L is the width (magnetic field units) of the absorption line at half intensity, and H_o is the field at maximum absorption.

The spin-spin or dipolar broadening mechanism is a consequence of the local variations of magnetic field due to the individual dipole fields. The absorption line associated with this mechanism is the

$$G(H_o - H) = \frac{1}{\sqrt{2\pi}} \cdot \frac{1}{\sigma_G} \cdot \exp\left[- \frac{(H_o - H)^2}{2(\sigma_G)^2} \right] \qquad (4.18)$$

where now the parameter σ_G is the half width of the line at maximum slope.

Relating the dipolar process to a relaxation time T_2 we have, (4.2,4.5,4.7,4.8):

$$\sigma_L = \frac{h}{g\beta} \cdot \frac{1}{\pi T_1} \qquad (4.19)$$

$$\sigma_G = \frac{h}{g\beta} \cdot \frac{1.254}{2\pi T_2} \qquad (4.20)$$

The characteristic shapes of the functions, and the significance of the linewidth parameters σ_L and σ_G are shown in Figure 4.5.

4.2 Experimental Results

Part 1: Spectra from the glass samples

After γ irradiation all of the glass samples gave a spectrum consisting essentially of two lines, the first originating from a hole centre ($g > 2.0023$), and the second an electron centre identified as a Ti^{3+} ion.

4.2.1 The Ti^{3+} spectra

Figure 4.6 shows the experimental spectra from the range of glass compositions studied, the dominant lines being marked 'hole centre' and 'Ti^{3+}'. The spectrum from glass 1 is not included because, containing no TiO_2, it does not show a Ti^{3+} line.

After correcting for spectrometer gain, sample quantity, etc., the Ti^{3+} spectra of the untreated glasses were found to be almost identical throughout the range of compositions. Slight quantitative differences are present, as indicated in Table 4.1, where the g values of the characteristic points of the line are tabulated.

Within any given composition, pre-crystallization heat treatment has no effect on the g values, the form, or the intensity of the Ti^{3+} line. This is shown in Figure 4.7 where spectra from glass 4 exemplify this point.

In essence therefore, throughout the range of compositions and pre-heat treatments the Ti^{3+} line remains constant, and we next consider the g values and site symmetry associated with this line by comparing the spectrum from glass 3 with computer simulations of the line.

4.2.2 Simulations of the Ti^{3+} line in glass 3

Figures 4.8 and 4.9 show trial simulations assuming an axially symmetric site for the titanium ion, and employing g values derived from the peaks of the experimental first derivative.

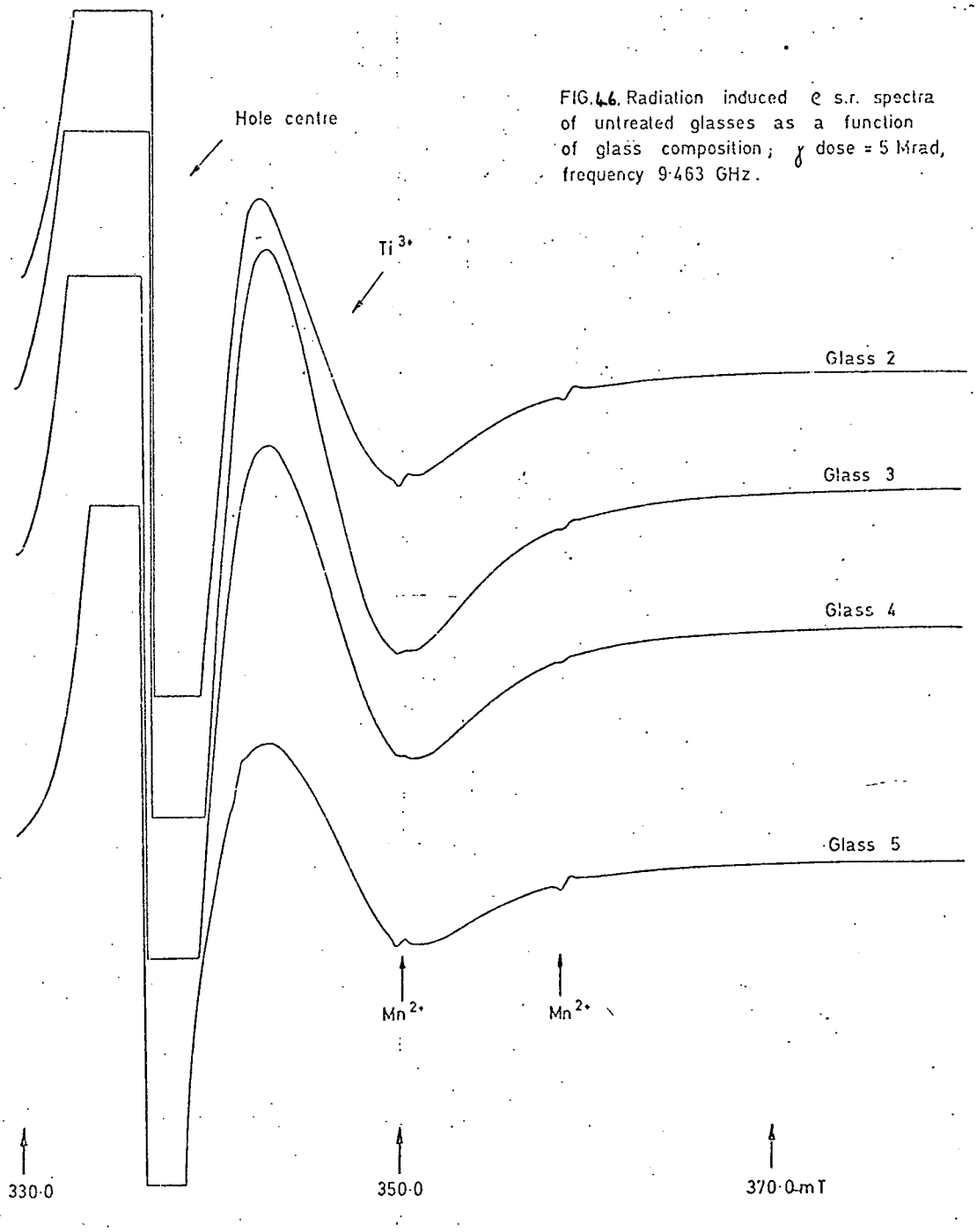

FIG. 46. Radiation induced e.s.r. spectra of untreated glasses as a function of glass composition; γ dose = 5 Mrad, frequency 9·463 GHz.

TABLE 4.1 :- THE g VALUES OF THE Ti^{3+} LINE ASSOCIATED WITH :-

a) The positive peak (G1)
b) The base line crossing (G2) } i.e.
c) The negative peak (G3)

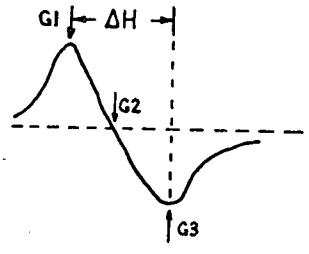

① SPECTRA FROM GLASS SAMPLES :-

Sample	G1	G2	G3	ΔH (pk-pk width)
Glass 2	1·975(0)	1·953(1)	1·929(8)	78 gauss.
Glass 3	1·973(7)	1·951(3)	1·928(5)	78 gauss.
Glass 4	1·971(7)	1·948(2)	1·926(6)	78 gauss.
Glass 5	1·971(2)	1·947(2)	1·924(9)	80 gauss.

② SPECTRA FROM CERAMIC SAMPLES :-

SAMPLE	Crystalliz^{n} Temp.	G1	G2	G3	ΔH
GLASS 2	1000°C	1·958(9)	1·946(7)	1·911(4)	86 gauss
"	1200°C	1·959(8)	1·944(7)	1·911(6)	87 "
GLASS 3	1000°C	1·959(0)	1·946(6)	1·911(6)	85·5 "
"	1200°C	1·960(1)	1·944(6)	1·911(9)	87 "
GLASS 4	1000°C	1·960(7)	1·944(7)	1·923(4)	67 "
"	1200°C	1·959(9)	1·943(9)	1·911(8)	87 "
GLASS 5	1000°C	1·960(2)	1·943(8)	1·922(9)	67 "
"	1200°C	1·960(4)	1·942(9)	1·911(4)	88·5 "

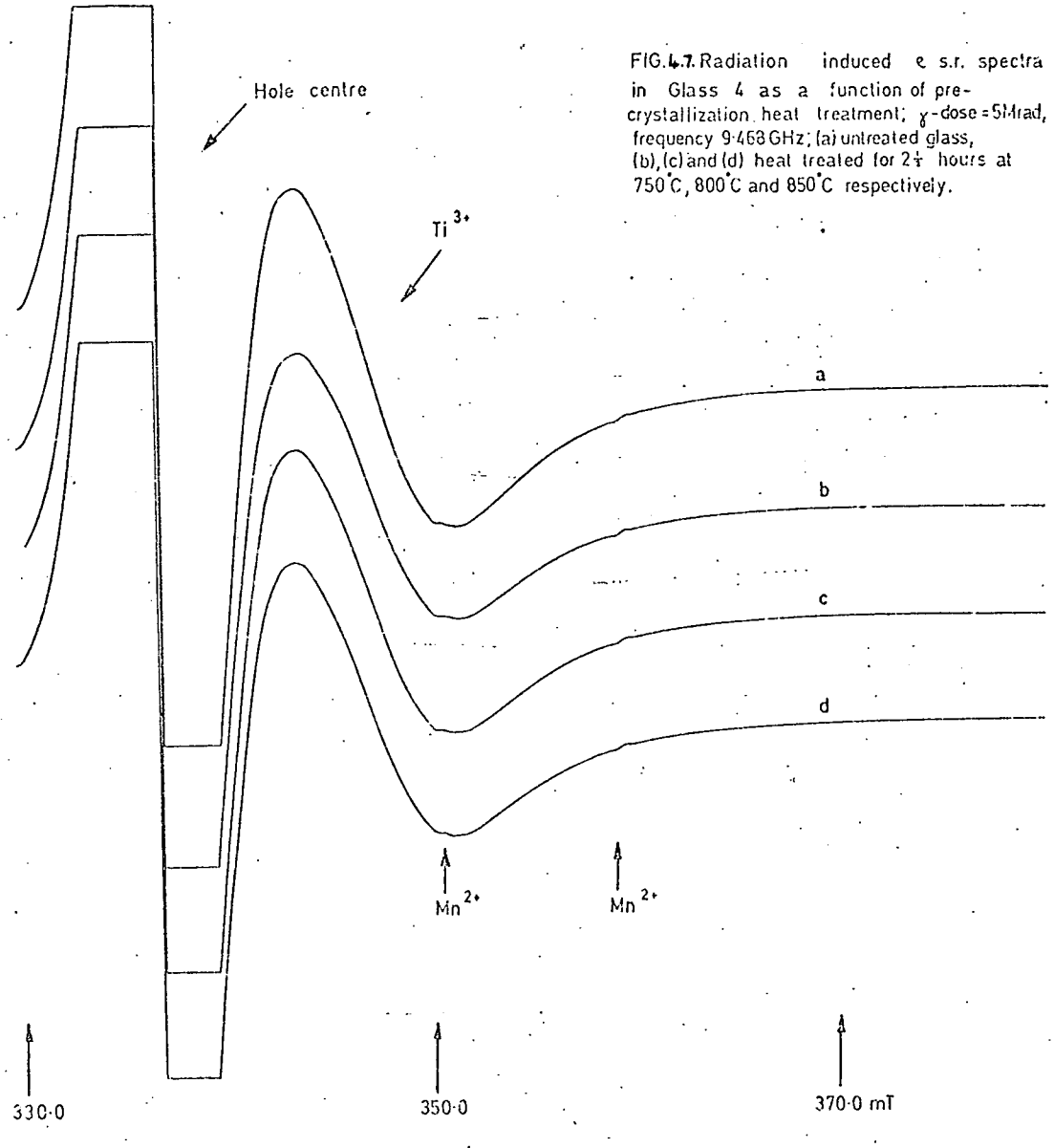

FIG. 4.7. Radiation induced e s.r. spectra in Glass 4 as a function of pre-crystallization heat treatment; γ-dose = 5 Mrad, frequency 9·468 GHz; (a) untreated glass, (b), (c) and (d) heat treated for 2½ hours at 750°C, 800°C and 850°C respectively.

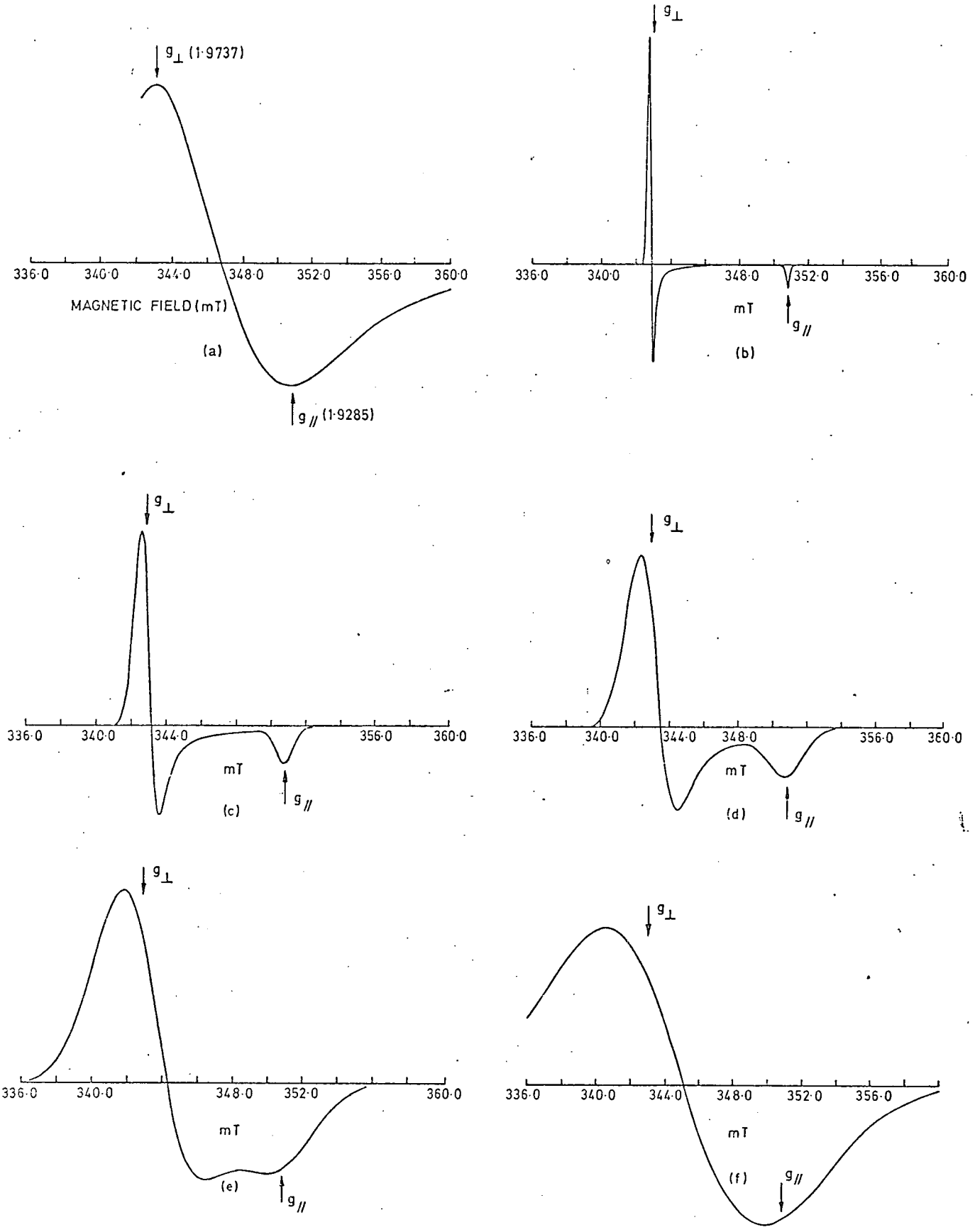

FIG. 4.8. Computer simulations of the Ti^{3+} spectrum in Glass 3. The field axis is plotted for a frequency of 9·472 GHz; (a) experimental spectrum, (b),(c),(d),(e), and (f) simulations with σ_G = 1gauss, 5 gauss, 10 gauss, 20 gauss, and 40 gauss respectively. Axial symmetry is assumed; the g values employed in the accompanying simulations are derived from the points shown on the experimental spectrum.

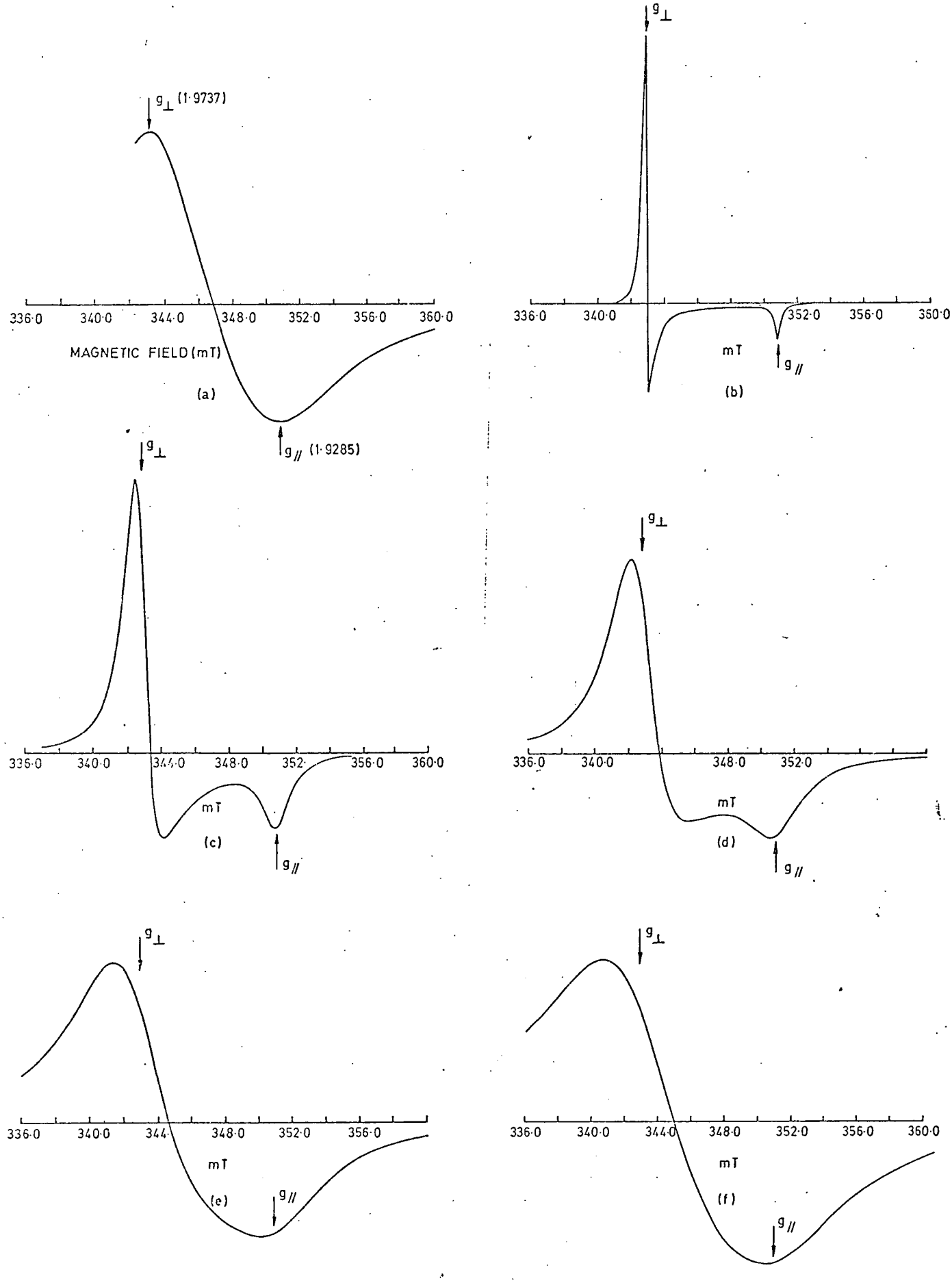

FIG. 4.9. Computer simulations of the Ti^{3+} spectrum in Glass 3. The field axis is plotted for a frequency of 9·472 GHz; (a) experimental spectrum, (b), (c), (d), (e) and (f), simulations with σ_L = 4 gauss, 20 gauss, 40 gauss, 80 gauss, and 120 gauss respectively. Axial symmetry is assumed; the g values employed in the simulations are derived from the points shown on the experimental spectrum.

The Gaussian and Lorentzian line functions generate spectra which are broadly similar with some features discernably different, notably the slower return to the base line of the Lorentzian derivatives. It is precisely this feature of the spectrum, i.e. the return to the base line from the peak associated with $g_{\perp}$, which allows the determination of the most suitable lineshape function. Unfortunately, because of the hole centre, this feature is lost from the experimental spectrum.

Simulations assuming an orthorhomic titanium site are shown in Figure 4.10. In this case only the Gaussian broadened spectra are shown.

At low and moderate values of the line broadening parameters σ_G and σ_L, the spectra from axial and orthorhombic sites are quite different, but as σ_G and σ_L are increased the simulations become remarkably similar. It is also apparent that at high values of σ_G and σ_L the 'peaks' of the derivative cease to correspond to $g_{\perp}$ and $g_{\parallel}$ (or g_1 and g_3).

Figure 4.11 shows the best fit simulations for both symmetries after adjustment of the g values to give peaks and base line crossings corresponding to the field positions of these features on the experimental spectrum. It is clearly impossible on the basis of this figure to be certain of the site symmetry, indeed, even the most suitable line shape function cannot be determined. The feature which is consistent across the best fit spectra is the smaller 'negative' peak of the experimental trace when compared with the simulations.

Figures 4.12 and 4.13 show the effects on the spectrum of a distribution in the $g_{\parallel}$ or g_3 parameters. The discrepancy in the experimental and simulation peak heights is eliminated, although the high field 'tail' cannot be reproduced exactly. Further simulations were not attempted, it now being clear that the broad, featureless Ti^{3+} line could be simulated with reasonable accuracy by various sets of parameters, no one set of which could be given precidence over the others.

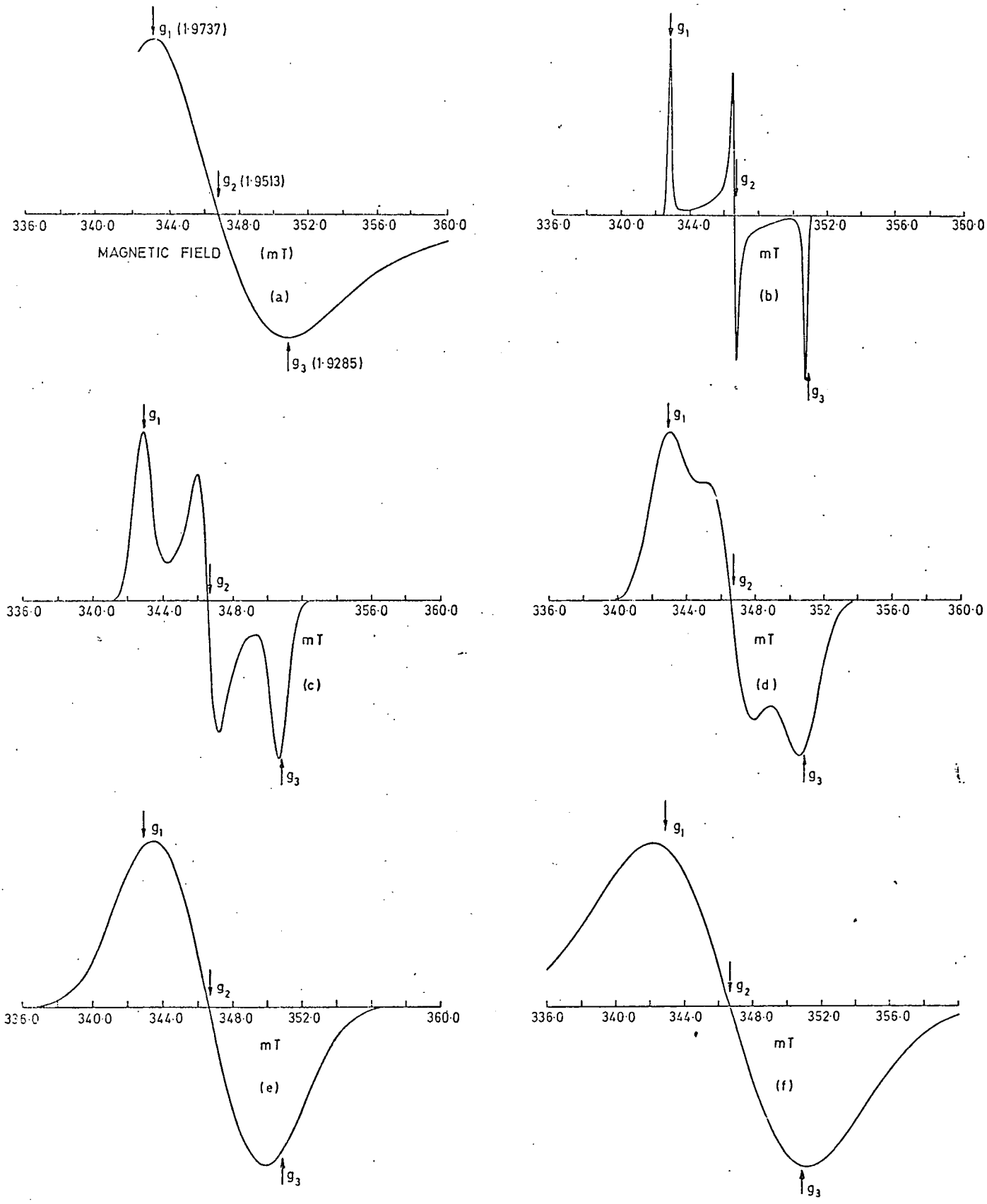

FIG. 4.10. Computer simulations of the Ti^{3+} spectrum in Glass 3. The field axis is plotted for a frequency of 9·472 GHz; (a) experimental spectrum, (b), (c), (d), (e) and (f) simulations with σ_G = 1 gauss, 5 gauss, 10 gauss, 20 gauss, and 40 gauss respectively. Orthorhombic symmetry is assumed; the g values employed in the simulations are derived from the points shown on the experimental spectra.

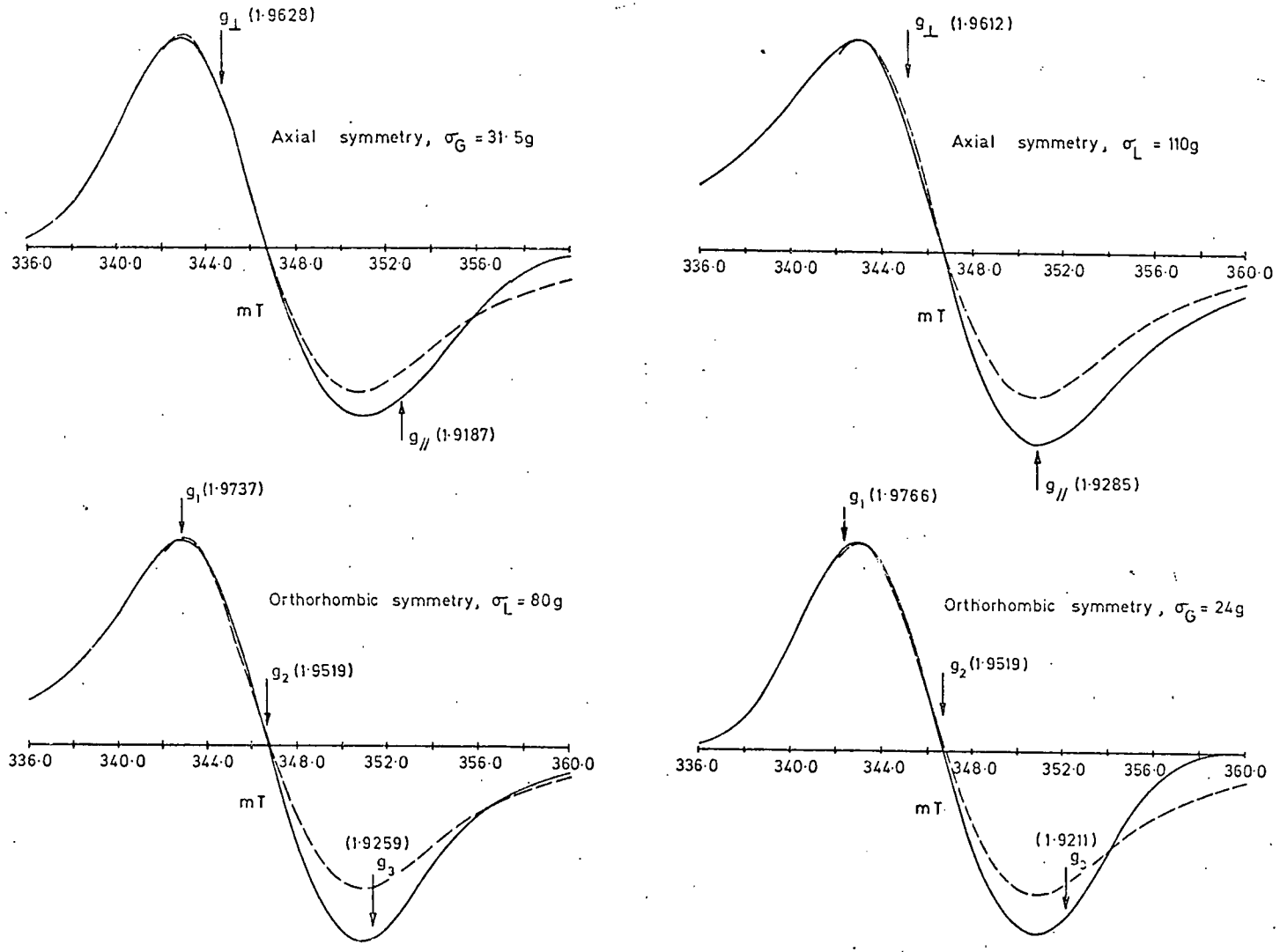

FIG. 4.11. Comparison of experimental Ti^{3+} spectrum with best fit computer simulations. The field axis is plotted for a frequency of 9.472 GHz ; (key, — — experimental, —— simulation)

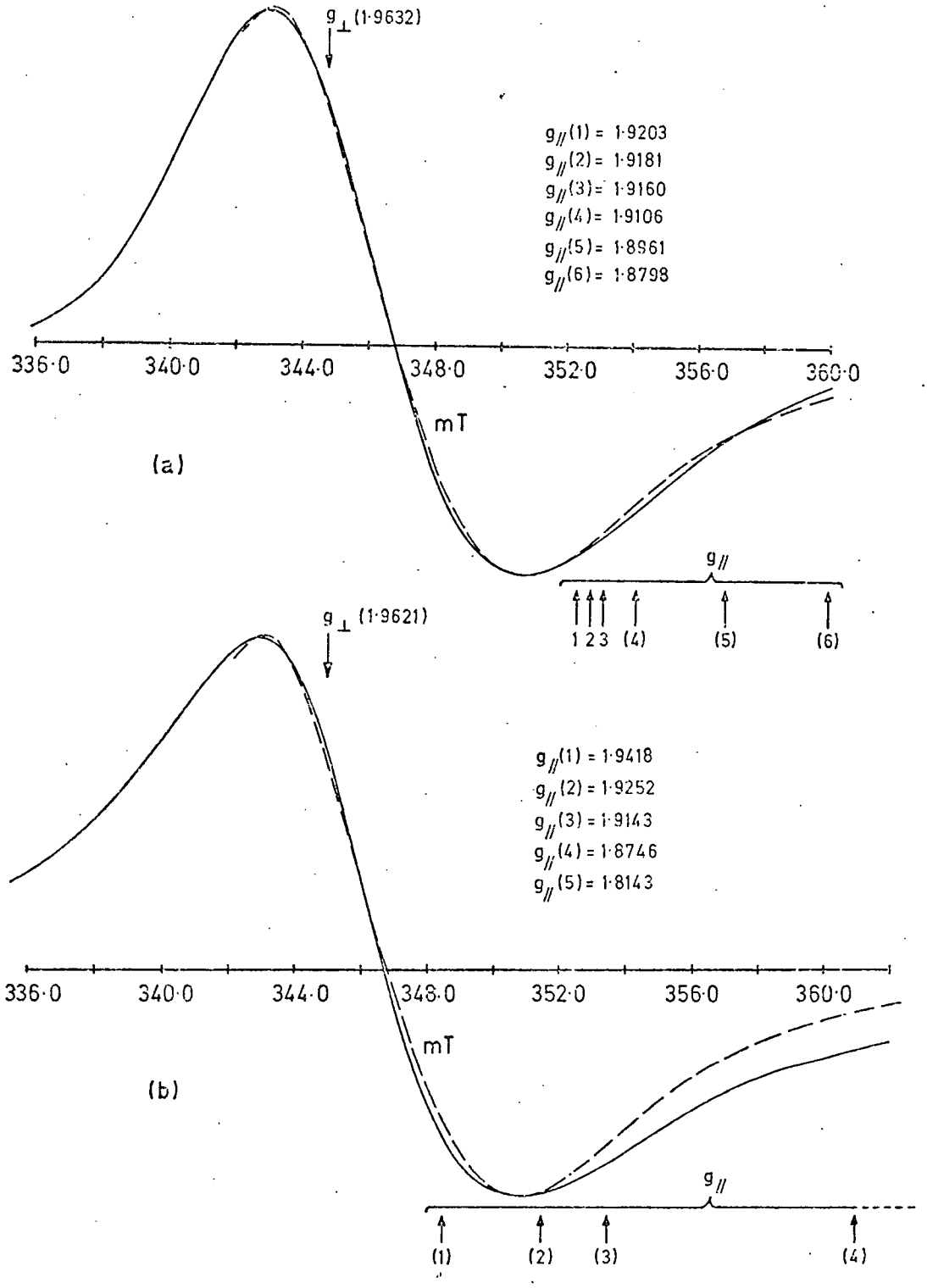

FIG. 4.12. Comparison of experimental Ti^{3+} spectrum with best fit simulations using distributed values for $g_{//}$. (— — experimental, —— simulation)
(a) axial symmetry, $\sigma_G = 31g$; (b) axial symmetry, $\sigma_L = 105g$. The field axis is plotted for a frequency of 9·472 GHz.

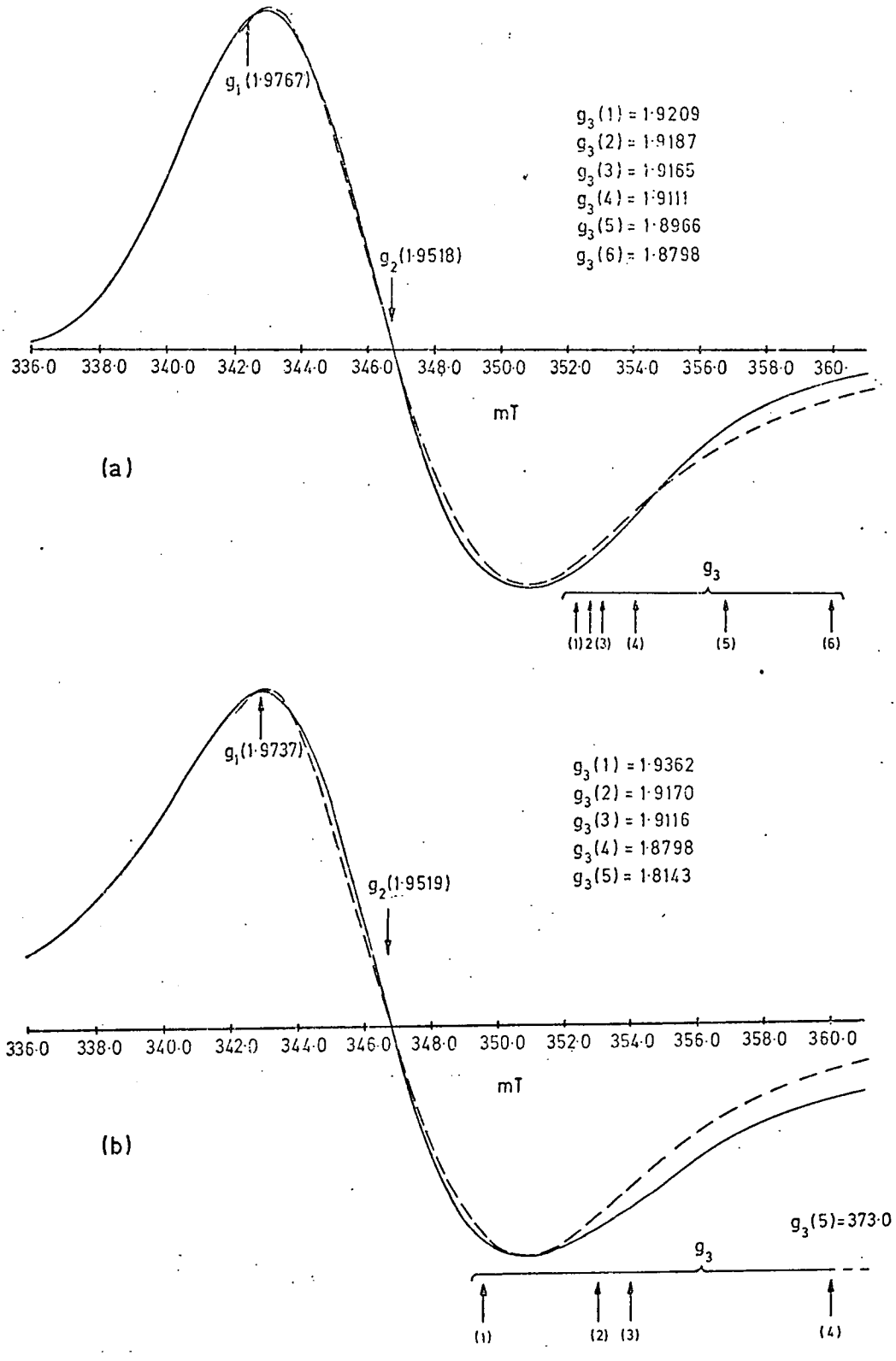

FIG. 4.13. Comparison of experimental Ti^{3+} spectrum with best fit simulations using distributed values for g_3. (a) orthorhombic symmetry σ_G = 24g; (b) orthorhombic symmetry σ_L = 80g. The field axis is plotted for a frequency of 9·472 GHz; (key, --- experimental —— simulation)

4.2.3 The Hole Centre Spectrum

The hole centres from each of the glass compositions before heat treatment are shown in Figure 4.14. Unlike the Ti^{3+} line, significant differences are present in the hole centres of the different compositions. Glasses 1 and 2 have identical spectra which are in most ways comparable with the glass 3 spectrum, but on moving to glasses 4 and 5 the spectrum is noticeably changed.

Within a given glass composition the hole spectrum is unaltered by pre-crystallization heat treatments. This is illustrated in Figure 4.15 wherein the spectra from samples of glass 4 are represented.

Consequently, there are two basic lineshapes to account for, one associated with the low TiO_2 glasses and one with the higher TiO_2 glasses.

4.2.4 Simulations of the glass hole centres

The base glass, (glass 1), centre is plotted on a reduced field axis in Figure 4.16 and 4.17 along with trial simulations employing both lineshape functions. It is clear that in particular a Lorentzian function of suitable half-width, combined with a correct choice of g_1 and g_2, could give a reasonable fit to the portion of the line below the base line, but that no combination of parameters would adequately account for the line shape above the base line. A reasonable fit to the experimental spectrum could only be achieved by greatly distributing the g_3 parameter, (combined with a very slight distribution of g_2). The best fit simulation and its associated parameters is shown in Figure 4.18.

The spectrum of the 10% TiO_2 sample (glass 5), being typical of the high TiO_2 (5% and 10%) hole centre spectrum, is plotted on a reduced field axis in Figure 4.19, and accompanied by trial simulations; the g_2 value was chosen by inspection of the second derivative of the absorption line.

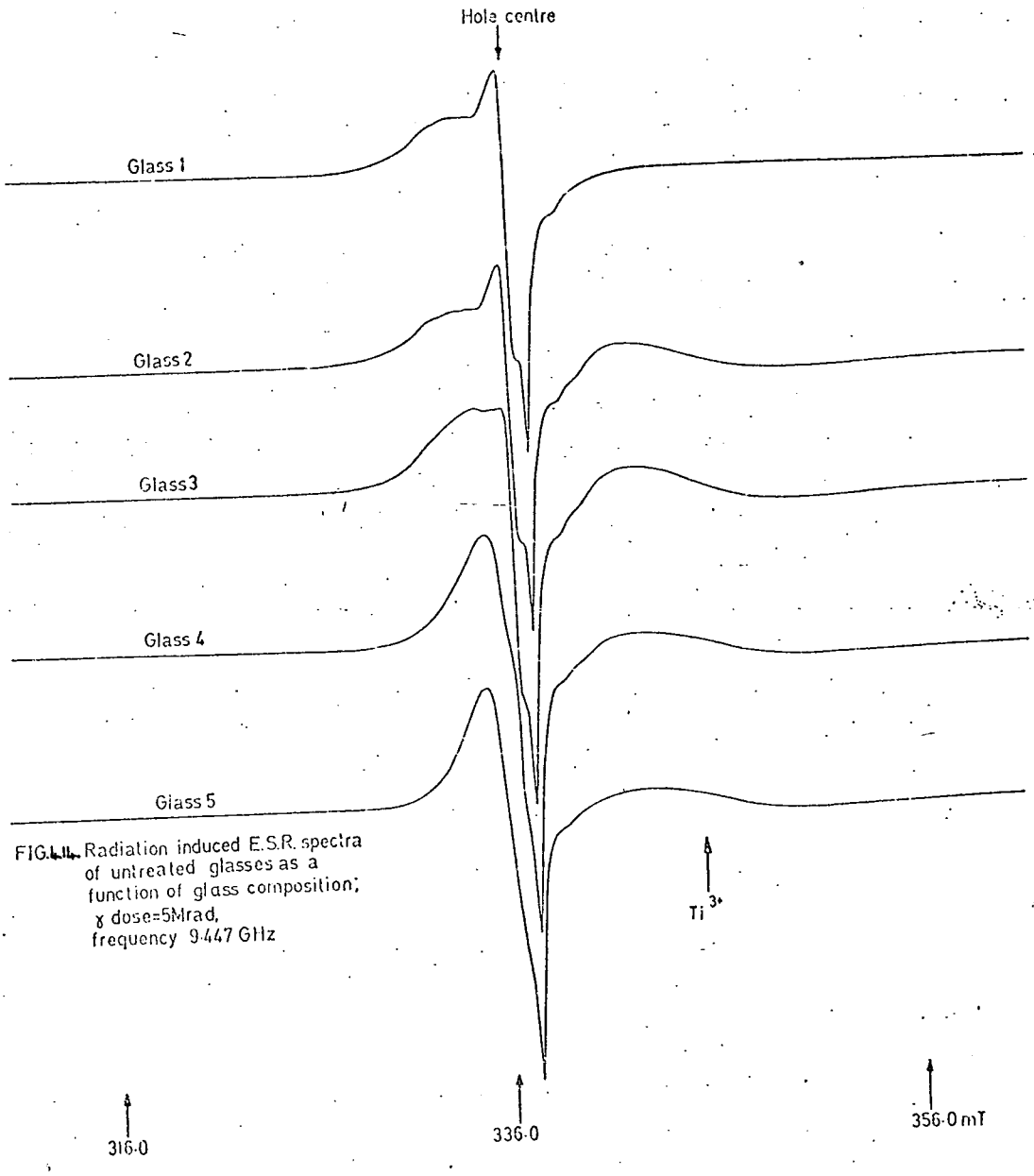

FIG. 4.14. Radiation induced E.S.R. spectra of untreated glasses as a function of glass composition; γ dose=5Mrad, frequency 9·447 GHz

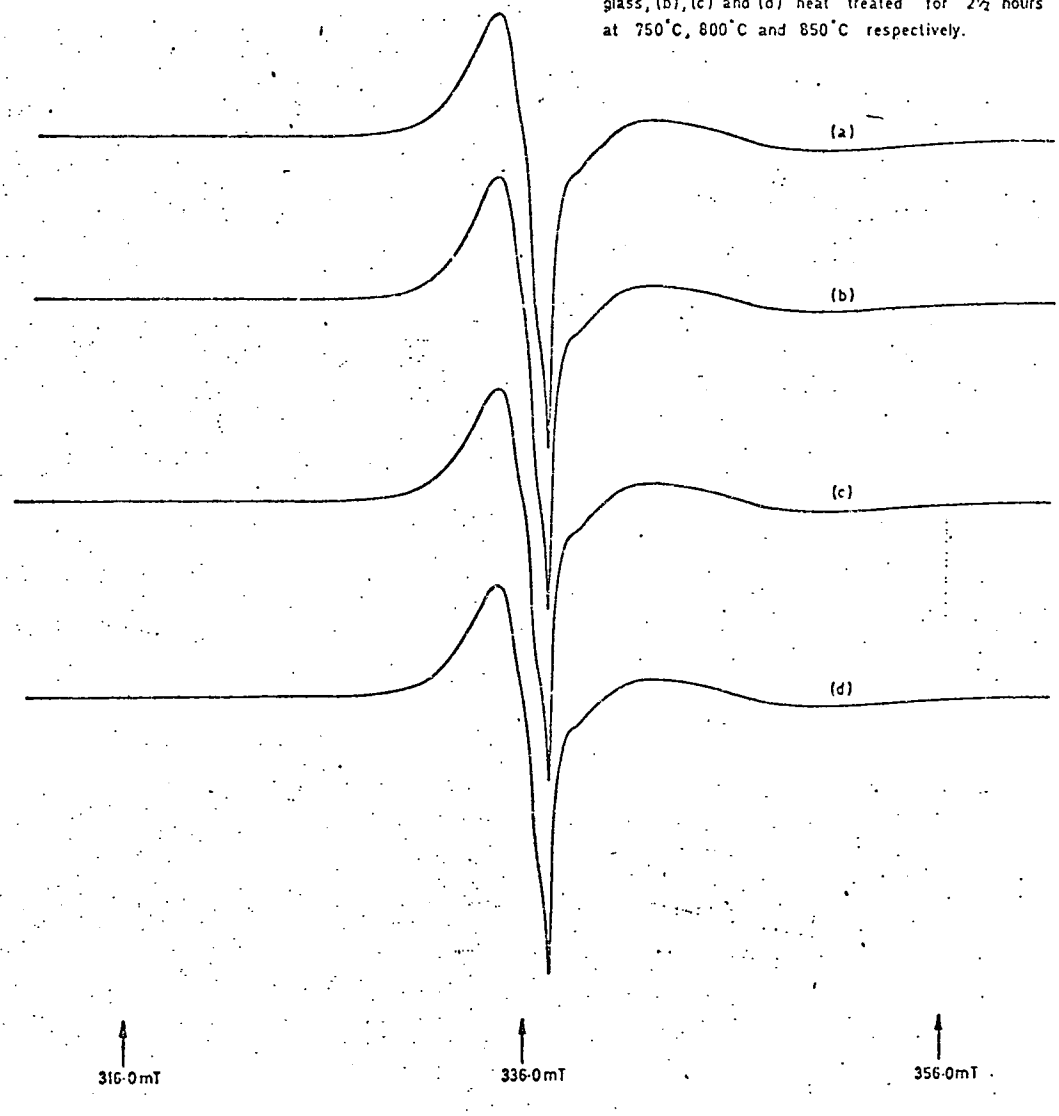

FIG. 15 Radiation induced e.s.r. spectra in Glass 4 as a function of pre-crystallization heat treatment; γ-dose = 5 Mrad, frequency 9·468 GHz; (a) untreated glass, (b), (c) and (d) heat treated for 2½ hours at 750°C, 800°C and 850°C respectively.

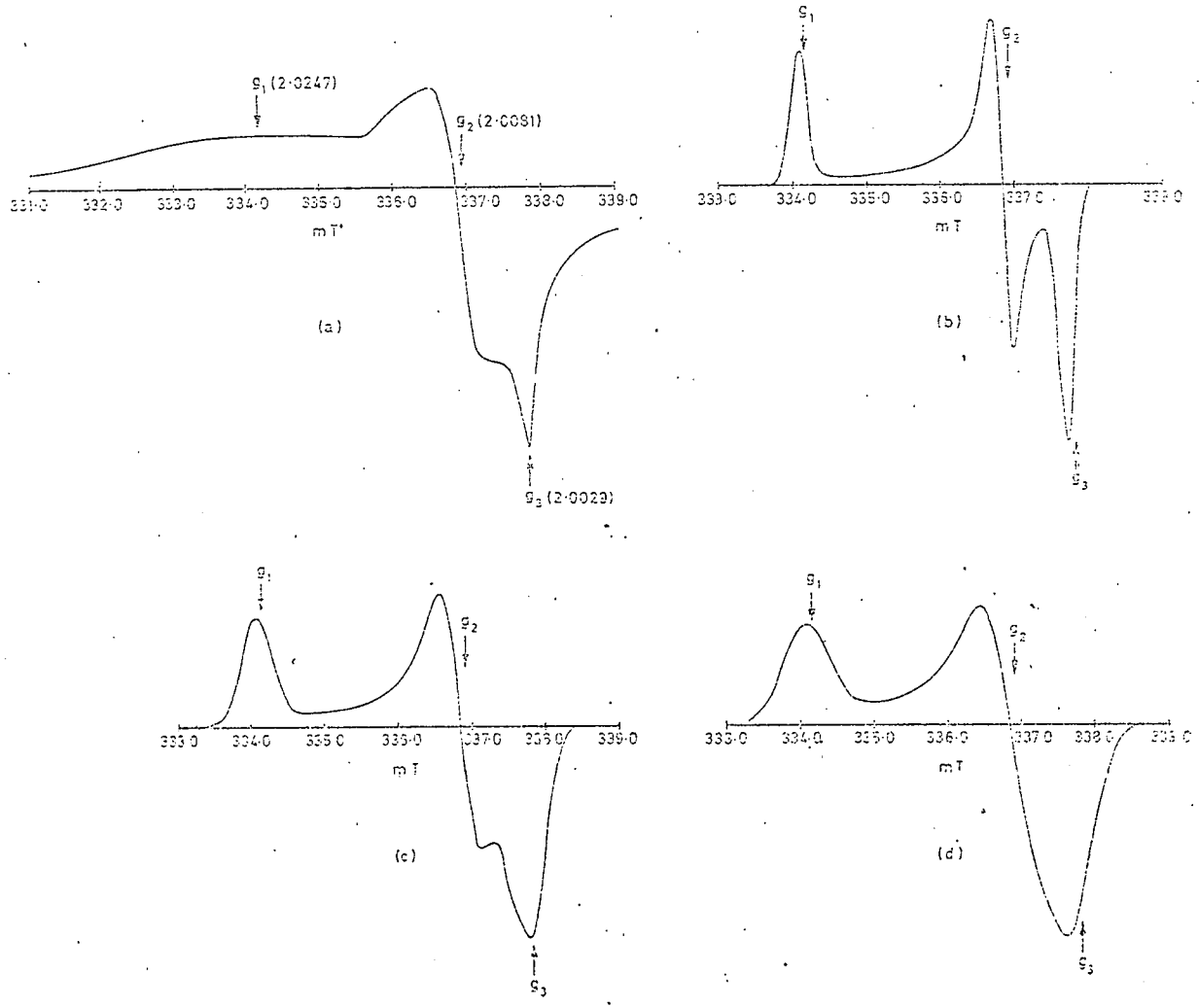

FIG.4.16. Computer simulations of the Hole Centre in the Base Glass. The field axis is plotted for a frequency of 9·47 GHz ; (a) experimental spectrum , (b), (c) and (d) simulations with σ_G = 1 gauss, 2 gauss, and 3 gauss respectively. The g-values marked on the experimental spectrum are those used for the accompanying simulations.

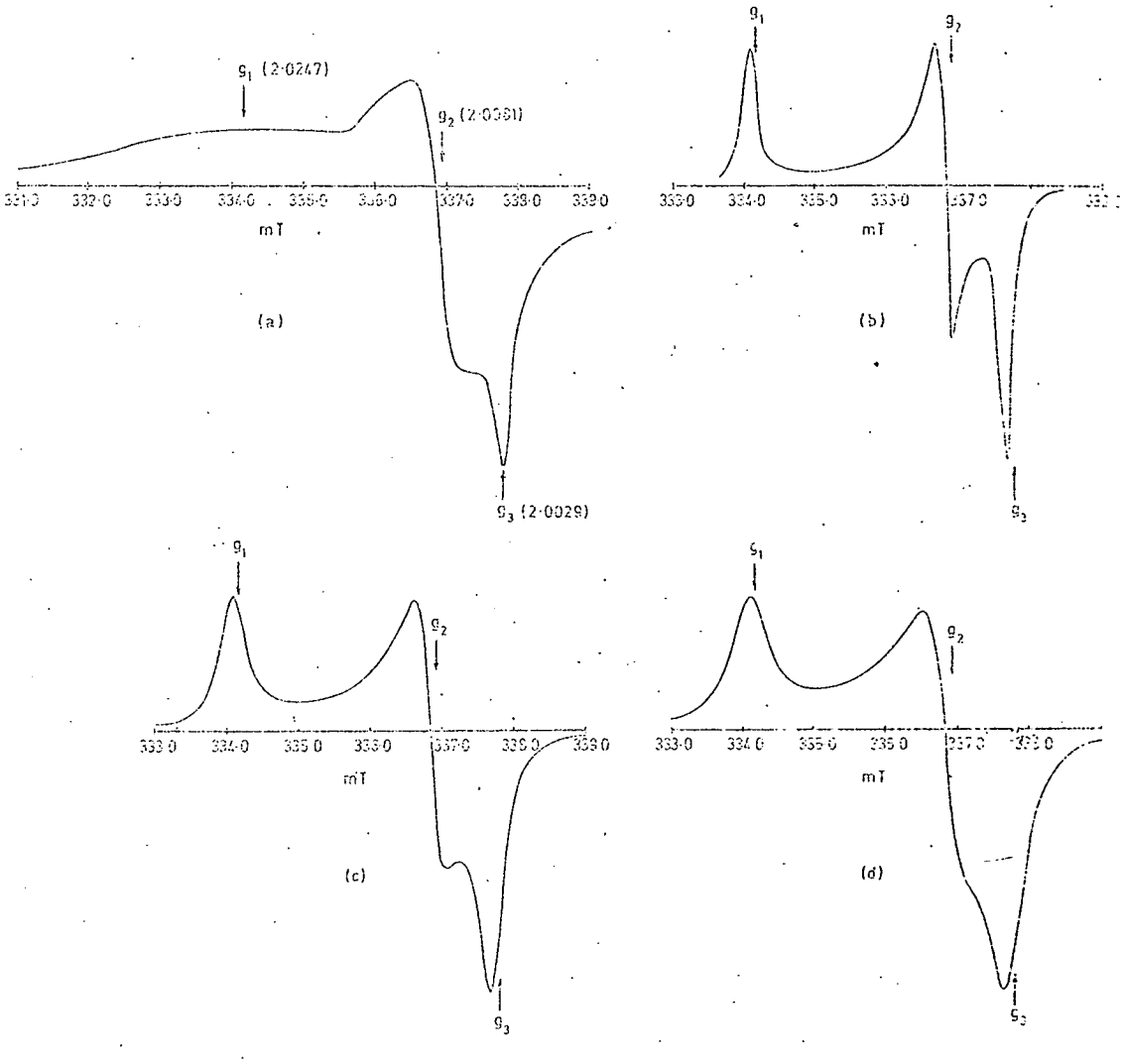

FIG. **4.17.** Computer simulations of the Hole Centre in the Base Glass. The field axis is plotted for a frequency of 9·47 GHz ; (a) experimental spectrum, (b), (c) and (d) simulations with σ_L = 2 gauss, 4 gauss and 6 gauss respectively. The g-values marked on the experimental spectrum are those used for the accompanying simulations.

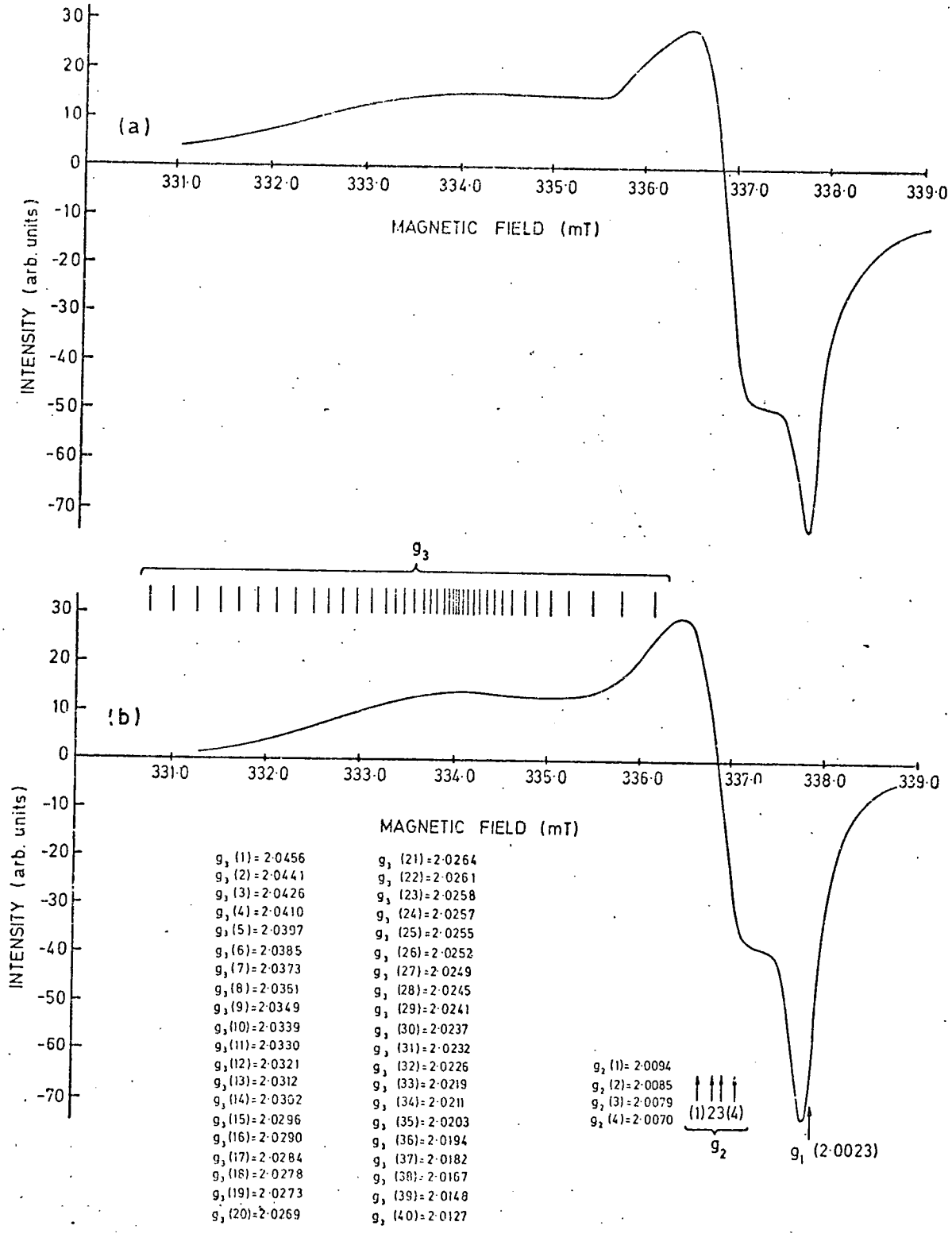

FIG. 4.18. Comparison of (a) experimental hole spectrum in base glass and (b) best fit computer simulated spectrum combining a distributed g_3 with $\sigma_L = 4{\cdot}2g$. The field axis is plotted for a frequency of 9·470 GHz.

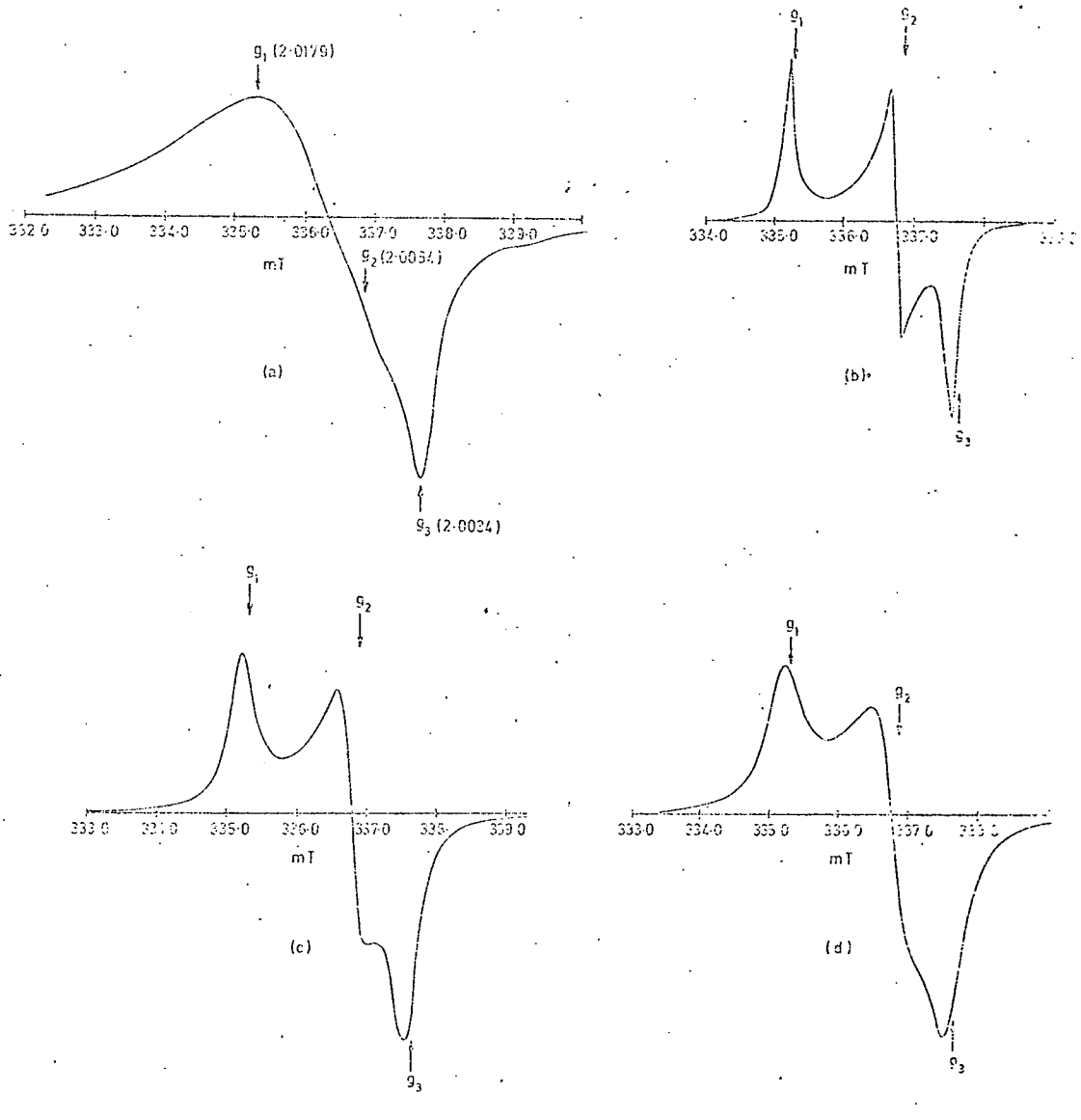

FIG. 4.9. Computer simulations of the Hole Centre in Glass containing 10wt % TiO_2, (Glass 5). The field axis is plotted for a frequency of 9·47 GHz; (a) experimental spectrum, (b), (c) and (d) simulations with σ_L = 2 gauss, 4 gauss and 6 gauss respectively. The g-values marked on the experimental spectrum are those used for the accompanying simulations.

Again, the simulations suggest that no combination of g_1, g_2 and g_3 combined with either lineshape function could adequately account for the observed spectrum. In this instance it was necessary to invoke significant distributions of both g_2 and g_3 in order to account for the experimental spectrum. The simulation and best fit parameters are shown in Figure 4.20.

Thus the hole spectrum in the low TiO_2 glasses derives from a centre with two reasonably well defined principal g values, and one rather ill defined g value. On the other hand, the spectrum in the high TiO_2 glasses is a consequence of a centre with one well defined g value, (identical to one of the principal g values in the low TiO_2 glasses), and two much less well defined g values.

The glass 3 spectrum, not explicitly considered here, is characterised by the absence of the positive peak, although in other details it more closely resembles the low TiO_2 line. This is a consequence of a slight broadening of g_2, although not nearly to the extent found in the high TiO_2 glasses.

Part 2 Spectra from the crystallized, i.e. ceramic samples

After γ-irradiation two lines dominate the spectrum from these samples. The extremities of the lines merge, with one line displaced slightly below and one line slightly above the free spin resonance field. The high field line is absent in the glass 1 composition, and only appears upon the addition of 0.2% TiO_2, i.e. in glass 2, and consequently the two lines are designated as a 'hole centre' and a 'Ti^{3+} centre.'

4.2.5 The Ti^{3+} spectra

The spectra from each glass composition, with and without pre-crystallization heat treatment, and crystallized for both two and twenty

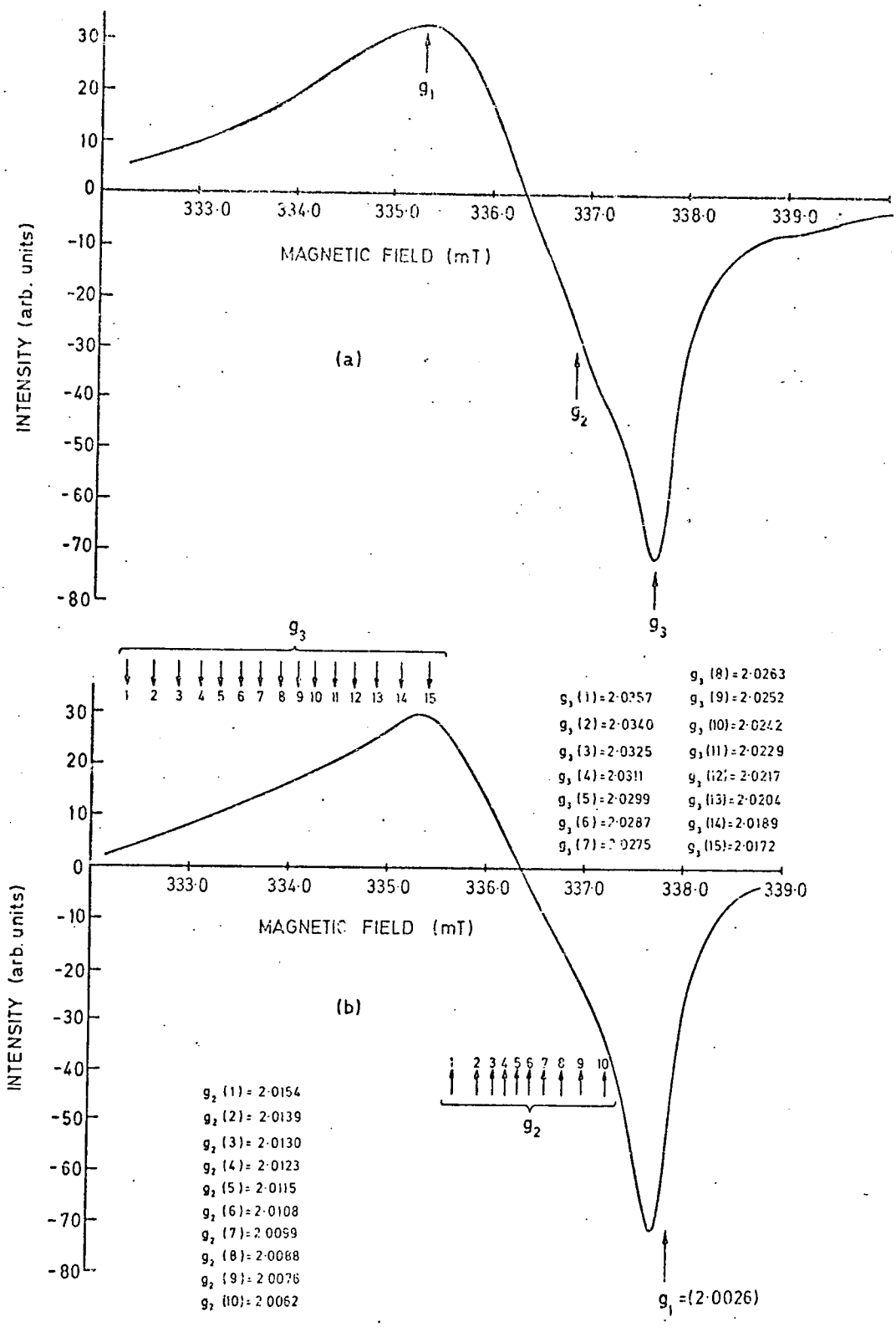

FIG. 4.20. Comparison of (a) experimental hole spectrum in 10 wt. % TiO_2 glass and (b) best fit computer simulated spectrum combining a distributed g_2 and g_3 with $\sigma_L = 4{\cdot}4\,g$. The field axis is plotted for a frequency of 9·47 GHz.

hours at both 1000°C and 1200°C were studied. Specimens of glasses 2 and 3 crystallized for 2 hours at 1000°C exhibited only surface crystallization, and spectra from these samples under the above conditions are not considered. Before analysing the spectra, we consider the effect of the above variables on the Ti^{3+} spectrum.

The spectra from the bulk crystalline specimens of glasses 2 and 3, crystallized at 1000°C for 20 hours are typified by the spectra of Figure 4.21. The figure suggests, and closer analysis confirms, that the pre-crystallization heat treatments have no effect on the spectrum.

Glasses 2 and 3 are bulk crystalline after only 2 hours at 1200°C, and Figure 4.22 shows spectra from samples of glass 3, (as typical of both glasses), with varying pre-heat treatments and crystallization periods. Again, the figure suggests that neither of these variables materially affect the spectrum, and closer analysis shows this to be true, although small variations between the spectra of samples crystallized at 1000°C and 1200°C are present.

Specimens of glasses 4 and 5 are bulk crystalline after 2 hours at both 1000°C and 1200°C. Figure 4.23 shows spectra from glass 4, (as typical of both compositions), crystallized at 1000°C for 2 and 20 hours, with and without pre-heat treatment. After allowing for spectrometer gain and sample quantity, analysis shows that the line shape and position are unaltered by either pre-heat treatment or crystallization period, but clearly the form of the line differs from that of the low titania specimens crystallized at the same temperature.

The spectra from glasses 4 and 5 crystallized at 1200°C are typified by Figure 4.24, where it is yet again apparent that the shape and position of the resonance line is independent of the pre-heat treatment or crystallization period. Compared with the low TiO_2 1200°C line there is a discerable change in the form of the high TiO_2 line, but not to the extent

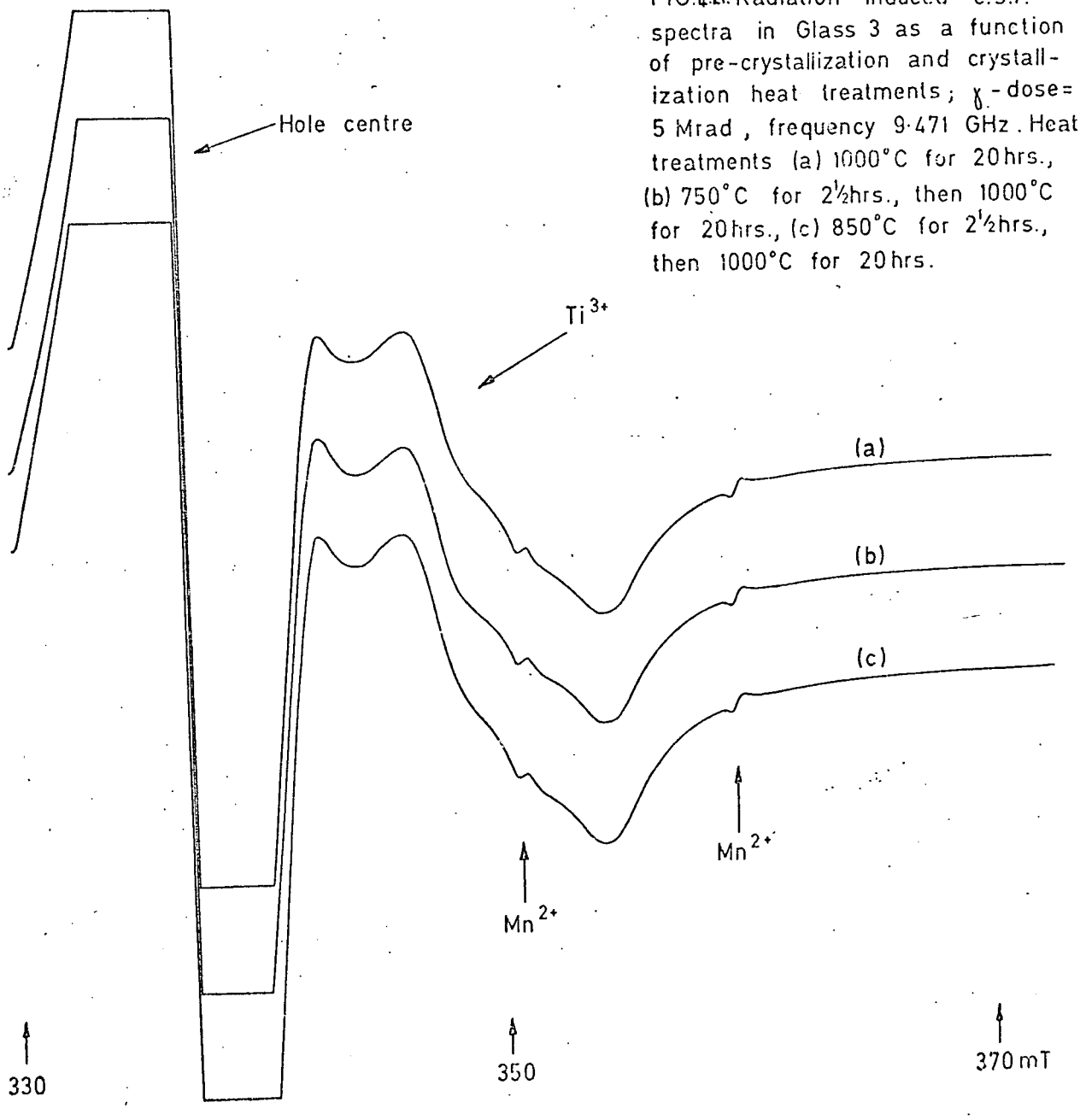

FIG.4.21. Radiation induced e.s.r. spectra in Glass 3 as a function of pre-crystallization and crystallization heat treatments; γ-dose = 5 Mrad, frequency 9·471 GHz. Heat treatments (a) 1000°C for 20 hrs., (b) 750°C for 2½hrs., then 1000°C for 20 hrs., (c) 850°C for 2½hrs., then 1000°C for 20 hrs.

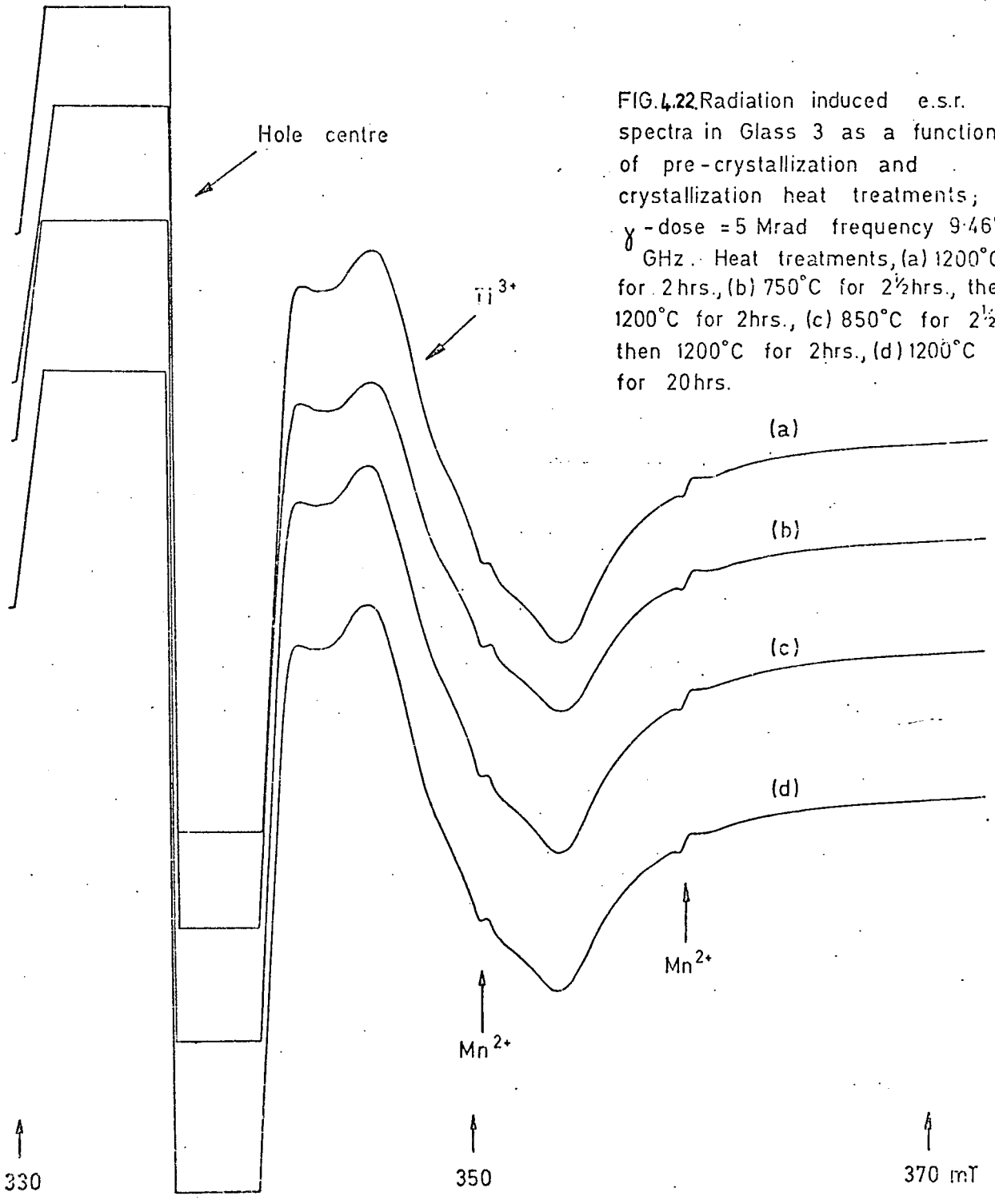

FIG. 4.22. Radiation induced e.s.r. spectra in Glass 3 as a function of pre-crystallization and crystallization heat treatments; γ-dose = 5 Mrad frequency 9·467 GHz. Heat treatments, (a) 1200°C for 2 hrs., (b) 750°C for 2½hrs., then 1200°C for 2hrs., (c) 850°C for 2½hrs. then 1200°C for 2hrs., (d) 1200°C for 20hrs.

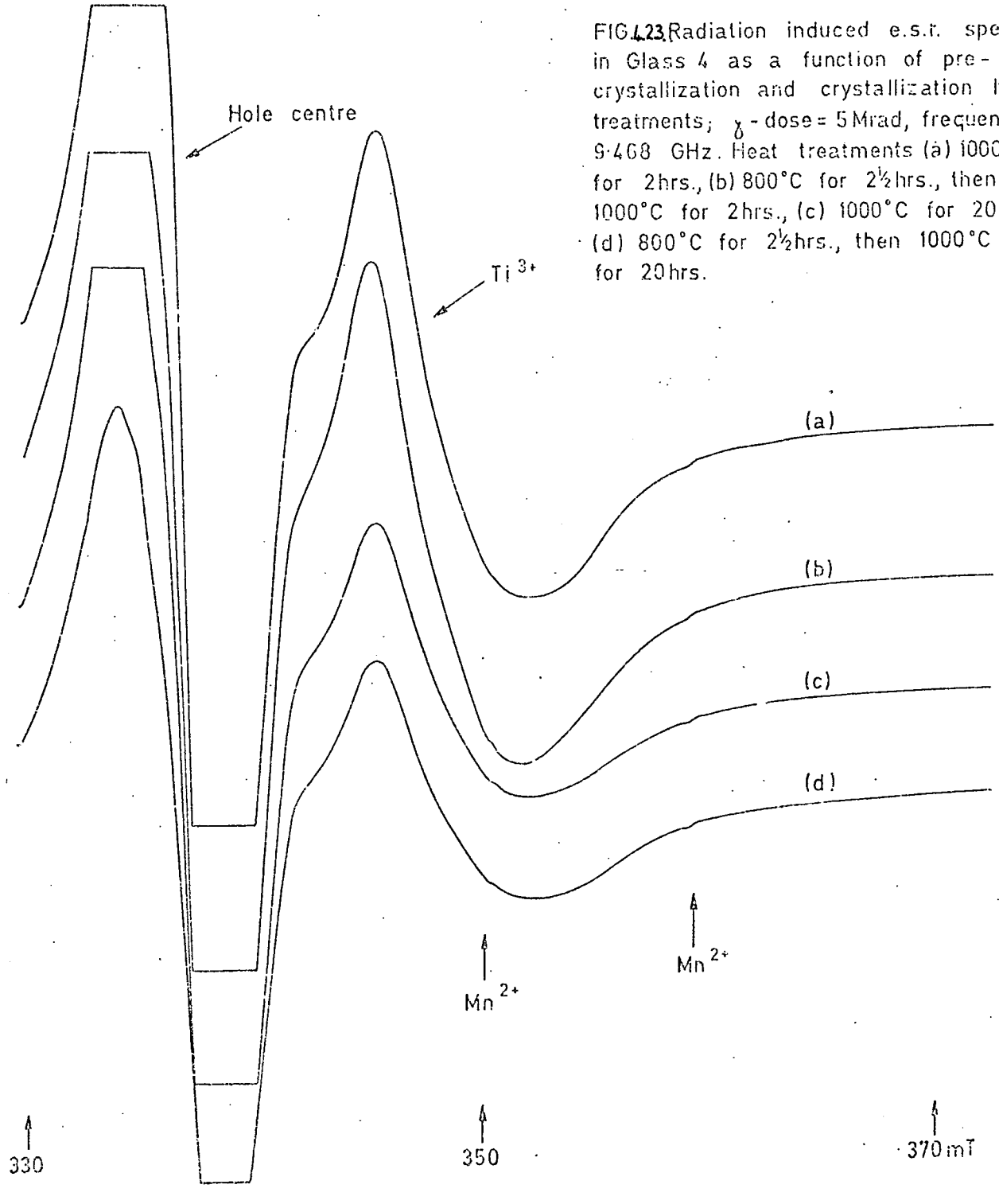

FIG 4.23 Radiation induced e.s.r. spectra in Glass 4 as a function of pre-crystallization and crystallization heat treatments; γ-dose = 5 Mrad, frequency 9·468 GHz. Heat treatments (a) 1000°C for 2 hrs., (b) 800°C for 2½ hrs., then 1000°C for 2 hrs., (c) 1000°C for 20 hrs., (d) 800°C for 2½ hrs., then 1000°C for 20 hrs.

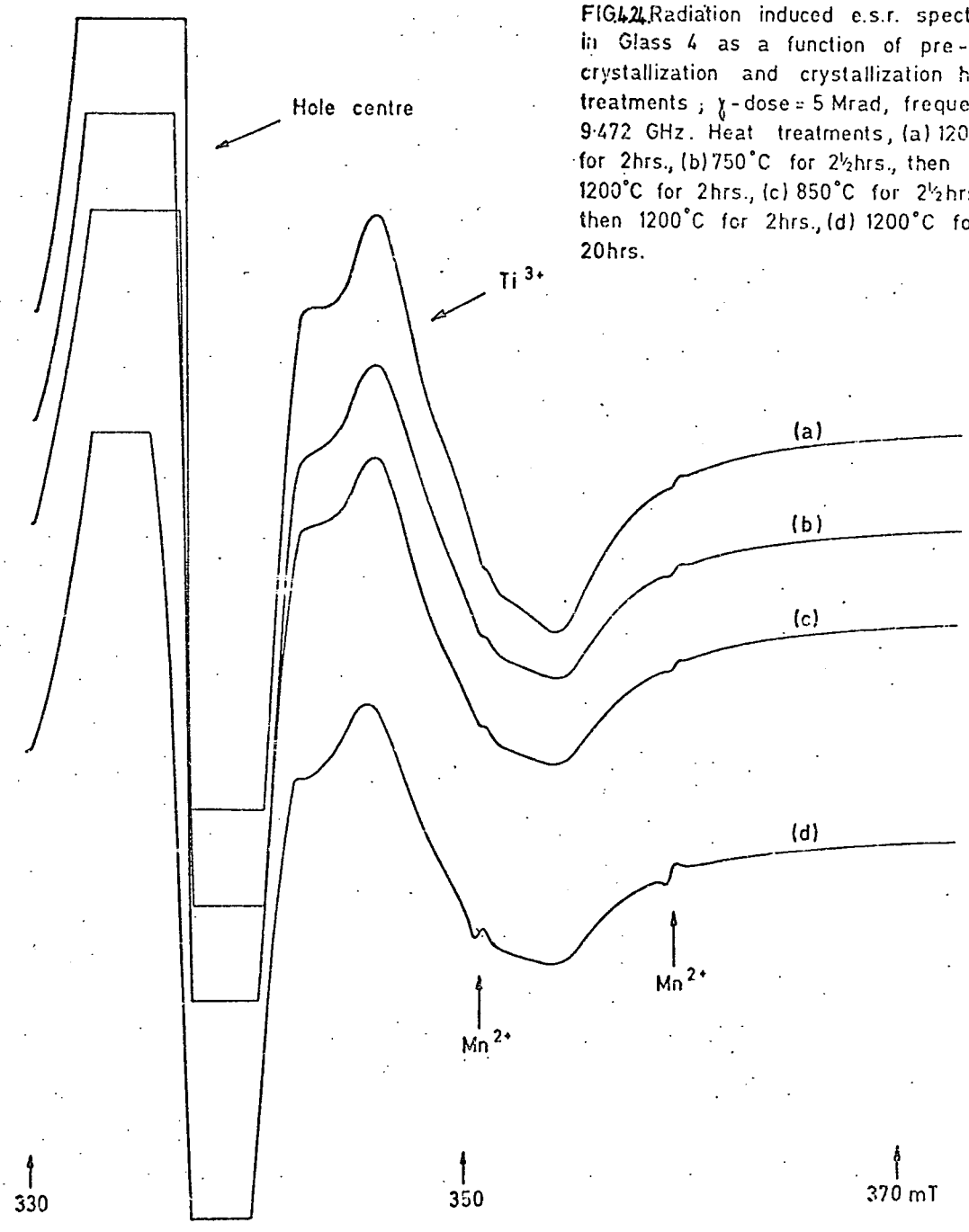

FIG.4.24. Radiation induced e.s.r. spectra in Glass 4 as a function of pre-crystallization and crystallization heat treatments ; γ-dose = 5 Mrad, frequency 9·472 GHz. Heat treatments, (a) 1200°C for 2hrs., (b) 750°C for 2½hrs., then 1200°C for 2hrs., (c) 850°C for 2½hrs., then 1200°C for 2hrs., (d) 1200°C for 20hrs.

of the low to high TiO_2, 1000°C line noted previously.

The g values of the characteristic points on the crystallized Ti^{3+} line are listed in Table 4.1.

4.2.6 Analysis and simulation of the Ti^{3+} lines in the ceramic samples

We consider first the high TiO_2 (glasses (4) and (5) 1000°C line, (Figure 4.23). This line may be simulated by assuming a centre with orthorhombic symmetry and a distribution (greater than g_1), in the g_2 and g_3 parameters. Figure 4.25 shows the beat-fit simulation; the Hamiltonian parameters employed are indicated on the diagram, and, as the figure shows, the correlation of simulation and experiment is good.

The experimental line from the low TiO_2 specimens (e.g. glass (3), crystallized at 1000°C (Figure 4.21) has features which again require a site of orthorhombic symmetry and a distribution in g_2 and g_3. Figure 4.26 (upper) compares the experimental and simulated lines. The simulation adequately reproduces the essential features of the experimental line, i.e. the suggestion of a double positive peak and the greater intensity of the negative peak; (note that the second, more intense, positive peak is absent on the experimental trace due to the merging of this peak into the even more intense hole centre line). Nevertheless, this line cannot be reproduced with the exactness of the high TiO_2 line, and the possibility of an underlying resonance emerges. Consequently, included in Figure 4.26 (upper) is a low intensity trace of the high TiO_2 line previously considered. A summation of this line and the simulation gives, after scaling, an almost exact fit to the experimental line. This is shown in the lower trace of the same Figure, the high TiO_2 line being 7% - 8% of the composite line, although this value could reasonably be between 4% and 12% depending upon the precise choice of simulation parameters and the smoothing of the

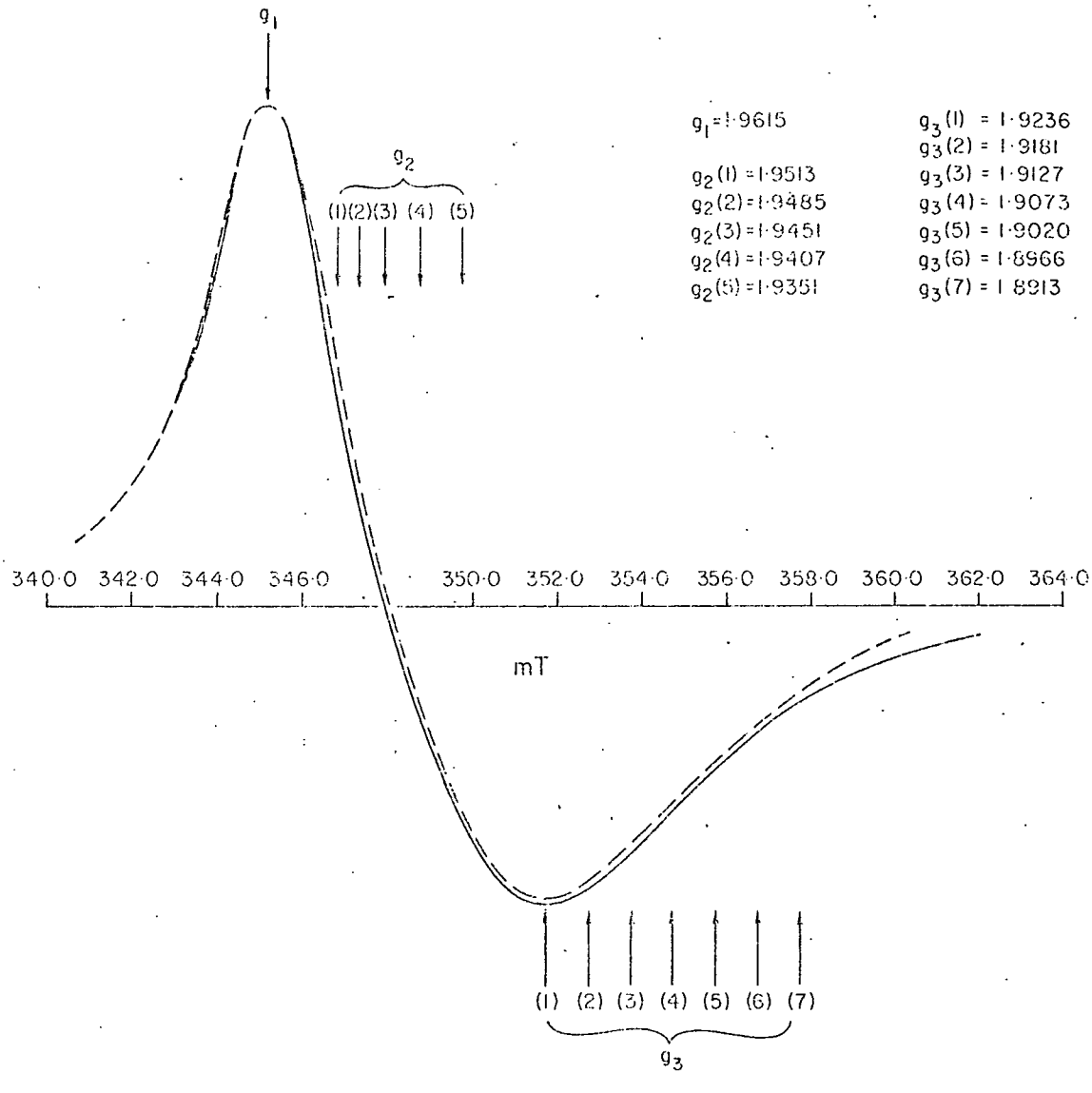

Fig. **4.25.** Comparison of the experimental Ti^{3+} spectrum from Glass 4 crystallized at 1000°C with best fit simulation employing σ_L = 35 gauss. (————), experimental; (– – – –) line, simulation. Frequency 9·472 GHz, γ-dose = 5 Mrad.

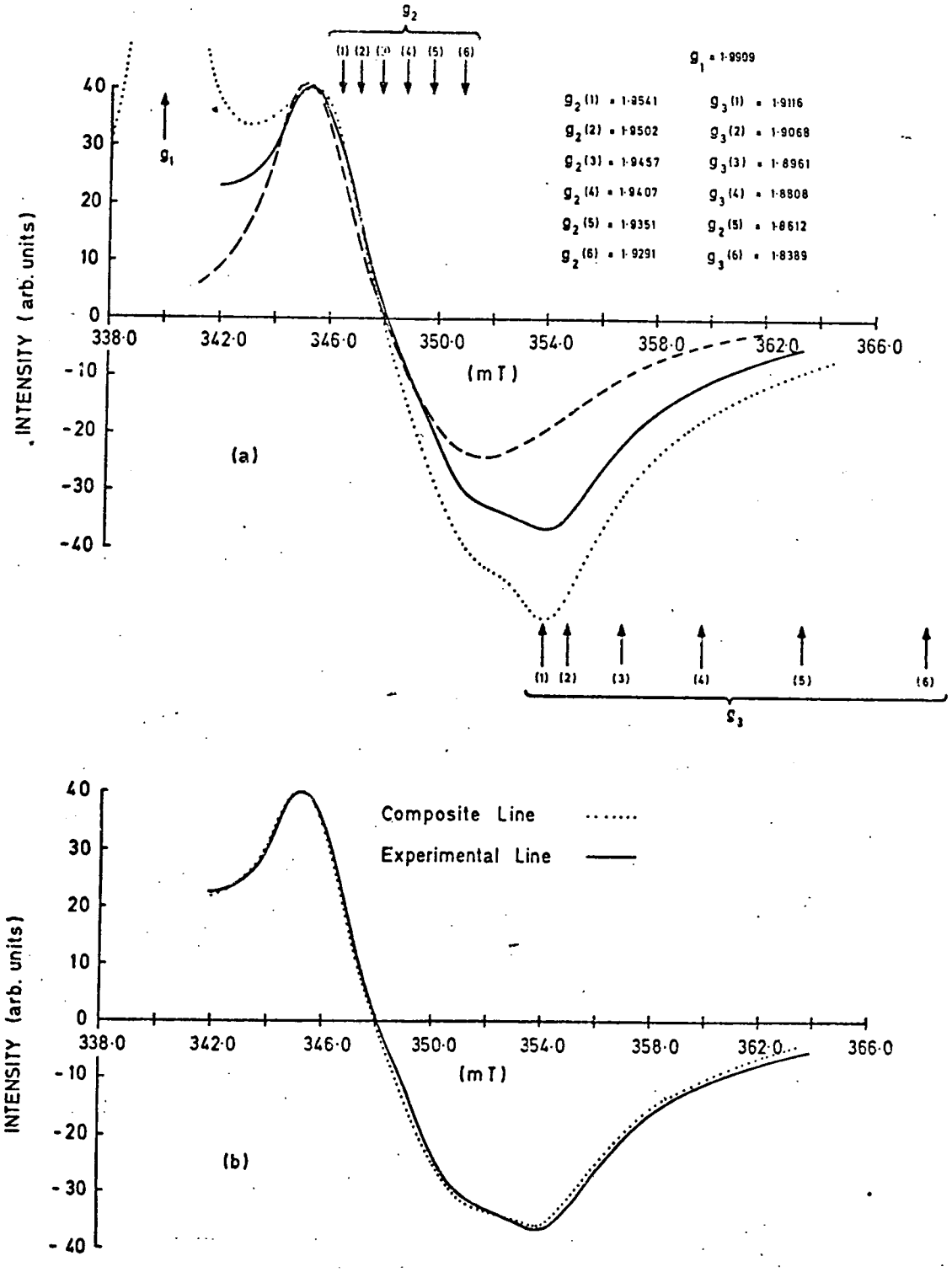

FIG. 4.26. Experimental and simulated lineshapes for Glass 4.

(a) —— Experimental, crystallized at 1200°C

– – – Experimental, crystallized at 1600°C

····· Simulated, taking σ_L = 26 gauss and g-values shown.

(b) Comparison of 1200°C experimental line with the composite line derived by summation and normalization of the ····· and – – – lines of (a). Fields plotted for 9·472 GHz.

simulated trace necessarily involved when a range of discrete values are used to reproduce the effects of a smooth distribution in a g parameter, (this approximation produces undulations in the simulated line whenever the separation of the discrete components becomes comparable with the line width of the broadening function).

The lines from the ceramics crystallized at 1200°C, (both low and high TiO_2), are closely related in their quantitative features, i.e. the peak positions and base line crossings, to the line just considered, the low TiO_2 1000°C line. The most striking changes are qualitative, i.e. change of shape, and in particular the ratio of the positive and negative peak intensities. The previous line having been shown to be a mixture of two lines, it was not surprising when it was found that a single site was not responsible for either of the 1200°C lines. No combination of Hamiltonian parameters could adequately simulate the 1200°C lineshapes.

Figure 4.27 therefore attempts to reproduce the 1200°C lines from combinations of the 1000°C (experimental) lines. The upper trace shows the low TiO_2 1200°C line compared with a composite line derived from the low and high TiO_2 1000°C experimental lines in the ratio indicated in the figure, i.e. 100 (low TiO_2) : 20 (high TiO_2). (The ratios quoted are on the basis of area of first derivative which is not directly related to the abundance of the particular paramagnetic site). The lower trace of Figure 4.27 compares the high TiO_2 1200°C line and a composite line derived from the 1000°C lines in the ratio 100 (low TiO_2) : 30 (high TiO_2).

The Figure shows that this procedure is, in essence, successful, verifying that the 1200°C lines are amalgums of resonances from two different sites. It is nonetheless true that some features of the lines are not reproduced by assuming a simple summation of the 1000°C experimental lines, i.e. the base line crossing point is not quite correct and the qualitative features of the positive peak of the low TiO_2 and the negative

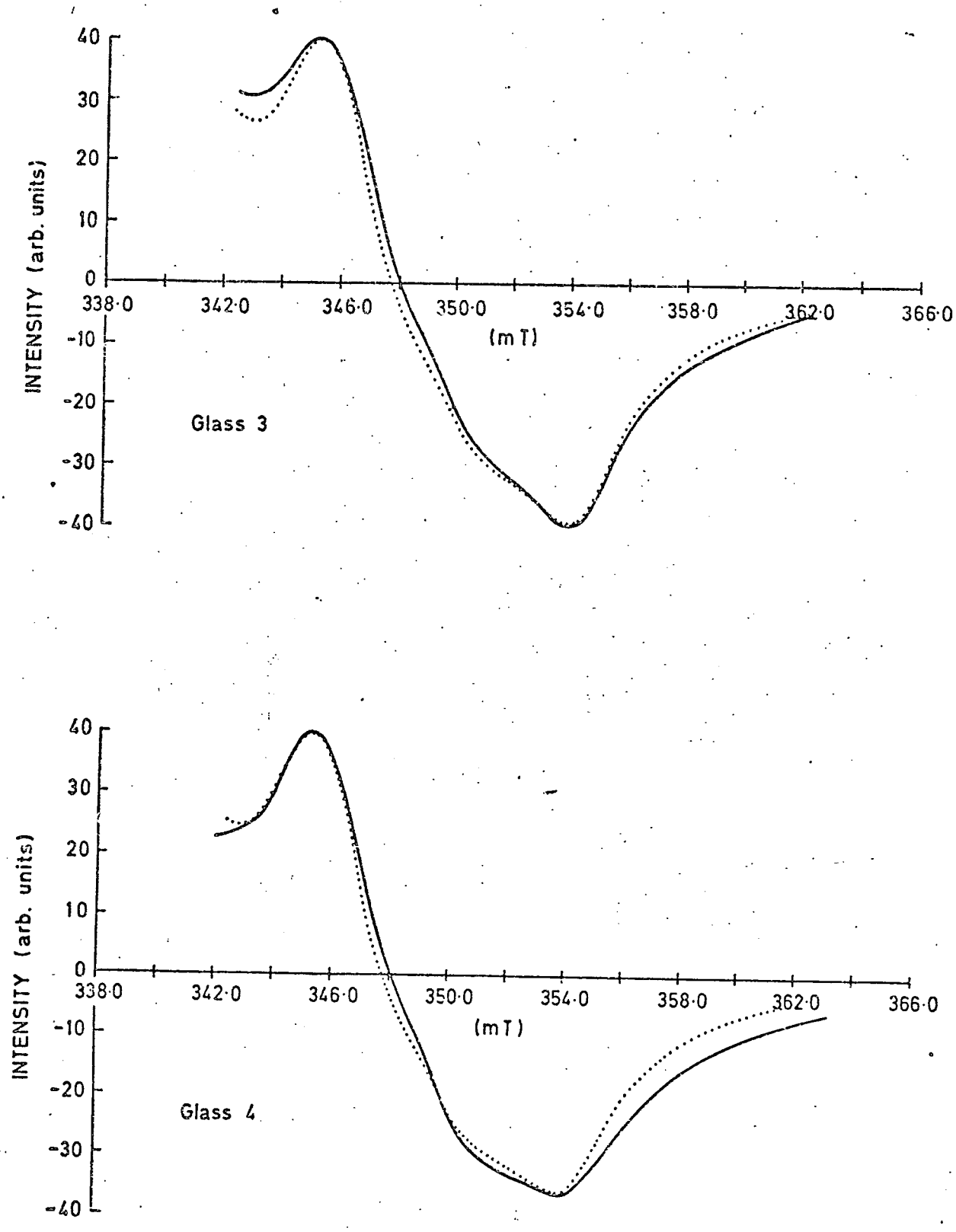

FIG. 4.27. Experimental and simulated lineshapes for glasses 3 and 4
——— Experimental spectra, (crystallized at 1200°C). ····· Composite lines derived by the addition of the experimental lines from glass 3 and 4, (crystallized at 1000°C).

peak of the high TiO_2 lines are not accurately reproduced. Thus one or both of the underlying lines have undergone some qualitative changes from their 1000°C lineshapes on increasing the crystallization temperature to 1200°C.

To establish the degree of variation of the Hamiltonian parameter of the 1000°C sites when moving to the 1200°C resonance lines, we analyse the high TiO_2 1200°C line by assuming that the resonance line from the high TiO_2 1000°C specimens is unchanged. This procedure is shown in Figure 4.28, where the upper trace shows the experimental line together with a new simulated line, having the Hamiltonian parameters on the figure, and the appropriate intensity experimental line from the high TiO_2 1000°C data, (40% of the simulation intensity). The lower trace of this Figure compares the 1200°C experimental line with a composite line derived from the component lines shown in the upper trace. The correspondence is now very good, significantly better than that of Figure 4.27. Comparison of the Hamiltonian parameters of the simulation in Figure 4.28 with those previously employed in the analysis of the low TiO_2 1000°C line (Figure 4.26) shows that only slight variations in the parameters have occurred when the crystallization temperature is increased to 1200°C, although the precise nature of the changes is admittedly a subject of speculation.

To summarise the analysis of the Ti^{3+} spectra from the ceramic specimens, we find that the lines from the ceramics crystallized at 1000°C are satisfactorily accounted for by resonances from two sites with differing Hamiltonian parameters. In the case of the high TiO_2 1000°C specimens almost complete correlation with the experimental trace is afforded by the simulation of Figure 4.25, i.e. the resonance line originates from a single Ti^{3+} site, but to account for the low TiO_2 1000°C line we must invoke a composite line whose predominant component is from a new Ti^{3+} site (Figure 4.26), with the high TiO_2 line again present as a minor,

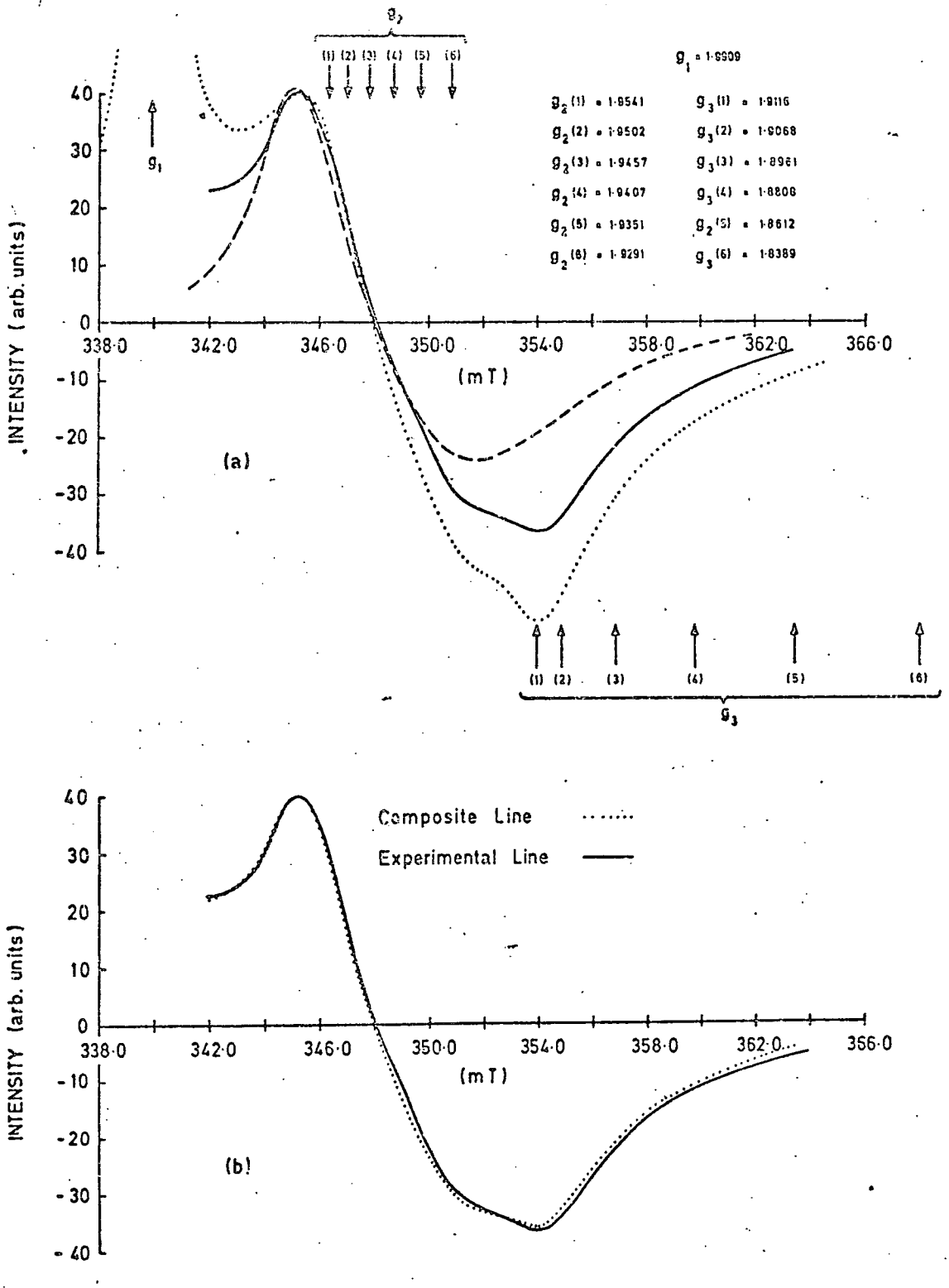

FIG. 4.28. Experimental and simulated lineshapes for Glass 4.

(a) —— Experimental, crystallized at 1200°C

— — — Experimental, crystallized at 1600°C

..... Simulated, taking σ_L = 26 gauss and g-values shown.

(b) Comparison of 1200°C experimental line with the composite line derived by summation and normalization of the ..... and — — — lines of (a). Fields plotted for 9·472 GHz.

(7% - 8%), component. The lines from the 1200°C ceramics do not originate from a single Ti^{3+} site; rather, they are composite lines of what are essentially the 1000°C experimental lines, one or both of which has undergone small changes in its Hamiltonian parameters.

4.2.7 The hole centre spectra

Spectra from all of the glass compositions under all combinations of pre-crystallization and crystallization heat treatments were studied and the spectra are typified in Figures 4.29, 4.30 and 4.31.

Figure 4.29 shows the variations in the spectrum as a function of glass composition, (1000°C crystallizations being chosen). Figure 4.30 shows the spectra from glass (4) crystallized at 1000°C with varied pre-crystallization heat treatments. As with all previous spectra, compositional differences are present, but pre-crystallization heat treatments have no effect on the e.s.r. line.

The essential 1200°C spectra are shown in Figure 4.31 with glasses (3) and (4) as examples. Slight differences are present between these spectra and the 1000°C spectra, and even a change in the crystallization period alters the form of the spectrum slightly, but overall, the crystallization hole centre has a characteristic multiple peaked structure, and a constant resonance field position, only the envelope of the line is changing.

4.2.8 Analysis and simulation of the ceramic hole centre spectra

For analysis we take two lines at the apparent extremes of the lineshape, the lines from glasses (2) and (4) crystallized at 1000°C (Figure 4.29). These lines are plotted on extended field axes in Figure 4.32 where it is clear that the field positions of the multiple peaks in the lines are identical, and that it is the envelope, particularly in the

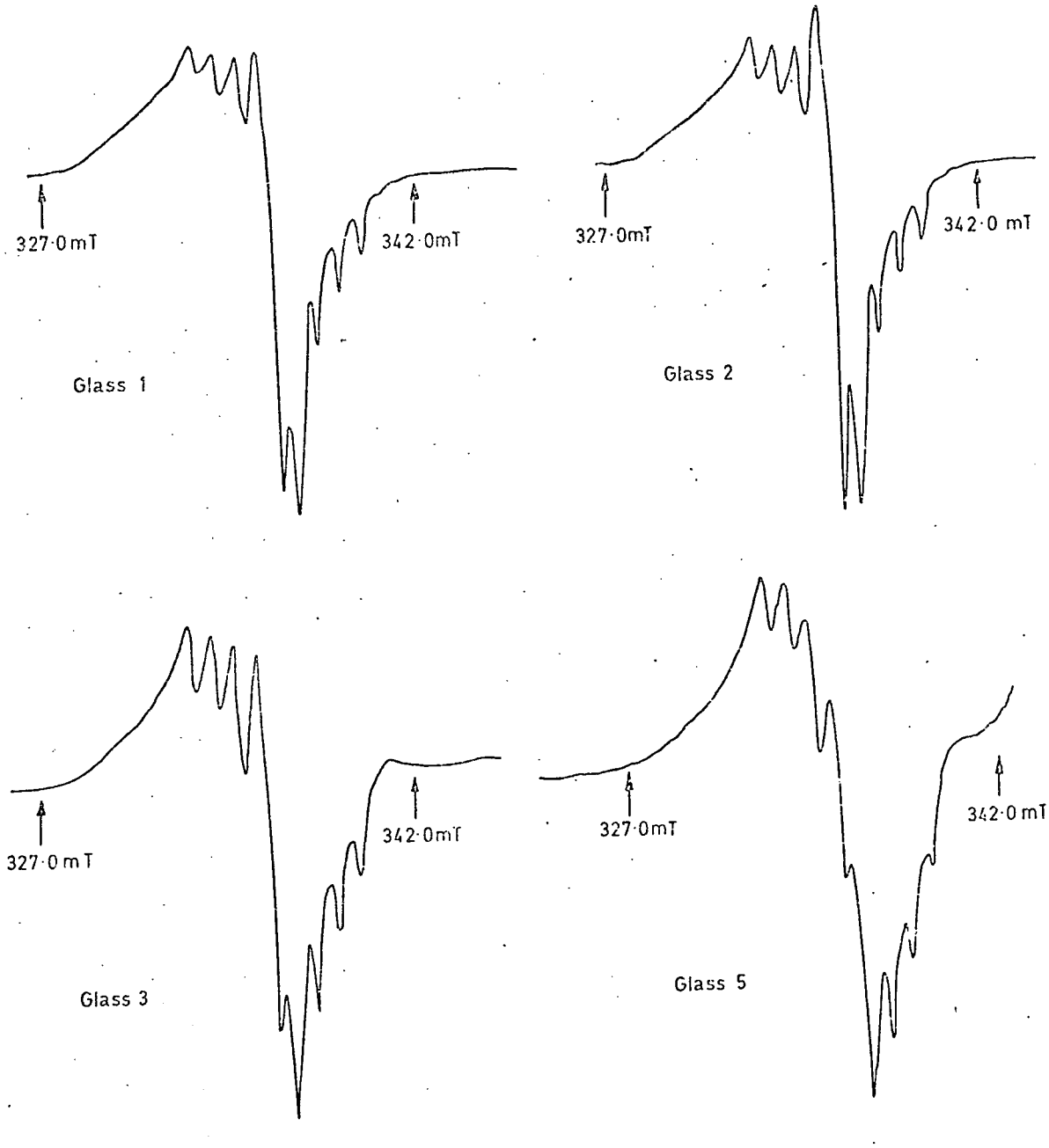

FIG.4.29. Radiation induced e.s.r. spectra of hole centre as a function of glass composition; all glasses crystallized by heating at 1000°C for 20 hours. (γ - dose = 5 Mrad)

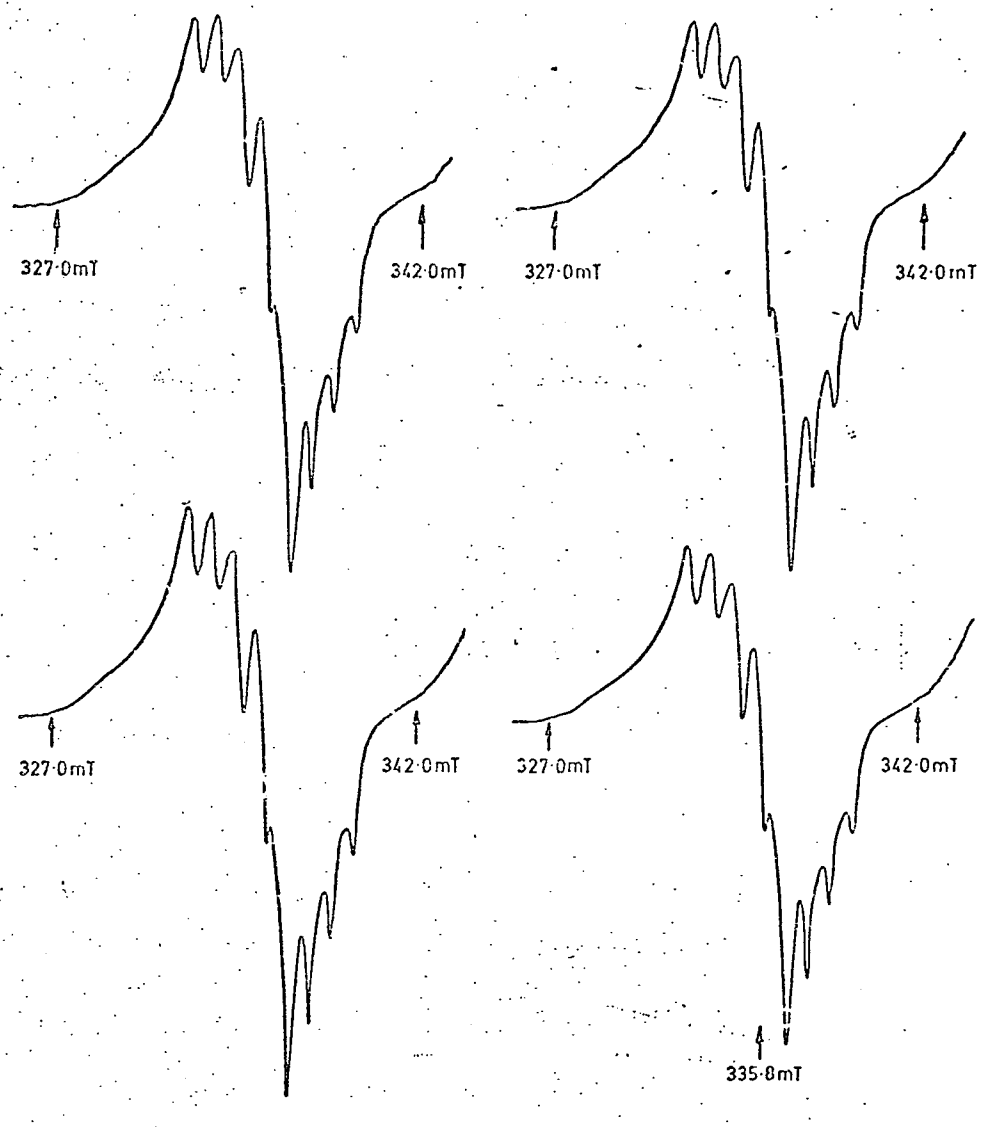

FIG430. Radiation induced e.s.r. spectra of hole centre in Glass 4 as a function of pre-crystallization heat treatment; (a) untreated; (b), (c), and (d) heat treated for 2½ hours at 750°C, 800°C and 850°C respectively and subsequently crystallized at 1000°C for 20 hours. (γ - dose = 5 Mrad)

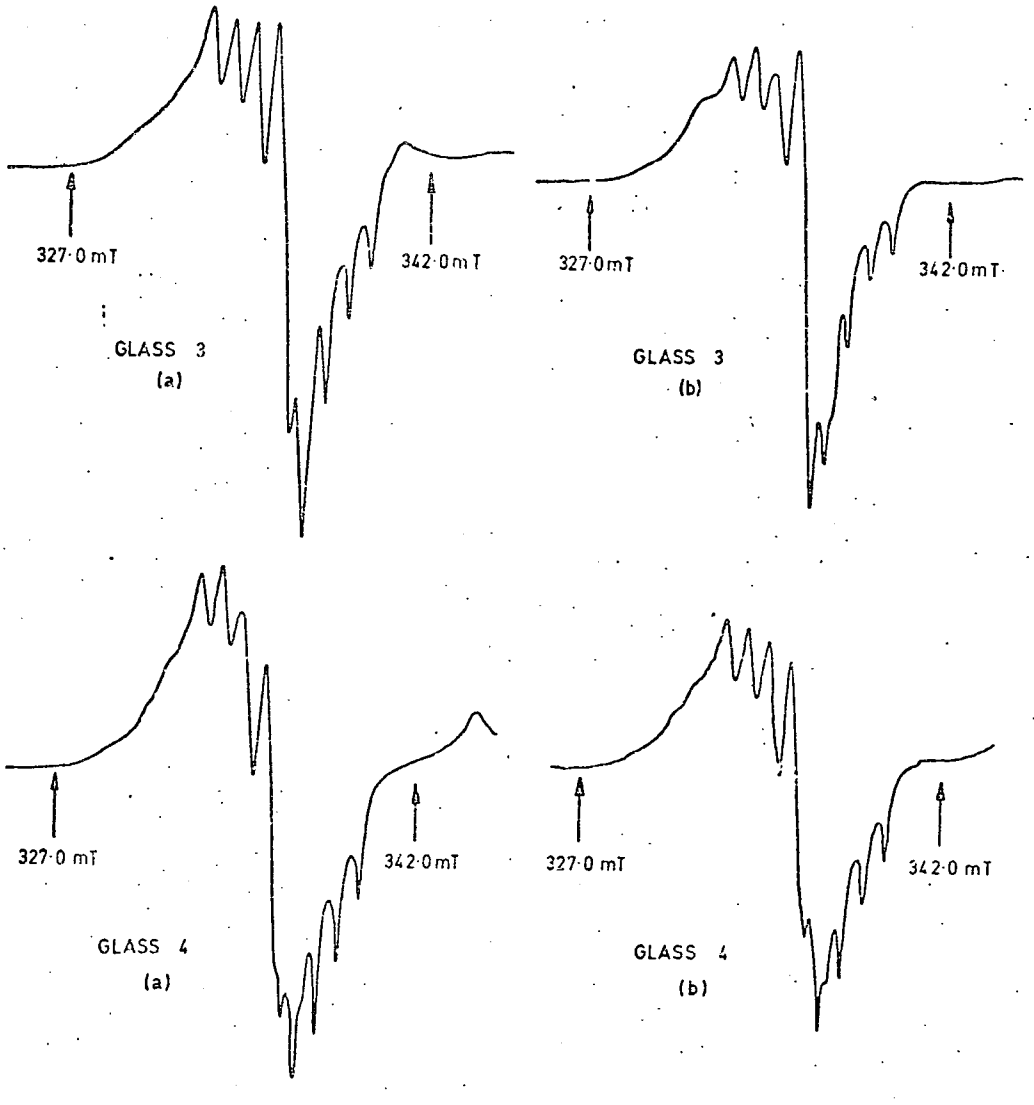

FIG.4.31. Radiation induced e.s.r. spectra of hole centre in glasses 3 and 4 crystallised (without pre-heat-treatment) at 1200 °C (a) for 2 hours, (b) for 20 hours.

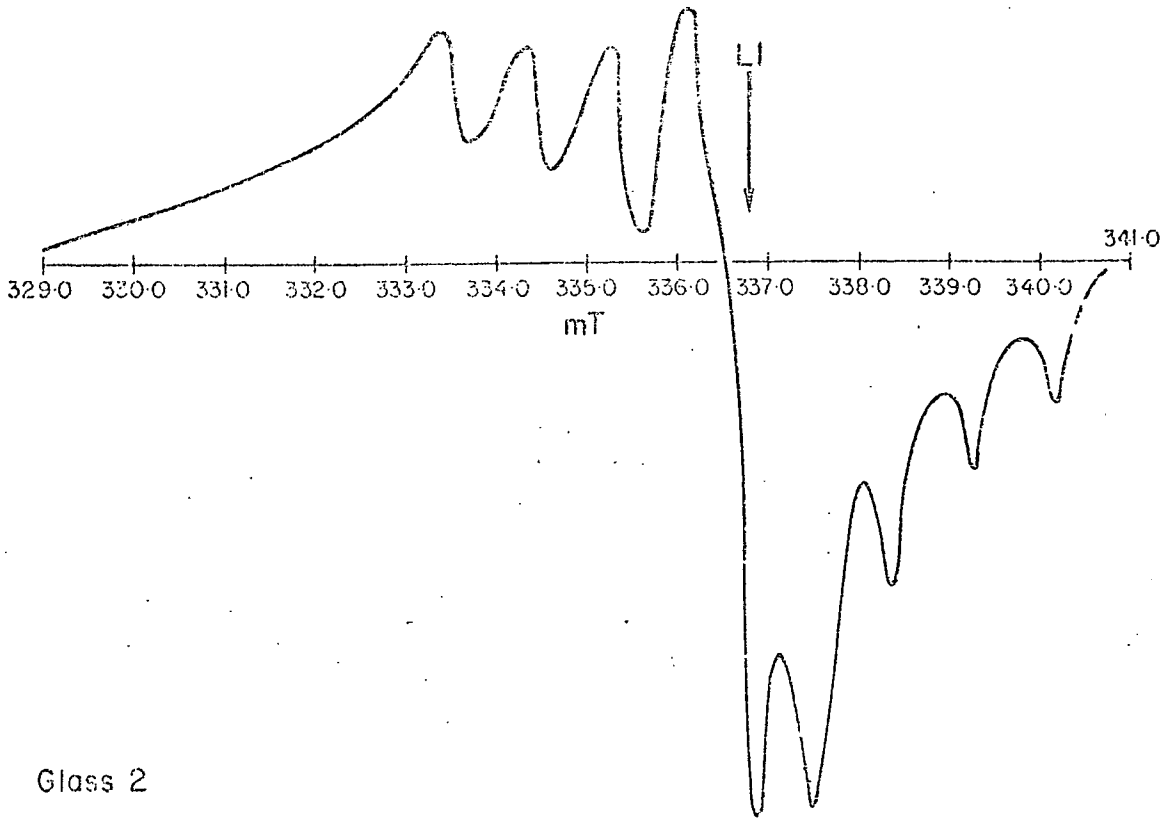

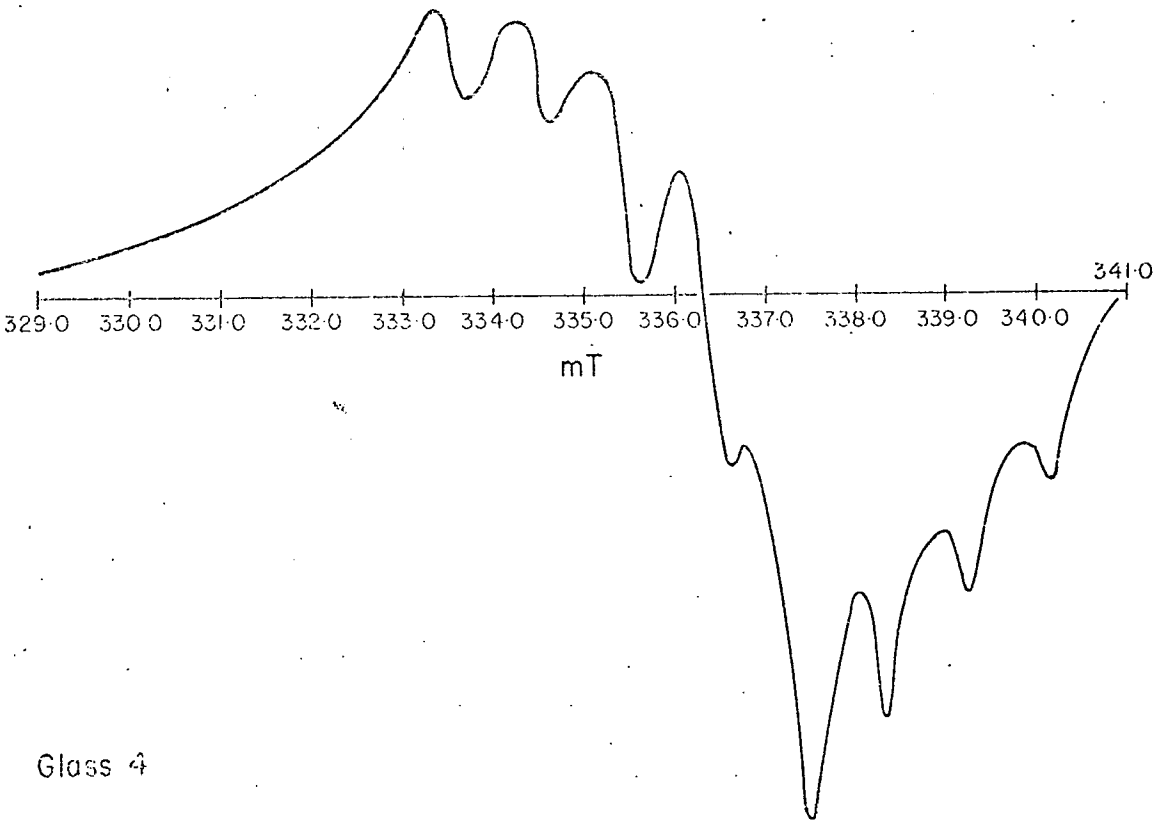

Fig. 4.32. Radiation induced hole centres in Glasses 2 (upper) and 4 (lower) crystallized at 1000°C for 20 hours. The field axis is plotted for a frequency of 9·470 GHz; γ-dose = 5 Mrad

region 336 to 337 mT, which differentiates the lines.

Figure 4.33 shows the second derivative tracings of the hole centres in glasses (2) and (4) crystallized at 1000°C (i.e. the second derivative spectra corresponding to the first derivative tracings of Figure 4.32). The spectrum of both glasses consists of two sets of six equally spaced lines (marked 1 to 6 and A to F in Figure 4.33). In addition, the spectrum of glass (2) has the extra peaks marked L1 and L2, and the glass (4) spectrum the peaks L2 and L3. The constant field separation within each set of six indicates a hyperfine interaction with a nuclear spin of $^5/_2$.

Extending the crystallization period to 100 hrs. produced, on the second derivative, a suggestion of a third set of six lines, (not discernable on the first derivative). An attempt was thus made to simulate the hole centre spectrum assuming a site with orthorhombic symmetry, an interaction with a nucleus of spin $^5/_2$, and an isotropic coupling constant of 8.4×10^{-4} cm^{-1} (i.e. $|A_1| = |A_2| = |A_3| = 8.4 \times 10^{-4}$ cm^{-1}); the principal g values were evaluated from the second derivative tracings, i.e. the central value of each set of six hyperfine lines.

The trial simulations are shown in Figure 4.34 where they are compared with the crystallized glass (4) centre. The simulation assuming a unique value for g_3 although reproducing the field positions of the experimental 'peaks' fails to reproduce the correct envelope, (note the base line crossing point), and also generates three 'peaks' on the low field side of the simulation not present in the experimental spectrum. A slight distribution of g_3 successfully removes the surplus of peaks, replacing them with a low field 'shoulder', but the incorrect envelope remains.

At this point we refer to the glass (4) second derivative tracing (Figure 4.33). Superimposed on to the tracing from the crystallized glass (4) is the second derivative spectrum from an uncrystallized specimen of

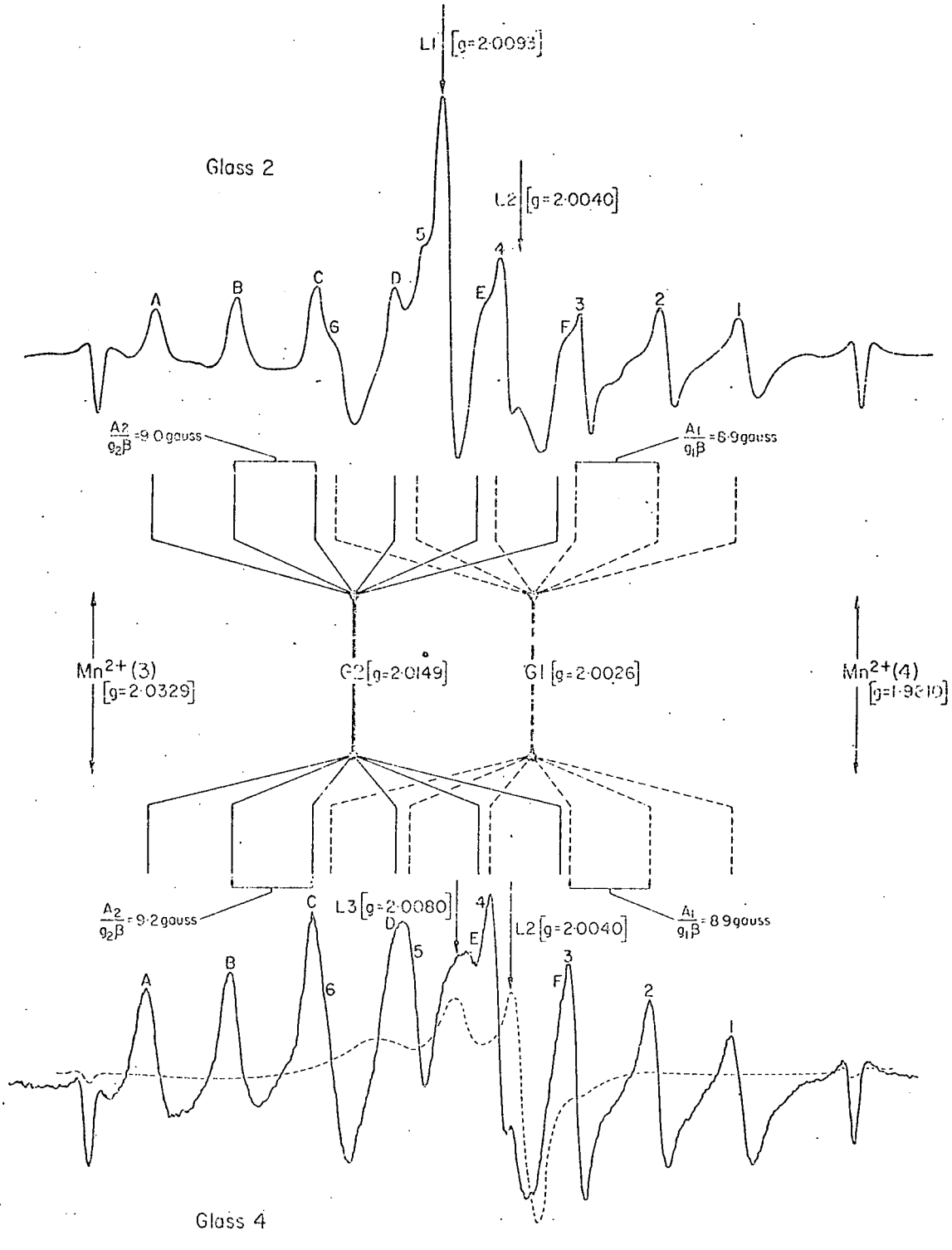

Fig. 4.33. Second derivative tracings of the radiation induced hole centres Glasses 2 (upper) and 4 (lower) crystallized at 1000°C for 20 hours. The dotted line on the lower tracing is the second derivative of the hole centre in the uncrystallized Glass 4.

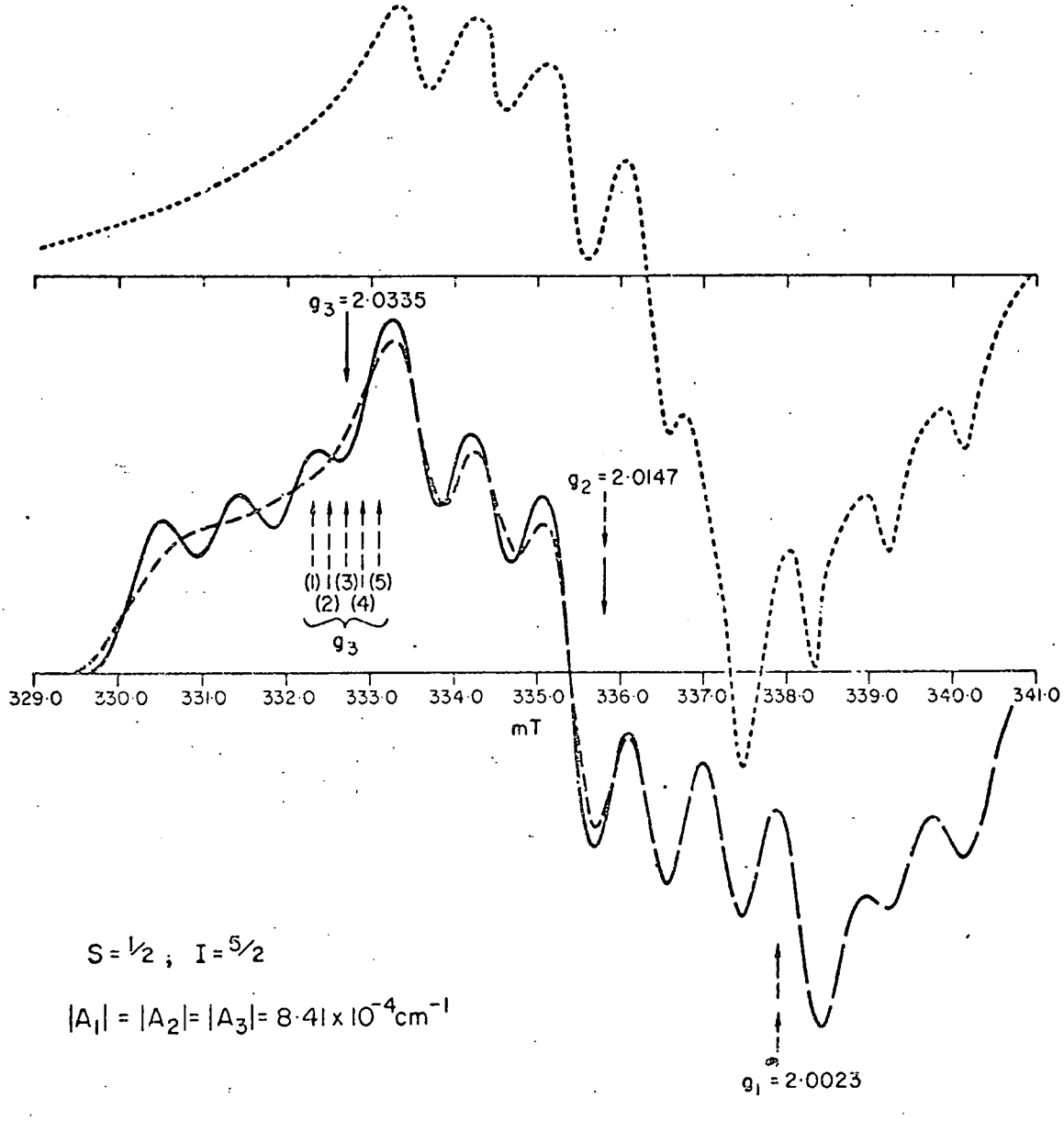

Fig. 4.34. Comparison of the hole centre in Glass 4 (--------) with trial simulations assuming orthorhombic symmetry and (a) a precise value for g_3 (————), (b) a distributed g_3 (— — —).
The field axis is plotted for a frequency of 9·470 GHz and a Gaussian lineshape function with $\sigma_G = 3$ gauss is used in the simulations.

this glass. The additional peaks marked L2 and L3 on the crystallized tracings, correspond to the peaks on the second derivative of the high TiO_2 glassy specimens. This suggested a contribution to the total spectrum from the glassy hole centre in the high TiO_2 glasses.

Figure 4.35 (upper) shows the crystallized centre with the uncrystallized centre superimposed. The difference spectrum, i.e. the crystallized defect, (full line), minus the uncrystallized defect (dashed line) is shown below, where it is compared with the best-fit simulation employing the Hamiltonian parameters indicated on the diagram. The fit is very good, the only significant variation occurring in the region 360 to 370 mT, and we conclude therefore that the crystallized hole centre is essentially an amalgam of the glassy hole centre for this composition and a line from a site with the symmetry and Hamiltonian parameters indicated in Figure 4.35.

A similar analysis of the crystallized glass 2 centre, assuming that there is a contribution from the centre in the uncrystallized glass of this composition, is not so successful, almost certainly due to the presence of a strong additional centre indicated by the peak L_1 at $g = 2.0093$ on the second derivative from this composition. The effect of this resonance is to markedly alter the first derivative in the region 360 to 370 mT, and the simulation, although reproducing the position and the number of the hyperfine peaks, is only a reasonable fit to the envelope at the 'wings' of the difference spectrum. Nevertheless it is certain that the centre responsible for the hyperfine structure in the glass (4), whose essential features have been evaluated from the analysis of the line from this glass, is again present in the crystallized glass 2 specimens, although in this case combined with a line or lines whose exact nature cannot be determined.

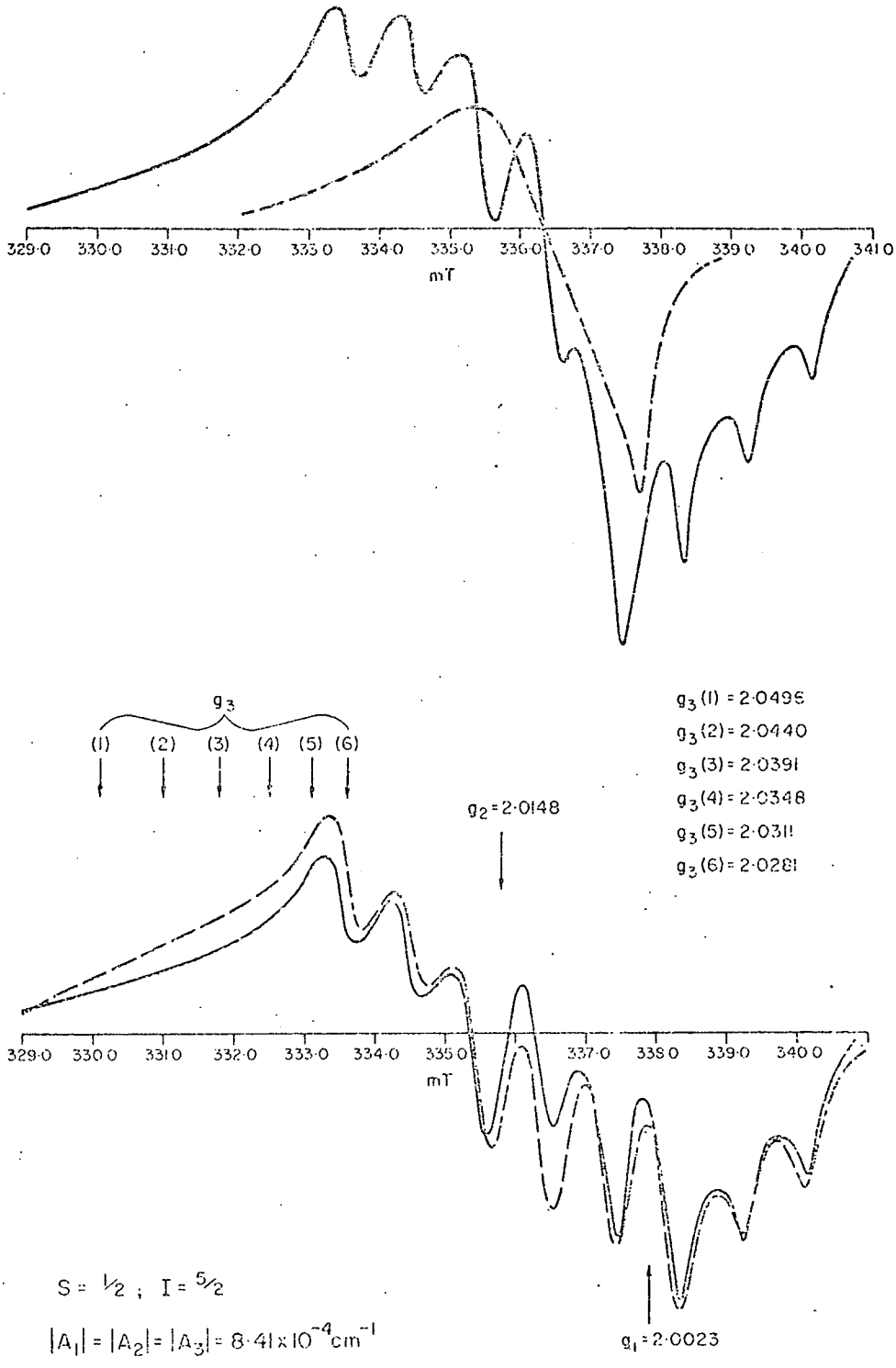

Fig. 4.35. UPPER TRACES :- The hole centres of the crystallized (———) and uncrystallized (— — —) Glass 4.

LOWER TRACES :- Comparison of the difference spectrum (———) of the crystallized and uncrystallized Glass 4 hole centres with the best fit computer simulation (— — —) employing a Lorenzian lineshape (σ_L = 5·5 gauss).

4.3 Discussion

The nature of the radiation produced hole and electron centres and the structural information which may be inferred from their spectra are now discussed. We consider first the Ti^{3+} spectra.

4.3.1 E.S.R. d' ions in cubic, tetragonal and trigonal crystal fields

Isofrequency plots of the rotational symmetry of the e.s.r. lines from an ion in a single crystal will often allow the coordination number of the ion and the detailed nature of the paramagnetic site to be resolved. In polycrystalline or glassy specimens e.s.r. measurements provide only the shape and field position of the resonance line, and of itself, being dependent only upon the point symmetry of the site, the shape of the line is not sufficient to infer the coordination state of the ion (4.9). In some cases, notably the Fe^{3+} ion, sites with a defined symmetry have been correlated with resonance lines at three specific field positions, (i.e. three g values) (4.10). No such agreement exists as to the nature of the sites responsible for the Ti^{3+} resonance lines in glass. We consider therefore the characteristics of the resonance line expected from the Ti^{3+} ion, (d' configuration), in octahedral coordination and under distortions of the cubic field which leave axial symmetry, (minimum 3-fold axis), at the central ion. The appropriate orbital level diagrams are shown in Figure 4.36 (4.11-4.15). The electronic ground state is an orbital doublet whenever the octahedron is elongated along the triad or tetrad axes, and an orbital singlet for compressions of the ligands along the 3 and 4-fold axes. Theory shows that when an orbital doublet is the ground state, then, as with perfect octahedral coordination, one or both principal g values are zero and no resonance line is observed, (4.14)(4.16). When the perturbation of the octahedron is such as to leave an orbital singlet ground state, then the nature of the perturbation may be discerned from the shape of the e.s.r. line by noting that

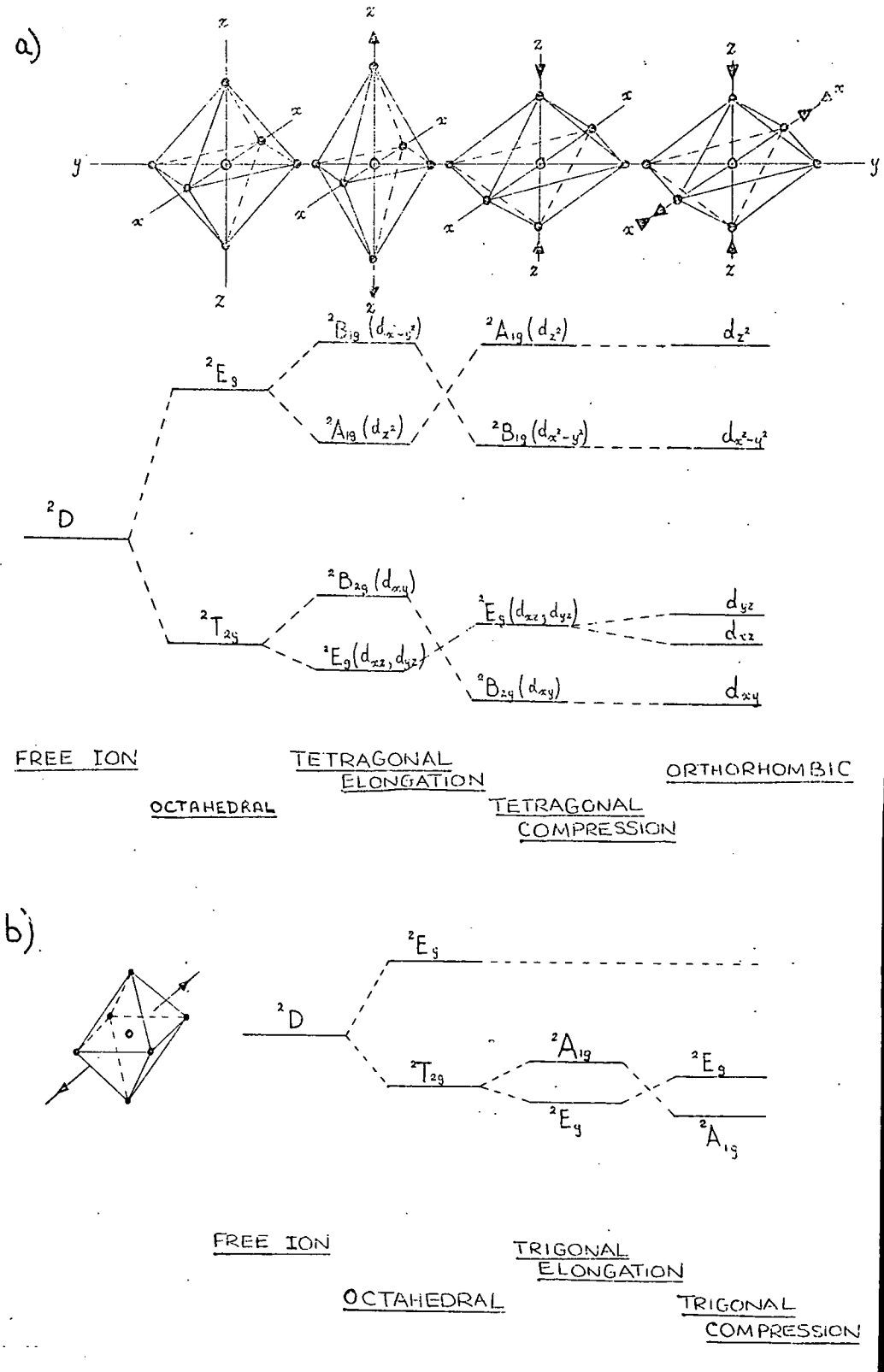

FIG. 4.36. ORBITAL SPLITTINGS OF THE ^2D FREE ION GROUND STATE OF THE Ti^{3+} ION, (o), IN OCTAHEDRAL, (O_h), TETRAGONAL, (D_{4h}), AND TRIGONAL, (C_{3V}), SYMMETRIES.

$g_\perp > g_\parallel$ in D_{4h} symmetry, and $g_\perp < g_\parallel$ in C_{3v} symmetry (4.14,4.16,4.11). Rhombic terms in the crystal field eliminate all but the Kramers degeneracy, (Figure 4.36).

At room temperature, only the lowest orbital is populated in a d' system. The displacement of the principal g values from g_e, the free electron value (2.0023), is due to the admixing of the higher orbital levels into the ground state wavefunction (4.2), and is therefore dependent upon the magnitude of the orbital splittings and spin-orbit coupling constants (λ). For ions in a tetragonally distorted cubic field Pryce (4.17) gives,

$$\left.\begin{aligned} g_\perp &= 2.0023\left[1 - \frac{\lambda}{E(xz)(yz) - E(xy)}\right] \\ g_\parallel &= 2.0023\left[1 - \frac{4\lambda}{E(x^2 - y^2) - E(xy)}\right] \end{aligned}\right\} \quad (21)$$

in terms of λ and the orbital splittings (Figure 4.36). When the separation within the lower triplet is small, i.e. for small tetragonal distortions, the g values depart markedly from g_e (equation (21)). In addition, the spin-lattice relaxation time T_1 is very short, (Van Vleck (4.18) proposes $T_1 \sim$(lower triplet splitting)^6), leading to very broad resonance lines, (equation (19)), and resonance can only be observed at cryogenic temperatures.

As examples of the general principles outlined above we would site the Titanium Alums and the crystalline TiO_2 polymorphs. The Alums, (and most hydrated titanium solutions), have the Ti^{3+} ions in sites which have a small trigonal distortion of the octahedral ligands. In all instances, measurements at LN_2 temperature and below are necessary to observe the resonance line, and in addition all the spectra have $g_\perp < g_\parallel$ (4.14,4.19,4.20). The room temperature stable form of TiO_2, rutile, has the Ti ions in D_{4h} symmetry with two long and four shorter bonds to oxygens, i.e. in a tetragonally elongated octahedron. Resonance lines from d' ions, (e.g. Ti^{3+},V^{4+}),

at substitutional titanium sites have not been confirmed. In fact, although most of the e.s.r. lines from rutile and anatase anneal out at between 77 K and 300 K, it has been shown (4.21 ,4.22) that the d^1 resonance signals originate from ions at interstitial sites, where the symmetry is again D_{4h}, but now the essential deformation of the octahedron of ligands is a compression along the tetrad axis, i.e. there are four long and two short bonds to oxygen. The resonance lines from this site have $g_\perp > g_\parallel$.

Our analysis of the Ti^{3+} spectra from the glass specimens indicates $g_\perp > g_\parallel$ and when combined with the field position and room temperature stability of the resonance lines, our discussion above strongly suggests that the Ti^{3+} ions are most likely to be situated at the centre of a group of octahedral ligands which have a significant compression along the 4-fold axis. We now consider published spectra and models of the Ti^{3+} sites in glass.

4.3.2 Spectra and Models of the Ti^{3+} sites in glass

In some quartz and high silica glasses quadravalent titanium can assume four coordination, substituting for Si^{4+} and acting as a glass former (4.23). Some authors (4.24) consider that up to 10 mol.% of TiO_2 can be incorporated into the network, and consider that this replacement is responsible for the extremely low expansion coefficients of Ti-Si glasses. Other workers (4.25,4.26) place the solubility limit at less than 1%, arguing that above this level $[TiO_4]$ groups are replaces by $[TiO_6]$ groups. However, in all multicomponent glasses containing significant amounts of glass modifiers, (i.e. Na, K, Mg etc.), the overwhelming evidence suggests that the titanium is quadravalent and in octahedral groups.

Almost all authors (4.27 - 4.40) have ascribed the broad, usually assymetric line, with a baseline crossing in the region of $g \sim 1.93 - 1.96$, and a peak to peak first derivative width of from 40 to 110 gauss, to the

Ti^{3+} ion in their glasses. This line is observed at room temperature in all irradiated titania doped silicate and borate glasses, although occasionally measurements at 77 K are necessary to observe the resonance in phosphate glasses (4.27). The Ti^{3+} ion is universally concluded to be at the centre of a distorted octahedron of oxygen ions. Yafer et al (4.28) consider the distortion to be essentially trigonal, whereas Garif,yanov et al, (4.32) consider the distortion essentially tetragonal. Kim et al (4.33) in a study of Alkali-Titanate glasses, observe two irradiation lines which they ascribe to Ti^{3+} ions in different sites. A sharp line with $g_{\perp} = 1.9904$ and $g_{\parallel} = 1.9810$ is associated with an electron trapped at a $[TiO_6]^{2-}$ unit (i.e. two non-bridging oxygen ions, (n.b.o.), per octahedron), and a much broader line with $g_{\perp} = 1.975$ and $g_{\parallel} = 1.89$ is ascribed to electrons trapped at $[TiO_6]^{-}$ units (i.e. one n.b.o. per octahedron). Arafa and co-workers (4.35-4.39) in a series of papers on silicate and borate glasses, also observe a sharp and a broad line due to Ti^{3+} in two sites. The sharper line, denoted T_2, has $g_{\perp} = 1.975$ and $g_{\parallel} = 1.936$ and is ascribed to a $[TiO_6]^{4-}$ unit (4 n.b.o. per octahedron). The broad line, denoted T_1, has a base line crossing at $g \sim 1.946$ and is ascribed to $[TiO_6]$ units (all oxygen bridging). In both Arafa's and Kim's work the sharp line dominates the spectra from the low titania, high alkali glasses, and, as the titania content is increased beyond $\sim$1 mol.%, the broad line intensifies and dominates the spectrum at moderate TiO_2 concentrations.

We consider here that neither of the models above describing the centres responsible for the broad resonance lines, are appropriate to the Ti^{3+} e.s.r. line observed in this work. The analysis of the irradiation produced optical bands, described in the next chapter, indicates that the radiochemically reduced Ti^{3+} ions are in centrosymmetric sites, and as such, Kim's $[TiO_6]^{-}$ units are not appropriate here. Arafa's T_1 centre, with

four non-bridging and two bridging oxygen ligands would seemingly produce the site symmetry of a tetragonally elongated octahedron at the Ti^{3+} ion, and our previous arguments have indicated that it is unlikely that such sites would produce room temperature e.s.r. lines except in the presence of very strong tetragonal or othorhombic distortions. We have proposed that our resonance spectra are most likely to arise from titanium sites where two of the six titanium-oxygen bonds are significantly shorter than the remaining four. It is speculation to define the complex exactly. However, in the formalism of the bridging oxygen non-bridging oxygen approximation, $[TiO_6]^{2-}$ units would provide suitable trapping sites, and we cautiously ascribe the glassy Ti^{3+} spectra to these units.

4.3.3 E.S.R. as a probe of the glass structure

The most formidable problem in work involving radiochemical reduction is the one of generality, in that inferences must be made about the general behaviour of an ion (or paramagnetic centre), by observing only a small fraction of the total number of ions. In this work the concentration of Ti^{3+} was 5×10^{17} spins per gram, and, within a factor of two, was constant for all glass compositions. This represents from 3% of the total Ti ions in glass (2) to 0.07% in glass (5). Nevertheless, this limitation has not prevented other workers postulating general behaviour for their ions and we shall do likewise, although qualifying all assertions because of the necessary extrapolation.

The e.s.r. parameters which may alter during a structural change within the glass due to compositional changes or heat treatments, are line-shape, line position (changes in the g values), and line intensity. With reference to the Ti^{3+} ion we discuss the significance of each in turn, the discussion in most cases being appropriate to any $S = \frac{1}{2}$ centre whether intrinsic or radiation produced.

(a) Changes in line position

There is not a unified method of interpreting the shape and positional changes of an e.s.r. line from a glass which is undergoing structural changes. Positional changes, i.e. g value changes, result from changes in the chemical environment of the ion and in some cases (4.41,4.42) the g values of a given ion in known crystalline compounds, have, by interpolation of these values, been used to infer the presence of intermediate chemical compounds from the measured g values of the ion in the glass. We in this work can only equate g value changes to either (i) stereochemistry changes, i.e. changes in the site symmetry, or (ii) covalency changes, i.e. bonding of identical TiO_6 groups to different complexes, resulting in a change of the covalency of the Ti - O bond (4.41).

(b) Changes in line shape

It is possible for the dominant change to be a 'sharpening' of the e.s.r. line, i.e. a reduction in the single crystal linewidth without significant changes in the principal g values. Some authors equate such a reduction in the linewidth with an 'ordering' in the neighbours of the paramagnetic ion (4.33,4.34,4.43), i.e. 'sharper' lines ≡ more 'ordered' glass. Other authors, (4.31,4.32), contend that a broadening of the line is indicative of an ordering in the paramagnetic ion ligands. Only studies which involve observations of the line at different temperatures and at different microwave frequencies can give an unequivocal interpretation of lineshape changes. The principal line broadening mechanism must be established. If, as is likely in glasses, a statistical distribution of the crystal fields experienced by an ion causes distributions in the g parameters, then these distributions will become progressively less important as the microwave frequency is lowered, and a linewidth reduction upon reduction of the microwave frequency is sufficient to establish that g distributions

are the main cause of line broadening. Measurements of this nature have been made by Peterson et al (4.29) on a Ti doped borate glass, where it was established that indeed g distributions were responsible for the broad glassy lines at X-band frequencies.

On the other hand, if spin-lattice relaxation mechanisms are principally responsible for the linewidth, then one should expect the lines to 'sharpen' as the observation temperature is lowered, (dipolar broadening mechanisms are not considered here because the Ti^{3+} concentration is well below the level at which one might expect significant broadening due to this mechanism (4.43) T_1 is reduced and the relaxation broadening intensified when the splitting between the ground state orbital and the higher orbitals is reduced. This would result from a reduction in the distortions of the TiO_6 units, i.e. in the spin-lattice broadening regime, a broadening of the line could reasonably be interpreted as an 'ordering' within the glass.

To establish the dominant line broadening mechanism the spectra from some glasses and some ceramics were recorded at 77 K on a Varian spectrometer. A reduction of the single crystal linewidth by a factor of three or four could be expected if spin-lattice effects were dominant, ($T_1 \propto (\text{Temp.})^{-1}$ in the 'direct' region (4.7) and $\sigma_L \propto (T_1)^{-1}$ - equation (19)). The concomitant lineshape changes from such a reduction in σ_L (e.g. Figures 4.8 and 4.9) were entirely absent from the spectra, which although the quality was moderate, appeared quite unchanged from the room temperature spectra. In this work, therefore, we interpret lineshape changes to be an indication of changes in the distributions of the g parameters.

(c) Line Intensity Variations

More than one e.s.r. line from the same ion, particularly if that ion has a d^1 or d^9 electronic configuration, is a clear indication of the

presence of that ion in different chemical environments (4.42,4.44,4.45). The reverse however is not true, i.e. that one e.s.r. line is indicative of the presence of the ion in a single site only, because, as previously discussed, many site symmetries would not produce R.T. spectra, even for ions which are paramagnetic in their normal oxidation state. Intensity changes from lines associated with paramagnetic ions are indicative of changes in the relative abundances of the different sites, but in a competitive trapping situation, then, as Friebele points out (4.46), the various sites compete for the radiation produced holes and electrons, and the final intensity of a line is as much a measure of the trap depth as of the relative abundance of the site with which it is associated. Thus the intensity of the line from a specific site may change greatly as a result of changes in structures (perhaps in a separate glass phase), with which it is in competition, and equally, a centre may have a constant intensity e.s.r. signal even though the number of its potential trapping sites increase, if the number of trapping centres providing charge compensation remains constant. Without therefore some knowledge of the probably structural changes attendant upon a change of composition or upon heat treatment, an interpretation of the intensity changes of the e.s.r. signals is largely meaningless (4.47).

(d) Relative distributions of the Hamiltonian parameters

We draw no conclusion in this section on the Ti^{3+} spectra, from the extra distributions of the g_3 or $g_{\parallel}$ parameters which are evident from the computer simulations. This feature of the experimental spectra is discussed in more detail in the next section which considers the hole spectra.

4.3.4 Structural Inferences from the Ti^{3+} spectra

In the light of the previous discussion we now make our final conclusions.

The spectrum from each of the different glass compositions contains a single Ti^{3+} line only. We have suggested that this line originates from titanium ions at the centre of a tetragonally compressed octahedron of oxygen ions. The invariance of this line with composition changes suggests that no new titania complexes are formed as the TiO_2 content of the glasses is increased, although it must be admitted that were rutile nuclei to form it is extremely unlikely that these regions would produce a R.T. e.s.r. signal, and thus their presence would not be detected. In addition, the fact that the form of the Ti^{3+} lines are unaffected by pre-crystallization heat treatments, is an indication that the statistical distributions of the crystal field parameters at the Ti sites, responsible for the broad glassy lines, are not reduced by these heat treatments, i.e. there is no evidence of an 'ordering' within the sphere of the Ti ions, and, by implication, there is no suggestion of an 'ordering' of the glass. We interpret the constant intensity of the resonance lines to be a consequence of the constancy in the number and nature of the other hole and electron trapping sites in the glass, rather than an indication that new Ti sites, which do not give R.T. e.s.r. signals, are formed at TiO_2 concentrations above $\sim 0.2\%$.

On crystallization of the glasses, two Ti^{3+} lines become evident. The inference must be that each line is characteristic of a different Ti^{3+} site each with orthorhombic symmetry. In the crystallization process, the distributions of the Hamiltonian parameters are reduced, i.e. the lines become sharper, although the parameters of the 'crystalline' lines (Figures 4.25 and 4.26) are certainly different to those of the 'glassy' line (Figures 4.12 and 4.13), neither 'crystalline' line arising simply from an

'ordering', i.e. a reduction in the g parameter distributions of the 'glassy' sites, and thus some change in the environment of the titanium ions has occurred. The extent of the g parameter changes are not so great as to imply large changes within the Ti sites, indeed the spectra suggest that whilst becoming less random on crystallization, the titanium complexes are not appreciably changed.

The Hamiltonian parameters of the two 'crystalline' lines which form the composite Ti^{3+} e.s.r. lines of the ceramic specimens, remain essentially unchanged throughout the range of ceramics from the various glass compositions and crystallization temperatures, only their relative proportions in a given ceramic vary. The ceramics whose principal crystalline phase is Enstatite-like, i.e. melts (4) and (5), crystallized at 1000°C, have a 'pure' e.s.r. line, that is, it can be simulated assuming a single Ti site only. The Cordierite ceramics have composite lines which are dominated by a Ti^{3+} line from a second site and which contain varying proportions of the first, i.e. Enstatite, line. The X-ray diffraction results show that whenever Cordierite is the major crystalline phase, there is an indication of the presence of some Enstatite-like phase. The diffraction lines D and E, characteristic of the Enstatite phase are, for a given glass composition, some two to four times more intense on the diffractograms of the 1200°C ceramics than on those from the 1000°C ceramics (c.f. Figures 3.1 and 3.3). When we observe that the analysis of the e.s.r. lines shows that ~ 8% of the Ti^{3+} line intensity from a specimen of melt (3) crystallized at 1000°C is due to the 'pure' e.s.r. line from the Enstatite ceramics, and that this contribution increases to ~ 30% in the same glass crystallized at 1200°C, the correlation of the proportions of the two crystal phases, (i.e. Enstatite and Cordierite), with the intensities of the two component lines, becomes evident. (We would not expect, from previous discussion, that the relative intensities of the component e.s.r. lines be in <u>direct</u> relationship with the relative proportions of the crystal phases).

It appears therefore that some Ti ions are incorporated into the Enstatite and Cordierite crystal phases, and, in the simultaneous presence of both phases, Ti ions are located in each phase. Measurements reported later in this thesis suggest that the parent glasses have a phase separated structure and that the primary crystal phases are heterogeneously nucleated by a metastable phase which crystallizes from a separate titanium rich glass phase. Thus, although by no means indicating that such a process is active, the ubiquitous nature of the titanium ions in the ceramic specimens, (X-Ray diffraction also indicates a TiO_2 phase, Rutile, in the Cordierite ceramics), is perhaps to be expected.

We consider now the e.s.r. hole spectra.

4.3.5 Oxygen associated hole centres (O.H.C.)

Radiation produced paramagnetic centres, (R.P.C.), in oxide glasses have been widely reported, e.g. references (4.31,4.33,4.34,4.40,4.48-4.55) specifically concern $S = \frac{1}{2}$ hole centres. The general nature of radiation 'damage' centres in glass has been reviewed by Griscom (4.56). Figure 4.37 is a schematic showing the most common 'defects' of the glass nework itself, (excluding modifier associated traps), and the associated paramagnetic centres after irradiation. Considering only the hole centres, then, 'defect' (1) is a non-bridging oxygen (n.b.o.) singly bonded to a network former, in our case a Silicon ion. The n.b.o. may be considered a negative point defect if its charge compensating cation is absent or displaced, and may therefore trap a positive hole. 'Defect' (2) may occur if R_B is Al or B, (trivalent ions), and R is Si (quadravalent). Then, the negative Si-O-Al complex may also provide a trapping site for a positive hole. The above centres are generally referred to as oxygen associated hole centres, (O.H.C.), because the Hamiltonian parameters of these centres have been found to be

a). BEFORE IRRADIATION

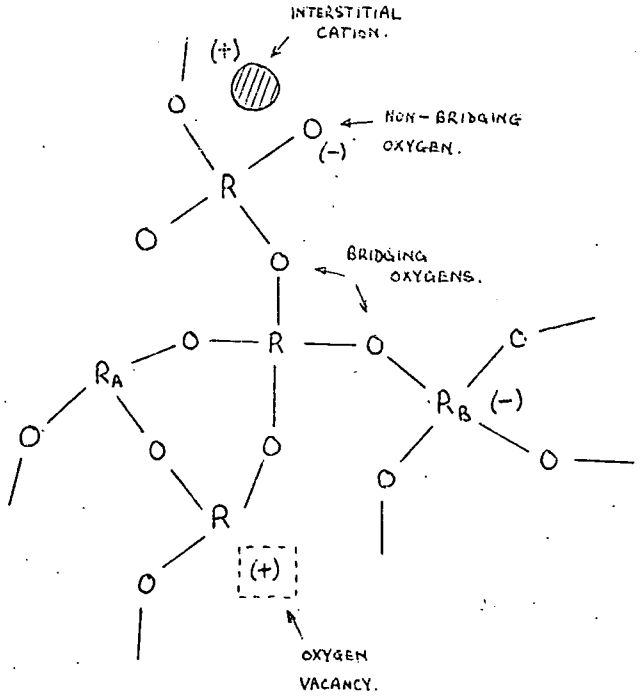

b). AFTER IRRADIATION

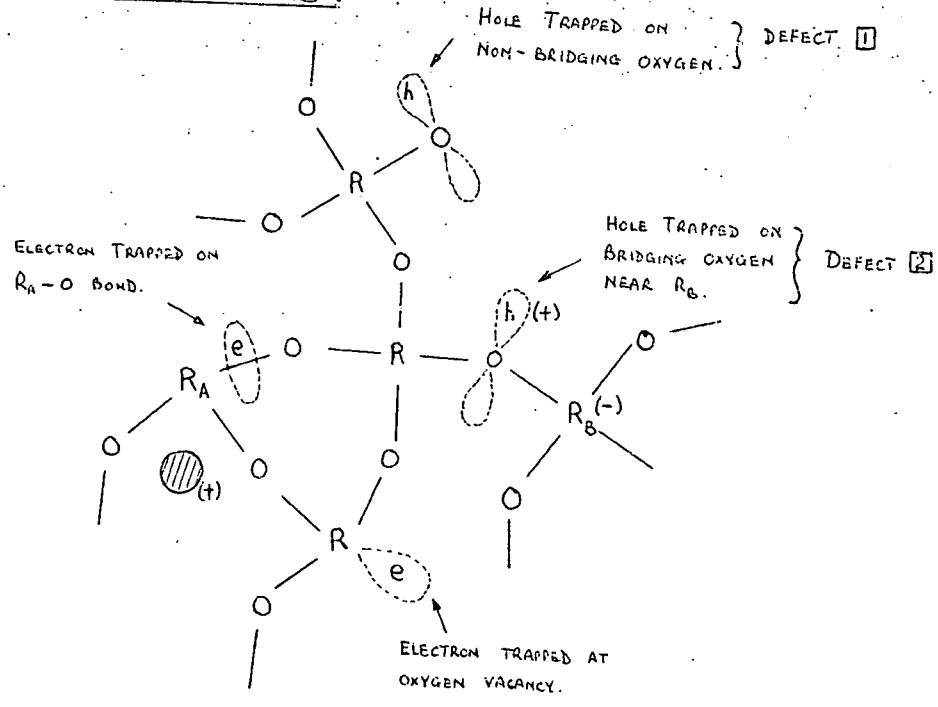

FIGURE 4.37. CONDENSED SCHEMATIC SHOWING SOME RADIATION INDUCED PARAMAGNETIC CENTRES AND THEIR RELATIONSHIP WITH PRE-EXISTING 'DEFECTS' OF THE GLASS NETWORK. (AFTER GRISCOM).

largely independent of the type of alkali in the glass (4.49), or indeed of the main glass-forming cations, e.g. Boron (4.55), Titanium (4.33) or Silicon (4.54). Griscom (4.56) and Taylor (4.56a) have collated the published results from oxide glasses, and by comparison of the derived Hamiltonian parameters of our 'glassy' hole centres (Figures 4.18 and 4.20), with the published data we can be reasonably certain that the centres responsible for our e.s.r. lines are holes trapped at oxygen ions, i.e. O.H.C's. For reasons discussed later we feel that, in the glass specimens, the specific defect involved is that of defect (1),i.e. holes trapped at n.b.o. bonded to Si ions. Radicals of the type O^- and O_2^- are unlikely to be present in significant quantities in silicate glasses (4.57) and, even then, the g values of these centres are not so well correlated with the g's of our centres as are the O.H.C. parameters. O_2^- radicals in TiO_2 have similar g's to our low titania centre (4.58). However the quantity of TiO_2 in the base glass, (melt 1), is less than the number of paramagnetic centres and so an O_2^- radical associated with TiO_2 is also an unlikely centre for our e.s.r. line.

4.3.6 Models of the O.H.C. in glass

Schreurs (4.54) has proposed that a hole centre with $g_1 = 2.003$, $g_2 = 2.009$, $g_3 = 2.019$ and which he denotes HCl, is due to a hole localized at the two n.b.o's. of an $\left[SiO_4\right]^{2-}$ tetrahedron, i.e. a SiO_4 unit with two bridging and two non-bridging oxygens. A second hole centre HC2 which has axial symmetry, and which Schreurs proposes is a hole trapped at a silicate tetrahedron with three n.b.o's. ($\left[SiO_4\right]^{3-}$), is dominant in high alkali glass.

Griscom (4.55,4.56) has proposed molecular orbital bonding schemes for the O.H.C's. involving bridging and non-bridging oxygen ions, (defects (2) and (1) respectively of Figure 4.37). The proposed steric

bonding picture and electronic levels of the n.b.o. defect are shown in Figure 4.38. The ground state of the hole is in a π type orbital which Griscom considers is at a slightly higher energy than the lone pair non-bridging level ($\sigma_Y^{N.B.}$). The g values of such a centre are given by

$$\begin{aligned} g_1 &\sim g_e \\ g_2 &\sim g_e \left(1 + \frac{C_2\lambda}{\Delta_1}\right) \\ g_3 &\sim g_e \left(1 + \frac{C_3\lambda}{\Delta_2}\right) \end{aligned} \qquad (22)$$

where C_2 and C_3 are constants of the order of 0.1 - 1.0 (4.7), λ is the spin-orbit coefficient of the O^- ion, and Δ_1 and Δ_2 are the energy separations of the levels shown in Figure 4.38. Using this model we consider the significance of the distributions in the g parameters.

4.3.7 Relative distributions of the principal g values

The slower base line return of the first derivative tracing on the high field side of electron spectra, and on the low field side of hole spectra, is a feature both of the spectra recorded here, and of all published spectra from S = ½ paramagnetic sites in glass, and although noted uncritically by many authors, and ascribed to an excess distribution of one principal g value relative to the other(s) by some (4.50,4.53), only one group of workers (4.55,4.59) have attempted to interpret from fundamental theory the structural significance of these apparent distributions. This final group have analysed the bridging oxygen defect, (defect (2)), and we consider their results in the next section, wherein we consider the spectra from the ceramic specimens. At present we are concerned with the analysis of defect (1), which for reasons presented later, appears to be the centre responsible for the hole spectra in the glass specimens.

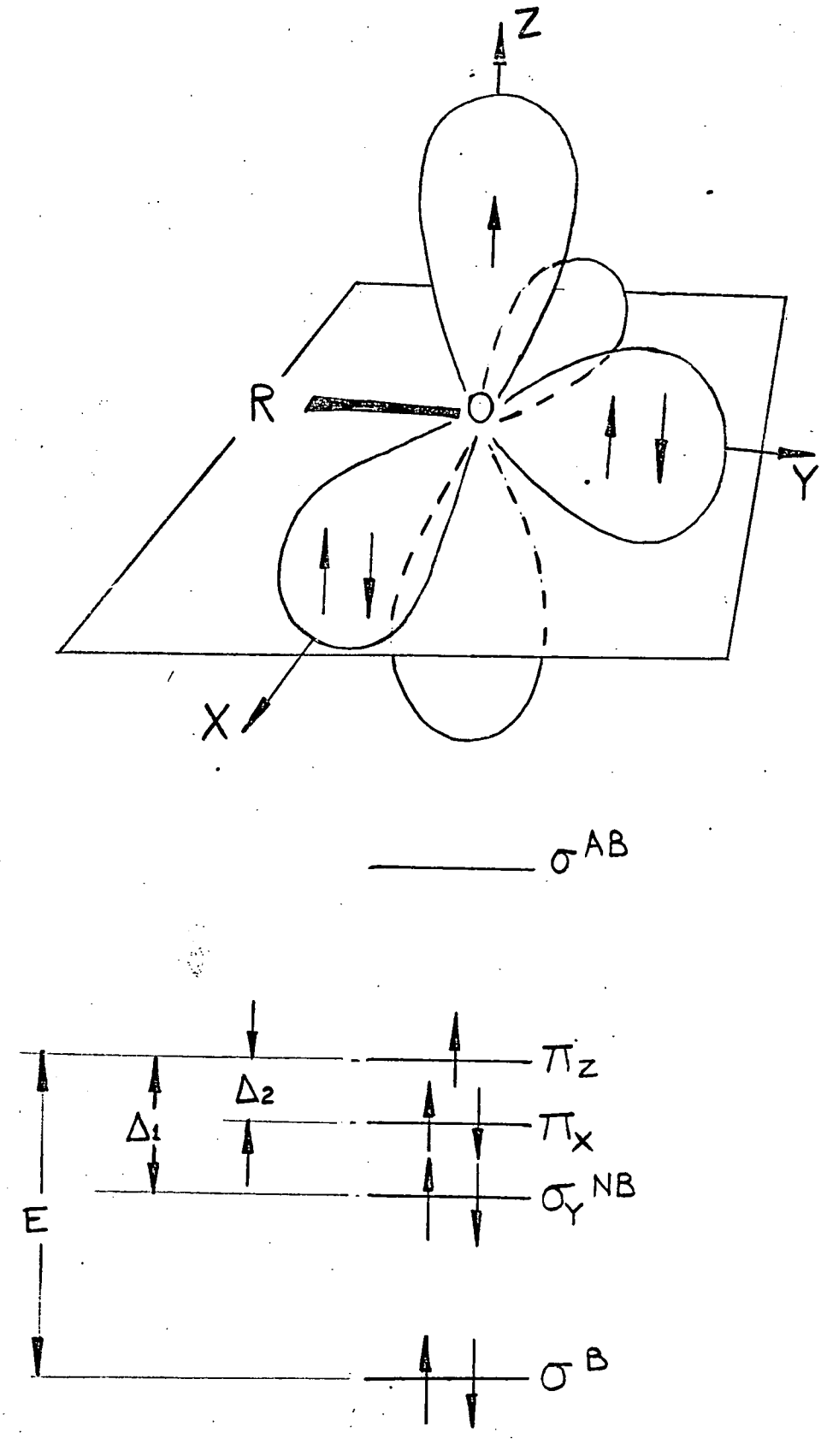

FIGURE 4.38. SCHEMATIC OF A NON-BRIDGING OXYGEN TRAPPED-HOLE CENTRE. UPPER: STERIC PICTURE. LOWER: ELECTRONIC ENERGY LEVELS.

In amorphous materials one would expect a statistical distribution of the crystal fields at the paramagnetic sites. Thus the orbital ground states of the S = ½ hole and electron systems observed in this work would have a distribution of energies, i.e. there would be a 'spread' in the d_{xy} ground state of the Ti^{3+} ion, (Figure 4.36), and of the π_x ground state of the O.H.C. (Figure 4.38). As a proportion of the energy separation between the ground and higher orbitals this spread is greatest for the levels lying closest to the ground state, (assuming no additional distributions of the higher levels). Thus inspection of equations (21) and (22) shows that

$$\delta g_1 < \delta g_2 < \delta g_3 \quad \text{or} \quad \delta g_\perp < \delta g_{\parallel}$$

where δg represents the distribution of a parameter and g_1 or $g_\perp$ is the principal value closest to g_e. Thus additional distributions of the principal g's furthest displaced from g_e is a result to be expected from the ground state distributions generated by isotropic crystal field variations. This argument of course is peculiar to glassy materials, the effect would be absent for sites experiencing identical crystal fields such as might be expected in well formed crystalline materials.

Quantifying the expected distributions requires a knowledge of the appropriate orbital level diagram and the relationship between the crystal field splitting parameters and the principal g values for the site under consideration. Using the well documented relationships for the Ti^{3+} ion, i.e. Figure 4.36 and equation (21), and the standard results:

$$\delta g_\perp = \frac{\partial g_\perp}{\partial \Delta_1} \cdot \delta \Delta_1$$

and

$$\delta g_{\parallel} = \frac{\partial g_{\parallel}}{\partial \Delta_2} \cdot \delta \Delta_2$$

where Δ_1 and Δ_2 are the energy splittings between the ground xy and xz/yz levels and the xy and $(x^2 - y^2)$ levels respectively, we have by

substituting the partial differentials from equation (21)

$$\frac{\delta g_{\perp}}{\delta g_{\parallel}} = \frac{\Delta_1^{-1}\left(\frac{\delta\Delta_1}{\Delta_1}\right)}{\Delta_2^{-1}\left(\frac{\delta\Delta_2}{\Delta_2}\right)} \qquad (23)$$

On entering the crystal field parameters Δ_1 and Δ_2 calculated from the g values derived in the simulation of Figure 4.12, and with the simplifying assumption that $\delta\Delta_1 \sim \delta\Delta_2$ we have

$$\frac{\delta g_{\perp}}{\delta g_{\parallel}} \sim 0.85$$

i.e. the distribution of $g_{\parallel}$ is some 20% greater than that of $g_{\perp}$. An estimated figure of

$$\frac{\delta g_{\perp}}{\delta g_{\parallel}} \sim 0.6$$

is plausible from the simulations of Figure 4.12. This is not sufficiently removed from the calculated figure, given the uncertainties in the calculation and of the contributions of the different linewidth broadening mechanisms to the experimental line, that any safe conclusions regarding the nature of the crystal fields at the Ti sites, can be drawn from the additional distributions evident in both the glassy and crystalline Ti^{3+} spectra.

Partial differentiation of equation (22) could in principle give an estimate of the expected relative distributions in the principle g's of the O.H.C. due to statistical distributions within the π_z ground state. However the values of the constants C_2 and C_3 in these equations have not been quoted in the literature and are difficult to estimate accurately enough to make such an exercise meaningful. We speculate therefore upon the interpretation of the broad distributions found in a single parameter,

(g_3), in the low titania glasses (Figure 4.18), and in two of the parameters (g_2 and g_3), in the high titania glasses (Figure 4.20).

The energy level scheme shown in Figure 4.38 implies that distributions of g_3 and g_2 arise from distributions in the crystal field parameters Δ_2 and Δ_1 which, from the steric bonding picture of this same figure, would result from variations in the crystal fields experienced by the π_x and σ_y^{NB} orbitals respectively, (ignoring at this stage the distributions within π_z). Thus in this scheme, distributions of g_2 and g_3 (beyond that expected from ground state distributions), reflect the 'randomness' of the crystal field in directions approximately perpendicular to the Si-O bond (π_x), and parallel to the bond (σ_Y^{NB}). It is pure speculation to equate distributions of g_2 or g_3 to specific directions relative to the Si-O bond unless it is known which of the levels, π_x or σ_Y, lies closest to π_z, e.g. a large distribution of g_3 implies that the crystal field is most 'random' in a direction parallel to the Si-O bond if σ_Y^{NB} is closest to π_z, but, with the level scheme of Figure 4.38 a distribution in g_3 implies that the randomness is greatest in a direction perpendicular to the Si-O bond. The mechanism responsible for the splitting of the π_2 and π_x molecular orbitals is not known (4.56), and thus the uncertainty in the orientation of the random field directions cannot be resolved. Nevertheless, <u>if</u> a ground state distribution is not responsible for the distributions observed here, then we may conclude that the n.b.o's. which provide the hole trapping sites, are, in the low Ti glasses, at sites where the crystal field is well defined in two dimensions and rather less well defined in the third dimension, and in the high Ti glasses the n.b.o. sites have crystal fields which are well defined in a single direction only.

This argument appears to this author reasonable for the M.O. scheme of the n.b.o. defect proposed by Griscom (4.56). It cannot be taken however as a general result for other paramagnetic centres with quite different bonding schemes - see later.

4.3.8 Structural Implications of the O.H.C. spectra from the glass specimens

The question is now in what type of silicate structure would the non-bridging oxygens bonded to a single silicon ion be expected to experience crystal fields of the nature discussed above? In general terms, structures in which the n.b.o's. are attached to SiO_4 units which are in two dimensional 'sheets', and in which the 'sheets' are joined by the predominantly ionic bonds of alkali or alkali earth ions, would appear to satisfy the requirement for a crystal field which is well defined in the two dimensions of the silicate 'sheets', and rather less well defined in a third, i.e. 'across' the 'sheets', under the reasonable assumption that the arrangement of the SiO_4 tetrahedra within the sheets is rather better than the ordering between the layers of tetrahedra. Structures consisting of silicate chains, i.e. one dimensional silicate structure might be expected to give oxygen sites where the crystal field is well defined in the dimension along the silicate chain, and rather more random in the remaining two dimensions corresponding to the ordering of the chains relative to one another.

The proposal is therefore that the glass hole centres are oxygen associate centres, and, more specifically, that the holes are located in the π orbitals of oxygen ions bonded to a single silicon ion, i.e. at n.b.o's. in the silicate framework. A speculative explanation of the shape of the resonance lines and the variations observed upon the addition of titanium to the base glass, is that the silicate units to which the n.b.o. are bonded have a two dimensional (sheet) arrangement in the low titania glasses, and a one dimension (chain) arrangement in the high titania glasses.

We show in the next chapter the correlation of an optical band found in all of the glasses with the e.s.r. hole centres. This absorption band is sufficiently near to the optical band associated by Schreurs (4.54) with the HC2 centre, that the location of our O.H.C. at $\left[SiO_4\right]^{2-}$ units is

reinforced. $[SiO_4]^{2-}$ tetrahedra are present in both of the principal crystalline silicates found on devitrification of the glasses, and their presence in the glasses themselves is not surprising. There is however a conflict with the proposal just discussed in that $[SiO_4]^{2-}$ tetrahedra may form silicate chains but not sheets which require the disilicate $[SiO_4]^{-}$ unit. This paradox can be solved by detailed consideration of the Cordierite and Enstatite structures. This is deferred until further experimental results relevant to the argument have been presented.

4.3.9 The Ceramic Hole Centres

The hole centres of the ceramic specimens are markedly different from the glassy hole centres, having a hyperfine interaction with a single ^{27}Al nucleus, ($I = {}^5/_2$). In addition, the principal g values of this centre are significantly different from those of the glassy centres.

Hole centres having a h.f. interaction with Al are also widely reported, (4.12,4,31,4.60-4.68). O'Brien (4.60) showed that in her Al doped quartz crystals, X-irradiation produced holes residing in the non-bonding orbital of an oxygen ion bridging between a Si ion and a substitutional Al ion. Most workers since have confirmed this analysis, concluding that the radiation produced centre with a h.f. interaction with Aluminium, is, in both aluminosilicate glasses and crystals, a hole at a π type orbital of an oxygen bridging between $[SiO_4]$ and $[AlO_4]$ tetrahedra, e.g. (4.12,4.66). This is the centre shown schematically in Figure 4.37, i.e. defect (2).

The uniformity in the reported g values of the O.H.C. discussed previously, (defect (1)), is not matched by a similar uniformity in the g parameters of the Al associated hole centre - although the analyses are often questionable, and we cannot therefore positively identify the centre observed here from a comparison of its derived g values with those values

published in the literature. However, the coupling constants $|A_1|$, $|A_2|$ and $|A_3|$ of our centre, ($\sim$ 9 gauss), compare well with the reported coupling constants of the Al associated centres, which range from 6 gauss (4.65) to 9.5 gauss (4.63), and with a reasonably certainty we assign our ceramic hole centres to holes trapped at Si-O-Al bridging oxygens.

The evidence in the literature suggests that Al ions in octahedral groups do not produce a h.f. hole spectrum. This is probably a consequence of the sp^3 hybridization of Al in tetrahedral coordination which would increase the Fermi contact interaction (4.2) and thus the hyperfine interaction compared with the non-hybridized p-type bonding of Al in AlO_6 groups. Alternatively, covalent-ionic changes in the nature of the bonds, giving the converse of an effect found by Taylor (4.69) for the h.f. splitting in the resonance from Mn^{2+} ions, may be responsible. Whatever the reason, the result seems well established, e.g. Grunin et al (4.12,4.66) found in crystalline aluminoscilicates that α-Spodumene with Al in 6-fold coordination gave an irradiation hole spectrum without h.f., and, on heat treatment of the crystals and the conversion to the β form where Al is in 4-fold, a hole spectrum with an Al associated h.f. interaction appeared after irradiation.

We must consider therefore whether the appearance of a resonance signal with resolved hyperfine only in the crystallized specimens is evidence of a coordination change of the Al ions from 6 in the glass to 4 in the ceramics. We think not. The great majority of workers have, like ourselves, observed a 'featureless' resonance in the glass, with the h.f. lines only in the ceramics, e.g. (4.31). It is extremely unlikely that, of the great variety of glasses studied, none would contain AlO_6 groups. In addition, the work of Royak et al (4.61) wherein Gehlenite crystals ($CaO-Al_2O_3-SiO_2$), were slowly fused, resulting in the disappearance (in the glass), of the h.f. lines present in the crystalline spectra, would not support a coordination change hypothesis.

Is therefore the random nature of the glassy phase responsible for this general effect? We would argue so, but, it cannot simply be an inherent line broadening, i.e. reduced resolution, effect, because two groups of workers have observed, albeit poorly resolved, hole centres with an Al associated h.f. interaction, in their silicate glasses (4.62,4.65). In addition, in studies of Borate glasses (4.55,4.56a), which are not thought to be less 'disordered' than silicate glasses, the glass hole spectrum is almost entirely the Boron Oxygen Hole Centre (B.O.H.C.), characterised by a clearly resolved h.f. interaction with a ^{11}B nucleus, and which has been analysed as a hole trapped at an oxygen ion bridging between 3 and 4 coordinated boron ions, and as such is analogous to our Al associated centre. Also against a simple 'randomization' hypothesis is the g analysis which has shown that two distinct sites are responsible for the lines in the glass and ceramic specimens.

We are left therefore with the concept of competitive trapping (4.46). We must conclude that defect (1) is the dominant capture centre in the glass specimens and that defect (2) is dominant in the ceramics, and that the intensity of the resonance signals from these centres is not a direct measure of the relative numbers of each of the centres in the glasses and the ceramics. In the crystal structure of Cordierite and Enstatite there are large numbers of n.b.o., i.e. defect (1), and equally, the glasses must contain Si-O-Al structures, i.e. defect (2).

The work of Bikbau et al (4.63) is most illuminating to this argument. His observations of the radiation induced hole centres in Al doped ($\sim$0.2 wt.%) orthosilicate crystals, (i.e. $\left[SiO_4\right]^{4-}$ units - 4 n.b.o. per tetrahedra,) showed that the Al associated centre with its h.f. structure dominated the spectrum. Clearly the ratio of Si-O-Al structures to $Si\text{-}O^-$ structure was very small in these crystals, nevertheless, the hole resided at the bridging rather than the non-bridging oxygen. We proposed here therefore

that in the glass the variations of local charge neutrality are much greater than in the crystals, giving many $Si-O^-$ sites where the charge compensating ion is further removed, or even absent from, its steric position expected in the crystalline form. Thus traps of this nature, i.e. defect (1), have a larger capture cross-section or trap depth than the bridging oxygen traps in the glass specimens, and the e.s.r. line shows no h.f. lines.*

In the spectra from the low Ti glasses we have observed on the high field side of g_1, two very weak lines separated by 8 - 10 gauss. Interestingly this pair of lines are not present in the hole spectrum of the high Ti glasses. These weak lines may be evidence of a weak resonance with an Al associated h.f. interaction, underlying the dominant 'featureless' line. This result was not consistently studied because of the very weak signals and because its possible relevance was not appreciated. However, we note that Pavlushkin et al (4.31.) have observed an Al associated h.f. centre in all crystalline compounds derived from the crystallization of a glass of Cordierite composition, with the exception of an unstable Magnesium-Aluminium-Titanate phase, wherein the e.s.r. line remains unchanged from the 'featureless' glassy line, (not unreasonably as there are no Si-O-Al bonds in this phase). Placing these observations together, we note that an association of the Al ions with Ti ions when titanium is added to the glass, would produce the admittedly weak effects in the hole spectrum just described, i.e. the disappearance of the pair of 'hyperfine' lines.

The analysis of the hole centres has shown that identical centres exist in both the Cordierite and Enstatite-like ceramics. We note that in

---

* The only isotope of Si with a non-zero nuclear spin, i.e. ^{29}Si is only 4.7% abundant (4.70), and thus h.f. interactions with Si nucleii are not observed in glasses without isotopic enrichment (4.56a).

the Cordierite structure, all of the Al ions are tetrahedrally co-ordinated, and all are bonded through a bridging oxygen to a Si ion (4.71), and thus the presence of Si-O-Al centres is expected. The Enstatite structure contains no Si-O-Al bonds and we must consider where the Al ions are located in these ceramics given that the e.s.r. spectra demand SiO_4 - AlO_4 groups bridged by Si-O-Al bonds. Previous arguments show that we cannot exclude the existence of Al ions in both the crystalline and glass phases of the ceramic, although it is unlikely that these ions are solely in the residual glass, and we consider their probable position in the Enstatite structure. The two non-equivalent interstitial sites between silicate chains are 6-fold coordination sites and thus the direct substitution of Al ions for Si ions of the chain seems more probable than the existence of the Al ions between the chains.

Finally, we consider the distribution of g_3 relative to g_1 and g_2 found for all of the bridging oxygen centres in this work. This distribution is a feature of the B.O.H.C. discussed previously. Griscom (4.56) observed that the molecular orbital bonding scheme for the oxygen ion bridging Si and Al ions may be expected to be similar to the M.O. scheme for the oxygen bridging between 3 and 4 coordinated boron ions, and therefore the analysis by these workers of the B.O.H.C. (4.55,4.56,4.59), should be relevant to the O.H.C. in our ceramics. They conclude that the excess distributions in g_3 result from variations of the B(III)-O-B(IV) bond angles, i.e. by analogy the Si-O-Al bond angles in our specimens. This is an attractive postulate in that it is well established that such statistical distributions of the bond angles is a feature of all glasses (4.72,4.73), and we can perhaps infer that these distributions are still present in the ceramics crystallized from the glasses.

The principal conclusions of this chapter will be summarised in the final chapter of this thesis, where they will be combined with the results from the following experimental chapters to produce a scenario of the structural changes which occur as TiO_2 is added to the base glass composition.

REFERENCES

CHAPTER 4

4.1 A Abragam and M H L Pryce, Proc. Roy. Soc. 951, A, 205, 135

4.2 A Abragam and B Bleaney, Electron Paramagnetic Resonance of Transition Ions. Clarendon Press 1970

4.3 R H Sands, Phys. Rev. V.99, No.4, 1955, P.1222-1226

4.4 F K Kneubuhl, J. of Chem. Phys. V.33, No.4, 1960, p.1074-1078

4.5 P C Taylor and P J Bray, J. of Mag. Res. 2 , (305-331), 1970

4.6 P C Taylor, J F Baugher and H M Kriz, Chem. Revs. 1975, V.75, No.2 p.203-240

4.7 P B Ayscough, Electron Spin Resonance in Chemistry, Methuen 1967

4.8 H M Assenheim, Introduction to Electron Spin Resonance, Adam-Hilger 1966

4.9 H Boim and G Bayer, J. Phys. Chem. Solids V.3 (1970) 2125-2137

4.10 D Loveridge and S Parke, Phys. and Chem of Glasses V.12, No.1 (1971) 19-27

4.11 J Baugher and S Parke in Amorphous Materials, Eds. R W Douglass and B Ellis, Pub. Wiley Interscience 1970 p.399-408

4.12 V S Grunin et al, J. of Non-Cryst. Solids 13 (1973/74) 243-250

4.13 F G Burns, 'Mineralogical Applications of Crystal field Theory' C.U.P. 1970

4.14 Gladrey and Swalen, J. of Chem. Phys. V42, No.6 (1965) 1999-2010

4.15 A Carrington and H C Longuet-Higgins

4.16 J S Griffiths in 'The Theory of Transition Metal Ions' C.U.P. 1964

4.17 M H L Pryce, Proc. Phys. Soc. A63 (1950) 25

4.18 J H Van Vleck, Phys. Rev. 57 (1940) p.426

4.19 B Bleaney et al, Proc. Phys. Sco. A68 (1955) p.57

4.20 R C Wilson and R J Myers, J. Chem. Phys. 64 5 (1976) 2208-2211

4.21 T Purcell and R A Weeks, J. Chem. Phys. 54 7 (1971) 2800-2810

4.22 Y Boudeville and P DeMontgolfier, Chem. Phys. Lett. 30 3 (1975) 469-471

4.23 Bl. V J Rao, Phys. Chem. of Glasses 4 1 (1963) 22-34

4.24 D L Evans, J. Amer. Ceram. Soc. 53 7 (1970) 418-419

4.25 D G Ostrizhko and G A Pavlova, Inorg. Mater. Consult. Bur. Transl, 6(1) (1970) 58-61

4.26 G J Copley et al, Phys. Chem. of Glasses 14 1 (1973) 73-76

4.27 A Paul, J. Mat. Sci. 10 (1975) 692-696

4.28 N R Yafaev and Yu. V Yablokova, Sov. Phys. Solid State V4 No.6 (1962) 1123-1127

4.29 G E Peterson and C R Kurkjian, Sol. State Comm. 11 (1972) 1105-1107

4.30 C R Kurkjian and G E Peterson, Phys. Chem. of Glasses 15 1 (1974) 12-17

4.31 N M Pavlushkin et al, Inorg. Mater. Consult. Bur. Transl. 10(10) (1974) 1852-1857

4.32 N S Garif'yanov and L V Tokareva, Soviet Phys. Sol. State 6 5 (1964) 1137-1139

4.33 Y M Kim and P J Bray, J. Chem. Phys. 53 2 (1970) 716-723

4.34 T A sidorov and V A Tyul'kin, Inorg. Mater. Consult. Bur. Transl. 2 (1966) 1763-1767

4.35 S Arafa, J. Amer. Ceram. Soc. 55(3) (1972) 137-141

4.36 S Arafa and F Assabghy, J. App. Phys. 45 12 (1974) 5269-5271

4.37 S Arafa, Int. Cong. Glass (Pap.) 10th 1974, Pub. 1974 V5 (1974) 24-29

4.38 S Arafa, Phys. Chem. of Glasses 15 1 (1974) 42-46

4.39 S Arafa et al, J. Amer. Ceram. Soc. 58 5-6 (1975) 203-206

4.40 E I Abrakhmanova and R Ya Khodakovskaya, Fiz. Khim. Stekla 3 2 (1977 (1977) 100-102

4.41 P C Taylor and P J Bray, J. Phys. Chem. Solids 33 (1972) 43-58

4.42 L D Bogomalova et al, Int. Cong. Glass (Pap.) 10th, Pub. 1974 V12 (1974) 71-78

4.43 D L Griscom and R E Griscom, J. Chem. Phys. 47 8 (1967) 2711-2722

4.44 L D Bogomolova et al, J. Mag. Res. 15 (1974) 283-291

4.45 TT I Barry and L A Lay in 'Reactivity of Solids' Wiley Intersci. Proc. 6th Int. Symp. on the React. of Solids 1968, Eds. J U Mitchell et al, Pub. 1969 pgs. 685-693

4.46 E J Friebele et al in Int. Cong. Glass (Pap.) 10th, Pub. 1974 V.6 (1974) 16-22

4.47 N M Pavluskin et al in 'The Structure of Glass' Ed. E A Porai-Koshits, Consult. Bur. N.Y. 1973 V.8 (1973) 139-144

4.48 V A Tyul'kin et al, Izv. Acad. Nauk. Consult. Bur. Transl. 9(3) (1973) 413-415

4.49 V A Tyul'kin and L G Gerasimova, Ibid 9(8) (1973) 1463-1465

4.50 E A Zamotrinskaya, Ibid 7(1) (1971) 148-153

4.51 E I Abrashitova and R Ya Khodakobskaya, Fiz. Khim. Stekla V.3 Pt.5 (1977) 434-438

4.52 M Kayshima et al, J. Amer. Ceram. Soc. V.61 Pt.7-8 (1978) 311-314

4.53 E A Zamotrinskaya, Izv. Vyss. Uch. Zav. Fiz. 6(109) (1971) 788-791

4.54 J W H Schreurs, J. Chem. Phys. 47(2) (1967) 818-830

4.55 D L Griscom, P C Taylor, D A Ware and P J Bray, J. Chem. Phys. 48(11) (1968) 5158-5173

4.56 D L Griscom, J. Non-Cryst. Solids 13 (1973-74) 251-285

4.56a P C Taylor in 'Treatise on Mater. Sci. and Technol.' V12 p.223-281 Eds. M Tomazawa, R H Doremus, Academic Press 1977

4.57 R A Weeks in 'Interaction of Radiation with Solids' Ed. A Bishay Pub. Plenum Press N Y 1967

4.58 R D Iyengar and M Codell in 'Adv. in Colloid and Interface Sci' 3 (1972) 365-388

4.59 D L Griscom, G H Sigel and R H Ginther, J. Appl.Phys. 47(3) (1976) 960-967

4.60 M C M O'Brien, Proc. Roy. Soc. A231 (1955) 404-414

4.61 S M Royak et al, ZL. Prikl. Khim. 46(1) (1973) 16-19

4.62 G O Karapetyan et al, Sov. Phys. Solid State 6(5) (1964) 1197-1203

4.63 M Ya Bikban and R Akramov, Izv. Acad. Nauk. Consult. Bur. Transl. 14(3) (1978) 397-400

4.64 D Zwingel, Sol. Stat. Comm. 20 (1976) 397-400

4.65 S Lee and P J Bray, Phys. Chem. Glass 3 (1962) 37-42

4.66 V S Grunin et al, Sov. Phys. Solid State 14(7) (1973) 1589-1593

4.67 E A Zamotrinskaya, Inorg. Mater. Consult. Bur. Transl. 6 (1970) 544

4.68 V A Ioffe and I S Yanchevskaya, Sov. Phys. Solid State 10(2) (1968) 370-374

4.69 P C Taylor and P J Bray, J. Phys. Chem. Solids 33 (1972) 43-58

4.70 Table of Nuclear Properties, Produced by Varian Associates, Palo Alto California

4.71 W A Deer, R A Howie and J Zussman in 'Rock Forming Minerals' Longmans 1962

4.72 B E Warren and R L Mozzi, J. App. Cryst. 2 (1969) 164

4.73 D L Griscom et al, Solid St. Comm. 15 (1974) 479-483

CHAPTER 5

OPTICAL ABSORPTION SPECTRA

This Chapter presents the results of optical absorption studies on the glasses as produced, and after γ irradiation. The differential spectra are analysed into Gaussian component bands and the significance of these bands discussed.

5.1 Experimental Spectra

The absorption spectra of each of the five glass compositions, with and without pre-crystallization heat treatment, were measured, and, as representative of the range of glasses, spectra from melts (1), (3) and (5) are presented in Figures 5.1, 5.2 and 5.3. The absorption coefficient (α) is calculated from the measured transmission I_t according to

$$\alpha = \frac{\text{Ln}\left[\frac{I_o}{I_t} \cdot \frac{(16\ n^2)}{(n+1)^4}\right]_t}{d}$$

where I_o is the beam intensity, n is the refractive index and d is the sample thickness, (see Appendix II). Also shown in these figures are the absorption spectra of the same specimens after irradiation with 1 Mrad of γ-rays.

The most noticeable effect of the addition of TiO_2 on the pre-irradiation spectra is the increased u.v. absorption which, in melts (4) and (5) produced a brown-red colouration, melt (5) being rather darker than melt (4) and melts (1), (2) and (3) have no colouration. Of particular interest in this work, however, is the additional aborption produced by the γ-irradiation, and, in Figures 5.4, 5.5 and 5.6 the differential absorption (i.e. the absorption coefficient at a specific wavelength after irradiation minus the absorption at that wavelength prior to irradiation) is presented. The lower traces of each of these figures show the differential absorption

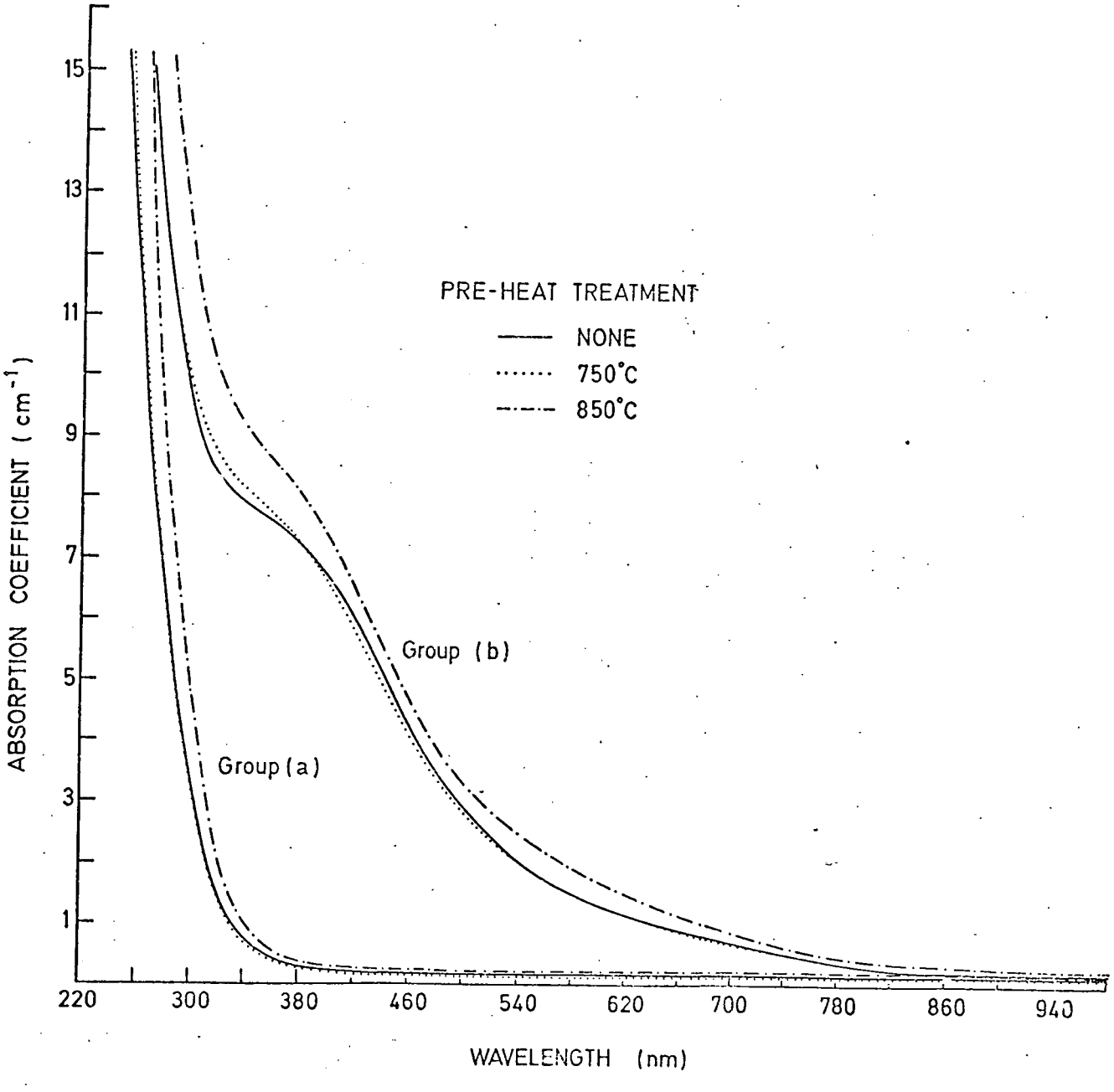

FIG. 5.1. OPTICAL ABSORPTION IN GLASS 1 . GROUP (a) BEFORE γ – IRRADIATION ; GROUP (b) AFTER γ – IRRADIATION.

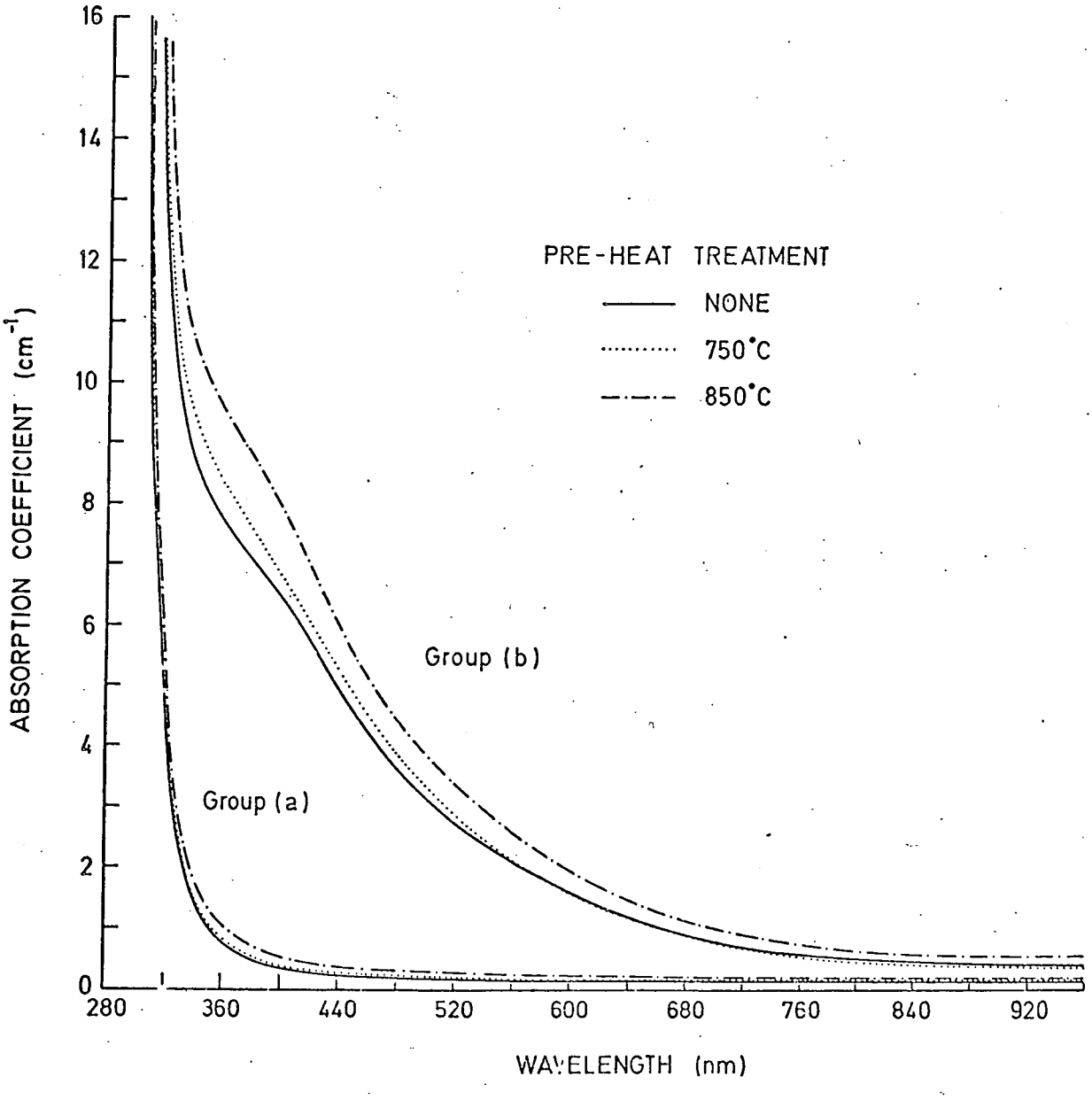

FIG. 5.2. OPTICAL ABSORPTION IN GLASS 3 . GROUP (a) BEFORE γ – IRRADIATION ; GROUP (b) AFTER γ – IRRADIATION.

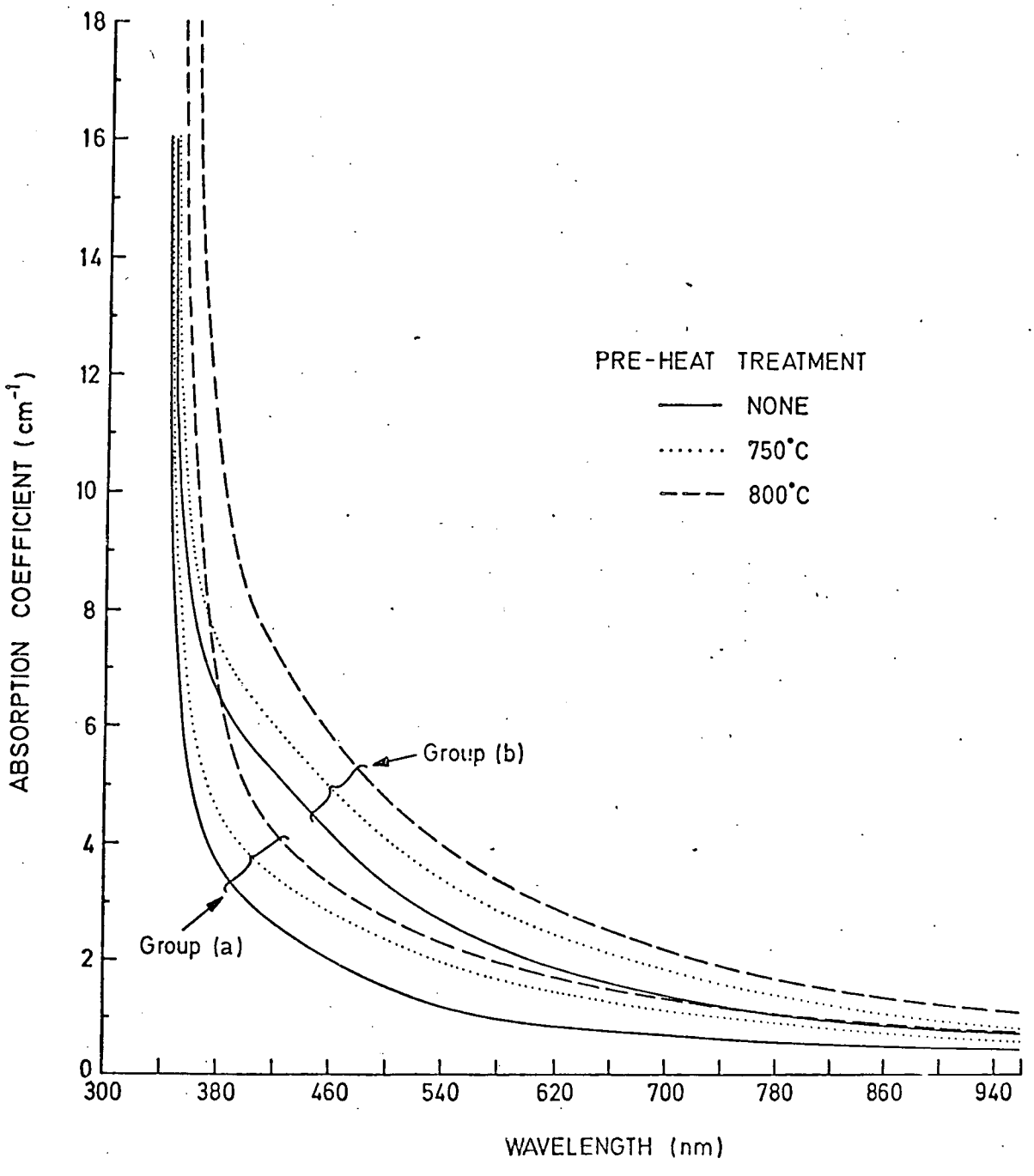

FIG. 5.3. OPTICAL ABSORPTION IN GLASS 5 . GROUP (a) BEFORE γ – IRRADIATION ; GROUP (b) AFTER γ – IRRADIATION.

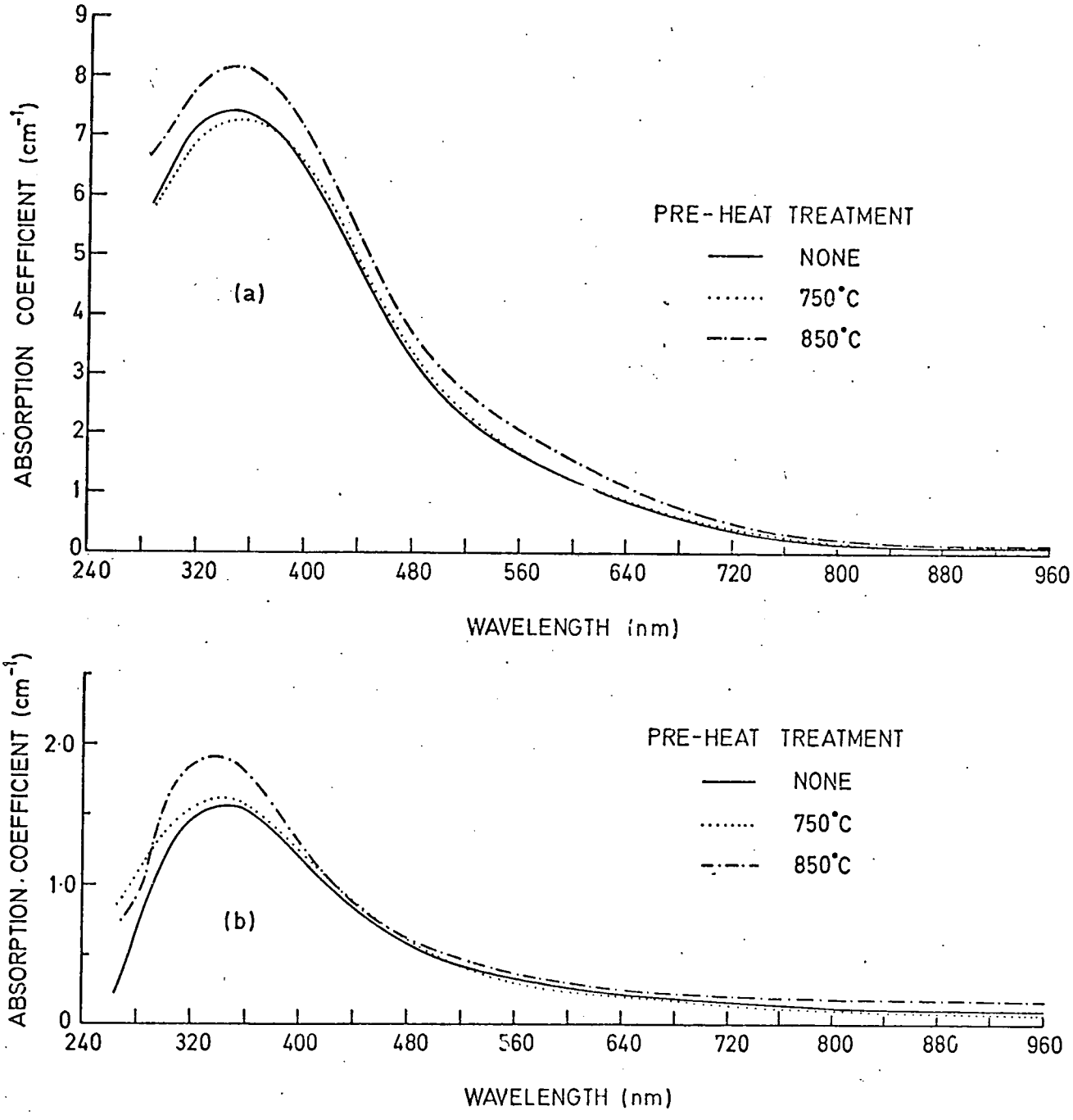

FIG. 5.4. DIFFERENTIAL ABSORPTION BETWEEN IRRADIATED AND UN-IRRADIATED SPECIMENS, (GLASS 1) ; (a) BEFORE AND (b) AFTER "SOAKING" AT 200 °C FOR 4 HOURS.

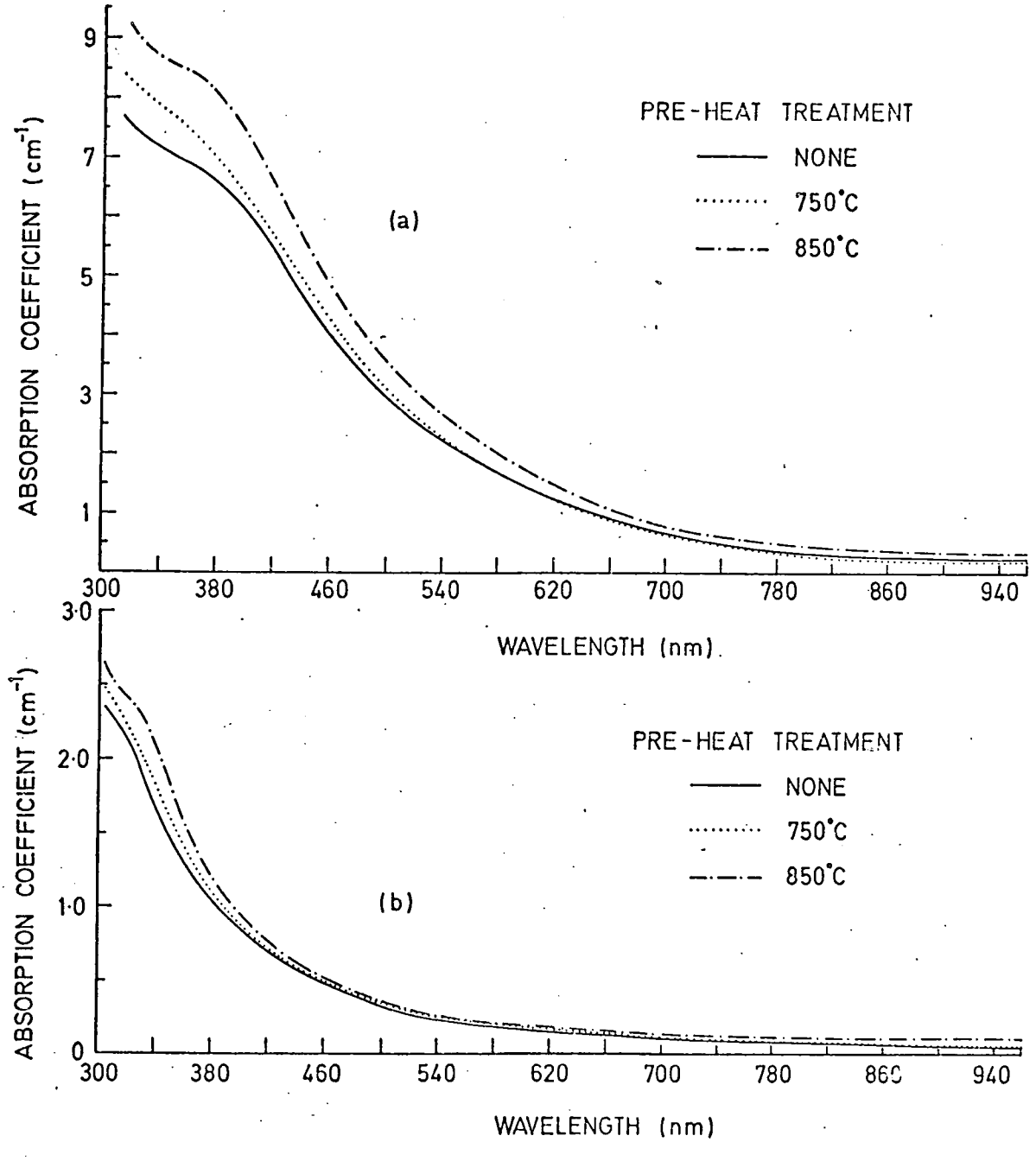

FIG. 5.5. DIFFERENTIAL ABSORPTION BETWEEN IRRADIATED AND UN-IRRADIATED SPECIMENS, (GLASS 3) ; (a) BEFORE AND (b) AFTER "SOAKING" AT 200 °C FOR 4 HOURS .

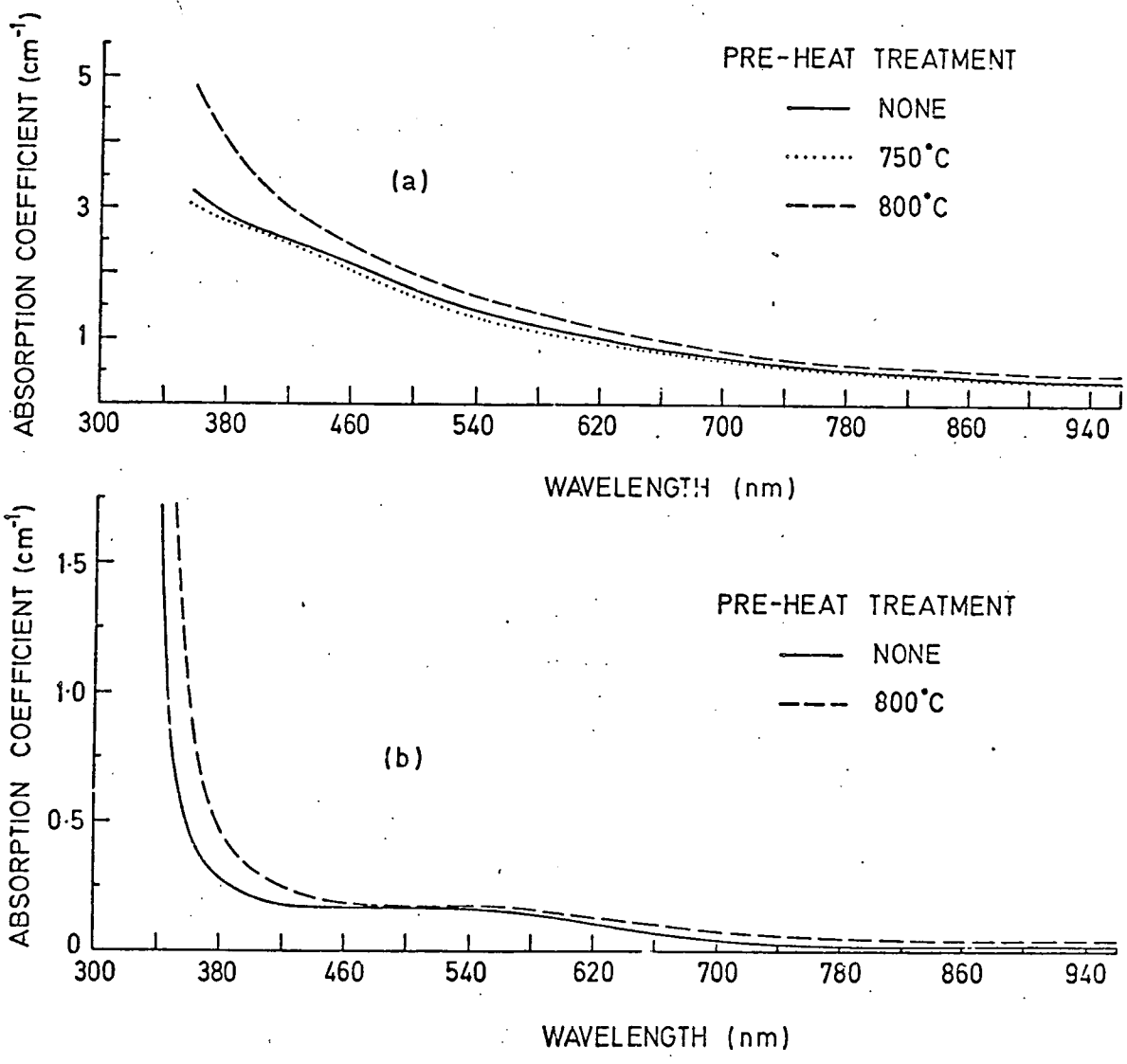

FIG. 5.6. DIFFERENTIAL ABSORPTION BETWEEN IRRADIATED AND UN-IRRADIATED SPECIMENS, (GLASS 5) ; (a) BEFORE AND (b) AFTER "SOAKING" AT 200 °C FOR 4 HOURS .

after an 'annealing' heat treatment at 200°C.

Figures 5.1, 5.2 and 5.3 show that the pre-crystallization heat treatments, particularly at the higher temperatures, shifts the 'u.v. edge' to longer wavelengths. This effect is small in melts (1), (2) and (3) and more pronounced in melts (4) and (5). However, Figures 5.4, 5.5 and 5.6 show that the induced γ-ray absorption is independent of pre-crystallization heat treatment, apart from a slightly increased absorption at higher heat treatment temperatures. Certainly, no new irradiation centres giving rise to an absorption in the wavelength range studied, (240 nm → 1000 nm), are produced by heat treatment and from this point, as with the e.s.r. spectra, we deal with compositional effects only.

The analysis of the differential spectrum of melt (1), (Figure 5.4), is shown in Figure 5.7 (the abscissa is now a linear energy scale, i.e. wavenumber). Three bands of Gaussian form (5.1) can be resolved in the upper trace, and, as the lower trace shows, these bands, although diminished in intensity, are still the principal components after the sample has been annealed for four hours at 200°C. The analysis of the melt (2) and (3) differential spectra yield similar results, but the melt (4) and (5) spectra are different enough to warrant separate discussion. The analysed spectrum of melt (5), as typical of both melts (4) and (5), is shown in Figure 5.8(a), traces (b) and (c) being the differential spectra after one hour and four hours at 200°C. Five bands are resolved in this spectrum and these bands remain the components of the spectrum after 'annealing' heat treatments. Figures 5.7 and 5.8 therefore encompass the optical bands created in the glasses upon γ-irradiation and the decay characteristics of these bands upon heat treatment of the speciments at 200°C.

Finally, therefore, in Figure 5.9, the growth characteristics of the optical bands are typified. The figure shows the differential spectra of a Melt (4) specimen after irradiation with doses of 1 Mrad and 300 Mrad.

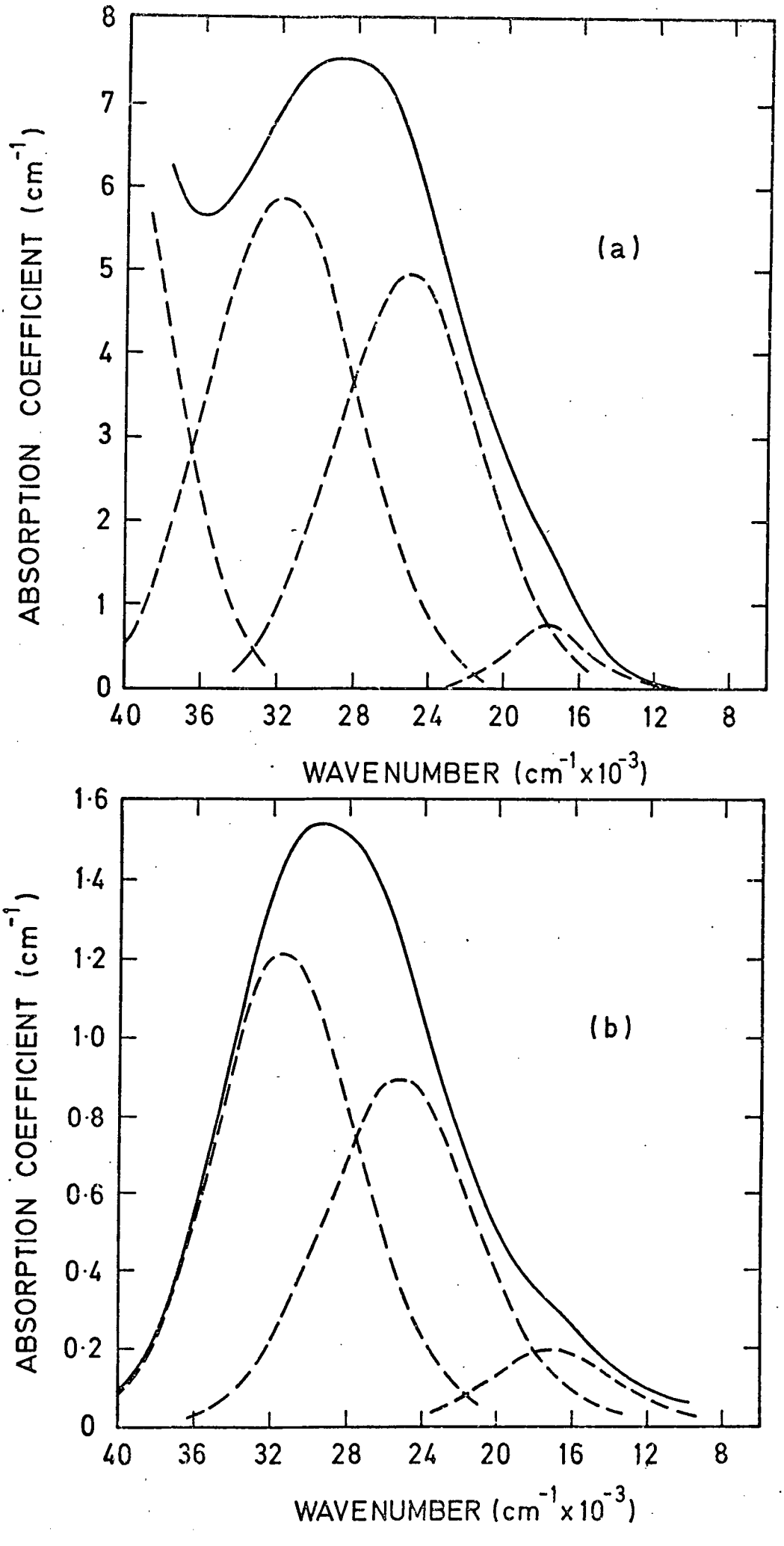

FIG. 5.7. Differential absorption in glass 1. (1 M rad)
a) before. b) after 4hrs at 200°C.

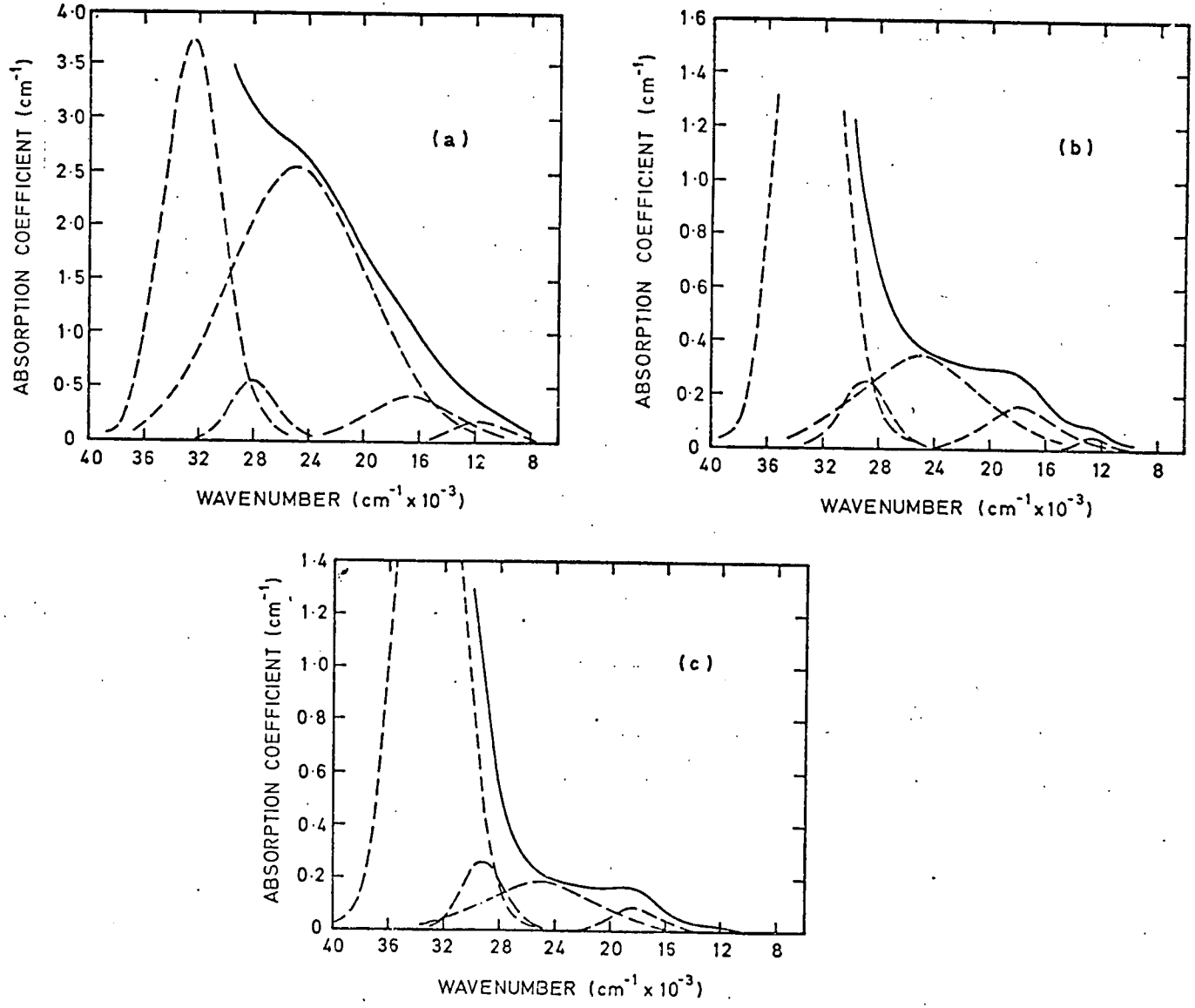

FIG. 5.8. Differential absorption in glass 5, (1 M rad)
a) before. b) after 1 hr. at 200°C. c) after 4 hrs. at 200°C.

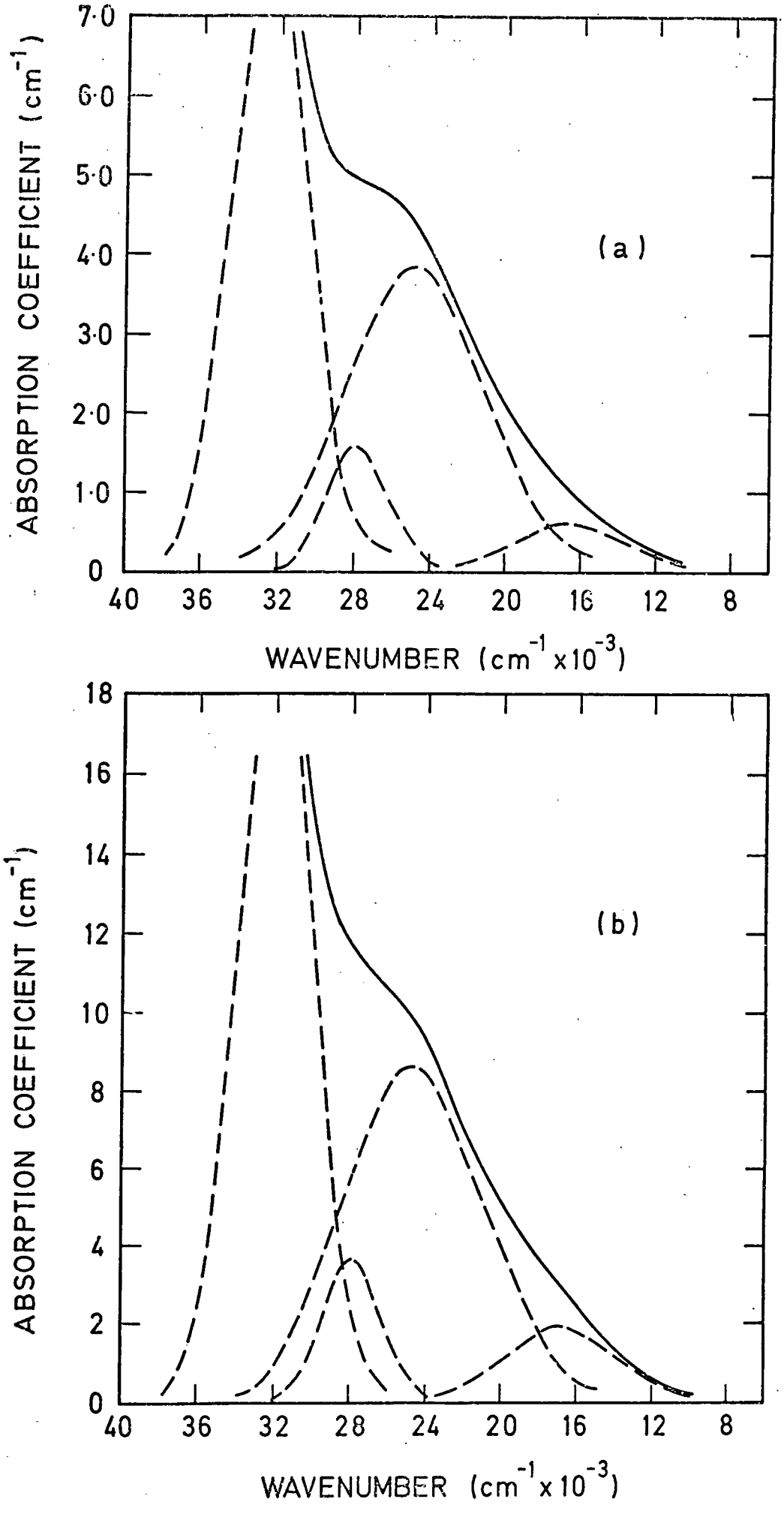

FIG. 5.9. Differential absorbtion in glass 4
a) after 1 Mrad b) after 300 Mrads.

No new bands are created, and, to varying extents, all of the induced bands increase in intensity upon prolonged irradiation beyond 1 Mrad. This general statement is true for all of the glasses studied, and a more detailed discussion of growth characteristics follows in the next section.

5.2 Discussion of the Experimental Spectra

Radiation induced colour centres in silicate, phosphate and borate glasses, and in crystalline silicates, have been extensively studied and the early definative work is reviewed by Lell,[5.2] (simple and binary silicates and glasses), and by Bishay,[5.3] (multicomponent glasses). The E.M. radiation is not capable of creating structural defects, but only of changing the electronic distribution, and thereby generating trapped holes and electrons at 'defects' already present in the specimen.[5.4] In quartz and fused silica there are numerous bands between 200 nm and 230 nm[5.5] due to hole and electron traps at defects (e.g. oxygen vacancies, Si-Si bridges etc.), in the silica network, but in the region studied here, most published spectra from irradiated silicate glasses resolve to three principal bands in the region of 620 nm (16.1×10^3 cm^{-1}); 430 nm (23.3×10^3 cm^{-1}); and 310 nm (32.3×10^3 cm^{-1}).[5.6] Indeed, the similarity in the form of the spectra from silicate, phosphate and borate glasses, indicated a common origin for the defects.[5.6] One defect common to all glasses is the non-bridged oxygen, and it seems likely that holes trapped at n.b.o's. are responsible for each of the three aforementioned bands. The precise nature of each defect is returned to later.

We consider now the analysis of the spectra reported here (Figures 5.7 and 5.8). Absorption bands at approximately 25×10^3 cm^{-1} and 17×10^3 cm^{-1} are present in both samples and indeed in the spectra of all of the glasses studied. A band at approximately 32×10^3 cm^{-1} is clearly identified in the glass (1) specimen, (and also in glasses (2) and (3),

and, although a precise position and intensity cannot be established for this band in melts (4) and (5), it is probable that it is present in these melts too. In addition, the melts (4) and (5) have bands at approximately $28 - 29 \times 10^3$ cm^{-1} which are not present in melts (1), (2) and (3). There is also some indication of a weak band in the 11.5×10^3 cm^{-1} region in melt (5). The possibility of a correlation between an optical band and the e.s.r. hole centre previously discussed is now considered.

The area beneath the Gaussian optical bands is proportional to the product $\alpha_m U$ where α_m is the peak value of the absorption coefficient and U is the band width at half peak intensity, and, from Smakula's equation,[5.7] the number of colour centres is given by

$$N = \frac{0.87 \times 10^{17}}{f} \times \frac{n}{(n^2 + 2)^2} \alpha_m U$$

where f is the oscillator strength and n is the refractive index. Considering f to be constant and knowing n to vary by only 5% across the range of glasses, we assume proportionality between the product $\alpha_m U$ and the number of colour centres. The number of spins contributing to a given e.s.r. line is also proportional to the area beneath the absorption curve, which we find by double integration of the experimental first derivative spectrum.[5.8]

Throughout the range of glass samples studied the intensities of the hole and electron e.s.r. resonances could be correlated to within a factor of two, and within this experimental accuracy the intensities of the signals in different glasses was found to be constant. However, to compliment the optical absorption studies, in a limited number of specimens of melts (1) and (5), the irradiation growth and heat treatment decay of the e.s.r. intensities were measured with greater care, (i.e. as regards the sample position in cavity, sample quantity, microwave power, etc.). An examination of the e.s.r. and optical data for these melts revealed a correlation between the 25×10^3 cm^{-1}) optical band and the e.s.r. hole centre. The results

are summarised in Tables 5.1 and 5.2.

Table 5.1 shows that the general decrease in the 25 x 10^3 cm^{-1} band as the titania content in the glasses increases, is mirrored by a similar decrease in the e.s.r. hole centre intensity, at least at each end of the composition range. In addition, Table 5.2 shows that within a given glass composition the irradiation growth and 'annealing' decay of the two signals is, within the limits of measurement, identical. That is, although the 25 x 10^3 cm^{-1} optical band in melt (1) increases at a greater rate with irradiation dose than the same band in melt (5), the e.s.r. signal behaves correspondingly, increasing in melt (1) rather more quickly than in melt (5). Also, the optical band in melt (1) decays more slowly than in melt (5), and this effect is paralleled by the e.s.r. signals in these melts. There is, therefore, a strong correlation between the 25 x 10^3 cm^{-1} optical band and the radiation induced e.s.r. hole centre considered in the previous Chapter.

The work of Stroud et al[5.9] on Soda-Silica glass doped with cerium, established that bands at 22.7 x 10^3 cm^{-1} and 16.1 x 10^3 cm^{-1} are hole traps. His interpretation, later confirmed by Mackey,[5.10] is that the traps are normally filled π-orbitals associated with non-bridged oxygens on glass forming tetrahedra. Schreurs[5.11] extended this work and correlated the HC1 and HC2 e.s.r. lines discussed previously, with the optical bands above. On the basis of the intensity changes in the optical and e.s.r. signals with glass composition, Schreurs assigned the HC1 centre to the $\sim$23 x 10^3 cm^{-1} optical band and the HC2 centre to the $\sim$16 x 10^3 cm^{-1} optical band, and proposed that the HC1/23 x 10^3 cm^{-1} absorption was due to a hole trapped at a n.b.o. attached to an $(SiO_4)^{2-}$ tetrahedron, i.e. an SiO_4 unit with two non-bridging oxygens. This work has correlated an e.s.r. hole centre with an optical band at $\sim$25 x 10^3 cm^{-1}. The similarity of the hole centre found in this work and the HC1 centre has been previously

Table 5.1: A comparison of the intensities of the 25×10^3 cm^{-1} optical band and the e.s.r. hole centre in glasses (1) and (5) after a 1 Mrad dose of γ-rays.

Glass No.	Optical ($a_m U$)	e.s.r. ($\iint \frac{dX''}{dH} \cdot dH$).
1*	1.0*	1.0 *
2	0.9	**
3	0.9	**
4	0.8	**
5	0.7	0.6

* e.s.r. and optical intensities are relative to the melt (1) intensities which are normallized to unity for both signals.

** These specimens were not examined.

Table 5.2: The growth and decay characteristics of the 25×10^3 cm^{-1} optical band and the e.s.r. hole centre in glasses (1) and (5).

IRRADIATION GROWTH (^{60}Co γ-rays)				
Dose (Mrad)	Glass 1		Glass 5	
	e.s.r.	optical	e.s.r.	optical
0.5	0.7	0.8	0.8	0.8
1.0*	1.0 *	1.0	1.0 *	1.0
10	2.0	1.8	1.5	1.4
300	3.2	2.8	2.4	2.2
600	3.5	3.1	2.5	2.3

HEAT TREATMENT DECAY (at 200°C following 1 Mr)				
Time	Glass 1		Glass 5	
	e.s.r.	optical	e.s.r.	optical
0 hrs.*	1.0 *	1.0	1.0 *	1.0
1 hr	0.40	0.34	0.17	0.13
4 hrs.	0.21	0.18	0.09	0.07

* The e.s.r. and optical intensities of <u>both</u> glasses are normalized to unity after a 1 Mrad exposure. Thereafter, intensity figures are relative to the intensity at 1 Mrad.

noted, and we now consider the association of the 23 x 10^3 cm^{-1} band found by Schreurs and the 25 x 10^3 cm^{-1} band found in this work.

Kats[5.4] established that the position of the ∿ 23 x 10^3 cm^{-1} band was quite sensitive to the type of alkali in the glass. Studies of 30 mol.% of differing alkalis showed that although the 32 x 10^3 cm^{-1} and 16 x 10^3 cm^{-1} bands changed very little throughout the range of alkalis studied, the 23 x 10^3 cm^{-1} band had its peak at 24.1 x 10^3 cm^{-1} for Li_2O at one extreme and at 20.4 x 10^3 cm^{-1} for Cs_2O at the other. They ascribed this effect to the size of the alkali ion, i.e. its ionic radius. However, as each of the ions studied was monovalent perhaps the criterion may well have been the ionic field strength, (Z/r^2). Continuing the series of modifier ions to Mg^{2+} therefore, with its relatively high field strength,[5.12] may well account for the shift to shorter wavelengths which we observe for this band.

With caution therefore, we ascribe the 25 x 10^3 cm^{-1} optical band and the e.s.r. hole resonance to a single centre, that centre, following Schreurs, being a hole trapped at a non-bridged oxygen ion in an $[SiO_4]^{2-}$ unit.

Thus we return to the remaining bands present in all of the glass specimens, those at 32 x 10^3 cm^{-1} and 17 x 10^3 cm^{-1}. The 17 x 10^3 cm^{-1} band is ascribed by Schreurs[5.11] to a hole trapped at a n.b.o. at an $[SiO_4]^{3-}$ unit, (the HC2 centre), and Yokota[5.13] and Karapetyan[5.14] ascribe the 32 x 10^3 cm^{-1} band to a hole trapped at an alkali vacancy neighbouring a non-bridging oxygen ion. We should therefore consider the apparent absence of any aluminium associated or Ti^{3+} optical bands.

Aluminium in glass terms is an intermediate oxide,[5.12] and in both crystals and glass it is found in both 4- and 6-fold co-ordination with oxygen. Due to this undertainty of co-ordination state in glass there is a corresponding uncertainty in the position and assignment of aluminium associated colour centres in glass. However, in known co-ordination states,

e.g. when quartz is doped with Al as an impurity, (Al in 4-fold), the main irradiation band is at 21.0 x 10^3 cm^{-1} and is associated with a hole trapped at an oxygen atom bonded to the Aluminium in an $[AlO_4]^-$ unit.(5.15) There is also a much weaker band at 16.1 x 10^3 cm^{-1}. The e.s.r. properties of this defect, i.e. its associated hyperfine structure, have been discussed previously. In silicate glasses, the hole trapped at an oxygen on an $[AlO_4]^-$ unit is correlated with an optical band at 18.2 x 10^3 cm^{-1}.(5.16) Thus we must conclude, due to the absence of bands in the 18 - 21 x 10^3 cm^{-1} region that there is no evidence of $[AlO_4]$ units, although this must be a very weak statement.

In structures where Al is known to exist in 6-fold co-ordination, e.g. corundum, (Al_2O_3), there are many γ-irradiation produced bands,(5.17) most notably in the wavelength range studied here at 24.8 x 10^3 cm^{-1}. This band has also been found by Bauer(5.18) in γ-irradiated Al_2O_3, and ascribed to a hole on an n.b.o. attached to an $[AlO_6]$ unit and stabilized by an associated divalent impurity, (Fe^{2+}). They find that an axial e.s.r. signal with Hamiltonian parameters $g_\perp = 2.007$ and $g_\parallel = 2.012$ is associated with the optical band. Other authors have correlated this band, (at 25.6 x 10^3 cm^{-1} in their work), with a six line hyperfine e.s.r. signal.(5.14) Neither of the above e.s.r. lines are present in the glasses studied here, and as before we conclude that the band at 25 x 10^3 cm^{-1} is most likely due to a hole trapped at an $(SiO_4)^{2-}$ unit. We consider now the optical absorption produced by the titanium ion in other glass and crystal systems.

Quadravalent titanium, i.e. Ti^{4+}, is a d^o system and produces no 'crystal field' bands, although charge transfer absorption, which is Laporte allowed(5.19) and thus intense, is possible between the Ti^{4+} ion and the surrounding ligands. We return to charge transfer absorptions later. The splitting of the ^2D ground state of the Ti^{3+} ion by various types of distortion of the ligand octahedron has been discussed in the

previous chapter, and, from previous arguments, we reproduce in Figure 5.10 the most probably energy level diagram (neglecting the possible orthorhombic splitting). The optical transitions from the ground state are indicated in the diagram. The crystal field splitting parameter, Δ, is the energy separation between the lower levels of the original doublet and triplet created by the cubic crystal field, (in perfect octahedral co-ordination it is the energy difference between the E_g and T_{2g} levels), and gives rise to the strongest crystal field absorption. δ, represents the energy splitting within the lower triplet due to the tetragonal distortion and this gives rise to a weaker, longer wavelength absorption which is often observed as a shoulder on the main band.[5.19,5.20,5.21] Pryce[5.22] developed relationships between the position of the e.s.r. resonance absorption and the optical bands, which, in terms of Figure 5.10, may be written,

$$\Delta = \frac{4\, g_e\, \lambda}{(g_e - g_{\parallel})} \qquad (5.1)$$

and

$$\delta = \frac{g_e\, \lambda}{(g_e - g_{\perp})} \qquad (5.2)$$

where g_e is the free electron g value, (2.0023), and λ is the spin-orbit coupling constant. For the free T_i^{3+} ion $\lambda = 154\ cm^{-1}$.[5.23] Using the above relationships and the values of $g_{\parallel}$ and $g_{\perp}$ deduced from the simulated resonance spectra, (Figure 4.12) we obtain

$$\Delta = 17.1 \times 10^3\ cm^{-1} \quad (585\ nm)$$

and

$$\delta = 7.9 \times 10^3\ cm^{-1} \quad (1266\ nm)\ .$$

In fact, most of the reported T_i^{3+}, $^2B_{2g} \rightarrow {}^2B_{1g}$ optical bands lie in the

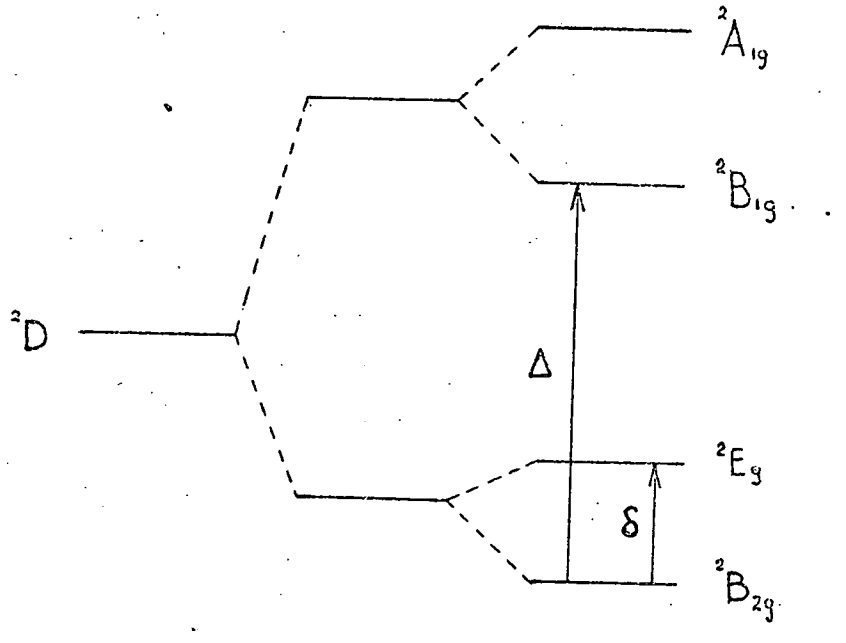

FIG. 5.10. ORBITAL LEVELS OF THE Ti^{3+} ION IN THE D_{4h} SYMMETRY OF A TETRAGONALLY COMPRESSED OCTAHEDRON.

region of 20 x 10^3 cm^{-1}, (500 nm).[5.19,5.20,5.21] We should, therefore, consider whether or not the 17 x 10^3 cm^{-1} band in our glasses is due to Ti^{3+} absorption.

At the onset this would seem improbable, noting that the band is observed in all glasses, including glass (1) with no added TiO_2. This glass shows only a very weak absorption in the region $g \sim 1.96$ and therefore at most a very small quantity of Ti^{3+} is present, at least two orders of magnitude smaller than that in the glasses with added TiO_2. Nevertheless, a comparison of the irradiation growth and thermal annealing of the Ti^{3+} e.s.r. signal and the 17 x 10^3 cm^{-1} optical band is made in Table 5.3 for a sample of Glass 5. The table clearly shows that a single centre is not responsible for both of these signals, and we must conclude that the Ti^{3+} optical absorption is either too weak to be observed, or that it is so broad that it cannot be resolved. Thus we consider the expected intensity of the Ti^{3+} optical absorption.

For states which have wavefunctions of the same parity, (either even or odd), the integral of the electronic dipole moment between the states vanishes,[5.24] and transitions induced by E.M. radiation are Laporte forbidden, i.e. the selection rule becomes

$$\Delta \ell = \pm 1$$

The 'd' electron wave functions are all of even parity and thus inter-d transitions are forbidden. Relaxation of this rule occurs whenever the ion is not at a centre of symmetry, due to the mixing of the 'd' and 'f' orbital wavefunctions, or, if the ion is in a centrosymmetric environment, vibronic coupling allows some, although a lesser, relaxation of the rule.[5.25] It is found therefore[5.26] that the 'crystal field' bands, (inter-d transitions), of the iron group transition metals in tetrahedral co-ordination are some 10 - 100 times more intense than those of the same

Table 5.3: The growth and decay characteristics of the 17 x 10^3 cm^{-1} optical band and the Ti^{3+} e.s.r. signal in glass (5).

IRRADIATION GROWTH (^{60}Co γ-rays)		
Dose (Mrad)	e.s.r.	optical
1 Mrad*	1.0*	1.0*
300 Mrad	1.2	3.2

HEAT TREATMENT DECAY (at 200°C following 1 Mrad)		
Time	e.s.r.	optical
0 hrs.*	1.0*	1.0*
1 hr.	0.6	0.3
4 hrs.	0.5	0.12

* The e.s.r. and optical intensities are normallized to unity after a 1 Mrad exposure. Thereafter intensity figures are relative to the intensity at 1 Mrad.

ion in octahedral co-ordination. For the Ti^{3+} ion in centrosymmetric encironments, e.g. $[Ti(H_2O)_6]^{3+}$ (crystal) [5.27] and titania doped Na_2O - B_2O_3 glass,[5.20] the peak value of the extinction coefficient ε is found to be between 5 and 15 litre per mole per cm, ($\ell\, m^{-1}\, cm^{-1}$), whereas in glasses where the Ti^{3+} ion has lost it s centrosymmetric site due to the co-ordination of one of its surrounding oxygen ions with a hydroxyl (O-H) group,[5.21,5.26] the value of ε is found to be in the range 250-500 $\ell m^{-1}\, cm^{-1}$ and significant colouration of the glass results. The concentration of radiochemically produced Ti^{3+} ions in the glasses studied here was 5×10^{17} spins per gram, and was constant within a factor of two through the range of glasses studied (Chapter IV). Thus we expect, (Appendix II), the peak value of the absorption coefficient (α) to be within the range 0.05 - 0.15 cm^{-1} when the Ti^{3+} ion is in a centrosymmetric site and 1.0 - 2.5 cm^{-1} if it is in a non-centrosymmetric environment.

An upper limit to the peak Ti^{3+} absorption can be estimated by assuming that after annealing, the residual absorption in the 17×10^3 cm^{-1} region is due entirely to the Ti^{3+} ion. The e.s.r. resonance signal decay, (Table 5.3), shows that the signal is 50% of its original intensity after four hours at 200°C, i.e. there are now 2.5×10^{17} Ti^{3+} ions per gram of melt. Thus the 17×10^3 cm^{-1} band peak value of $\alpha = 0.1$ cm^{-1} after annealing, gives a maximum molar extinction coefficient of 40 $\ell m^{-1}\, cm^{-1}$ for the Ti^{3+} ion. It is concluded therefore that the radiochemically produced Ti^{3+} giving rise to the e.s.r. electron centre is at the centre of symmetry of an octahedral site.

The presence of Ti^{3+} in tetrahedral symmetry was excluded by optical absorption measurements, (not presented here), which were extended to longer wavelengths (up to 2 μm). In a tetrahedral field the ^2D ground state is again split intro a triplet T_{2g} and a doublet E_g with, in this case, the doublet lying below the triplet. The total splitting between

the doublet and triplet is $^4/_9\ \Delta$, where Δ is the octahedral splitting parameter, and thus from previous considerations one would expect the absorption band from tetrahedral Ti^{3+} to be intense, ($\varepsilon \sim 100 - 500\ \ell m^{-1} cm^{-1}$), and in the region $7 \rightarrow 8 \times 10^3\ cm^{-1}$, (1300 - 1400 nm). No such band is found and tetrahedral Ti^{3+} is excluded from the present considerations.

Finally, on the topic of Ti^{3+} absorption, we note that it is to be expected that the optical band due to this ion would be broadened by the range of crystal field parameters suggested in the simulations, (note relations (5.1)) (5.20). However the conclusion of a centrosymmetric octahedral site for the Ti^{3+} ion is still the most reasonable conclusion.

The effect or effects responsible for the colouration of the 5% and 10% glasses remains unclear. As TiO_2 is added to the base glass the absorption 'edge' is shifted to lower frequencies and, in melts 4 and 5, the 'tail' of this edge extends well into the visible and gives these glasses their red/brown colour. Pre-crystallization heat treatments of melts 4 and 5 causes a further shift to lower frequencies and a consequent darkening of the glasses.

The colouration is unlikely to be due to charge transfer absorptions of the Ti^{4+} ion, which are in the u.v. (5.28,5.29). However in other glass systems the presence of transition elements in addition to titanium (e.g. Fe, V, Cu, etc.) has been observed to produce Ti-O-M charge transfer bands in the short wave visible region, (5.28,5.30,5.31,5.32), and it is argued, (5.28,5.30), that upon heat treatment , the displacement of the u.v. 'edge' which is observed in some of these systems, is due to an increase in the number of Ti-O-M bonds, i.e. an increase in the intensity of the band. Fe^{3+} is the most abundant metallic impurity in our glasses, ($\sim$ 5 p.p.m.), and from the published data upon Fe^{3+} - O - Ti^{4+} complexes, (5.30), we have extrapolated from the comparatively large Fe^{3+} concentrations of the published work ($\sim$1 wt.%), to an expected absorption coefficient at our Fe^{3+}

concentrations. Although this is precarious, we arrive at an expected absorption at 350 nm, the observed peak of the Fe-O-Ti charge transfer group, which is two orders of magnitude greater than that observed in this work and thus iron titanate groups in the glass seem unlikely to be responsible for the shortwave visible absorption.

Maurer (5.33) and Varshal et al (5.34) ascribe the darkening of their glasses as TiO_2 is added to a light scattering effect. In a phase separated glass, the point to point variations in the refractive index causes the light beam to be scattered, and in the standard spectrophotometer used in this work this scattering would be indistinguishable from a true absorption process. The 'absorption edge' shift which is attendant upon the pre-crystallization heat treatments, is also observed by these workers and ascribed to a change in the wavelength position of the scattering peak due to changes in the dimensions of the phase separated regions.

The measurements of this work were primarily intended to study the behaviour of the radiation induced bands, and the comparatively high intensity of this short wavelength absorption has prevented us from identifying whether the changes in the 'edge' position are due to intensity variations of a fixed wavelength peak or, to changes in the position of a fixed intensity peak, and therefore we cannot effectively differentiate between the charge-transfer and the scattering mechanisms. We note the effect principally because it is one of the few measurements made in this work which proved to be sensitive to the pre-crystallization heat treatments.

REFERENCES

CHAPTER 5

5.1 P W Levy, Journ. Am. Ceram. Soc. 43 1960 p.389

5.2 E Lell, N J Kreidl and J R Hensler, Prog. in Ceram. Sci. Vol. 4, Ed. J Burke (Pergamon Oxford 1966)

5.3 A Bishay, Journ. of Non-Cryst. Solids 3 1970 pp.54-114

5.4 A Kats and J M Stevels, Philips Res. Repts. V.11 1956 pp.115-156

5.5 R A Weeks and C M Nelson, Journ. Amer. Ceram. Soc. 43 (1960) pp.399-404

P W Levy, Phys. Chem. Solids 13 (1960) pp.287-295

5.6 A Bishay and K R Fergusson, 'Advances in Glass Technol' Proc. VI Int. Congr. on Glass Washington 1962 (Plenum Press N.Y. pp.133-148)

5.7 A Smakula, Z Phys. 59 (1939) p.603

5.8 P B Ayscough, E.S.R. in Chemistry 1967 Methuen pp.442-443

5.9 J S Stroud, J W H Schreurs and R F Tucker, Proc. VII Cong. on Glass Brussels 1965 (Gordon and Breach N.Y. 1966)

5.10 J H Mackay, H L Smith and J Nahum, J. Phys. Chem. Solids 27 1966 p.1773

5.11 J W H Schreurs, Journ. of Chem. Phys. V.47 No.2 1967 p.818

5.12 P W McMillan, Glass Cermics, Academic Press 1964

5.13 R Yokota, Phys. Rev. 95 1954 p.1145

5.14 G O Karapetyan, S A Stepanov and D M Yudin, Soviet Phys. Solid State V.6 No.5 1964 p.1197

5.15 M C M O'Brien, Proc. Roy. Soc. A231 1955 pp.404-414

5.16 E Lell, Phys. Chem. Glass 3 1962 pp.84-94

5.17 P W Levy, Phys. Rev. V.123 No.4 1961 p.1226

5.18 C F Bauer and D G Whitmore, J. of Solid State Chem. 11 1974 pp. 38-52

5.19 T Bates, Modern Aspects of the Vitreous State, V.2 pp.195-254 (Ed. J D Mackenzie, Butterworths and Co. 1962)

5.20 A Paul, J. of Mater. Sci. 10 1975 pp.692-696

5.21 D S Carson and R D Maurer, J. of Non-Cryst. Solids 11 1973 pp.368-380

5.22 M H L Pryce, Proc. Phys. Soc. Lond. A64 1950 p.25

5.23 J J Davies and J E Wertz, J. Mag. Res. VI 1969 p.500

5.24 R M Eisberg, Fundamentals of Modern Physics, Wiley 1961

5.25 R G Burns, Minerological Application of Crystal Field Theory' C.U.P. 1970

5.26 C R Kirkjian and G E Peterson, Phys, Chem. of Glasses, V.15 No.1 1974 p.12

5.27 H Hartman and F E Ilse, Z. Phys. Chem. 197 1951 p.239

5.28 T I Veinberg, Izv. Acad. Nauk. SSSR Neorgan. Mater. 11(3) 1975 pp.440-443

5.29 J A Duffy, Phys. and Chem. of Glasses 13(3) 1972 pp.65-69

5.30 M A C G van de Graaf et al, Phys. and Chem. of Glasses 14(3), 1973 pp.53-59

5.31 A Paul, Phys. and Chem. of Glasses 17(1) 1976 pp.7-9

5.32 J A Duffy, Phys. and Chem. of Glasses 16(1) 1975 pp.22-26

5.33 R D Maurer in Symp. pn Nucleation and Crystallisation in Glass and Melts. Amer. Ceram. Soc. 1962 p.5

5.34 V G Varshal et al, Izv. Acad. Nauk. SSSR Neorgan. Mater. 10(7) 1974 pp.1140-5.

CHAPTER 6

VIBRATIONAL SPECTRA

In this Chapter the results of infra-red (I.R.) absorption and Raman scattering measurements are presented and discussed.

6.1 Results and Analysis

Both I.R. and Raman spectra were recorded for all of the glass specimens. The I.R. absorption of a limited number of ceramic specimens were also recorded.

6.1.1 I.R. absorption spectra

Figure 6.1 is a composite diagram of the I.R. absorption spectra from Glasses 1, 3 and 5, both with and without pre-crystallization heat treatments. The absorption peaks are broad and ill-defined but it is clear that no substantial changes in the spectra have resulted from the addition of TiO_2 to the base glass composition, or indeed within any particular composition due to pre-crystallization heat treatments. The main 'high' and 'low' frequency peaks occur at 1080 cm^{-1} and 450 cm^{-1} with shoulders on these peaks at $\sim$1200 cm^{-1}, $\sim$940 cm^{-1} and $\sim$550 cm^{-1}. The absorption on all traces at $\sim$3500 cm^{-1} is due to O-H 'group' vibrations.(6.1)

Ceramic specimens at each end of the compositional range, i.e. melts 1 and 5, were also studied and the spectra are presented in Figures 6.2 and 6.3. Again a common feature is that the pre-crystallization heat treatments have no effect upon the resulting spectra. The spectra from melt 1 crystallized at 1000°C and 1200°C and from melt 5 crystallized at 1200°C are qualitatively similar, the most striking change occurring between these two spectra and those from the ceramic made from melt 5 crystallized at 1000°C. This is not unexpected, X-ray diffraction having

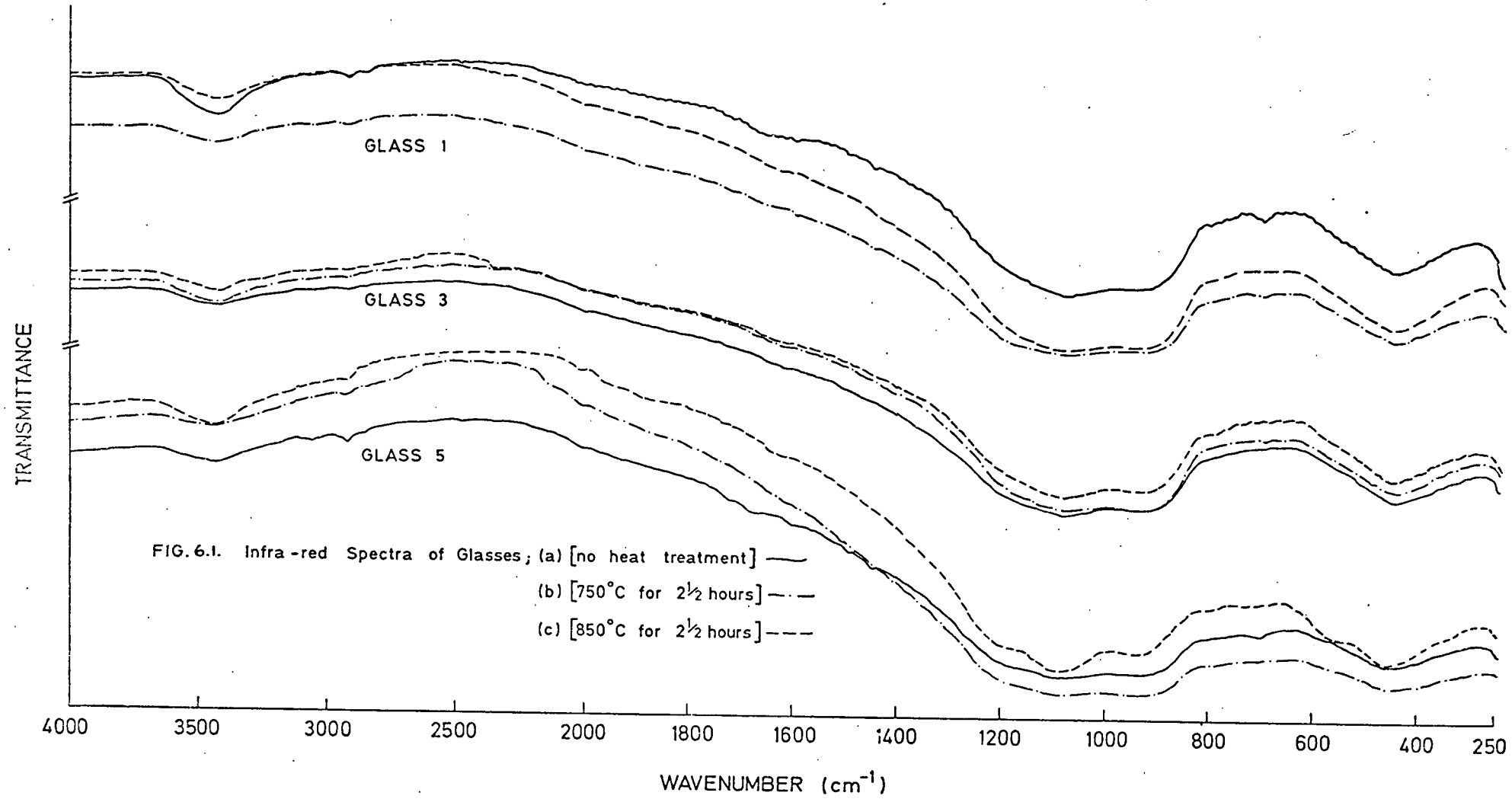

FIG. 6.1. Infra-red Spectra of Glasses; (a) [no heat treatment] ——
(b) [750°C for 2½ hours] —·—
(c) [850°C for 2½ hours] – – –

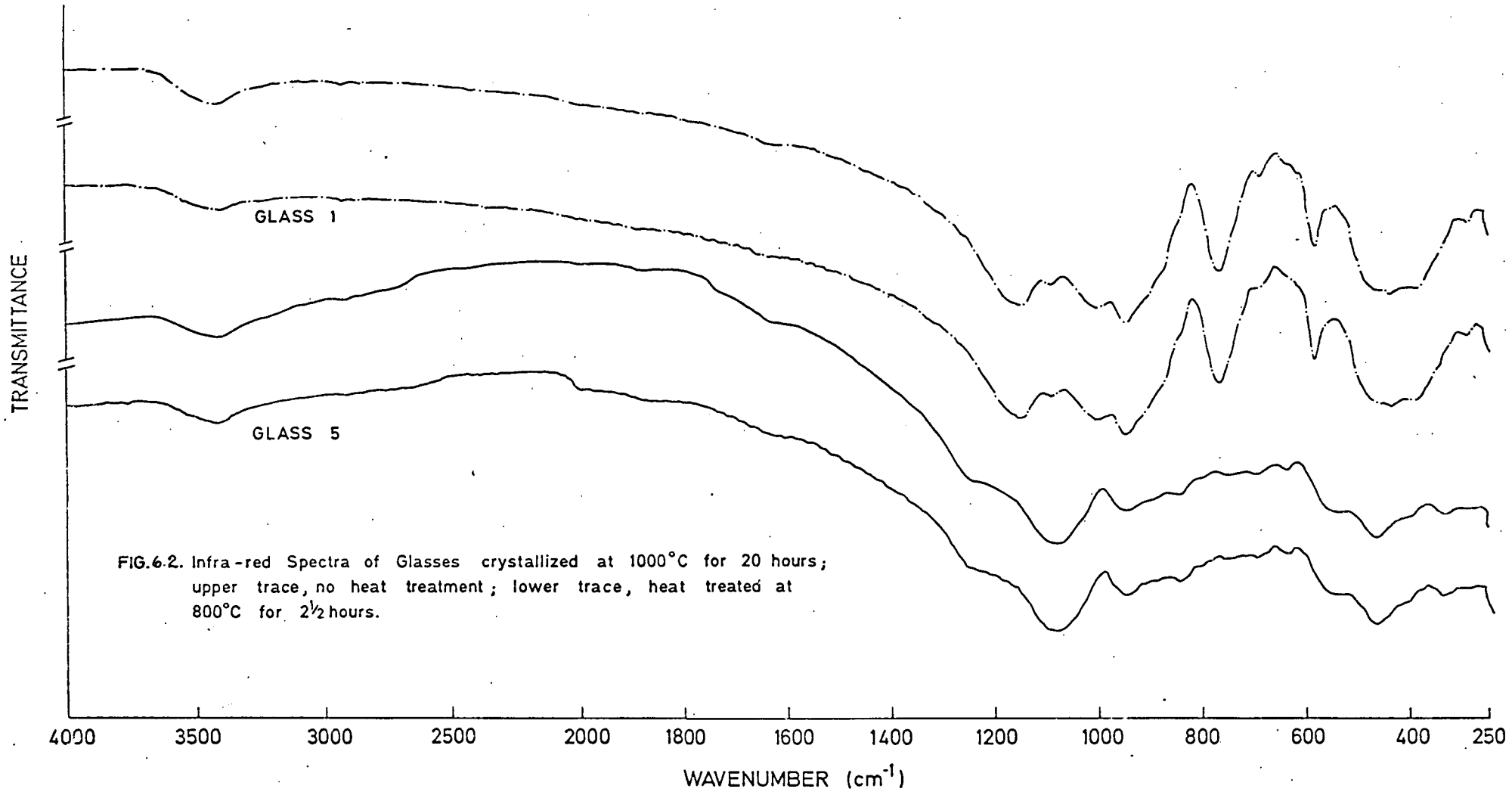

FIG.6.2. Infra-red Spectra of Glasses crystallized at 1000°C for 20 hours; upper trace, no heat treatment; lower trace, heat treated at 800°C for 2½ hours.

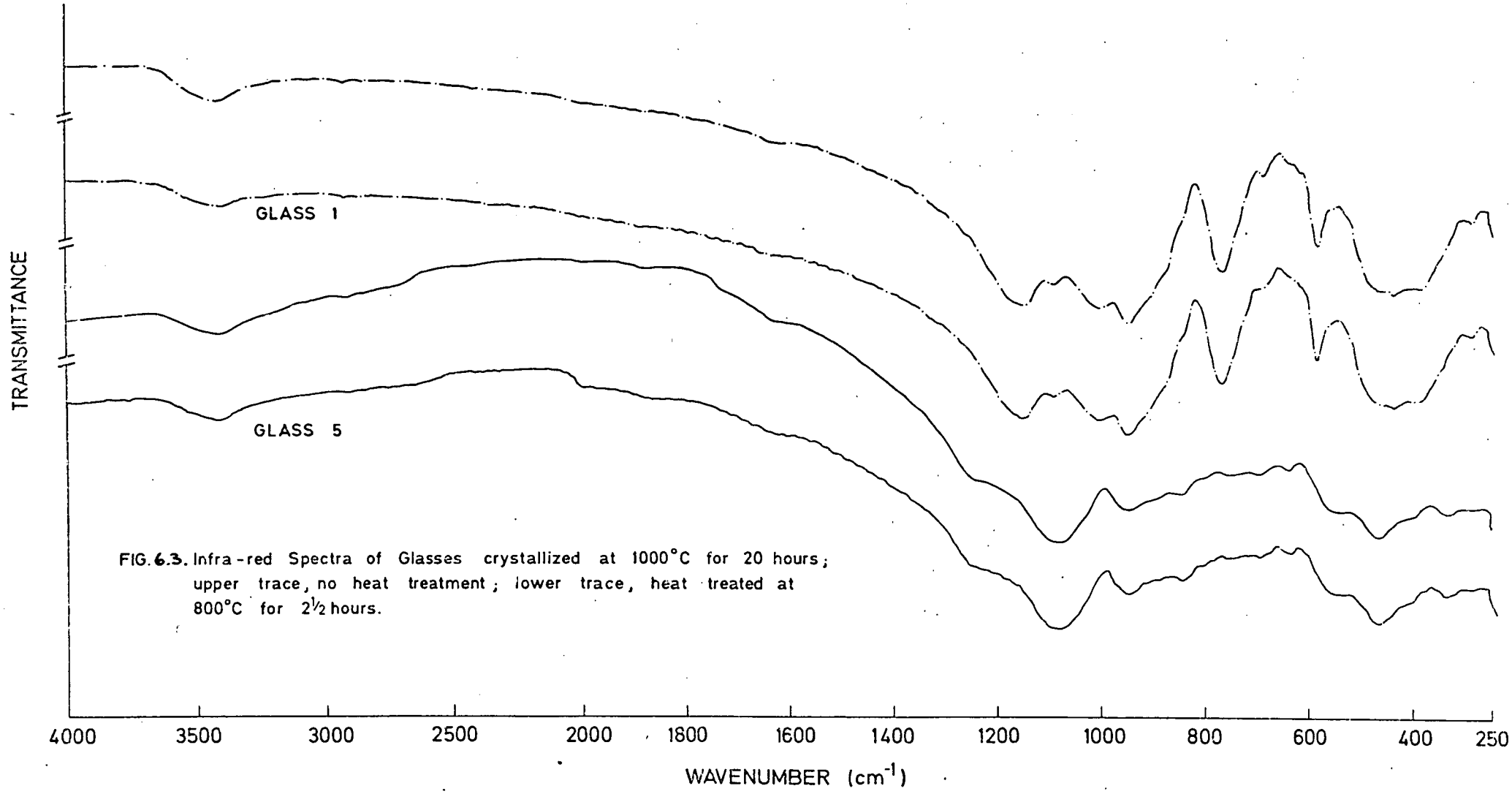

FIG. 6.3. Infra-red Spectra of Glasses crystallized at 1000°C for 20 hours; upper trace, no heat treatment; lower trace, heat treated at 800°C for 2½ hours.

shown a broadly similar principal crystal phase in the first three ceramics and a markedly different phase in the latter specimen. We consider now the results of the Raman scattering experiments.

6.1.2 Raman Scattering Spectra

The spectra from melts 1, 2, 3, 4 and 5 are shown in Figures 6.4 and 6.5. Again, it is clear that within a composition, the pre-crystallization heat treatments leave the spectra unaltered. There are, however, unlike the I.R. spectra, clear differences in the spectra from the different glasses. The analysis of these spectra into their component Gaussian bands is shown in Figures 6.6, 6.7, 6.8 and 6.9. Essentially, but for melt 4, which has at least three strong bands, the glassy Raman spectra between 300 cm^{-1} and 1300 cm^{-1} resolve into two main bands plus two or three minor bands. The most striking change in the spectra as TiO_2 is added to the base glass, is the shift to lower frequencies of the main high frequency band, and the smaller but definite shift in the same direction, of the low frequency peak. The minor bands remain largely unchanged during the compositional and main peak changes, although there is an increase in the relative intensity of the ~ 730 cm^{-1} band as the titania content increases.

6.2 Discussion

6.2.1 Vibrational Spectra in Silicate Glasses

Absorption of I.R. radiation is possible whenever a vibrational mode changes the permanent electric dipole moment of the molecular unit. Raman scattering however will occur whenever a vibrational mode changes the polarizability of the molecule. In this case the incident radiation of frequency v is scattered with sidebands $\pm v_f$ where v_f is a fundamental of the molecule.

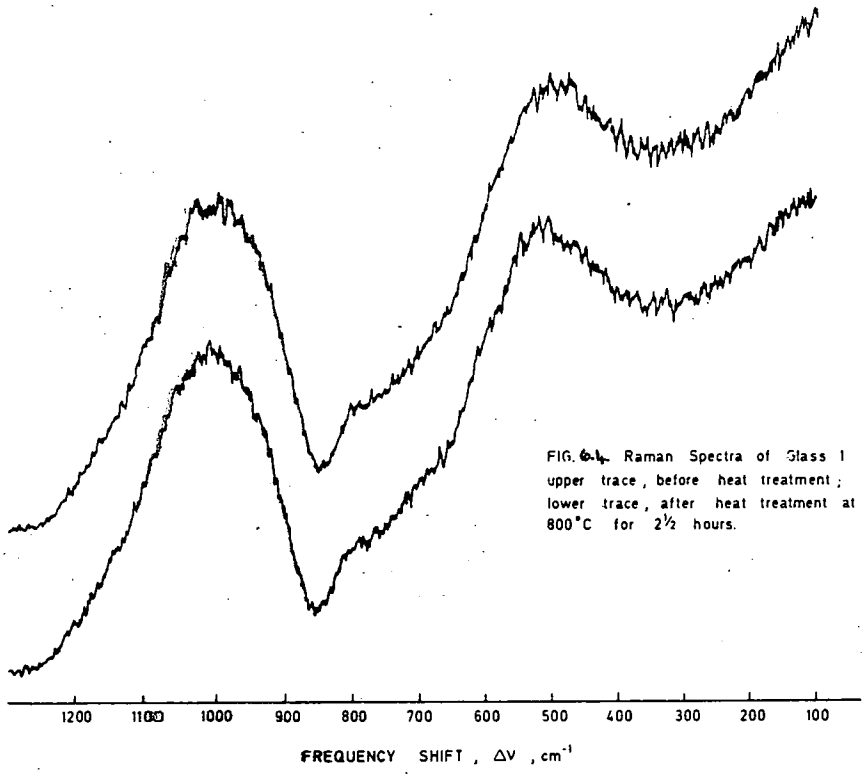

FIG. 6.4. Raman Spectra of Glass 1 upper trace, before heat treatment; lower trace, after heat treatment at 800°C for 2½ hours.

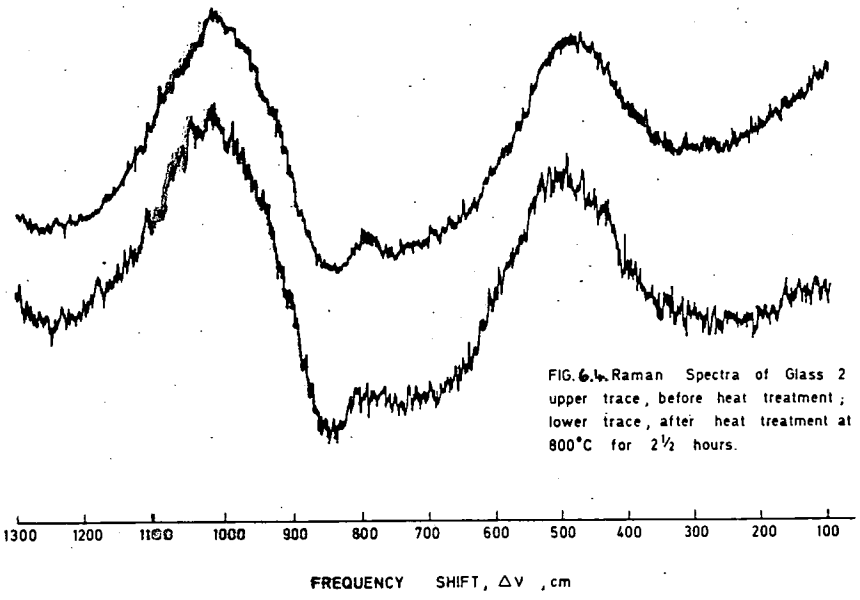

FIG. 6.4. Raman Spectra of Glass 2 upper trace, before heat treatment; lower trace, after heat treatment at 800°C for 2½ hours.

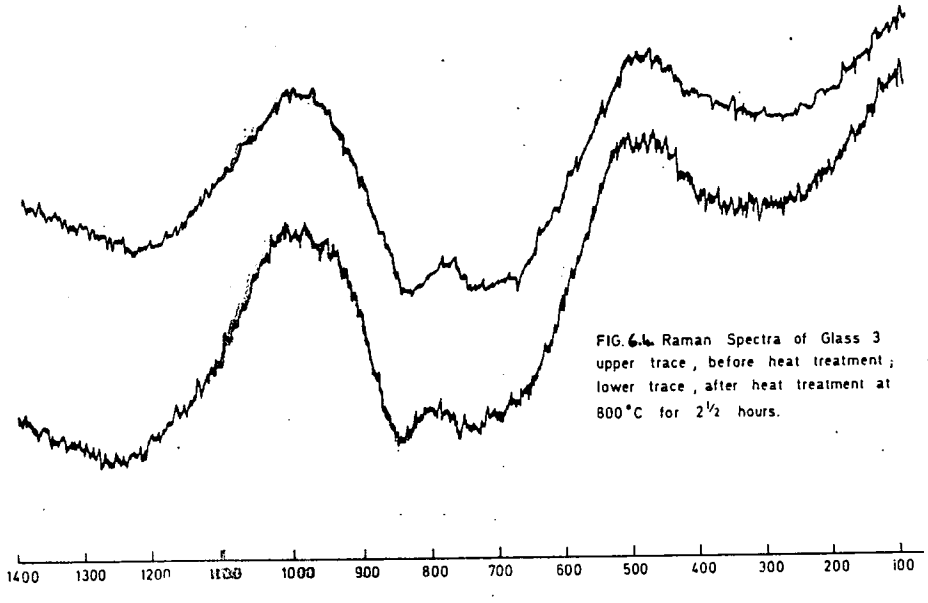

FIG. 6.4. Raman Spectra of Glass 3 upper trace, before heat treatment; lower trace, after heat treatment at 800°C for 2½ hours.

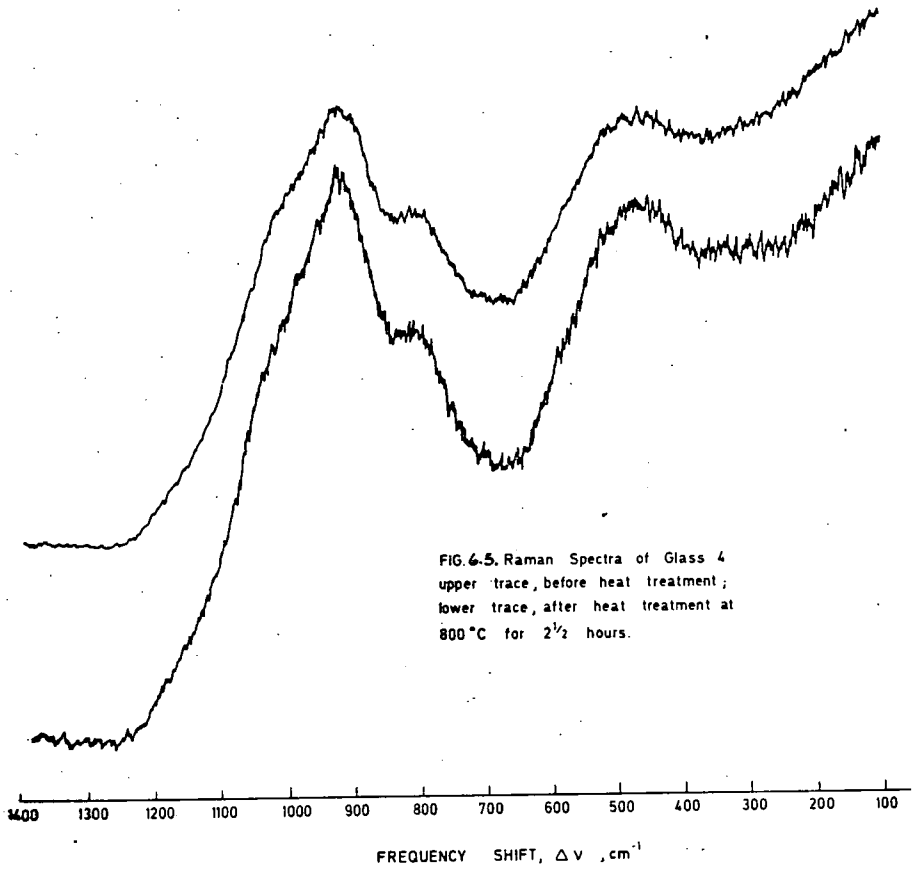

FIG. 6.5. Raman Spectra of Glass 4 upper trace, before heat treatment; lower trace, after heat treatment at 800 °C for 2½ hours.

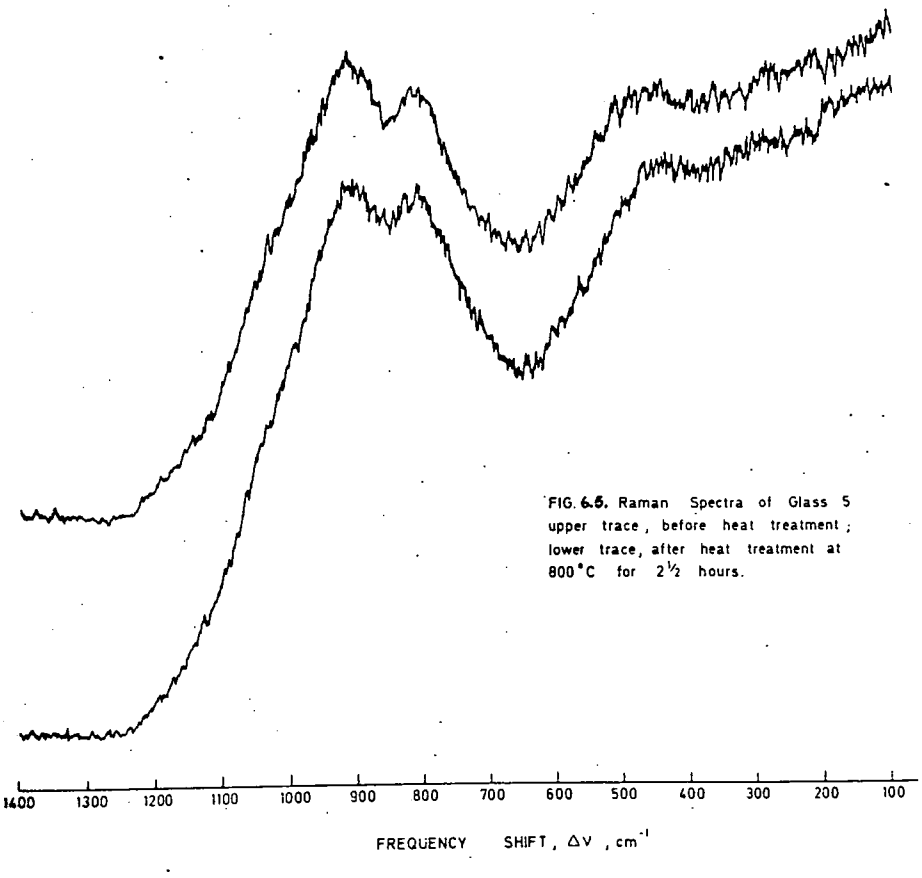

FIG. 6.6. Raman Spectra of Glass 5 upper trace, before heat treatment; lower trace, after heat treatment at 800 °C for 2½ hours.

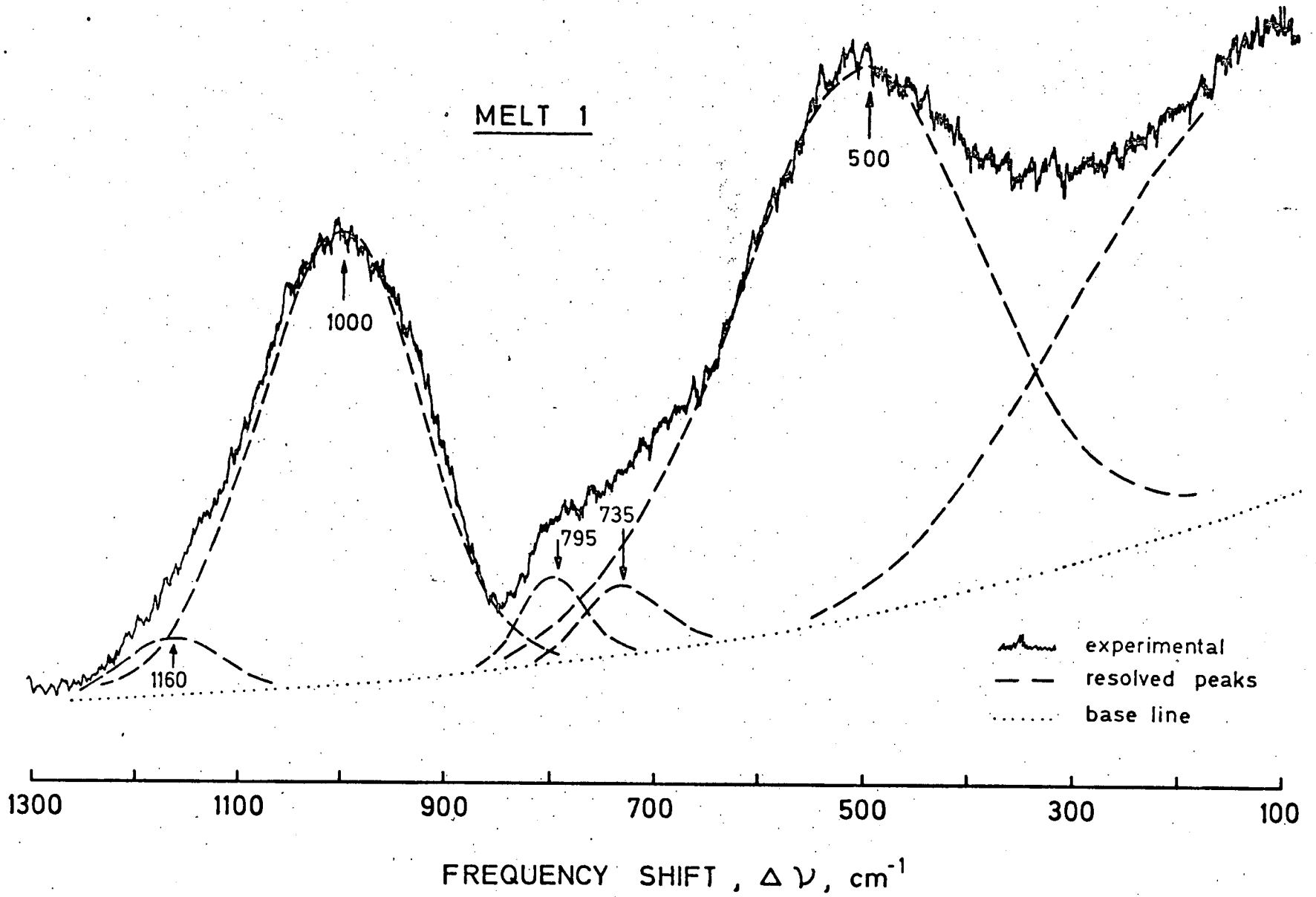

FIG.6.6.ANALYSIS OF RAMAN SPECTRA.

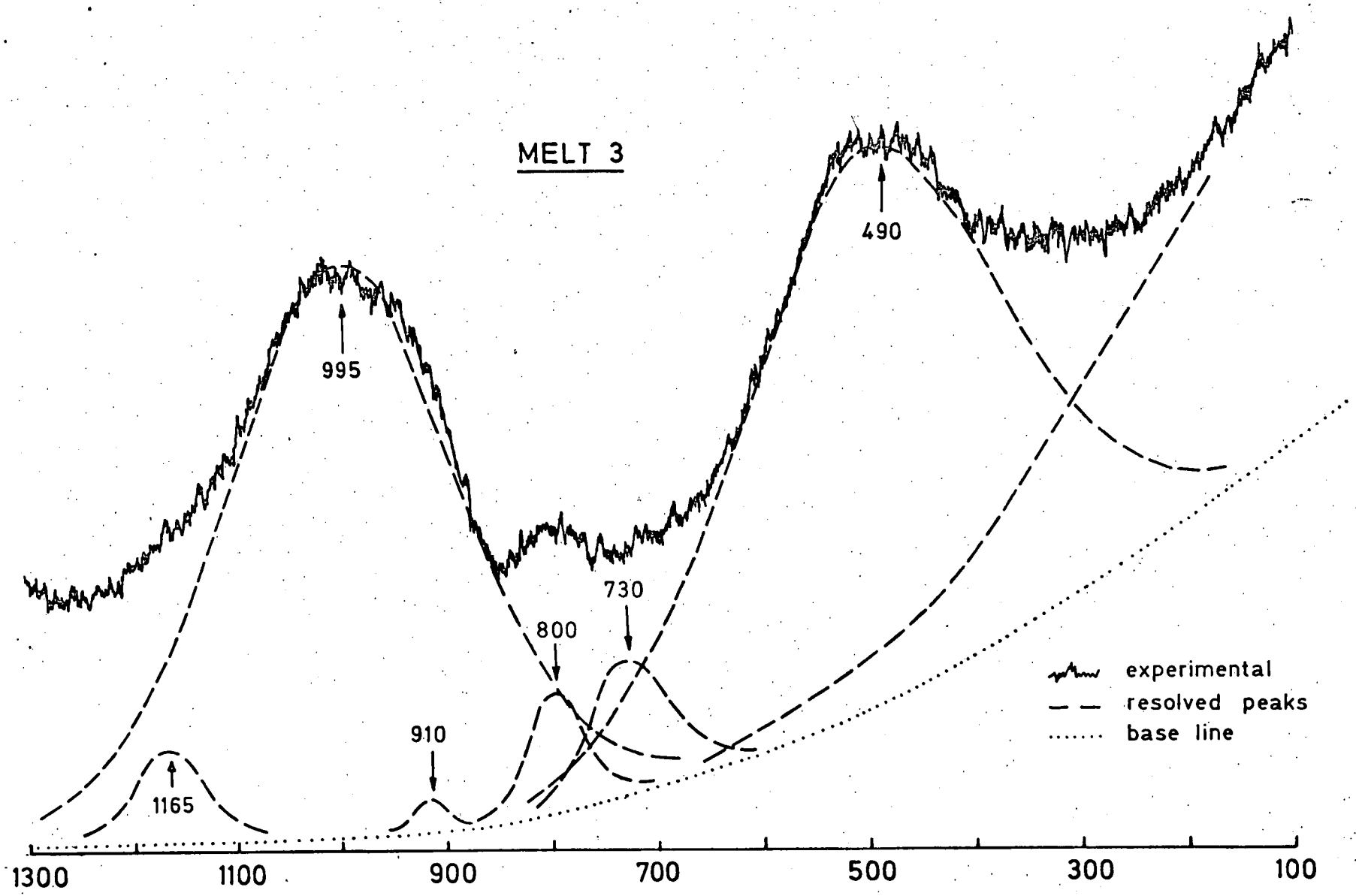

FIG6.7. ANALYSIS OF RAMAN SPECTRA.

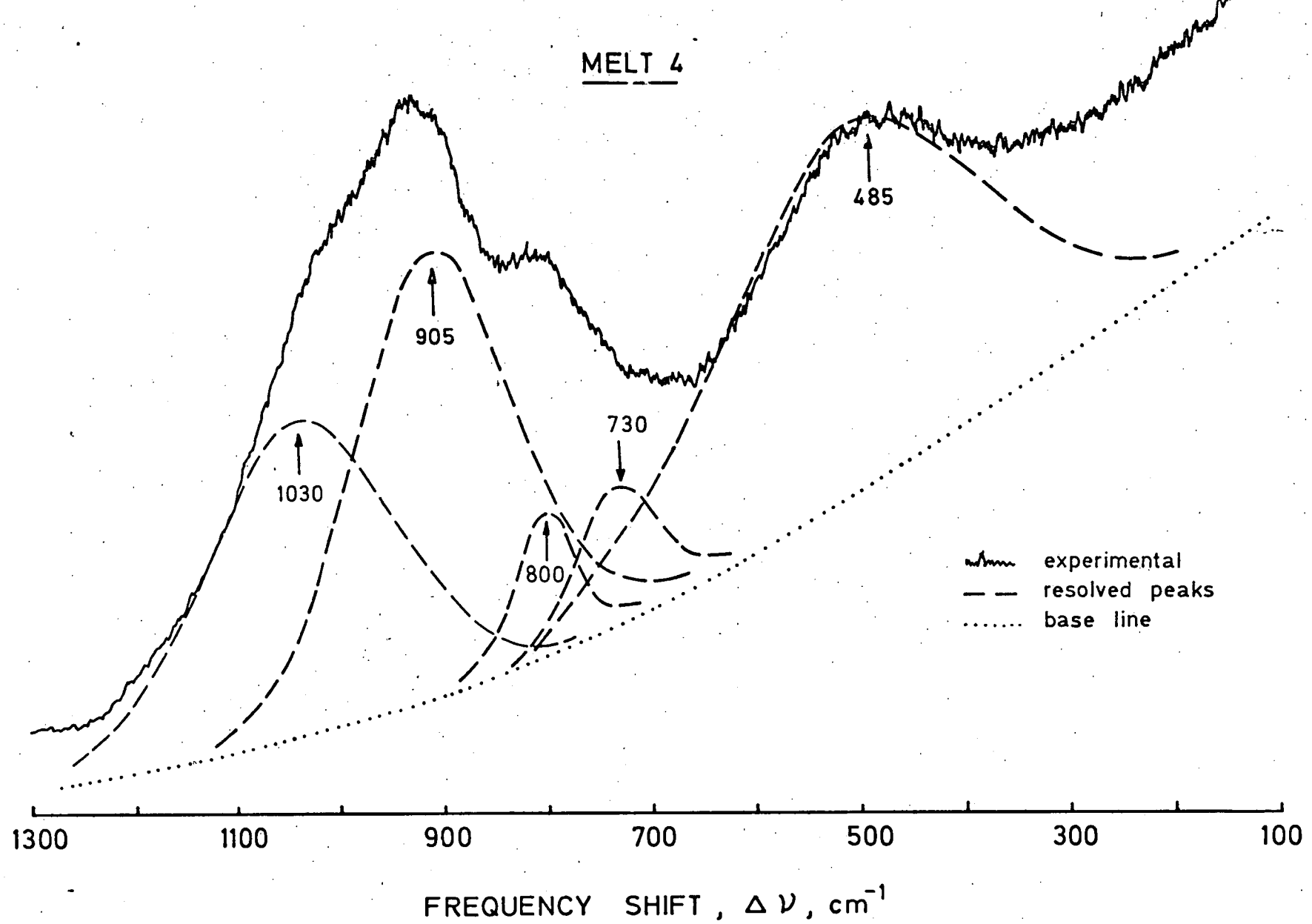

FIG.6.8. ANALYSIS OF RAMAN SPECTRA.

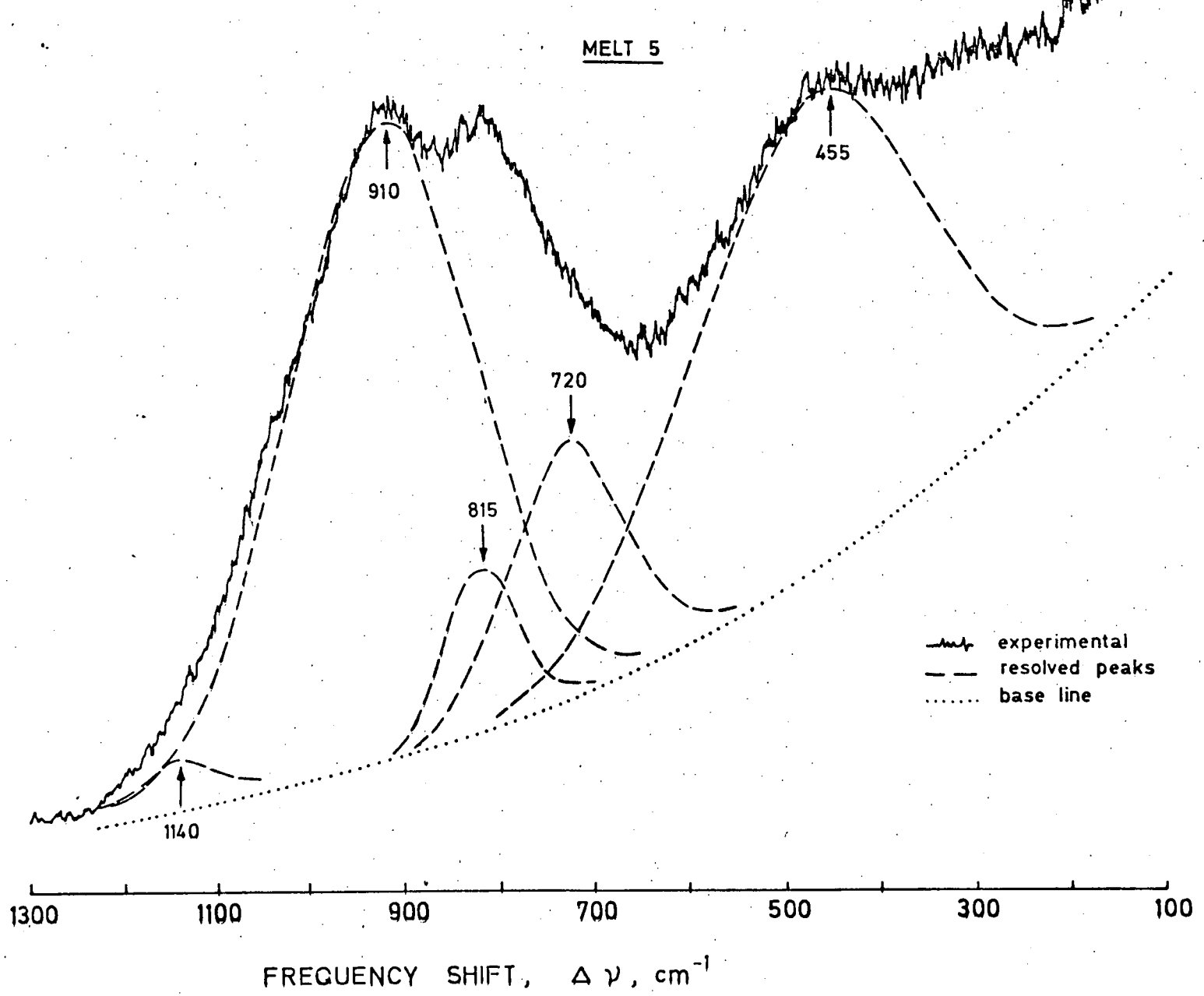

FIG.6.9 ANALYSIS OF RAMAN SPECTRA.

For molecules whose point group is known, the number of vibrational modes and their Raman and/or I.R. activity, may be found from the group character tables.[6.2] The activities are mutually exclusive if the molecule has a centre of symmetry, but, if there is no centre of symmetry, e.g. the SiO_4 group in T_d symmetry, then some, but not necessarily all, of the modes of vibration may be both I.R. and Raman active. Thus the qualitative features, i.e. the number of bands in the vibrational spectrum, may be predicted. The vibrational energy levels however are determined by the force constants of the specific molecular bonds; the intensity of a given band depends upon the derivative of the electric dipole moment with respect to small displacements, (I.R. spectrum), or of the polarizability, (Raman spectrum), for the vibrational mode concerned. Thus the Raman and I.R. spectrum of a given material often have markedly different appearances although the information from each spectrum may be complementary.

The vibrational spectra of α and β quartz have been successfully computed,[6.3,6.4] and, assuming a disordered quartz structure, i.e. a distribution of bond angles and strengths around those found in quartz, as a model of vitreous silica,[6.5] the main features of the glassy spectrum have been derived.[6.6,6.7,6.8] Multicomponent glasses, however, contain silica tetrahedra with one, two, three or four non-bonding oxygens (n.b.o.), i.e. their basic structural units may be the $[SiO_4]^-$, $[SiO_4]^{2-}$, $[SiO_4]^{3-}$, or the $[SiO_4]^{4-}$ groups. Theoretical studies,[6.8,6.9] have shown that these units incorporated into a crystalline or vitreous material will have characteristic 'group' frequencies.[6.1] Thus the existence of these silicate groups in a glass, can, in principle, be inferred by a comparison of the vibrational spectrum of the glass, and the vibrational spectra of crystalline silicates known to contain specific silicate groups. This approach has been successfully employed by Konijnendijk[6.10] in identifying borate groups in borate and borosilicate glasses, and by numerous authors

involved with lunar glasses. This technique, i.e. the use of the published spectra from silicate minerals and glasses to 'fingerprint' structural units within the glasses, has been used here. The lack of translational symmetry causes the glassy spectra to be weak, the peaks broad, and the detail simple, compared with the intense, sharp, complicated spectra from the crystals. However, in most cases, the crystalline spectra and the spectra from the glass of the same composition do have similar features, although there are exceptions.[6.10,6.11] To facilitate further discussion we now classify the silicate minerals according to the SiO_4 groups which they contain.

(a) Orthosilicates

These structures are formed with isolated $[SiO_4]^{4-}$ radicals, e.g. the olivines, garnets, etc.

(b) Metasilicates

When two $[SiO_4]^{4-}$ tetrahedra cross link the metasilicate compounds of $[Si_2O_7]^{6-}$ units are formed. As the chain lengthens the basic structural unit becomes $[SiO_3]^{2-}$, i.e. long chains of tetrahedra each with two non-bridging oxygens. The $[SiO_3]^{2-}$ chains, in various morphologies form the pyroxene group of minerals, e.g. Enstatite, Diopside etc.

(c) Disilicates

Cross linking of the $[SiO_3]^{2-}$ chains forms the double chains of the amphibole group of minerals. Further cross linking produces a sheet structure of basic unit $[Si_2O_5]^{2-}$, i.e. one n.b.o. per tetrahedron. This is the structural unit of the micas.

(d) Framework Silicates

All tetrahedra now share each of their four corners, i.e. the basic unit is now $[SiO_4]$. All of the crystalline polymorphs of silica have this structure at S.T.P. Isomorphous substitution of Si by Al and other ions also produces a three dimensional network typified in the feldspar and ultramarine group of minerals.

The metasilicates are of particular interest here, X-ray diffraction having shown that they are the main crystalline products in all of the devitrified glasses. Within this class of silicates, structures exist with from two to seven SiO_4 tetrahedra in the repeat units of the chain[6.9] forming either infinite chains or in some cases rings with three or more $[SiO_3]^{2-}$ tetrahedra per ring. This final group can be classified as Ring or Cyclo-silicates.[6.12] Because the I.R. absorption is determined primarily by short range dipole forces of essentially nearest neighbour interactions it is not expected to be sensitive to configurational changes within a metasilicate chain. The Raman scattering however is sensitive to the break-up of translational order over several unit cells in a crystalline material[6.13] and one may expect configurational changes to be reflected in changes in the Raman spectrum.[6.13,6.11] We return to this point later during the discussion of the experimental Raman spectra, but first we consider the I.R. spectra.

6.2.2 The I.R. Spectra

Tartre[6.14] established that the co-ordination state of many ions in glass may be inferred from the position of the main high frequency I.R. bands. For a given ion, XO_4 tetrahedral groups will vibrate at higher frequencies then XO_6 octahedral groups. In addition, a given group

will vibrate at a higher frequency in a 'condensed', (multiply bonded) state than in an 'isolated', (free radical) state. For most ions therefore there are two frequency 'bands' corresponding to 'condensed' and 'isolated' XO_4 and XO_6 groups. Silica is the principal component of the glasses studied here and we consider first the characteristic frequencies of SiO_4 groups.

Most crystalline silica polymorphs, fused silica, and many commerical high silica glasses such as Vycor, have been studied and the main I.R. bands catalogued,[6.4,6.8,6.10,6.15,6.16] The framework $[SiO_4]$ tetrahedron has its main bands, (in both glasses and crystals), in the 1070 - 1090 cm^{-1} and 440 - 480 cm^{-1} regions. These bands are ascribed respectively to the asymmetric intratetrahedral stretching motion (v_3) $\leftarrow SiO \rightarrow \leftarrow Si$, and the bending modes (v_2) $\overset{\uparrow}{O} - \underset{\downarrow}{Si} - \overset{\uparrow}{O}$ between tetrahedra and $\overset{\uparrow}{Si} - \underset{\downarrow}{O} - \overset{\uparrow}{Si}$ within tetrahedra. In addition, an intertetrahedral stretching vibration (v_1) $\leftarrow Si - O - Si \rightarrow$ produces less intense bands at $\sim$700 and 800 cm^{-1}. The 1070 - 1090 cm^{-1} band has a shoulder on the high frequency side at $\sim$1180 cm^{-1} in the crystalline silicates. Lowering the symmetry of the tetrahedron from T_d, (or D_3 in α quartz), increases the number of I.R. bands,[6.17] i.e. the two F_2 I.R. active modes in T_d decompose to 8 I.R. modes in C_{2V}. Thus in the crystalline forms, the symmetry of the SiO_4 unit is indicated by the number of I.R. bands. The glassy bands are very much broader and often merge, preventing a symmetry assignment. However, the silicate glasses do mirror the 'shift' to lower frequencies which is observed in the main high frequency crystalline silicate bands when the number of n.b.o's. increase. Essentially, bands at frequencies lower than the 1070 - 1080 cm^{-1} main peak of the framework tetrahedron, become more intense, e.g. in most crystalline metasilicates, ($[SiO_4]^{2-}$ units), there are three main high frequency bands in the 850 - 1080 cm^{-1} region, all of comparable intensity.[6.10,6.18] The frequency 'shift' is continued

in the crystalline orthosilicates, where now the low frequency section of the group of bands between 850 and 1080 cm^{-1} has greatly increased in intensity at the expense of the high frequency section of this group, such that a band at $\sim$870 cm^{-1} is now the most intense I.R. peak, and the high frequency band at $\sim$1060 cm^{-1} has decayed almost completely.(6.20)

The multiple high frequency peaks of the crystalline silicates broaden to one or two main peaks in the glassy silicate spectra. At low concentrations of n.b.o's. a peak at $\sim$950 cm^{-1}, taken by many authors to be indicative of the Si - O terminal stretching mode,(6.14,6.17,6.19) appears as a shoulder on the intense 1050 - 1080 cm^{-1} vitreous silica peak. As the glass modifiers increase to the metasilicate ratio, these peaks assume approximately equal intensities.(6.10,6.14,6,19) In some systems the above peaks merge to a single broad peak at $\sim$980 cm^{-1}. The effect of increasing the modifier/silica ratio is to shift this peak to lower frequencies.(6.17) In all but cases of special founding techniques, (small volume melts, rapid quenching, etc.), the metasilicate ratio represents the approximate limit of glass formation in silicate melts,(6.21) and no I.R. data have been found for glasses beyond the metasilicate composition.

In most binary silicate glasses and crystals of disilicate and metasilicate compositions, the I.R. absorption in the region of 1200 cm^{-1} is very weak. Exceptions occur when the glass phases separate into high silica and high alkali regions;(6.22) it is suggested that then the high frequency part of the spectrum, and in particular the high frequency shoulder at $\sim$1200 cm^{-1} on the main $\sim$1060 cm^{-1} peak, is due to the high silica region, and the band in the region of $\sim$950 cm^{-1} is due to the high alkali phase. This explanation applies here, so the $\sim$1200 cm^{-1} and 940 cm^{-1} bands could be characteristic of a high silica region and a region of disilicate or metasilicate composition. The 1080 cm^{-1} band would be common to each of these glass phases.

The constancy of the spectra throughout the compositional range independently indicates a corresponding constancy of the silicate units within the glass. The bending modes in the region of 450 cm^{-1} are largely invariant in position as the proportion of n.b.o's. increases within the glass, changing only some 30 - 40 cm^{-1} between the extremes of vitreous silica and a metasilicate glass.(6.17) The broadness of the experimental bands would make such shifts to higher frequencies difficult to detect in our glasses. In contrast, the high frequency stretching peaks should reflect significant changes of the structural units (SiO_4 tetrahedra), in terms of the number of non-bridged oxygens per tetrahedron. This is not to say that configurational changes within a metasilicate or disilicate region could be discerned; a study of a range of pyroxene minerals, ($[SiO_4]^{2-}$ chains), showed that only very slight variations were present in the spectra from different pyroxene chains.(6.18) In principle, the number of $[SiO_4]^{2-}$ units in the repeat unit of the chain can be established from the number of bands in the 550 - 750 cm^{-1} region, and the positions of the three main high frequency peaks are characteristic of the particular pyroxene. However, first class crystalline spectra are necessary to detect these variations, and, in a glass, where the bands are greatly broadened, the I.R. spectra from pyroxenes with different configurations may be expected to be indistinguishable from one another. We turn now to the aluminium, magnesium and titanium groups present in the glasses.

The co-ordination state of the aluminium ion when moderate amounts ($\sim$10 mol.%), of Al_2O_3 are added to high silica melts is difficult to determine by I.R. spectroscopy. In the Feldspar minerals where large amounts of Al substitutionally replace Si in the lattice, there are significant changes in the form of the high frequency bands, and, because of the lower force constant of the Al - O bond, these bands are displaced to lower frequencies.(6.18) However when Al_2O_3 is added to silicate glasses

together with equimolar amounts of alkali to allow the Al ion to assume four-fold co-ordination, the changes in the I.R. spectra are barely discernable at 10 wt.% Al_2O_3, and the principal effect of 25 wt.% Al_2O_3 is to displace the main high frequency silicate bands by approximately 40 cm^{-1}.(6.14) The $[AlO_4]$ group bending vibrations are in the region of the $[SiO_4]$ bending modes, i.e. at 450 cm^{-1}.(6.23) The characteristic stretching bands of $[AlO_6]$ groups fall in the region 450 - 650 cm^{-1}.(6.14) These bands are weak, and in high silicate glasses are usually swamped by the low frequency silica bending modes. Thus, in multicomponent, possibly phase separated, silicate glasses, the clear identification of aluminium co-ordination is best accomplished by X-ray fluorescence spectroscopy,(6.24,6.25,6.26) using Corundum and Feldspar standards.

The $[MgO_6]$ group frequencies are in the region 360 - 480 cm^{-1}(6.14,6.23) and in silicate glasses are swamped by the Si-O-Si bending modes. $[MgO_4]$ groups absorb in the 500 - 700 cm^{-1} region.(6.14,6.23)

The characteristic asymmetric stretching mode, (F_{1u}), of the $[TiO_6]$ group gives rise to a series of bands in the 400 - 680 cm^{-1} region when titanium is incorporated into the octahedral sites of mineral structures such as the Perovskites.(6.14,6.18,6.24,6.27,6.28) In silicate glasses however, quite large quantities of TiO_2 ($\sim$ 25 mol.%) incorporated into an alkali silicate glass failed to produce any clear bands in the region of 600 cm^{-1},(6.17) and we therefore would not expect the presence of $[TiO_6]$ groups, in the proportions possible in our glasses, to produce new bands or even to alter noticeably the lower frequency region of the spectrum. $[TiO_4]$ groups in minerals, e.g. $BaTiO_4$, produce much stronger characreristic stretching bands in the 700 - 900 cm^{-1} region.(6.14,6.17,6.28) The apparent absence of any additional absorption in this region when TiO_2 is added to the base glass composition would seem to preclude the bulk of the titanium ions assuming this co-ordination, although our experimental spectra

are not sufficiently resolved to eliminate the possibility that some titanium is in $[TiO_4]$ groups. We now consider the spectra from the ceramic specimens.

Langer et al[6.29] devitrified a stochiometric Cordierite glass and studied both the glass and the crystalline products by I.R. spectroscopy. Their glass exhibited three broad maxima at $\sim$1100 cm^{-1}, 935 cm^{-1} and 440 cm^{-1} in close agreement with our glass spectra. The 1200 cm^{-1} shoulder found here is only just discernable in Langer's spectra. A comparison of the spectra from our ceramics which have Cordierite as the principal crystal phase, with the published spectra of Cordierite by Langer,[6.29] Lyon[6.30] and Gregory[6.31] shows that all of the major peaks in our spectra are ascribable to the Cordierite phase. The slight variations in the spectra from different ceramic specimens, all of which have Cordierite as the major phase, are probably due to the minor crystalline phases present in the specimens. For example, the spectra from glass 1 crystallized at both 1000°C and 1200°C, i.e. Figures 6.2 and 6.3, are identical in the position and the number of the I.R. bands. However, the 1200°C specimen shows some additional absorption at 570 - 580 cm^{-1} and at $\sim$1100 cm^{-1} when compared with the 1000°C specimen. Reference to the X-ray diffraction data for these specimens, Figure 3.1 and 3.3, shows the growth of the lines E and F, the main lines of the Enstatite-like phase, in the diffraction spectrum of the 1200°C specimen. Figure 6.2 shows that the Enstatite-like phase, typified by glass 5, crystallized at 1000°C, has absorption bands in the 570 - 580 cm^{-1} and 1100 cm^{-1} regions; and thus the variations in the spectra of the melt 1 ceramics are reasonably accounted for by the higher proportion of the Enstatite-like phase present in the 1200°C ceramics. It is equally true that the spectra from melt 1 and melt 5 show small differences, most notably in the additional absorption between 550 cm^{-1} and 750 cm^{-1} shown in the melt 5 spectrum. Both ceramics

have Cordierite as the major crystalline phase, however they differ in that the melt 5 specimen contains a significant quantity of rutile, (Figure 3.14). Rutile produces a single broad I.R. band with its 'peak' in the 600 - 650 cm^{-1} region,[6.32] and this most probably accounts for the extra absorption shown by the melt 5 specimen.

The I.R. spectrum of melt 5 crystallized at 1000°C, (Figure 6.2), is quite different from the other spectra, i.e. the Cordierite specimens. X-ray diffraction suggests an Enstatite-like phase in this specimen (Figure 3.8). Estep et al[6.18] have presented I.R. spectra from a range of pyroxene minerals, including Enstatite. A comparison of their reference spectra and that from the melt 5 ceramic, shows that whilst the ceramic spectra are less well resolved than Estep's spectra, they undoubtedly are of pyroxene form, exhibiting all of the major pyroxene absorption bands. The type of pyroxene cannot be distinguished, indeed the best fit is made with a specimen shocked to 1 Mbar, but the chain silicate nature of the principal crystal phase in these ceramics is established. The shoulder at $\sim$ 1260 cm^{-1}, present in the spectra of these ceramics, is absent from any of the reference pyroxene spectra. Our X-ray diffraction measurements have shown a strong <101> β-quartz line, and we speculate therefore that this I.R. band originates from a high quartz or high quartz solid solution crystal phase. We consider now the Raman spectra.

6.2.3 The Raman Spectra

High silica crystalline compounds and glasses, e.g. quartz and vitreous silica, have only weak Raman lines in the 800 - 1200 cm^{-1} wave-number region, i.e. the Si - O - Si antisymmetric stretch which produces the strong I.R. peak at 1080 cm^{-1} and the shoulder at 1180 cm^{-1}, is only a weak Raman scattering mode,[6.4] and produces only weak Raman bands at these positions. The Si - O - Si bending vibration is the strongest Raman mode,[6.4] producing a broad peak in the region of 440 cm^{-1} with a sharp

shoulder/peak at 490 cm^{-1}, and, in high silica glasses, these peaks dominate the Raman spectrum.[6.8,6.11] In addition in these glasses, there are medium-weak peaks at 800 cm^{-1} and 600 cm^{-1}.

The silicon ↔ terminal oxygen bond is more polarizable than the silicon ↔ bridged oxygen bond, and consequently, the Si - O^- stretching vibration produces strong Raman bands in the high frequency portion of the spectrum. Thus, as glass modifiers, i.e. K, Na, etc. are added to a high silica glass, a strong Raman band at ∿ 1080 - 1100 cm^{-1} appears, and increases in intensity as the modifier content is increased.[6.10] This band is assigned to an Si - O^- stretching mode within an $[SiO_4]^-$ disilicate unit,[6.8,6.11,6.33] and it dominates the high frequency region as the modifiers are increased up to approximately the disilicate composition. Indeed, all published spectra from crystalline and glassy disilicates have a characteristic band at ∿ 1100 cm^{-1},[6.8,6.11,6.33,6.13] (Interestingly, it is hazardous to assume the presence of disilicate units from the appearance of a peak at ∿1100 cm^{-1} in the I.R. spectrum of a glass which may possibly be phase separated and containing a high or vitreous silica phase, because of the strong band at this wavenumber from the Si - O - Si stretch of the framework $[SiO_4]$ unit. No such difficulty is present in the interpretation of the Raman spectrum from such a glass, because of the extremely weak scattering from the high silica phase at wavenumbers above 800 cm^{-1}).

As the modifier content is increased beyond the disilicate ratio, a band at 950 - 980 cm^{-1} grows in intensity.[6.10,6.11] This band is assigned to the Si - O^- stretching vibration within an $[SiO_4]^{2-}$ unit, i.e. a metasilicate tetrahedron.[6.11,6.33] The cataloguing of spectra from a series of pyroxene minerals,[6.10,6.13,6.34,6.35] has shown that almost all, (discussed later), have a characteristic high frequency peak in the 970 - 1010 cm^{-1} region. Equally, studies of metasilicate ratio glasses have shown an intense Raman peak in this region, (usually a slight downward

shift of frequency of some 20 - 30 cm^{-1} occurs, bringing the glass peaks into the region 950 - 990 cm^{-1}).[6.10,6.11,6.34]

Crystalline orthosilicates have a doublet at ∿820 and 850 cm^{-1} [6.13,6.34] characteristic of the $[SiO_4]^{4-}$ unit. Although some Lunar glass specimens have shown peaks in this region,[6.13] these peaks are rather 'sharp' for glass specimens, and, as previously noted, orthosilicate glasses are unlikely. We now interpret our Raman spectra.

The melt 1 glasses have their main high frequency peak in the metasilicate wavenumber region. The broad low frequency peak at 500 cm^{-1} may well be a composite of two bands. The I.R. spectra suggested the presence of a high silica glass phase, which would be expected to produce a strong broad peak at ∿440 cm^{-1}. Combined with the metasilicate peak at ∿590 cm^{-1}, this band may merge to give the observed maximum at 500 cm^{-1}. Certainly this effect is present in the spectra of Brower et al[6.11] where their lithium-silicate glasses, known to phase separate, produce broad peaks at 555 cm^{-1} and 470 cm^{-1}. The peaks are only just resolved in their spectra and we assume here that this resolution has been lost in the spectra from our glasses. Some additional support of this interpretation is afforded by the weak bands at 1160 and 795 cm^{-1}, which are compatible with the presence of a high or vitreous silica glass phase.

As TiO_2 is added to the base glass composition, the principal effect upon the Raman spectrum is the growth of a band at 910 cm^{-1} and the concomitant decay of the 1000 cm^{-1} band, until at the composition of melt 4, (5% TiO_2), the bands are of comparable intensity, and in the melt 5 (10% TiO_2) glasses, the 910 cm^{-1} band dominates the high frequency region. During this process the minor bands remain largely unchanged, although the ∿720 cm^{-1} band appears to increase in relative intensity, and the broad low frequency peak shifts some 40 - 50 cm^{-1} to lower wavenumbers. If the observed frequency shift of the high frequency band were ascribable

to a change in the average number of n.b.o's. per silica tetrahedron, then one should expect similar band changes in the I.R. spectra of the glasses, and certainly such major changes are absent from these spectra. We consider therefore the effect of configurational changes within the metasilicate chains.

Gaskell[6.9] has considered some simple pyroxene chain structures, and in particular the vibrational modes which are allowed for various arrangements of the $[SiO_4]^{2-}$ tetrahedra. He concludes that modes which involve phase relationships between the vibrations of atoms in adjacent tetrahedra, are quite sensitive to changes in the translational symmetry of the chain, although characteristic 'group' vibrations exist for all arrangements, corresponding to atomic motions within a single tetrahedron. The I.R. bands are determined primarily by the short range dipolar forces of nearest neighbour interactions,[6.13] and, whilst sensitive to changes in the co-ordination cations, these bands are largely constant for a specific $[SiO_4]$ group, i.e. for silica tetrahedra with none, one, two, three or four n.b.o's. per tetrahedron. The Raman intensities and frequencies are sensitive to changes in the translational order of a specific $[SiO_4]$ group,[6.13] and a plausible explanation of the constancy in the I.R. bands with simultaneous changes in the high frequency Raman peaks, is that the glasses all contain a phase whose structural groups are essentially similar, but that the arrangement of these groups relative to one another, is changing as TiO_2 is added to the base glass composition. The high frequency peaks in the Raman and I.R. spectra of our glasses indicate that the most probable common group is the $[SiO_4]^{2-}$ tetrahedron, and we now consider possible configurations.

The calculations,[6.9] and the experimental data,[6.11] suggest that high frequency peak changes somewhat less, ($\sim$30 cm^{-1}), than the observed value of 90 cm^{-1} would result from configuration changes within

the metasilicate chain. Data presented by Fabel et al[6.34] contain Raman spectra from a series of polycrystalline pyroxenes including Enstatite ($MgSiO_3$), Diopside ($CaMgSi_2O_6$), and Spodumene ($LiAlSi_2O_6$). The principal high frequency peaks of Enstatite and Diopside are displaced by only 10 cm^{-1} relative to one another, but compared with these minerals, the Spodumene peak is displaced some 60 cm^{-1} to higher wavenumbers. Spodumene is similar in structure to Diopside except for the replacement of the large Ca and Mg ions by the smaller, higher field strength Li and Al ions. The result is a closer packing of the SiO_4 tetrahedra and a smaller unit cell.[6.12] In our glass specimens therefore we could expect a shift of the Raman peaks to lower frequencies if Al ions co-ordinating $[SiO_4]^{2-}$ tetrahedra were removed from that sphere of co-ordination. Such frequency shifts are essentially due to changes in the force constant of the Si - O band, and as such we should expect to see similar changes in the I.R. spectra. Allowing for the poor resolution of the I.R. spectra, the large 90 cm^{-1} frequency shift of the high frequency Raman peaks does not appear in these spectra, and a mechanism additional to changes in the cation co-ordination must be responsible for the Raman spectra effects.

In the Cordierite structure, i.e. the main crystalline product of the low titania glasses, there are six membered rings of $[SiO_4]^{2-}$ tetrahedra. The six membered tetrahedral rings are ideally composed of five $[SiO_4]$ tetrahedra and one $[AlO_4]$ tetrahedron. These rings are linked laterally and horizontally by Mg ions in 6-fold and Al ions in 4-fold co-ordination.[6.12] Preferential removal of the Al ions would result in an enrichment of the Mg:Si ratio and the breaking of the six membered rings of silica tetrahedra, i.e. short chains of tetrahedra would be formed. We are not aware of any theoretical work which has considered specifically the extended vibrational modes of ring and chain metasilicate structures, and equally there are no reported measurements of the Raman spectra from cyclosilicates of the

metasilicate composition. Thus the configurational changes suggested above are speculative. However, if such a change is responsible for the Raman bands at 1000 cm^{-1} and 910 cm^{-1}, the fact that the latter peak falls outside of the range reported for other metasilicate glasses and pyroxene minerals, may be accounted for by the short chains which would result from the breaking of the six membered rings of silica tetrahedra. Gaskell's calculations[6.9] assumed short chains of tetrahedra, and he deduced a figure of 900 cm^{-1} for the terminal stretch of the metasilicate unit. However other calculations,[6.36] again using a limited number of tetrahedral units, have calculated this frequency to be at $\sim$960 cm^{-1} for the chains of a K_2SiO_3 glass in close agreement with the observed value.[6.11]

In whichever manner the Raman spectra are interpreted, it is clear that the addition of TiO_2 causes a change in the structure of the silicate network. Two distinct bands are present in the Raman spectrum and this indicates the formation of two distinct groups, rather than a gradual metamorphosis from one group to another, i.e. a configurational or gradual cation change within the silicate units. The nature of the change therefore is consistent with the process suggested above.

Turning now to the other changes in the Raman spectra upon the addition of TiO_2, and in particular the shift to lower frequencies of the main low frequency peak, we note that particularly if the glass has a phase separated structure, this change may have a number of possible origins. An increase in the amount of the silica rich phase, (relative to other glass phase(s)), or a decrease in the metasilicate phase, would produce such a displacement. An additional possibility is afforded by Brawer et al.[6.11] These authors have calculated the change in frequency of the strongest Raman bands of a disilicate sheet structure when the Si - O - Si intertetrahedral bond angle is increased from 130° to 180°, (vitreous silica has a range of bond angles between 120° and 180° with a

most probable value of 144°.[6.37] They conclude (as does Gaskell[6.9]), that the high frequency stretching modes are largely insensitive to bond angle changes, but that the low frequency bending modes move to lower frequencies as the bond angle increases. A change in the bond angle would be expected during a cyclosilicate → chain silicate configurational change. We do not know whether phase separation and changes in the relative quantities of phases within the glass, or bond angle changes, (or indeed some other mechanism), is responsible for the movement of the low frequency Raman peak during the addition of TiO_2, but in the next chapter we shall discuss a mechanism which is consistent with, i.e. would result in, both of the changes described above. Finally therefore we discuss the other ionic groups within the glass, i.e. Ti, Mg and Al groups.

The addition of large amounts (up to 30 mol.%) of Al_2O_3 to silicate and borosilicate melts has been shown[6.10] not to produce new bands in the 200 → 1200 cm^{-1} region ascribable to aluminium units. The only discernable effect was to slightly depress the frequency of the main silicate bands. Aluminium co-ordination is usually inferred from changes in the characteristic silicate peaks.

The Mg groups are expected to scatter in the low frequency region because of the much reduced Mg - O force constant,[6.36] and the strong silicate bending modes and the long Rayleigh tail found in most glasses, make Mg group vibrations difficult to detect in high silicate glasses. For these reasons there is little information in the literature regarding Mg Raman bands in silicate glasses.

Titanium groups have been reported to produce Raman bands in silicate glasses.[6.38,6.39] They conclude that the main stretching band is in the 900 - 980 cm^{-1} region for $[TiO_4]$ groups, and the 600 - 770 cm^{-1} region for $[TiO_6]$ groups. The bands are weak compared with the scattering by the silicate groups and the interpretation of the spectra in the above papers is equivocal. The most intense Raman modes of Rutile, the A_{1g} and

E_g modes, give bands at 450 cm^{-1} and 612 cm^{-1},(6.40,6.41) (titanium in octahedral co-ordination). Our experimental spectra do not indicate any new bands which may be ascribed to Ti units, and we conclude that the Ti co-ordination cannot be deduced from the Raman spectra. We note finally that the band at 730 cm^{-1}, present in all glasses has not been ascribed to any structural unit and its origin remains unclear.

6.3 Conclusions

The form of the I.R. spectra from the glasses is consistent with the co-existence of two glass phases, one of which is high silica, and one of which is high alkaline earth. The shoulder at $\sim$ 1200 cm^{-1} is suggestive of a high silica phase, and the position and intensity of the peak/shoulder at $\sim$940 cm^{-1} is indicative of a metasilicate phase. Allowing for the poorly resolved glassy spectra, the constancy of the I.R. spectra throughout the range of compositions and pre-crystallization heat treatments, is interpreted to mean that within each of the phases, the number of non-bridged oxygens per SiO_4 tetrahedron remains unaltered, i.e. the 'group' I.R. modes are unchanged.

The 'high frequency' Raman bands originate from the high alkaline earth phase, the high silica phase would be a weak scatterer in this wavenumber region. The occurrence of these bands in the wavenumber region in which the crystalline metasilicates and the metasilicate ratio glasses scatter, is strong confirmation of the present of $[SiO_4]^{2-}$ silicate units in the high alkaline earth phase. The two high frequency bands indicate two dissimilar metasilicate structures, and we have proposed that the two structures are the precursors of the major crystalline phases which precipitate upon devitrification of the glasses, namely Cordierite in the low Ti glasses (rings of $[SiO_4]^{2-}$ tetrahedra), and a pyroxene similar to Enstatite, (one dimensional chains of $[SiO_4]^{2-}$ tetrahedra.

A mechanism by which such changes could take place, involves the preferential removal of Al ions from the co-ordination spheres of the silica tetrahedra. This is discussed further in the next chapter. Although some changes in the I.R. spectrum could be expected through perturbations of the 'group' vibrational modes of the silicate units due to changes in the co-ordination cations, we have proposed that principally the 'extended' vibrational modes are affected by the configurational changes suggested, and that this is manifest in the Raman bands characteristic of each metasilicate configuration.

REFERENCES

CHAPTER 6

6.1 C N Banwell, Fundamentals of Molecular Spectroscopy, McGraw-Hill 1972

6.2 G Herzberg, Infrared and Raman spectra of polyatomic molecules, Van Nostrand New York 1946

6.3 J F Scott and S P S Porto, Phys. Rev. 161 1967 p.903

6.4 J Etchepare, M Merian and L Smetankine, Journ. of Chem. Phys. V.60 No.5 1974 pp.1873-1876

6.5 B E Warren and J Biscoe, Journ. of Amer. Ceram. Soc. 21 1938 p.49

6.6 N F Borrelli and G J Su, Mater. Res. Bull. V.3 1968 pp.181-192

6.7 G J Su and J Bock, Journ. of Amer. Ceram. Soc. 53 1970 p.69

6.8 M Hass, Journ. Phys. Chem. Solids V.3 1 1970 pp.415-422

6.9 P H Gaskell, Trans. Faraday Soc.

6.10 W L Konijnendijk, Philips Research Reports Supp.1 No.1 1975 p.143

6.11 S A Brawer and W B White, Jounr. Chem. Phys. V.63 No.6 1975 p.2421

6.12 W A Deer, R A Howie and J Zussman, 'Rock forming minerals' Vols. 1-4 Longmans 1962

6.13 J R Sweet, W B White, E W White and R Roy, Proc. 4th Lunar Sci. Conf. 1973 in Geochim Cosmochim, Acta. Supp.4 V.1 pp.389-396

6.14 P Tartre, Phys. of Non-Xtal. Solids North Holland 1975

6.15 J Wong and C A Angell, App. Spectosc. Revs. 4(a) 1971 pp.155-231

6.16 J R Ferraro, M H Manghrani and A Quattrochi, Phys. Chem. of Glasses V.13 No.4 1972 pp.116-121

6.17 M H Manghrani, J R Ferraro and L J Basile, App. Spectrosc. V.28 No.3 1974 pp.256-259

6.18 P A Estep, J J Kovach, P Waldstein and C Karr, Proc. 3rd Lunar Sci. Conf. Geochim Cosmochim. Acta. Supp.3 V.3 1972 pp.3047-3067

6.19 P A Estep, J Kovach and C Karr Jr., Proc. 2nd Lunar Sci. Conf. Geochim. Cosmochim. Acta. Supp.2 V.3 1971 pp.2137-51

6.20 J R Sweet and W B White, Phys. Chem. Glasses V.10 No.6 1969 p.246

6.21 P W McMillan, Glass-Ceramics Academic Press 1964

6.22 D Crozier and R W Douglas, Phys. Chem. of Glass 6(6) 1965 p.240

6.23 F Freund, 'Infra-red spectra of minerals" ed. V C Farmer, pub. Mineralogical Soc. 1974

6.24 M Tashiro, T Kokubo and M Nishimura, S. Info. 10th Int. Cong. on Glass 1974 Pt.II pp.129-135 pub. The Ceramic Soc. of Japan

6.25 K Kamiua, S Sakka and I Yamanaka, ibid pp.44-48

6.26 T Kokuko, K Yamashita and M Tashiro, Bull. Inst. Chem. Res., Kyoto Univ. V.50 No.6 1972 pp.608-620

6.27 G V Bazuev and G P Sjveikin, Izv. Acad. Nauk. SSSR Neorgan Mater. V.11 pt.12 1975 pp.1884-1887

6.28 E A Kopylova and L V Salmova, Russ. Jounr. of Phys. Chem. 49(10) 1975 pp.1614-1615

6.29 K Langer and W Schreyer, The Amer. Mineral. V.54 1969 pp.1442-1459

6.30 R J P Lyon, 'Minerals in the Infra-red - A critical bibliography' Stanford Res. Inst., Menlo Park, California 1962

6.31 A G Gregory and T J Veasey, Jounr. of Mater. Sci. 7 1972 pp.1327-1341

6.32 A M Rubenshtein et al, Journ. Catal. V.35 Pt.1 1974 pp.80-91

6.33 W L Konijnendijk, Glastech. Ber. V.48 1975 pp.216-218

6.34 G W Fabel, W B White, E W White and R Roy, Proc. 3rd Lunar Sci. Conf. 1972.
Geochim. Cosmochim. Acta. Supp.3 Vol.1 1972 pp.939-951

6.35 J Etchpare, Amorphous Materials, Eds. R W Douglass, B Ellis, Pub. Wiley Intersc. 1970 pp.337-346

6.36 S Brawer, Phys. Rev. V.11 No.8 1975 pp.3173-3194

6.37 B E Warren and R L Mozzi, Journ. Appl. Cryst. V.2 1969 p.164

6.38 Ya S. Bobovich, Optika i Spectroskopiya V.14 1963 pp.342-7

6.39 N Iwamoto, T Tsunawaki, M Fuji and T Hatfori, Journ. of Non-Cryst. Solids 18 1975 pp.303-306

6.40 G A Samara and P S Peercy, Phys. Rev. B V.7 No.3 1973 p.1131

6.41 S P S Porto, P A Fleury and R C Damen, Phys. Rev. V.154 No. 2 1967 pp.522-526

CHAPTER 7

FINAL DISCUSSION AND CONCLUSIONS

7.1 The Glass Structure

The glass specimens have given an e.s.r. line from the radiochemically reduced Ti^{3+} ions which is invariant with both compositional changes and pre-nucleation heat treatments. We consider that the titanium ions responsible for this resonance signal are six co-ordinated and at centrosymmetric sites of essentially D_{4h} symmetry resulting from a compression of the octahedral ligands along the tetrad axis. An orthorhombic component may be present at these sites although the broad resonance lines do not allow the existence of such a field to be substantiated or rejected. This result may not be taken uncritically to be typical of the whole of the titanium ions in the glass, because, as argued in Chapter 4, many possible titanium complexes, including the crystalline forms of titania, either do not provide stable electronic traps or do not produce room temperature e.s.r. signals. Such an effect appears to be present in the ceramic specimens. Here, we have observed two resonance lines whose relative intensities in a given specimen have been correlated with the relative quantities of the major crystalline phases Cordierite and Enstatite, and the inference was that the signals giving rise to the composite line originated from Ti ions in each of these phases. However we now note that the X-ray diffraction data eliminates the possibility of Ti ions existing in large quantities in these phases, both on the grounds that the index plane spacings are almost unchanged as Ti is added and therefore there is no suggestion of solid solutions forming, and because the quantitative analysis shows that at least 80% of the titanium is in the rutile phase. We conclude therefore that the ceramic resonance lines are not typical of the titanium as a whole in these specimens.

Although not rejected by direction observation of the Ti^{3+} resonance spectra, it is unlikely that the major part of the titania in the glasses exists as TiO_2 (e.g. Rutile) complexes. We argue that the 'inert' nature of such complexes does not properly explain the changes in the glass structure observed in this work, and we favour the concept of titanium as a chemically active agent in the glass structure.

The dominant e.s.r. hole centres in the glass specimens are non-bridging oxygen ions which are singly bonded to SiO_4 tetrahedra. From the lineshape analysis, and using a molecular orbital scheme suggested by Griscom et al (4.56), we have concluded that these n.b.o's. are bonded to SiO_4 units which have a 'sheet' structure in the base and low titania glasses and which convert to 'chain' structures as the titania content increases.

The principal low temperature phases which crystallize from the low and high titania glasses are Cordierite and Enstatite respectively. Enstatite is a chain silicate (7.1), consisting of infinite chains of $\left[SiO_4\right]^{2-}$ metasilicate units. Cordierite however is not a sheet silicate, it is classified (7.1) as a ring or cyclosilicate. The Cordierite structure is essentially one of six membered SiO_4 rings connected laterally and vertically by Al and Mg ions. Within the silicate rings half of the SiO_4 tetrahedra are associated with MgO_6 octahedra and may be considered metasilicate $\left[SiO_4\right]^{2-}$ units, and half are associated with AlO_4 tetrahedra and are therefore more properly disilicate units $\left[SiO_4\right]^{-}$. The silicate rings are arranged in 'sheets' with the rings of each sheet arranged vertically above one another in long 'columns'. We cannot here deduce from the Cordierite structure whether a lateral or vertical misregistry of the rings is more probable, we note only that if the basic randomness of the glass structure is achieved in our specimens by displacements of the 'sheets' of silicate rings relative to one another, then this would generate the type of silicate

structure and n.b.o. trapping sites which we have argued are responsible for the dominant hole resonance in the low titania glasses.

Our proposal is therefore that the hole centre spectra are indicating silicate structure in the glasses which are the precursors of the major low temperature crystalline phases.

The vibrational spectra give some support to this thesis. The main high frequency scattering peak from the low titania glasses is at rather higher frequencies than the high frequency peaks from the crystalline metasilicates and glasses of the metasilicate composition, but well below the high frequency peaks of the crystalline and glass disilicates. Thus the ring type silicate structure with its equal proportion of metasilicate and pseudodisilicate units, would seem to fit well the observed scattering frequency. The growth and ultimate dominance of a peak at lower frequencies as TiO_2 is added to the glass is interpreted as a breaking of the silicate rings into short chains of $\left[SiO_4\right]^{2-}$ tetrahedra. The observed frequency shift of $\sim 100\ cm^{-1}$ is not mirrored by similar changes in the I.R. spectra, and we have concluded that in addition to nearest neighbour coordination changes which may slightly increase the average number of n.b.o's. per SiO_4 unit, although not, (from the I.R. data), to the extent of a disilicate $\rightarrow$metasilicate conversion, this frequency shift must be partially, if not largely due to the ring $\rightarrow$chain configurational change, an effect which has some precident in the crystalline metasilicate spectra. The abnormally low wavenumber of the main high frequency peak from the high titania glasses may be due to the fact that the silicate chains are short, (originating from the six membered rings), or to the presence of Al ions substituting for Si ions in the chain. We have concluded from the study of the e.s.r. hole spectra of the ceramics that bridging SiO_4 and AlO_4 groups exist in both the crystalline ring and chain silicates (i.e. the Enstatite and Cordierite ceramics), and it is reasonable to suppose therefore

that the chain structures in the glasses should incorporate some AlO_4 tetrahedra into the silicate chains. Thus we feel that the Raman spectra are consistent with the existence of ring and chain silicate structures in the glasses, the conversion being effected upon the addition of TiO_2.

The high frequency shoulder at $\sim 1200\ cm^{-1}$ which is present in the I.R. spectrum of all of the glasses, is typical of a high silica framework structure, and there is a suggestion therefore of a phase separated glass structure. In addition, the micrographs of Chapter 3 show that all ceramics crystallized at $1000^{o}C$ have a surface and a volume crystallization which is typical of phase separated glasses, and that the addition of quite small amounts of TiO_2, i.e. below the level at which the changes in the glass structure just discussed take place, noticeably reduces the size of the volume crystallites, and therefore by implication perhaps the dimensions of the phase separated regions. We now introduce a mechanism whereby the addition of TiO_2 to the glass would generate the structural changes within the glass which we have suggested are implied by the e.s.r. and vibrational spectra.

7.2 The Role of TiO_2

Russian workers (7.2,7.3,7.4,7.5) have established that in the $MgO-Al_2O_3-SiO_2$ system there are regions of metastable phase separation, (sub-liquidus), which extend from the $SiO_2-Al_2O_3$ and SiO_2-MgO sides of the ternary phase diagram. If γ , the $MgO:Al_2O_3$ mole ratio, is greater than unity the system will phase separate into high Mg and high Si phases, and, if γ is less than unity, the system will separate into high Al and high Si phases. The approximate regions of immiscibility, (at $1000^{o}C$), suggested by these authors are shown in Figure 7.1. It has been argued (7.6) that it is the high ionic field strength of the Mg^{2+} ion, (compared with most

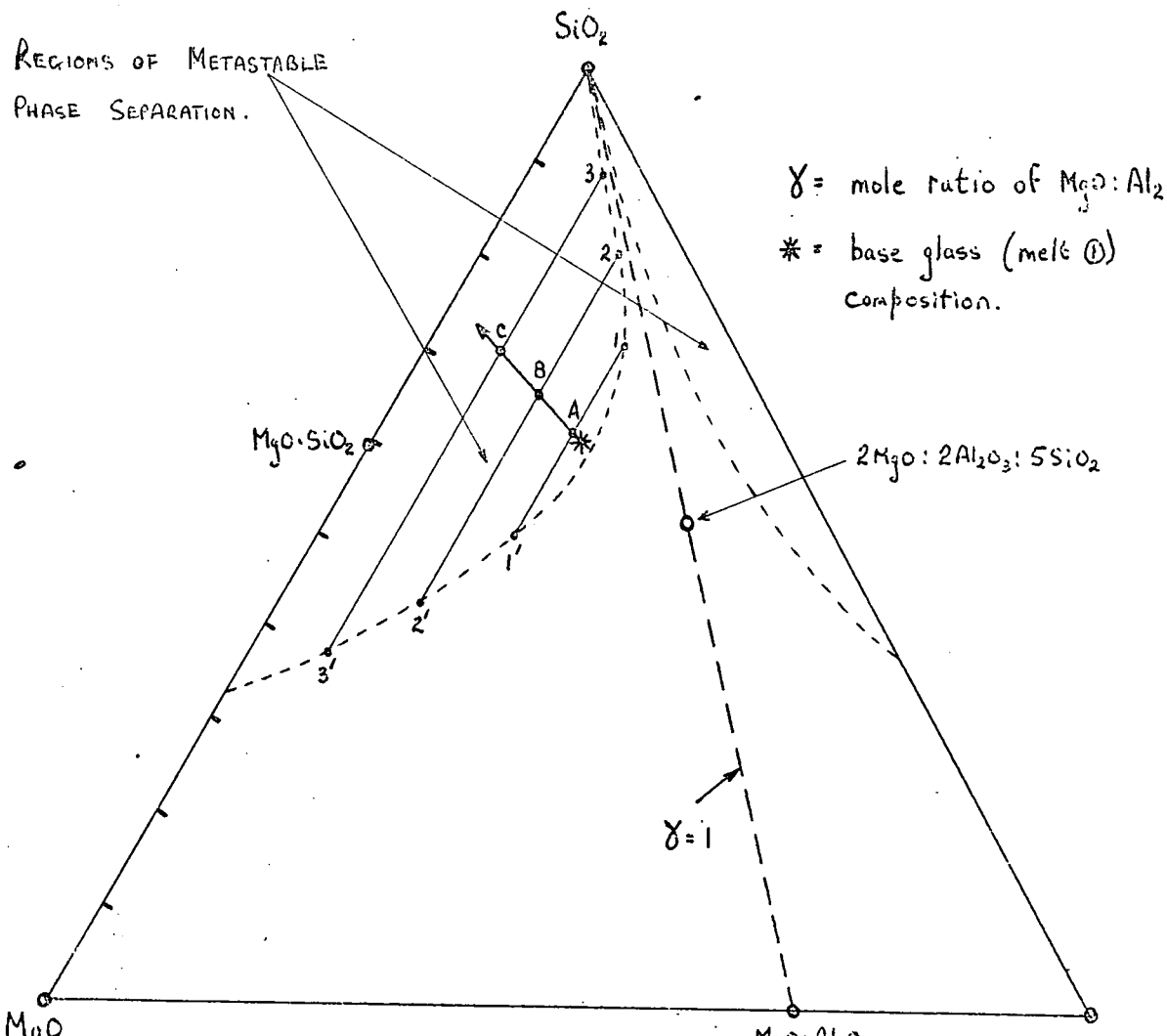

FIG. 7.1. THE $MgO - Al_2O_3 - SiO_2$ SYSTEM. WITH THE REGIONS OF PROBABLE PHASE SEPARATION, (AT 1000°C), SHOWN DOTTED.

other glass modifiers), which renders the Si-O-Al bond relatively unstable by the formation of $\left[AlO_4\right]Mg_{0.5}$ complexes, and thereby promotes the phase separation of the glass sytem. If, as TiO_2 is added to the glass, the titanium ions preferentially combine with Mg or Al ions in order to achieve their required oxygen coordination, the residual glass composition will be shifted toward the SiO_2-Al_2O_3 or MgO-SiO_2 sides of the phase diagram. Because one of the primary products of crystallization in our glasses is an Enstatite phase it would seem that the Ti ions are preferentially combining with Al ions. Such a process would displace the residual glass composition along the line ABC in Figure 7.1. If each mole of TiO_2 combines with one mole of Al_2O_3 to form Al_2TiO_5 complexes then the residual glass compositions would be A (1 wt.% TiO_2), B (5 wt.% TiO_2) and C (10 wt.% TiO_2). These compositions would then degrade to approximately 1 and 1', 2 and 2' and 3 and 3' respectively. The high silica glass phases represented by 1, 2 and 3 lie close to the $\gamma = 1$ mole ratio and would therefore have the Feldspar or framework silicate structure. These phases would give rise to the observed high frequency I.R. band. The increasingly high Mg phases represented by 1', 1' and 3' are, we consider, responsible for the high frequency Raman peaks, and are the phases from which the e.s.r. hole centre absorptions originate. This conclusion is essentially based upon the observations that the high silica phase is likely to be a weak Raman scattering phase, and that this phase would also contain many fewer non-bridging oxygen ions, (the 'defect' which we have concluded provides the hole trapping sites and gives rise therefore to the e.s.r. absorption at $g > g_e$), than the high Mg phase. Our previous discussion indicates therefore that the structural elements of 1' would be silicate rings, and consequently, upon crystallization, the ring silicate Cordierite is the primary phase. The structural elements of 3' would be silicate chains, and hence the emergence of the chain silicate Enstatite upon crystallization

of the glass. We presume the high silica phase to have a higher crystallization temperature than the high Mg phase.

7.3 Unresolved Problems

The phase separation mechanism and its promotion by the added TiO_2 accounts for many of the observations in this work. However we note that the formation of any titanate complex which displaces the residual glass further into the region of immiscibility would produce the structural changes discussed. In the $MgO-Al_2O_3-SiO_2$ glass system embryonic Al_2TiO_5 and $MgTiO_5$ crystals with a pseudo-brookite structure, and their solid solutions (Mg-Al-Titanates), have been observed (7.6,7.7). In the sister $Li_2O-Al_2O_3-SiO_2$ system Dohforty et al (7.8) have observed 50 Å $Al_2Ti_2O_7$ crystallites which heterogeneously nucleate the primary phase. In this work we have made no direct observation of Al-Ti or Mg-Al-Ti complexes, we have rather inferred their existence from the structural changes in the silicate networks of the glass. The point symmetry of the Ti ions, deduced from the nature of the Ti^{3+} e.s.r. line is, of itself, in the absence of published Hamiltonian parameters for this ion in structures which are possible in the glass, not sufficient to suggest a specific titanium containing complex.

There remains an important dilemma. Glasses of compositions such as B and C of Figure 7.1, without added TiO_2, do not produce the microcrystalline ceramics observed in this work. Thus, in addition to promoting the phase separation in the manner described, the Ti complexes must be involved in the crystallization process, most probably as discussed in Chapter I as surface active agents which reduced the interfacial free energy between the major glass phases and thereby reduce the dimensions of the phase separated regions, or as heterogeneous nucleii upon which the primary phase grows, or possibly in a combination of each of these processes.

We introduce therefore a pertinent observation. Figures 7.2 and 7.3 show the oxygen hole centre and Ti^{3+} e.s.r. spectra from a sample of Melt 5, the 10% TiO_2 glass. Traces (a) and (c) of each of these figures are typical of the glassy and crystalline materials, and these resonance lines have been analysed previously (Chapter IV). Trace (b) in each figure arises from a specimen in the early stages of crystallization and corresponds with the X-ray diffraction trace (b) of Figure 3.15, i.e. the trace having only the line marked 'U', (d = 3.70 Å). There is only one direct mention of this diffraction line in the literature, that of Christoserov et al (7.9), who also find the phase associated with the line to be unstable in that it exists only within a narrow temperature region, and who, like ourselves, have been unable to identify the phase. The point here is that our observation indicates that the change in the Ti^{3+} lineshape takes place when the unidentified phase appears and before there is any suggestion, (by standard X-ray diffraction), of the principal Enstatite phase. Although not identical to the 'stable' crystalline line (trace c), this Ti^{3+} line, (trace b), clearly resembles the 'crystalline' rather than the 'glassy' resonance line (Figure 7.3), and the inference is therefore that the Ti ions giving rise to the e.s.r. signals are part of, or closely associated with, the metastable phase responsible for the diffraction line 'U'. However, when this phase is replaced by the Enstatite phase, the Ti^{3+} line, although slightly broadened remains almost unchanged, (c.f. Figures 7.3 and 3.15). The structural implications of this result are not clear to us. It suggests that the earliest phase to crystallize is the Titanium containing phase, and that this phase is assimilated into the subsequent Enstatite phase, perhaps by a diffusion process similar to that described by Hench et al (7.10) during the growth of Li_2SiO_5 crystals from a metastable Li_2SiO_3 phase, although in our case probably involving the diffusion of Mg^{2+} ions. Inspection of Figure 7.2 trace (b), shows that although the Ti^{3+} line closely resembles

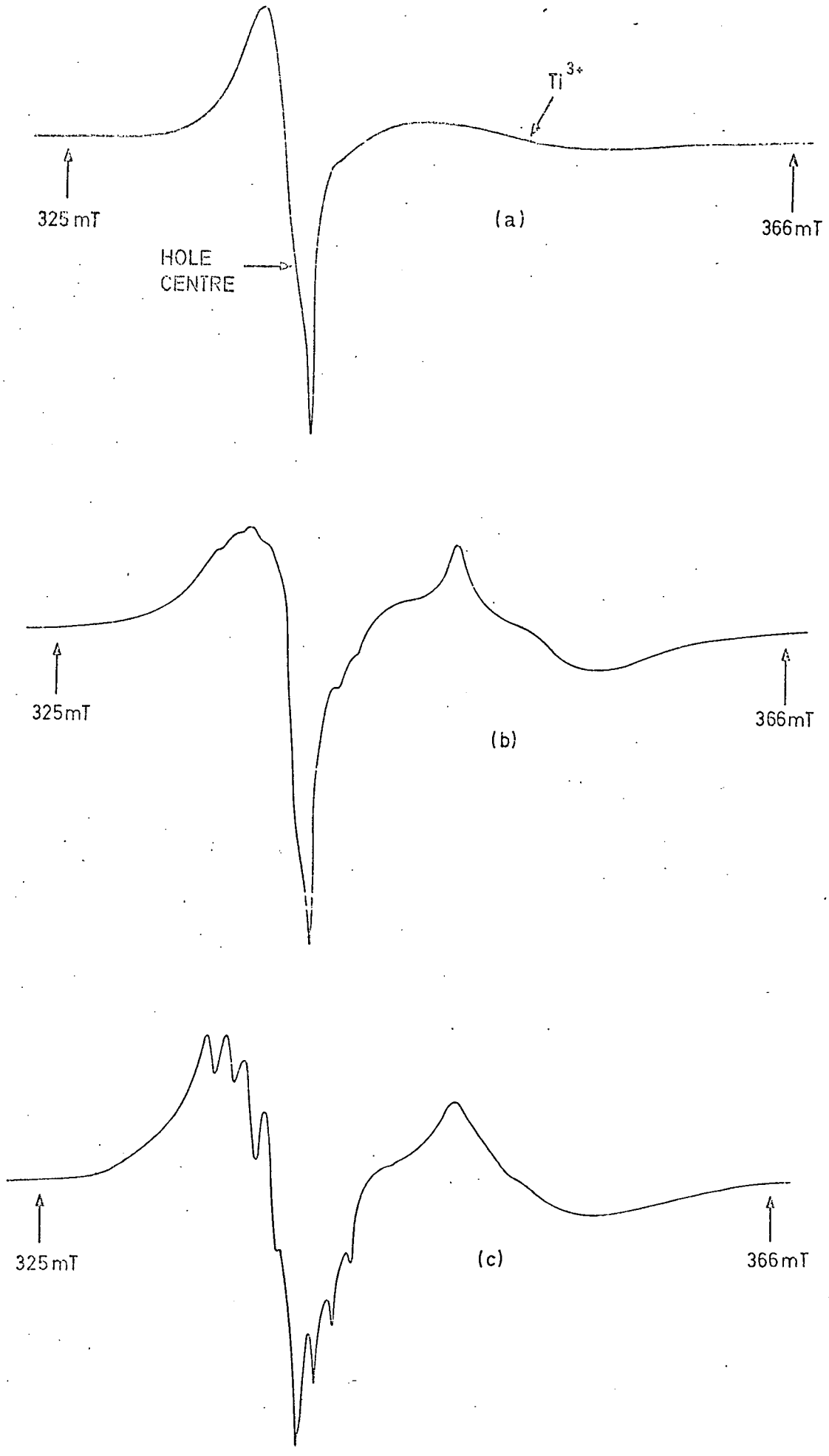

FIG. 7·2 E.S.R. SPECTRA OF HOLE CENTRE AND Ti^{3+} IN GLASS 5 ; δ - DOSE 1 MRAD, 9·48 GHz.
(a) GLASS AS MELTED, (b) HEAT TREATED AT 850°C FOR 2½ HOURS, (c) HEAT TREATED AT 1000°C FOR 2 HOURS.

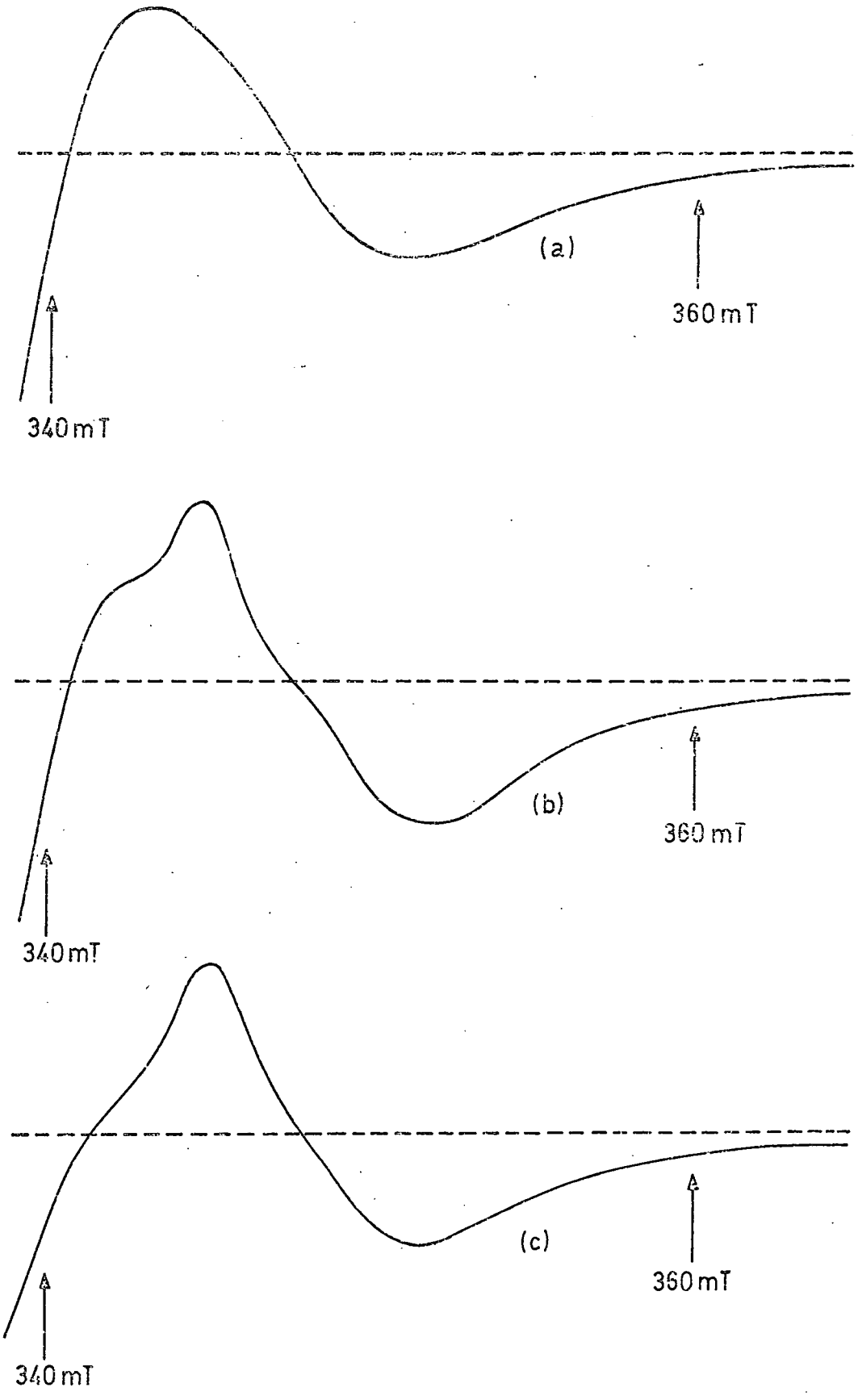

FIG. 7·3 E.S.R. SPECTRA OF Ti^{3+} FROM GLASS 5 ; γ - DOSE 1 MRAD , 9·47 GHz.
(a) GLASS AS MELTED, (b) HEAT TREATED AT 850°C FOR 2½ HOURS, (c) HEAT TREATED AT 1000°C FOR 2 HOURS.

its 'crystalline' form, the hole centre, whilst indicating the development of a hyperfine interaction, more closely resembles the 'glassy' line. We have in this work broadly divided the oxygen associated hole spectra into a line dominant in the glasses and which arises from holes trapped at non-bridging oxygen ions and a line dominant in the ceramics, displaying a hyperfine interaction with an Al nucleus, and arising from holes trapped at oxygen ions bridging four coordinated Si and Al ions. We have argued that the n.b.o. are primarily located in the high modifier glass phase, and thus it is not unexpected that the e.s.r. line associated with this 'defect' remains dominant in the metastable, partially crystalline, specimens because this phase is, at this stage, unaltered.

This final series of observations upon the chronology of the Ti^{3+} lineshape changes indicates that the Ti containing phase is involved in the initial stages of crystallization, although they do not clearly favour either the 'crystallite' or 'surfactant' mechanisms. They also suggest that the Ti^{3+} lines which have been observed in the glassy specimen are typical of those ions which are involved in the early stages of crystallization. The invariance of the glassy Ti^{3+} lines with pre-crystallization heat treatments now strongly suggests that there are no structural changes within the titanium containing glass phase as a result of such heat treatments.

7.4 Further Work

It would appear that 'nucleation' effects are compressed into a narrow temperature interval close to the temperature at which the first metastable crystalline phase appears, and indeed 'nucleation' may well consist entirely of the appearance of this phase. The present measurements have been spread over a range of compositions, pre-crystallization and crystallization temperatures and times, and the studies in the region of initial crystallization are not sufficiently detailed. We suggest therefore

a duality of measurements, both e.s.r. and transmission electron microscopy plus electron diffraction, upon specimens of a single composition, (e.g. Melt (5)), at temperature intervals of $5^{o}C$ in a range of $\pm 50^{o}C$ about the temperature at which the first crystalline phase appears. Such measurements would we think confirm our belief that it is the titanium containing glass phase which is the origin of the initial crystal phase, and place a better chronology upon the structural changes which are occurring in this phase prior to crystallization and during the growth of the Enstatite phase; in addition, the simultaneous data from the electron microscope could indicate the location of the initial crystallization and the nature of the glass phases, (i.e. whether the titanium phase is in droplet form or in a surface layer around the primary droplet phase). In this way it should be possible to distinguish between the 'crystallite' or surfactant' hypotheses discussed previously.

A clearer understanding of the chemical nature of the titanium containing glass phase could possibly be obtained in the following manner. If, as suggested, the addition of TiO_2 to the base glass causes Al ions to be removed from the coordination spheres of the silicate rings, and to form Al-Ti complexes, then this almost certainly implies a coordination change, (of the Al ions), from four to six. X-ray fluorescence studies using Corrundum and Feldspar standards could determine the porportion of four and six coordinated Al ions and a study of the changes would give an indication of the type of Ti-Al or Ti-Al-Mg complex formed (e.g. Al_2TiO_5 or Al_2TiO_7). The next stage would be an e.s.r. study of irradiated single crystals or powders of an appropriate Titanium containing complex, in the hope that the Hamiltonian parameters found would correlate with the resonance lines of the glasses studied here.

Finally , on a different vein, we note that the need to sensitise some titanium ions by radiochemical reduction is a severe limitation to

the general interpretation of the structural state of the titanium as a whole. There is some argument therefore for doping the glass with an ion which is chemically similar to titanium and which might be expected to form similar complexes, but which is paramagnetic in its most common oxidation state. In addition, an electronic ground state configuration giving spectra which are relatively easily interpreted in amorphous and polycrystalline materials is preferable. In both respects the V^{4+} ion (d^1) is attractive. This ion could be monitored, (by e.s.r.) through the glass to ceramic conversion without the need for radiochemical reduction.

CHAPTER 7

REFERENCES

7.1 W A Deer, R A Howie and J Zussman, 'Rock Forming Minerals' Longmans 1962

7.2 B G Varshal et al, Izv. Acad. Nauk. S.S.R. Neorgan. Mater. V6 1970 1314-20

7.3 B G Varshal et al, Ibid. V9 1973 1610-5

7.4 B G Varshal et al, Ibid. V9 1973 1946-51

7.5 B G Varshal et al, Ibid. V10 1974 1140-5

7.6 R C De Vekey and A J Majumdar, Proc. Brit. Ceram. Soc. 25 1975 1-11

7.7 N M Pavlushkin et al, 9th Int. Cong. Glass. Sci. Tech. Comm. 2 1971 1051-67

7.8 P E Dohferty et al, J. of Amer. Ceram. Soc. 1967 77-81

7.9 V G Chistoserdov et al in 'Structure of Glass' V5 Ed. E A Porai Koshits, Consult. Bur. 1965 pp.172-174

APPENDIX I

BOLTZMANN STATISTICS OF S = ½ SPIN STATES

For an S = ½ spin system the ratio of the number of spins in the upper $|+\tfrac{1}{2}>$ level to those in the $|-\tfrac{1}{2}>$ ground state is

$$\frac{N_{|+\frac{1}{2}>}}{N_{|-\frac{1}{2}>}} = \exp\left[-\frac{\Delta E}{kT}\right]$$

The energy separation, ΔE, of the states is given by the resonance condition

$$\Delta E = g\beta H$$

which for X-band frequencies gives $\beta = 9.273 \times 10^{-24}\ J\,T^{-1}$, and $H = 0.33$ T. Thus for the 'free' electron resonance, $g = 2.0023$, we have

$$\Delta E = 6.1 \times 10^{-24}\ J$$

At room temperature (300 K)

$$\frac{N_{|+\frac{1}{2}>}}{N_{|-\frac{1}{2}>}} = 0.999 \qquad (A1.1)$$

At liquid Helium temperatures (4.2 K)

$$\frac{N_{|+\frac{1}{2}>}}{N_{|-\frac{1}{2}>}} = 0.902 \qquad (A1.2)$$

Thus, of the ground state spins, $\sim 10^{-3}$ are 'available' for μ-wave absorption at R.T., and 10^{-1} are 'available' at liquid helium temperatures.

APPENDIX II

OPTICAL UNITS AND CALCULATIONS

I_o = beam intensity

I_t = transmitted beam intensity

d = specimen thickness

c = molar concentration of colour centres in moles/litre.

1. Optical Density (O.D.):-

$$O.D. = \text{Log}_{10} \frac{I_o}{I_t} .$$

2. Absorption Coefficient (α):-

$$\alpha = \frac{\ell n\left(I_o/I_t\right)}{d} \quad cm^{-1}$$

3. Molar Extinction Coefficient (ε):-

$$\varepsilon = \frac{O.D.}{c.d.} \text{ litre mol}^{-1} \text{ cm}^{-1}$$

Relationship between α, ε and O.D.:-

$$O.D. = \varepsilon.c.d = \frac{\alpha.d}{2.3}$$

Thus

$$\boxed{\alpha = 2.3 \ . \ c}$$

Calculation of absorption coefficient:-

In terms of the optical constant n and κ, the real and imaginary parts of the complex refractive index, the reflection at an interface, defined as

$$R = \frac{I_R}{I_o}$$

may be written

$$R = \frac{(n-1)^2 + \kappa^2}{(n+1)^2 + \kappa^2} \quad \text{(at normal incidence)} .$$

For $\alpha < 10^4$ cm^{-1}, i.e. at wavelengths sufficiently removed from the absorption edge, this reduces to

$$R = \frac{(n-1)^2}{(n+1)^2}$$

For multiple refections we have

$$\frac{I_t}{I_o} = (1-R)^2$$

$$= \left[1 - \frac{(n-1)^2}{(n+1)^2}\right]^2 e^{-\alpha d}$$

Therefore

$$\frac{I_t}{I_o} = \frac{16n^2}{(n+1)^4} e^{-\alpha d}$$

Thus

$$\boxed{\alpha d = -\ell n \left[\frac{I_t}{I_o} \cdot \frac{(n+1)^4}{16n^2}\right]}$$

Abscissa units:-

$$1 \text{ eV} = 8065.7 \text{ cm}^{-1} = 1239.8 \text{ nm} .$$

Thus

$$\boxed{\text{Wavelength in nm.} = \frac{10^7}{\text{Wavenumber in cm}^{-1}}}$$

The following programs generate the first derivative e.s.r.'powder' spectrum for systems with :-

PROG (1) :- (a) Zeeman term only in the Spin Hamiltonian.

(b) $S = \frac{1}{2}$.

(c) $g_1 \neq g_2 \neq g_3$.

(d) Distributed g_2 and g_3 parameters.

PROG (2):- (a) Zeeman plus Hyperfine terms in the Spin Hamiltonian.

(b) $S = \frac{1}{2}$, $I = \frac{5}{2}$.

(c) $g_1 \neq g_2 \neq g_3$.

(d) Distributed g_1 parameter.

F.

```
0001            FUNCTION F(H,H1,PAI,SIGMA)
0002            F=(2.0*SIGMA)/(PAI*(4.0*(H-H1)**2+SIGMA**2))
0003            RETURN
0004            END
```

G.

```
0001            FUNCTION G(H,H1,PAI,SIGMA)
0002            G=(1.0/((SQRT(2.0*PAI))*SIGMA))*EXP(-((H-H1)**2)/
               1(2.0*(SIGMA**2)))
0003            RETURN
0004            END
```

H.

```
0001            FUNCTION H(G1,G2,G3,THETA,FAY,UU,BETA,PLANK)
0002            G=SQRT((G1*SIN(THETA)*SIN(FAY))**2+(G2*SIN(THETA)
               1*COS(FAY))**2+(G3*COS(THETA))**2)
0003            H=(PLANK*UU)/(G*BETA)
0004            RETURN
0005            END
```

MAIN.

Prog. 1.

```
0001            DIMENSION HH(341),A(101),AA(201),BR(340),DIFF(340),IN(340),G3(6)
               1,G2(5)
0002            DATA HH/341*0.0/
0003            DATA A/101*0.0/
0004            DATA AA/201*0.0/
0005            DATA IN/340*0/
0006            DATA BR/340*0.0/
0007            DATA DIFF/340*0.0/
0008            SIGMAL=35.0
0009            SIGMAG=17.0
0010            G1=1.9874
0011            G2(1)=1.9518
0012            G2(2)=1.9496
0013            G2(3)=1.9451
0014            G2(4)=1.9385
0015            G2(5)=1.9291
0016            G3(1)=1.9116
0017            G3(2)=1.9095
0018            G3(3)=1.9062
0019            G3(4)=1.8998
0020            G3(5)=1.8892
0021            G3(6)=1.8694
0022            PL=0.66251E-26
0023            UU=0.9472E10
0024            BETA=0.92729E-20
0025            HH(1)=3320.0
0026            DO 1 I=2,341
0027            HH(I)=HH(I-1)+1.0
0028          1 CONTINUE
0029            DO 2 I=1,101
0030            A(I)=ARCOS(FLOAT(I-1)/100.0)
0031          2 CONTINUE
0032            PAI=4.0*ATAN(1.0)
0033            AA(1)=0.0
0034            DO 3 I=2,201
0035            AA(I)=AA(I-1)+PAI/200.0
0036          3 CONTINUE
0037            DO 16 M=1,5
0038            DO 15 L=1,6
0039            DO 4 I=2,100
0040            DO 5 J=2,200
0041            IF(J.EQ.101)GO TO 5
0042            X=H(G1,G2(M),G3(L),A(I),AA(J),UU,BETA,PL)
0043            DO 6 K=2,341
0044            IF(X.LE.HH(K))GO TO 7
0045            GO TO 6
0046          7 IN(K-1)=IN(K-1)+1
0047            GO TO 5
0048          6 CONTINUE
0049          5 CONTINUE
0050          4 CONTINUE
0051         15 CONTINUE
0052         16 CONTINUE
0053            DO 9 I=1,340
0054            YY=FLOAT(IN(I))
0055            S=HH(I)+0.5
0056            DO 10 J=1,340
0057            SS=HH(J)+0.5
0058            XX=G(S,SS,PAI,SIGMAG)
0059            YG=XX*YY
0060            BR(J)=BR(J)+YG
0061         10 CONTINUE
0062          9 CONTINUE
0063            DO 13 I=1,339
0064            DIFF(I)=BR(I+1)-BR(I)
0065         13 CONTINUE
0066            WRITE(6,100)
0067        100 FORMAT(//,12HINTERVAL NO.,5X,22HVAL. OF H AT BEGINNING,5X,
               19HFREQUENCY,5X,19HBROADENED FREQUENCY,5X,10HDERIVATIVE,/)
0068            DO 8 KK=1,340
0069            WRITE(6,200)KK,HH(KK),IN(KK),BR(KK),DIFF(KK)
0070        200 FORMAT(4X,I4,14X,E12.5,11X,I6,10X,E12.5,8X,E12.5)
0071          8 CONTINUE
0072            STOP
0073            END
```

F.

```
0001          FUNCTION F(H,H1,PAI,SIGMA)
0002          F=(2.0*SIGMA)/(PAI*(4.0*(H-H1)**2+SIGMA**2))
0003          RETURN
0004          END
```

G.

```
0001          FUNCTION G(H,H1,PAI,SIGMA)
0002          G=(1.0/((SQRT(2.0*PAI))*SIGMA))*EXP(-((H-H1)**2)/
             1(2.0*(SIGMA**2)))
0003          RETURN
0004          END
```

H.

```
0001          FUNCTION H(G1,G2,G3,THETA,FAY,UU,BETA,PLANK,WA1,WA2,WA3,AM)
0002          G=SQRT((G1*SIN(THETA)*SIN(FAY))**2+(G2*SIN(THETA)
             1*COS(FAY))**2+(G3*COS(THETA))**2)
0003          WW=SQRT((G1*WA1*SIN(THETA)*SIN(FAY))**2+(G2*WA2*SIN(THETA)
             1*COS(FAY))**2+(G3*WA3*COS(THETA))**2)
0004          H=(PLANK*UU)/(G*BETA)-(AM*WW)/G
0005          RETURN
0006          END
```

MAIN.

```
0001          DIMENSION HH(201),A(101),AA(201),BR(200),DIFF(200),IN(200),
             1AM(6),G1(5)
0002          DATA HH/201*0.0/
0003          DATA A/101*0.0/
0004          DATA AA/201*0.0/
0005          DATA IN/200*0/
0006          DATA BR/200*0.0/
0007          DATA DIFF/200*0.0/
0008          DATA AM(1),AM(2),AM(3),AM(4),AM(5),AM(6)/
             12.5,1.5,0.5,-0.5,-1.5,-2.5/
0009          DATA G1/5*0.0/
0010          SIGMAL=5.5
0011          SIGMAG=2.0
0012          G1(1)=2.0608
0013          G1(2)=2.0471
0014          G1(3)=2.0235
0015          G1(4)=2.0202
0016          G1(5)=2.0070
0017          G2=2.0148
0018          G3=2.0023
0019          PL=0.66251E-26
0020          UU=0.947E10
0021          BETA=0.92729E-20
0022          WA1=9.0
0023          WA2=8.9
0024          WA3=8.8
0025          HH(1)=3270.0
0026          DO 1 I=2,201
0027          HH(I)=HH(I-1)+1.0
0028        1 CONTINUE
0029          DO 2 I=1,101
0030          A(I)=ARCOS(FLOAT(I-1)/100.0)
0031        2 CONTINUE
0032          PAI=4.0*ATAN(1.0)
0033          AA(1)=0.0
0034          DO 3 I=2,201
0035          AA(I)=AA(I-1)+PAI/200.0
0036        3 CONTINUE
0037          DO 15 L=1,5
0038          DO 4 I=2,100
0039          DO 5 J=2,200
0040          IF(J.EQ.101)GO TO 5
0041          DO 20 M=1,6
0042          X=H(G1(L),G2,G3,A(I),AA(J),UU,BETA,PL,WA1,WA2,WA3,AM(M))
0043          DO 6 K=2,201
0044          IF(X.LE.HH(K))GO TO 7
0045          GO TO 6
0046        7 IN(K-1)=IN(K-1)+1
0047          GO TO 20
0048        6 CONTINUE
0049       20 CONTINUE
0050        5 CONTINUE
0051        4 CONTINUE
0052       15 CONTINUE
0053          DO 9 I=1,200
0054          YY=FLOAT(IN(I))
0055          S=HH(I)+0.5
0056          DO 10 J=1,200
0057          SS=HH(J)+0.5
0058          XX=G(S,SS,PAI,SIGMAG)
0059          YG=XX*YY
0060          BR(J)=BR(J)+YG
0061       10 CONTINUE
0062        9 CONTINUE
0063          DO 13 I=1,199
0064          DIFF(I)=BR(I+1)-BR(I)
0065       13 CONTINUE
0066          WRITE(6,100)
0067      100 FORMAT(//,12HINTERVAL NO.,5X,22HVAL. OF H AT BEGINNING,5X,
             19HFREQUENCY,5X,19HBROADENED FREQUENCY,5X,10HDERIVATIVE,/)
0068          DO 8 KK=1,200
0069          WRITE(6,200)KK,HH(KK),IN(KK),BR(KK),DIFF(KK)
0070      200 FORMAT(4X,I4,14X,E12.5,11X,I6,10X,E12.5,8X,F12.5)
0071        8 CONTINUE
0072          STOP
0073          END
```

PROG. 2.